

JPL PUBLICATION 85-41

# Proceedings of the Airborne Imaging Spectrometer Data Analysis Workshop

April 8, 9, 10, 1985

Editors

Gregg Vane

Alexander F.H. Goetz

Jet Propulsion Laboratory

(E86-10001 NASA-CR-176210) PROCEEDINGS OF  
THE AIRBORNE IMAGING SPECTROMETER DATA  
ANALYSIS WORKSHOP (Jet Propulsion Lab.)  
180 p HC A09/MF A01

CSCL 05b

G3/43

N86-11618  
THRU  
N86-11644  
Unclas  
00001

June 15, 1985



National Aeronautics and  
Space Administration

Jet Propulsion Laboratory  
California Institute of Technology  
Pasadena, California

JPL PUBLICATION 85-41

# Proceedings of the Airborne Imaging Spectrometer Data Analysis Workshop

April 8, 9, 10, 1985

Editors

**Gregg Vane**

**Alexander F.H. Goetz**

Jet Propulsion Laboratory

June 15, 1985



National Aeronautics and  
Space Administration

**Jet Propulsion Laboratory**  
California Institute of Technology  
Pasadena, California

This publication was prepared by the Jet Propulsion Laboratory, California Institute of Technology, under a contract with the National Aeronautics and Space Administration

## TABLE OF CONTENTS

INTRODUCTION TO THE PROCEEDINGS OF THE AIRBORNE IMAGING SPECTROMETER (AIS) DATA ANALYSIS WORKSHOP Gregg Vane and Alexander F. H. Goetz . . . . .	1
MINERALOGICAL MAPPING IN THE CUPRITE MINING DISTRICT, NEVADA Alexander F. H. Goetz and Vinay Srivastava . . . . .	22
REMOTE STRATIGRAPHIC ANALYSIS: COMBINED TM AND AIS RESULTS IN THE WIND RIVER/BIGHORN BASIN AREA, WYOMING H. R. Lang, E. D. Paylor, and S. Adams . . . . .	32
FIELD UTILIZATION AND ANALYSIS OF AIS 128-CHANNEL IMAGERY USING MICROCOMPUTERS: APPLICATION TO YERINGTON, NV FIELD AREA R. J. P. Lyon and Kai Lanz . . . . .	35
PRELIMINARY ANALYSIS OF AIS SPECTRAL DATA ACQUIRED FROM SEMI-ARID SHRUB COMMUNITIES IN THE OWENS VALLEY, CALIFORNIA Susan L. Ustin and Barrett N. Rock . . . . .	41
AIS SPECTRA FOR STRESSED AND UNSTRESSED PLANT COMMUNITIES IN THE CAROLINA SLATE BELT Diane E. Wickland . . . . .	46
SPECTRAL CHARACTERIZATION OF SUSPECTED ACID DEPOSITION DAMAGE IN RED SPRUCE (PICEA RUBENS) STANDS FROM VERMONT James E. Vogelmann and Barrett N. Rock . . . . .	51
A FIRST LOOK AT AIRBORNE IMAGING SPECTROMETER (AIS) DATA IN AN AREA OF ALTERED VOLCANIC ROCKS AND CARBONATE FORMATIONS, HOT CREEK RANGE, SOUTH CENTRAL NEVADA Sandra C. Feldman, James V. Taranik, and David A. Mouat . . . . .	56
INTERPRETATION OF AIS IMAGES OF CUPRITE, NEVADA USING CONSTRAINTS OF SPECTRAL MIXTURES Milton O. Smith and John B. Adams . . . . .	62
EVALUATION OF AIS DATA FOR AGRONOMIC AND RANGELAND VEGETATION: PRELIMINARY RESULTS FOR AUGUST 1984 FLIGHT OVER NEBRASKA SANDHILLS AGRICULTURAL LABORATORY Blaine L. Blad, Patrick J. Starks, Cynthia Hays, and Bronson R. Gardner . . . . .	68
SITE DESCRIPTION FOR THE UNIVERSITY OF NEBRASKA'S SANDHILLS AGRICULTURAL LABORATORY B. R. Gardner and Blaine L. Blad . . . . .	71
PRELIMINARY EVALUATION OF AIS SPECTRA ALONG A TOPOGRAPHIC/MOISTURE GRADIENT IN THE NEBRASKA SANDHILLS Donald C. Rundquist . . . . .	74

THE USE OF AIS DATA FOR IDENTIFYING AND MAPPING CALCAREOUS SOILS IN WESTERN NEBRASKA Scott A. Samson . . . . .	79
CALIBRATION OF AIS DATA USING GROUND-BASED SPECTRAL REFLECTANCE MEASUREMENTS James E. Conel . . . . .	84
ANALYSIS OF AIS DATA OF THE RECLUSE OIL FIELD, RECLUSE, WYOMING Jon D. Dykstra and Donald B. Segal . . . . .	86
HIGH RESOLUTION SPECTROMETRY OF LEAF AND CANOPY CHEMISTRY FOR BIOGEOCHEMICAL CYCLING Michael A. Spanner, David L. Peterson, William Acevedo, and Pamela Matson . . . . .	92
FOREST CANOPY CHEMISTRY FROM BLACKHAWK ISLAND, WISCONSIN James H. Fownes and John D. Aber . . . . .	100
ANALYTICAL TECHNIQUES FOR EXTRACTING MINERALOGICAL INFORMATION FROM MULTICHANNEL IMAGING SPECTROMETER DATA Fred A. Kruse, Gary L. Raines, and Kenneth Watson . . . . .	105
SPECTROSCOPY OF MOSES ROCK KIMBERLITE DIATREME Carle M. Pieters and John F. Mustard . . . . .	106
ANALYSIS OF AIRCRAFT SPECTROMETER DATA WITH LOGARITHMIC RESIDUALS A. A. Green and M. D. Craig . . . . .	111
COMPARISON OF AIS VS. TMS DATA COLLECTED OVER THE VIRGINIA PIEDMONT R. Bell and C. S. Evans . . . . .	120
A PRELIMINARY INVESTIGATION OF SYSTEMATIC NOISE IN DATA ACQUIRED WITH THE AIRBORNE IMAGING SPECTROMETER Edward Masuoka . . . . .	123
DISCRIMINATION OF COASTAL VEGETATION AND BIOMASS USING AIS DATA Michael F. Gross and V. Klemas . . . . .	129
AIS INVESTIGATION OF AGRICULTURAL MONOCULTURES Byron L. Wood and Robert C. Wrigley . . . . .	134
APPLICATION OF AIS TECHNOLOGY TO FOREST MAPPING Stephen R. Yool and Jeffrey L. Star . . . . .	141
A COMPARISON OF AIS DATA WITH OTHER AIRCRAFT AND GROUND DATA FOR THE GEOBOTANICAL DISCRIMINATION OF ROCK TYPES IN SOUTHWEST OREGON David A. Mouat . . . . .	146

FOREST SPECIES IDENTIFICATION WITH HIGH SPECTRAL  
RESOLUTION DATA

Charles E. Olson, Jr., and Zhiliang Zhu . . . . . 152

URBAN, FOREST, AND AGRICULTURAL AIS DATA: FINE SPECTRAL  
STRUCTURE

V. C. Vanderbilt . . . . . 158

APPENDIXES

1. ATTENDEES OF THE AIS DATA ANALYSIS WORKSHOP  
APRIL 8-10, 1985 . . . . . 166
2. AGENDA OF THE AIS DATA ANALYSIS WORKSHOP HELD  
APRIL 8-10, 1985 . . . . . 170

## ABSTRACT

The Airborne Imaging Spectrometer (AIS) Data Analysis Workshop was held at the Jet Propulsion Laboratory on April 8 to 10, 1985. It was attended by 92 people who heard reports on 30 investigations currently under way using AIS data that have been collected over the past two years. Written summaries of 27 of the presentations are in these Proceedings.

Many of the results presented at the Workshop are preliminary because most investigators have been working with this fundamentally new type of data for only a relatively short time. Nevertheless, several conclusions can be drawn from the Workshop presentations concerning the value of imaging spectrometry to earth remote sensing. First, work with AIS has shown that direct identification of minerals through high spectral resolution imaging is a reality for a wide range of materials and geological settings. Second, there are strong indications that high spectral resolution remote sensing will enhance the ability to map vegetation species. There are also good indications that imaging spectrometry will be useful for biochemical studies of vegetation. Finally, there are a number of new data analysis techniques under development which should lead to more efficient and complete information extraction from imaging spectrometer data. The results of the Workshop indicate that as experience is gained with this new class of data, and as new analysis methodologies are developed and applied, the value of imaging spectrometry should increase.

# INTRODUCTION TO THE PROCEEDINGS OF THE AIRBORNE IMAGING SPECTROMETER (AIS) DATA ANALYSIS WORKSHOP

GREGG VANE and ALEXANDER F. H. GOETZ,  
Jet Propulsion Laboratory, California Institute of Technology  
Pasadena, California 91109 U.S.A.

## OVERVIEW OF WORKSHOP AND SUMMARY OF KEY RESULTS

The AIS Data Analysis Workshop was held at the Jet Propulsion Laboratory on April 8 to 10, 1985. All investigators who have had a chance to work with AIS data were invited to attend and give a progress report on the status of their research. Of the 30 investigators who currently have AIS data sets, 27 attended the Workshop and made presentations. An additional 65 people attended who have interest in high spectral-resolution remote sensing. Of the total 92 attendees, 67 were from organizations other than JPL, including representatives from Austria, Australia, Canada, India, and Japan. A complete list of attendees is given in Appendix 1.

Most investigators have had only a relatively short time to work with AIS data; hence, many of the results presented at the Workshop should be considered preliminary. Imaging spectrometer data are of a fundamentally different nature from all previous types of remote-sensing data, and before meaningful results can be derived from them, new analysis methodologies must be developed. The development of new analysis methodologies in turn requires a certain amount of experience in working with this new class of data which has only become available in the past two years. In spite of this, several conclusions can be drawn from the reports presented at the Workshop. These reports are summarized in these Proceedings. Some of the conclusions are summarized here.

First, direct identification of minerals through high spectral-resolution remote sensing is a reality. Extensive work has been done in the hydrothermal alteration zone of the Cuprite Mining District, Nevada, where the minerals kaolinite, alunite, buddingtonite, and secondary quartz have been identified through spectral signatures derived from AIS imagery. Mineralogical maps of the Cuprite area have been produced directly from the AIS data and these maps have been substantiated by subsequent field work. In the Wind River Basin of Wyoming, the minerals calcite, dolomite, gypsum, and montmorillonite have been directly identified through their spectral signatures, and spectral stratigraphy, or the remote analysis of stratigraphic sequences, has been accomplished. OH-bearing minerals associated with sericite alteration in the porphyry copper deposit at Yerington, Nevada have been identified. The minerals kaolinite and montmorillonite have also been observed directly in AIS data in an area of altered and unaltered rhyolites and latites in the Hot Creek Range, Nevada. Serpentinized olivine-bearing soils have been tentatively identified with AIS spectra and a potential unmapped satellite dike associated with the Moses Rock diatreme in Utah has been detected. Also, the ability to discriminate between serpentinized and unserpentinized peridotite has been demonstrated at the Josephine Ophiolite

of southwestern Oregon. This finding was based both on spectral differences between the two rock types and spectral differences in the vegetation growing on the two different rock types. With the value of imaging spectrometry to mineral identification well demonstrated, the major effort now is in the development of efficient techniques for information extraction, and the application of these techniques to broader geological problems.

In addition to those data analysis methodologies under development at JPL, several other approaches to the analysis of high spectral-resolution remote-sensing data were discussed. A spectral mixture model is under development at the University of Washington that makes use of a spectral reference library, which has been used successfully to identify the origin of spectral variation in AIS images. The model has been applied to two data sets from Cuprite, Nevada, and has identified the spectral endmembers characteristic of the area imaged: playa silt, kaolinite, and alunite. A technique is also under development in Australia for mineral identification making use of the wavelength position, intensity, and shape of diagnostic absorption features. Extraction of the absorption features is done by ratioing the spectrum against its "upper convex hull," which is defined as the lowest convex curve lying above the spectrum. The resulting curve, called the "hull quotient," allows the isolation and extraction of individual features which provide the basis for automatic classification of spectra. The technique has been successfully applied to airborne spectroradiometer data. At the U.S. Geological Survey in Denver, analysis techniques under development include the normalization of spectra to remove albedo and illumination effects, and the calculation of reflectance relative to a standard spectrum to identify minerals. Standard spectral curves are formed by either calculating the simple average of all spectra along the flight line or using the low-order terms of a discrete Fourier series to fit each spectrum along the flight line by employing a fast Fourier transform method. The techniques used have allowed mineral identification in an area of hydrothermally altered quartz monzonite and carbonate rocks in Nevada. Other techniques are under study.

In the vegetation disciplines, the utilization of imaging spectrometry has not progressed quite as rapidly, due in part to the fact that vegetation spectra do not exhibit the wealth of spectral absorption features that are common in so many minerals. Further, vegetation spectra are highly variable as a function of time for most species. Hence, the techniques being developed for mineral identification are not always directly applicable. Nevertheless, several preliminary results were presented at the Workshop which could prove of great value if confirmed after further study. Variation in the width and depth of an absorption feature at about 1.19  $\mu\text{m}$  has been found to be related to forest type in the Slate Belt District of North Carolina. The absorption feature is consistently broader and shallower for pine forests than for deciduous forests. Subtle features in the near infrared plateau from about 1.18 to 1.31  $\mu\text{m}$ , and from 1.60 to 1.78  $\mu\text{m}$  suggest that high spectral-resolution data in these regions may be useful in discriminating between corn, soybeans, and alfalfa. Variations in the slope of the spectral reflectance curve between 1.4 and 1.9  $\mu\text{m}$  have made it possible to

separate four types of wetland vegetation in the Delaware Bay. In another study, over Blackhawk Island, Wisconsin, very strong correlations were observed between green wet-canopy weight and AIS data, as a strong indication of an important protein absorption feature at  $1.5 \mu\text{m}$  was inferred through a strong negative correlation between the AIS data at that wavelength and the nitrogen concentration and total nitrogen. Additional evidence of spectral signatures related to plant biochemistry was found in data acquired near Purdue University, Indiana, and over the Boreal Forest of Minnesota. The ratio of the AIS radiance of the ground cover to the radiance of a standard showed several ramp-like features thought to be due to the biochemical composition of the leaf or to the optical-scattering properties of its cuticle, or a combination of both. The size and shape of the ramps vary with ground cover, indicating the potential for species discrimination and identification, as well as assessment of health.

Contained in these Proceedings are the summaries of 27 of the progress reports that were presented at the Workshop. Further details pertaining to the foregoing synopsis can be found in the summaries. The meeting agenda is also included in the Proceedings as Appendix 2. The remainder of this Introduction to the Proceedings is devoted to an overview of the motivation for high spectral-resolution remote sensing, a brief discussion on how imaging spectrometry is accomplished, a summary of the analysis techniques under development at JPL, and an overview of the AIS and its operation.

#### MOTIVATION FOR IMAGING SPECTROMETRY

Imaging spectrometry is defined as the simultaneous acquisition of images in many narrow, contiguous spectral bands in such a way that a continuous reflectance spectrum can be reconstructed for each picture element (pixel) in the scene. The concept is shown diagrammatically in Figure 1. In the context of the ongoing NASA program at JPL, the spectral region to which this new approach to remote sensing is being applied spans the 0.4 to 2.5 micron ( $\mu\text{m}$ ) region at a typical spectral sampling interval of about 10 nanometers (nm). The goal of imaging spectrometry is to make possible the direct identification of those surface materials which have diagnostic features in their reflectance spectra. This cannot be done with sensors such as the Landsat Multispectral Scanner (MSS) or Thematic Mapper (TM) because of their low spectral resolution.

The physical and chemical characteristics of materials determine their reflectance and emittance spectra. Laboratory absorption and reflectance spectra from the ultraviolet to the far infrared have long been used for analysis and material identification. Although the two Landsat sensors mentioned above provide spectral information in several broad bands, this coarse sampling is insufficient to fully describe the material characteristics that can be determined through laboratory spectroscopy. This is because the spectral reflectance and emittance characteristics for surface materials, which are determined by electronic and vibrational energy states in the materials, are usually too highly structured to be observed at coarse spectral resolution.

EACH PIXEL HAS  
AN ASSOCIATED,  
CONTINUOUS SPECTRUM  
THAT CAN BE USED TO  
IDENTIFY THE SURFACE  
MATERIALS

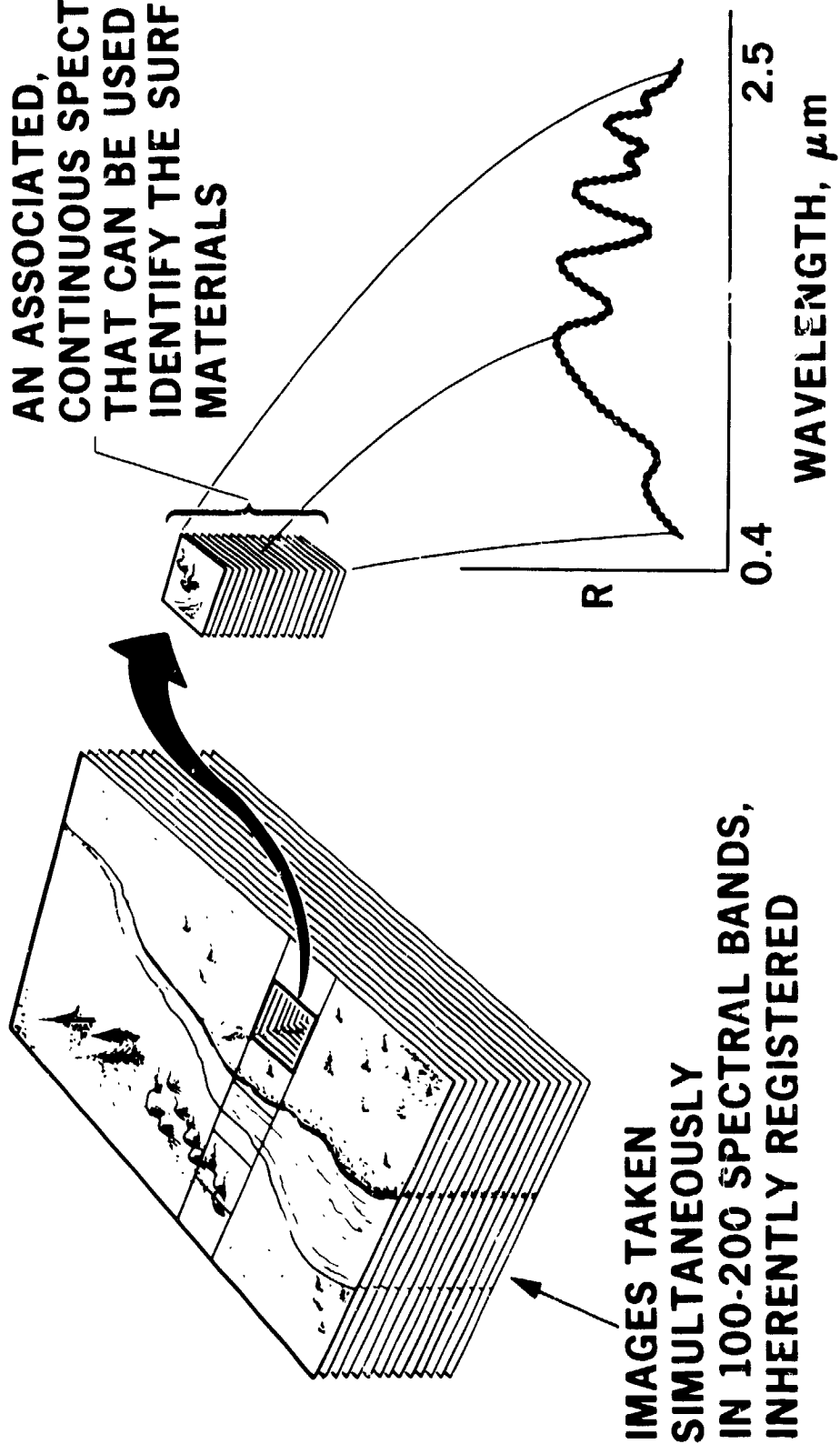


Figure 1. Imaging spectrometer concept showing a series of spectral images obtained simultaneously, allowing a spectrum to be derived for each pixel.

The reflectance characteristics short of 1.0  $\mu\text{m}$  for minerals are influenced by the presence of transition metals. Almost all minerals contain some iron, and that metal dominates the shape of most mineral reflectance curves in this spectral region. Charge transfer bands that are a result of the exchange of electrons between neighboring metal ions create absorptions in the UV region short of 0.4  $\mu\text{m}$ . The wings of these bands extend into the visible portion of the spectrum and are responsible for the general increase in reflectance between 0.4 and 0.8  $\mu\text{m}$ , as shown in Figure 2. Electronic transitions in the transition elements which result from energy level changes in the d-shell electrons within the crystal field of the mineral result in absorption features near 0.9  $\mu\text{m}$ , as seen in spectrums 2 and 3 in Figure 2 between 0.85 and 0.92  $\mu\text{m}$ , and this characteristic, as well as the steep rise in the reflectance curve in the visible region, is used to identify the presence of limonite in Landsat images (Rowan et al., 1974; Rowan et al., 1977).

At wavelengths beyond 1.0  $\mu\text{m}$ , vibrational features associated with bound and unbound water become important in determining the reflectance spectrum of the material. Major absorption features are seen at 1.4 and 1.9  $\mu\text{m}$ , but there are also strong atmospheric water bands at these wavelengths, making this region practically unuseable for remote sensing. Combination bending-stretching overtones of the fundamental OH vibration at 2.74  $\mu\text{m}$  are seen in the region of 2.1 to 2.4  $\mu\text{m}$ . Overtones for  $\text{SO}_4$  and  $\text{CO}_3$  are also found in this region. Minerals such as alunite, pyrophyllite, muscovite, kaolinite, montmorillonite, and calcite have uniquely diagnostic reflectance spectra in this region, as shown in Figure 3.

The use of high spectral-resolution remote sensing for the identification of minerals began in the last few years with the advent of remote-sensing instruments that sample at high spectral resolution. Chiu and Collins (1978) and Collins et al. (1983) have developed an airborne spectroradiometer with which they have demonstrated the ability to directly identify clay minerals through the presence of the overtone bands discussed above. Goetz et al. (1982), using a 10-channel radiometer flown aboard the Space Shuttle Columbia, made the first direct identification of kaolinite and carbonate rocks from orbit.

The spectral reflectance for vegetation in the 0.4 to 2.5  $\mu\text{m}$  region is not as highly structured as that for minerals. A typical reflectance curve for a growing plant is shown in Figure 2. This is a moderate resolution spectrum ( $\lambda/\Delta\lambda = 50$ ) which was acquired in the field (Goetz et al., 1983). The chlorophyll absorption features are centered at 0.48 and 0.68  $\mu\text{m}$ . The absorption at 0.48  $\mu\text{m}$  is the result of electronic transitions in the carotenoid pigments which function as accessory pigments to the chlorophyll pigments in the photosynthetic process. The 0.68  $\mu\text{m}$  absorption is the result of electronic transitions in the chlorophyll molecule, centered around the magnesium component of the photoactive site. The area between the two absorption features falls within the portion of the visible spectrum that results in the green color of plants. The steep rise in reflectance of vegetation beyond 0.8  $\mu\text{m}$  is called the red edge

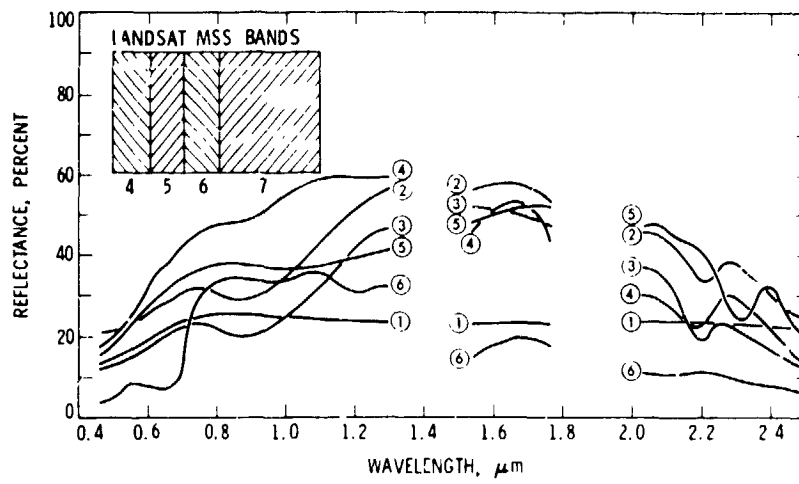


Figure 2. Field spectra of natural surfaces. The gaps correspond to the atmospheric water bands. (Goetz and Rowan, 1981.)

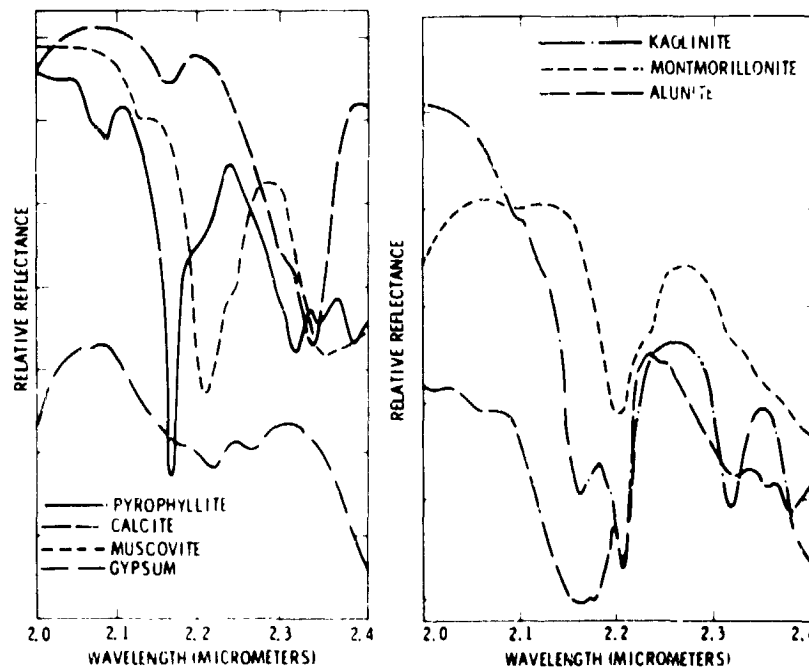


Figure 3. High resolution laboratory spectra for OH, CO<sub>3</sub>, and SO<sub>4</sub> bearing minerals. (Goetz and Rowan, 1981.)

of the chlorophyll band (Horler et al., 1980; Horler et al., 1983) and the slope of the red edge has been related to chlorophyll concentrations in the leaves (Horler et al., 1983).

The shape of the spectral reflectance curve short of 0.8  $\mu\text{m}$  changes significantly during the time the leaf goes from active photosynthesis to total senescence. In actively photosynthesizing plants, the spectral region most affected by geochemical stress lies between 0.55 and 0.75  $\mu\text{m}$ , where the most diagnostic feature is the position and slope of the red edge (Collins et al., 1981; Horler et al., 1983). Collins et al. (1982) and Milton et al. (1983) have recorded shifts in the red edge of the chlorophyll band toward shorter wavelengths on the order of 0.007 to 0.01  $\mu\text{m}$  in magnitude in plants influenced by geochemical stress. An example of this is shown in Figure 4. An airborne, 512-channel spectroradiometer covering the 0.4 to 1.1  $\mu\text{m}$  region (Chang and Collins, 1983) has been used to detect "blue shifts" of the chlorophyll red edge in both coniferous and deciduous tree stands growing in soils containing metal sulfides.

The near-infrared plateau is located between 0.8 and 1.3  $\mu\text{m}$ . The high reflectance in this spectral region is characteristic of the leaf tissue. The infrared plateau is by no means as uniform as its name implies, but contains potentially diagnostic features that may be related to both cellular arrangement within the leaf and to hydration state (Gates, 1970; Gausman et al., 1977; Gausman et al., 1978). The cellular arrangement within the leaf is genetically controlled and can therefore potentially be used for separating or identifying vegetation types (Esau, 1977). Figure 5 shows an example based on field spectra acquired during the fall foliage peak at Lost River, West Virginia (Goetz et al., 1983). The species shown can be separated from one another using the fine structure in the infrared plateau as well as the reflectance in the 1.6 to 2.2  $\mu\text{m}$  region, which is sensitive to leaf water content.

To briefly summarize the preceding discussion, there is considerable information in the 0.4 to 2.5  $\mu\text{m}$  spectral region which can only be acquired using high spectral-resolution sensors. For minerals, the short wavelength infrared from about 2.0 to 2.5  $\mu\text{m}$  is especially rich in narrow absorption features related to vibrational processes, while absorption features due to electronic processes are found throughout the 0.4 to 2.5  $\mu\text{m}$  region. Vegetation spectra do not differ as dramatically from one to another as mineral spectra, but they do exhibit spectral features associated with geochemical stress and leaf cellular structure that require high spectral-resolution measurements for detection, and work presented in these Proceedings indicates still other potentially very useful applications of high spectral-resolution remote sensing to studies of vegetation.

#### HOW IMAGING SPECTROMETRY IS ACCOMPLISHED

Simultaneous imaging in many contiguous spectral bands requires a new approach to sensor design. Sensors such as the Landsat MSS or TM are optomechanical systems in which discrete detector elements are scanned across the surface of the earth perpendicular to the flight path, the detectors converting the reflected solar photons from each pixel in the scene into a sensible electronic signal, as shown in

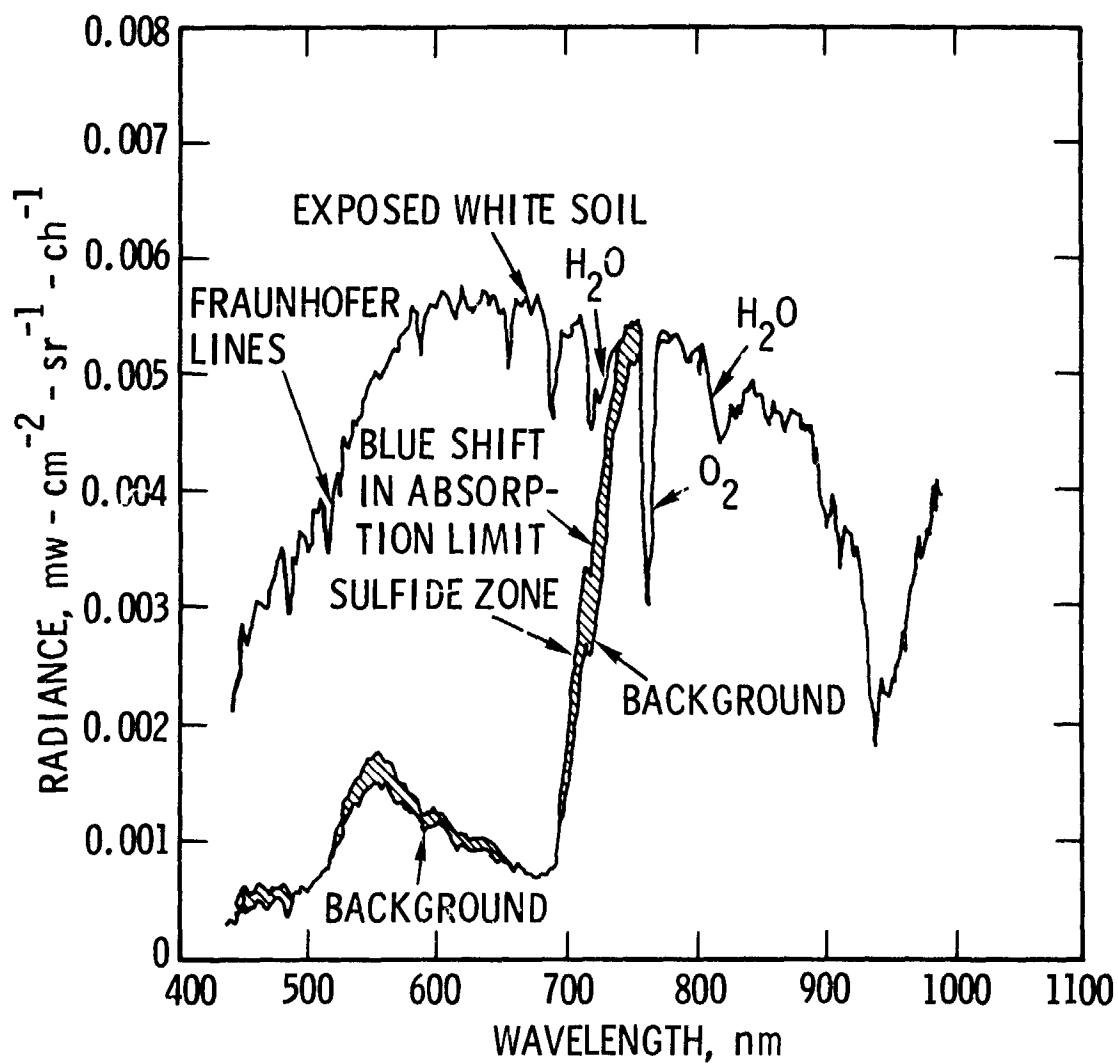


Figure 4. Blue shift in the chlorophyll red edge of conifers growing in a sulfide zone. (Collins, et al., 1983.)

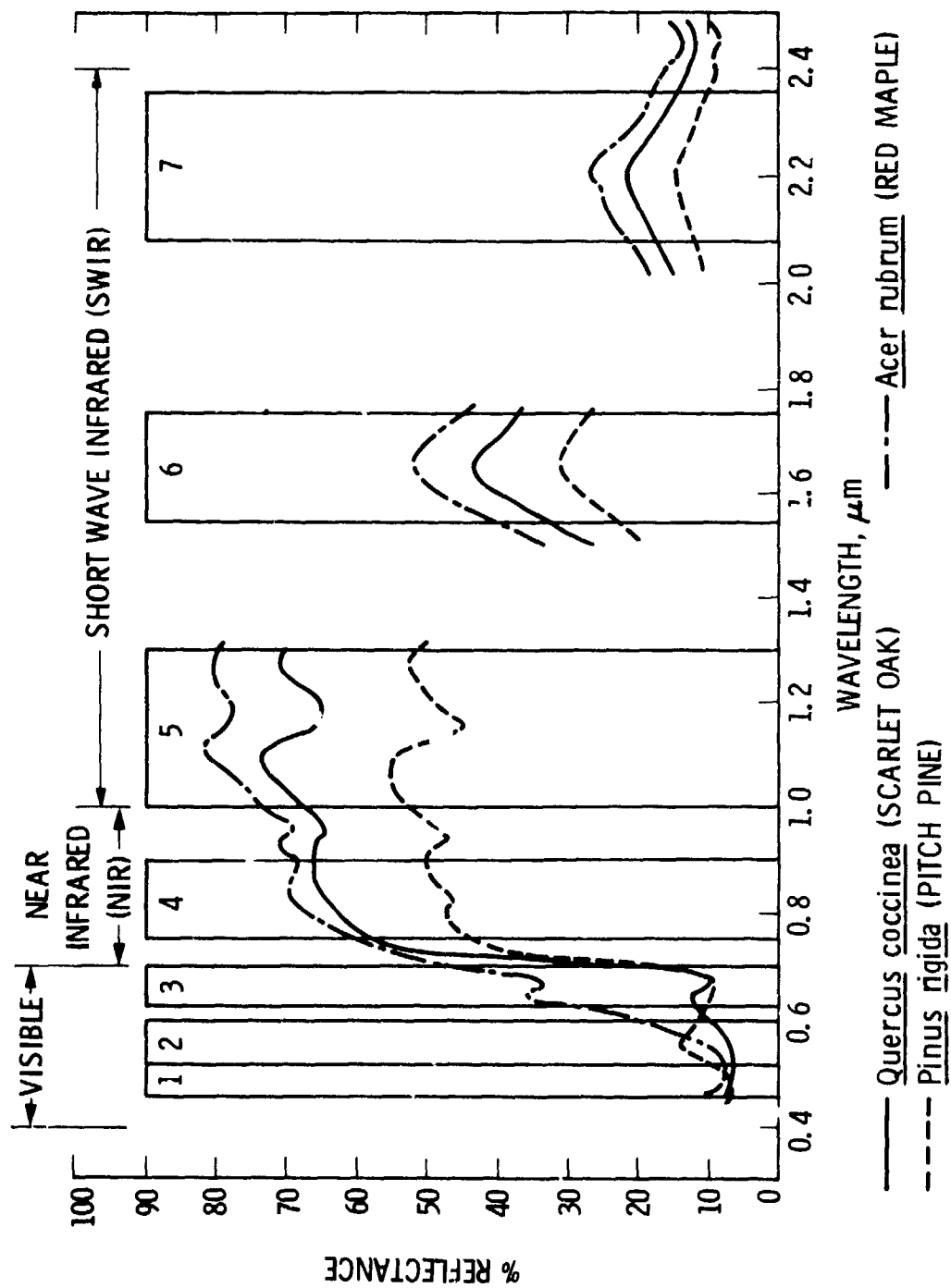


Figure 5. Reflectance spectra of three tree species in Lost River, West Virginia during the peak fall foliage display. (Goetz, et al., 1983.)

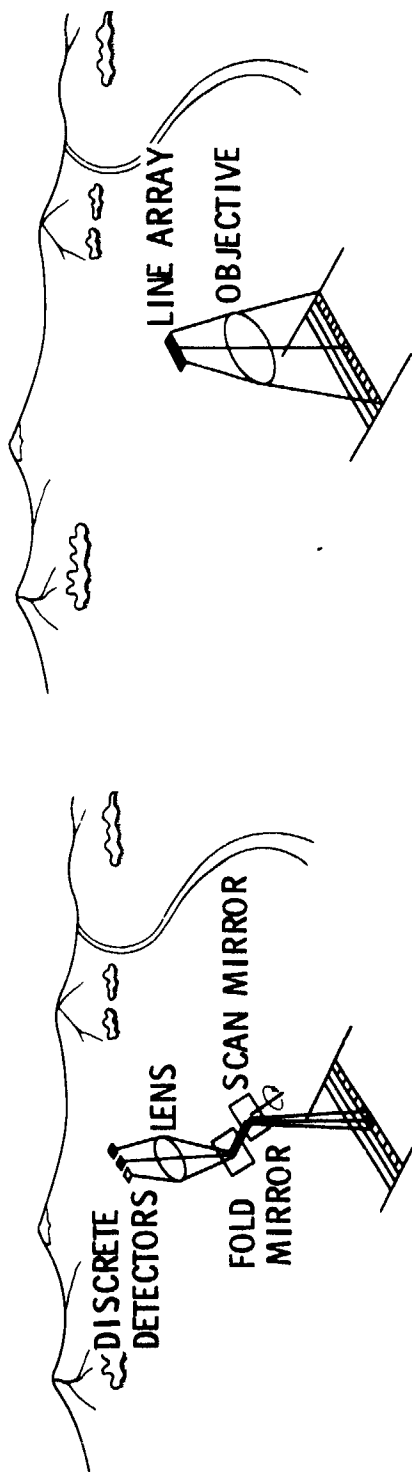
Figure 6(a). The detector elements are placed behind filters that pass broad portions of the spectrum. The MSS has four such sets of filters and detectors, while the TM has seven. The primary limitation of this approach is the short residence time of the detector in each instantaneous field of view (IFOV). In order to achieve an adequate signal-to-noise ratio without sacrificing spatial resolution, such a sensor must be operated in broad spectral bands of 100 nm or greater or must use optics with unrealistically small ratios of focal length to aperture (f number).

One approach to increasing the residence time of a detector in each IFOV is to use line arrays of detector elements as in Figure 6(b). In this configuration there is a dedicated detector element for each cross-track pixel, which increases the residence or integration time to the interval required to move one IFOV along track. Such an experimental two-spectral band instrument, called the modular optoelectronic multispectral scanner (MOMS), has been flown aboard the Space Shuttle (Meissner et al., 1983). The French satellite SPOT (Système Probatoire d'Observation de la Terre), which will use line array detectors, will be launched in 1985 (Brachet, 1981).

There are limitations associated with the use of multiple line arrays when each line array has its own spectral band-pass filter. If all the arrays are placed in the focal plane of the telescope, then the same ground locations are not imaged simultaneously in each spectral band. If beam-splitters are used to facilitate simultaneous data acquisition, the signal is reduced by 50 percent or more for each additional spectral band acquired in a given spectral region. Furthermore, instrument complexity increases substantially if more than six to ten spectral bands are desired.

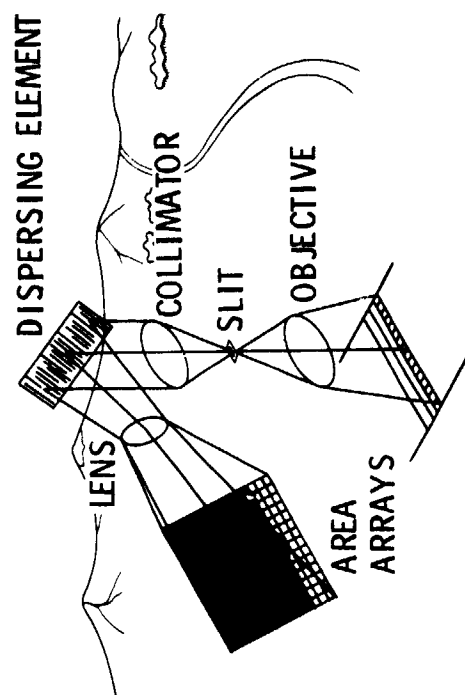
Two approaches to imaging spectrometry are shown in Figures 6(c) and (d). The line array approach is analogous to the scanner approach used for the MSS and TM, except that light from a pixel is passed into a spectrometer where it is dispersed and focused onto a line array. Thus, each pixel is simultaneously sensed in as many spectral bands as detector elements in the line array. For high spatial resolution imaging (ground IFOV's of 10 to 30 m), this approach is suited only to an airborne sensor which flies slowly enough that the readout time of the detector array is a small fraction of the integration time. Because of high spacecraft velocities, imaging spectrometers designed for earth orbit require the use of two-dimensional area arrays of detectors at the focal plane of the spectrometer [Figure 6(d)], obviating the need for the optical scanning mechanism. In this arrangement there exists a dedicated column of spectral detector elements for each cross-track pixel in the scene.

The first spaceborne imaging spectrometry of the earth will be done with the Shuttle Imaging Spectrometer Experiment (SISEX) which is now underway at JPL (Wellman et al., 1983). The first launch of SISEX is planned for 1990. Also in the design phase is a High Resolution Imaging Spectrometer (HIRIS) which has been identified by NASA as one of the three prime sensors to be placed into polar orbit in about 1994 on the Space Station Earth Observing System (EOS). Both SISEX and HIRIS are based on the area detector array approach described above. While area detector arrays made of silicon are now available for imaging spectrometry in the visible portion of the

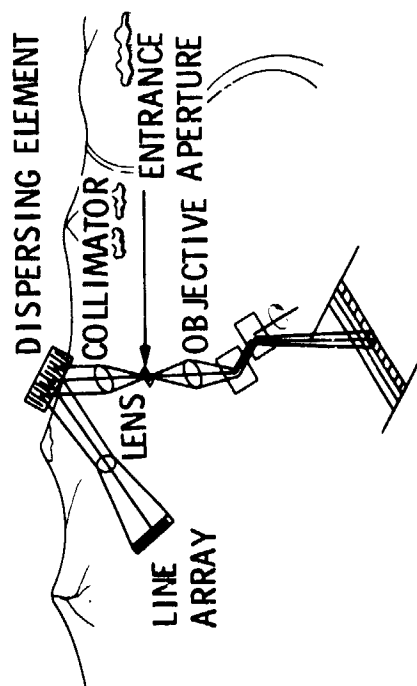


a. MULTISPECTRAL IMAGING WITH DISCRETE DETECTORS

b. MULTISPECTRAL IMAGING WITH LINE ARRAYS



d. IMAGING SPECTROMETRY WITH AREA ARRAYS



c. IMAGING SPECTROMETRY WITH LINE ARRAYS

Figure 6. Four methods of obtaining multispectral images.

spectrum, infrared area arrays of suitable dimensions for SISEX and HIRIS are still under development. AIS was designed as an engineering test bed for the prototype detector arrays that will lead to those to be used in space. To bridge the time between now and the flight of SISEX, another airborne instrument is under construction at JPL to provide complete coverage of the visible, near infrared and short-wavelength infrared, to provide the necessary data base for developing efficient algorithms for analyzing SISEX and HIRIS data. That instrument is the Airborne Visible/Infrared Imaging Spectrometer (AVIRIS) (Vane et al., 1984) and will become operational in 1987 as a NASA facility instrument. Its design is based on the approach illustrated in Figure 6(c) in order to achieve a large swath width on the ground using currently available detector technology. The characteristics of these four instruments are summarized in Figure 7; AIS will be discussed further shortly.

#### ANALYSIS OF IMAGING SPECTROMETRY DATA

Just as imaging spectrometry requires new technology for instruments and detectors, effective utilization of the data requires development of new analytic approaches and techniques. The dimensionality of imaging spectrometer data makes it necessary to seek new analytical methods if dependence on the raw computational power of supercomputers is to be avoided. The experience with AIS tends to confirm that the nature of imaging spectrometer data leads naturally to a more deterministic approach to scene analysis. The most compelling reason for turning to deterministic, as opposed to statistical, methods of analysis is the fact that imaging spectrometry provides spectral sampling sufficient to define unique spectral signatures.

The first problem to be addressed in the analysis of these data is visual interaction with hyperspectral images and their statistical properties. Current graphics and image display technology allow implementation of a variety of visual exploratory analysis tools. Among these are the ability to display a time-sequenced projection of the images in the spectral direction, the ability to have cursor-designated spectral plots of single pixels or averages over a spatial window, and the ability to rapidly locate pixels having similar spectral signatures. In addition, interactively locating and displaying spectra from a spectral library for visual comparison and interactively creating spectral data sets from specified regions in the scene are now possible. Another useful visual enhancement of the data is the application of an equal energy spectral normalization, which allows direct comparison of the shapes of spectral curves.

Manual examination of the spectral content of the images by cursor-designated plotting is a very useful tool. However, it becomes rather laborious when one is trying to locate spectrally similar units throughout an entire scene. To overcome this problem, a fast spectral-signature matching algorithm has been devised at JPL that can be used to find all the pixels in a scene having a spectral signature similar to a specified prototype spectrum. The prototype can be specified from the image data itself or from a spectral reference library. The technique relies on binary encoding of the

1983 AIS		1987 AVIRIS		1990 SISEX		1994 HIRIS	
	SPECTRAL REGION, $\mu\text{m}$	No. BANDS	WIDTH nm	SWATH	IFOV		
AIS	1.2 - 2.4	128	9.6	320 m	10 m		
AVIRIS	0.4 - 2.4	224	9.6	11 km	20 m		
SISEX	0.4 - 2.5	196	11	12 km	30 m		
HIRIS	0.4 - 2.5	196	11	50 km	30 m		

Figure 7. Characteristics of the four sensors in the JPL Imaging Spectrometer Program.

spectral data in order to achieve fast cross-correlation for signature matching. Details can be found in Goetz et al. (1985). The algorithm used provides a very fast means of searching a scene for the location of specific spectral classes and has been used with success on AIS data (Solomon and Lee, 1985, private communication).

Multispectral scene classification is especially affected by the dimensionality of the data. The general multispectral classification problem is illustrated in Figure 8. The key element in this problem is finding a feature extraction operator with efficient information-compression properties. The transformation operator can be linear or nonlinear but should reduce dimensionality and at the same time preserve the information necessary for identification of the spectral signature. One of the traditional transformations used is the Karhunen-Loeve or principal components transformation. However, construction of this transformation requires estimation of the covariance matrix, and this process would take on the order of  $10^{13}$  arithmetic operations for a typical 11-km-square scene such as will be acquired by AVIRIS. Clearly, more computationally efficient transformations are needed for the analysis of imaging spectrometer data.

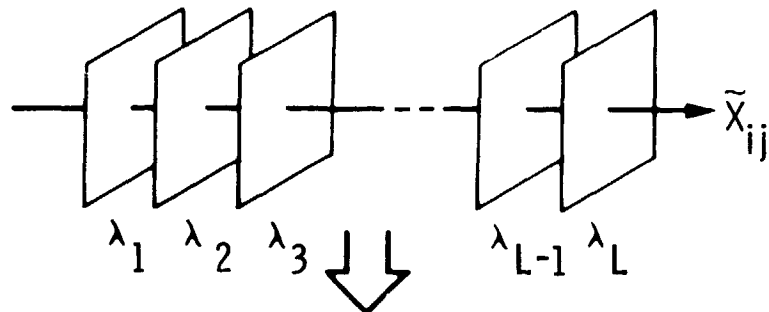
The nonlinear binary encoding and cross-correlation techniques discussed above are useful in this context. However, there is a large class of linear deterministic transformations having fast numerical implementations that are obvious candidates as feature extraction operators. Examples include Fourier, Walsh-Hadamard, and Haar (Gonzales and Wintz, 1979). All linear transforms provide dimensionality reduction. However, there remains the question of clustering properties and similarity measures in the reduced dimension pattern space. The Walsh-Hadamard transform is particularly attractive from the standpoint of computational speed, since it is even faster than the fast Fourier transform. Furthermore, early analytic results indicate that dimensionality reduction of eight-to-one can be achieved while maintaining good classification accuracy. This and other transforms are under study at JPL and elsewhere.

#### AIS DESCRIPTION AND OPERATIONS

As noted earlier, AIS was designed as an engineering test bed for use with prototype, infrared area-detector arrays of the type which will be flown in space on SISEX and HIRIS. At the time the instrument was proposed, it was intended to be flown only a few times, mostly over geological targets in California and the southwestern U.S. The desire to make AIS data as widely available as possible had led to a much more intensive operation of the instrument. AIS remains an engineering test bed, however, and data users ought to be aware of the implications of this. The following summary is an overview of the instrument and the changes it has undergone during the past two years.

The observational characteristics of AIS are summarized in Table 1. A complete description of the instrument can be found in Vane et al. (1983). AIS operates in the pushbroom imaging mode described earlier and illustrated in Figure 6(d). The foreoptics of the instrument consist of a concentric Schwartzchild telescope with a 24-mm-diameter collecting aperture. Light passes from the foreoptics

L-DIMENSIONAL PATTERN SPACE



L-DIMENSIONAL PATTERN VECTOR

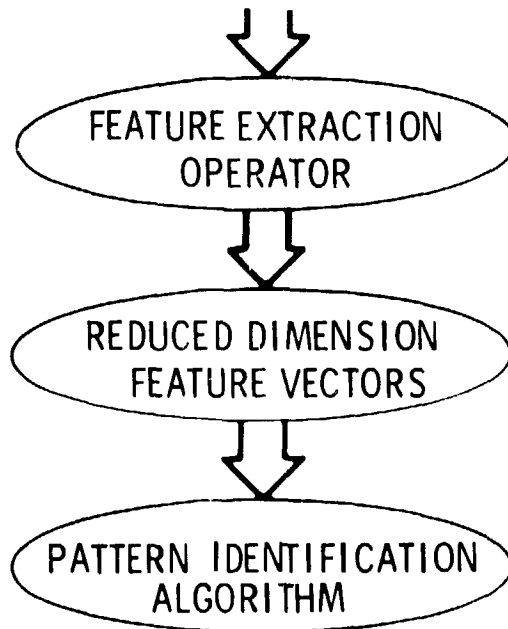
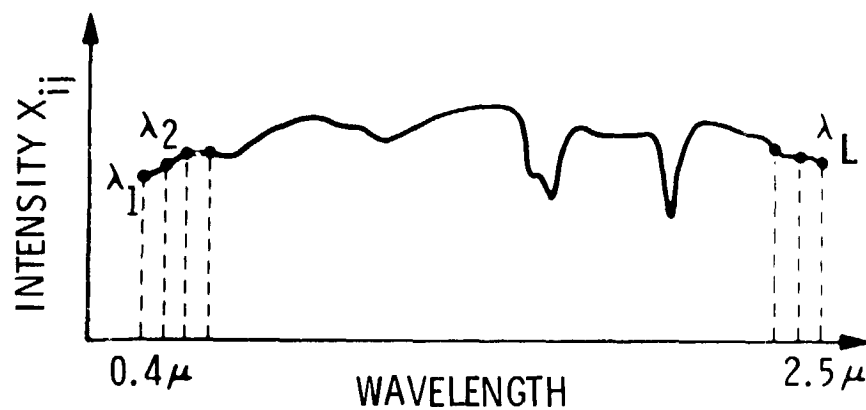


Figure 8. Generalized approach to the multispectral classification problem.

Table 1. AIS Performance Characteristics

IFOV	1.9 mrad
FOV	3.7 degrees
GIFOV at 6-km Altitude	~12 meters
Swath Width at 6-km Altitude	~400 meters
Spectral Coverage	9.3 nm
Spectral Sampling Interval	128
Data Rate	394 kbps
Grating Positions	
GPOS 0	~0.9 to 1.2 $\mu\text{m}$
GPOS 1	1.2 to 1.5 $\mu\text{m}$
GPOS 2	1.5 to 1.8 $\mu\text{m}$
GPOS 3	1.8 to 2.1 $\mu\text{m}$
GPOS 4	2.1 to 2.4 $\mu\text{m}$

through a slit which defines the cross-track footprint on the ground. In the spectrometer the light is dispersed with a diffraction grating and focused on a 32-by-32-element mercury cadmium telluride (HgCdTe) detector array located inside a dewar containing liquid nitrogen for detector cooling. The detector array consists of the HgCdTe chip mated via indium bumps to a silicon charge-coupled device (CCD) which serves as the multiplexer for reading the signal from the HgCdTe detector. It is therefore a hybrid detector array. To acquire 128 spectral images with a 32-by-32-element detector array, the grating is tilted through four positions during the time the aircraft flies forward one ground IFOV. A sketch and a photograph of the instrument are shown in Figure 9.

The first test flight of AIS was done in November 1982 aboard the NASA/Dryden C-47 aircraft. A detector array with a 4.7- $\mu$ m-long wavelength cutoff was used to successfully acquire images in one grating position or 32 spectral bands at a time. The original design for the grating drive was inadequate for moving the grating through the four required positions within the small stepping time allowed. In December 1982, AIS was installed on the NASA/Ames C-130, on which it has been flown ever since.

Data were acquired with the original 4.7- $\mu$ m cutoff detector over several test sites in the southwest U.S. and West Virginia in late 1982 and early 1983. In June 1983, a second-generation 32-by-32-element detector was installed that had a 2.5- $\mu$ m-long wavelength cutoff. Data collection continued with the improved detector, and a total of eleven investigators received data sets from the first season of operation. During the following winter, from November 1983 to April 1984, a new grating drive was designed and installed in AIS. Improvements were also made in instrument calibration with the acquisition of new laboratory equipment for that purpose. During the 1984 field season from April to October, data were acquired for an additional 19 investigators in spite of occasional instrument and C-130 failures and poor weather throughout the U.S. that year. This past winter, from November 1984 through April 1985, several additional improvements were made to the instrument including the removal of systematic noise in the instrument electronics, and the addition of a new boresited Nikon camera with automatic exposure. The instrument will be flown in this configuration during the 1985 field season until the next-generation detector is ready. Work is already under way to convert AIS to a HgCdTe area array which is 64-by-64 elements in size. The upgraded instrument should be ready by the end of this season. Further details of the AIS history can be found in the Airborne Imaging Spectrometer Science Investigator's Guide; this brief summary serves to make the point that although AIS is being used in an almost operational mode, it is still an engineering test bed and changes in the instrument will continue to be made as technology evolution permits.

By the end of the past season, some 30 investigators or groups of investigators had at least one AIS data set. There have been three approaches to obtaining AIS data. The first of these is through NASA-approved RTOP's of proposals which are submitted with a formal flight request for AIS data. The submission of a flight request with the proposal is essential for obtaining the necessary flight hour alloca-

ORIGINAL PAGE IS  
OF POOR QUALITY

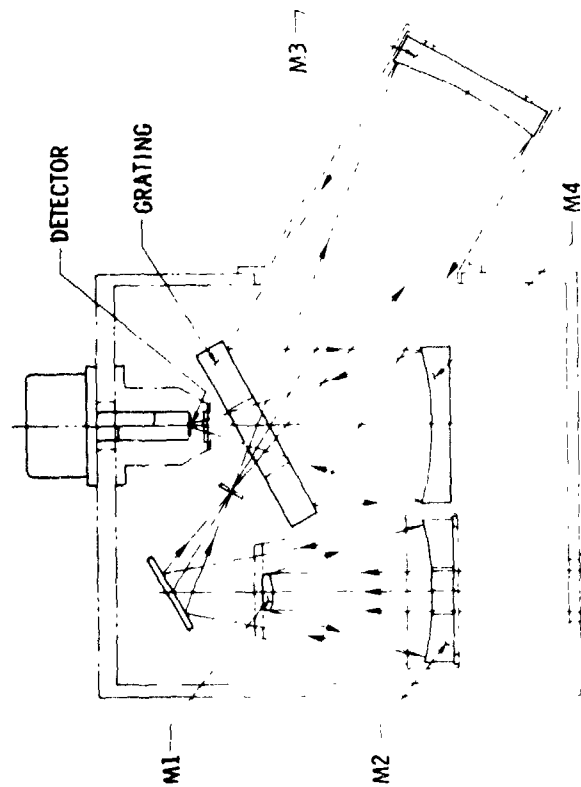
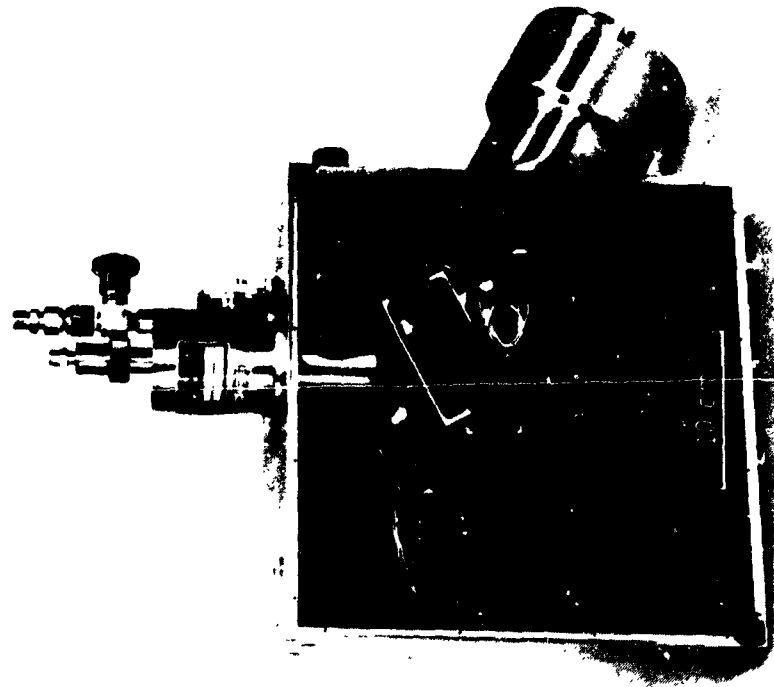


Figure 9. Instrument layout (left) and photograph (right) of the Airborne Imaging Spectrometer.

(4)

tion on the C-130 for data acquisition. Secondly, several investigators received data during the 1984 season, or have been approved for data acquisition in the 1985 season, through the "guest investigator" process in which a limited number of C-130 flight hours have been given to JPL by NASA for investigators who have not been formally funded by NASA for data acquisition. The purpose of the "guest investigator" process has been to bring new people into the imaging spectrometer program. By the end of this season about 20 experimenters will have benefitted. The final approach to obtaining AIS data is to acquire a copy of an existing data set. JPL will send a copy of a standard 128-spectral-band data set from Cuprite, Nevada, to anyone who requests it. Also, with the approval of the principal investigator concerned, a copy of any other data set that has been acquired can be provided.

AIS will continue in operation until AVIRIS becomes operational in 1987. NASA does not intend to continue the "guest investigator" process described above for acquiring AIS data, but formal proposals for data acquisition and analysis are being accepted for the 1986 season through the standard process. Contact Dr. Robert E. Murphy, Code EE, NASA Headquarters, Washington, D.C. 20546, (202) 453-1720, for details. Results from the 1985 season, as well as results from the continuing work described in these Proceedings, will be presented at JPL next spring (1986) in the next AIS Data Analysis Workshop. Also, a "dear colleague letter" soliciting proposals for AVIRIS data acquisition and analysis will be issued in late 1985 to select those investigators who will begin working with the first AVIRIS data in 1987.

#### REFERENCES

- Brachet, G., 1981, Spot Satellite Program. Proc. 1981 Int'l Geoscience and Remote Sensing Symp., IEEE Cat. No. 81CH8656-8.
- Chang, S. H., and Collins, W., 1983, Confirmation of the airborne biogeophysical mineral exploration technique using laboratory methods: Econ. Geol., Vol. 78, p. 723-736.
- Chiu, H. Y., and Collins, W., 1978, A spectroradiometer for airborne remote sensing: Photogramm. Eng. Remote Sensing, Vol. 44, p. 507-517.
- Collins, W., Chang, S. H., and Kuo, J. T., 1981, Detection of hidden mineral deposits by airborne spectral analysis of forest canopies: Final Rpt. NASA Contract NSG-5222, 61 p.
- Collins, W., Chang, S. H., Raines, G., Canney, F., and Ashley, R., 1983, Airborne biogeochemical mapping of hidden mineral deposits: Econ. Geol., Vol. 78, p. 737-749.
- Esau, K., 1977, Anatomy of seed plants: 2nd ed.. Wiley and Sons, New York, 550 p.
- Gates, D. M., 1970, Physical and physiological properties of plants in Remote Sensing With Special Reference to Agriculture and Forestry: Nat. Acad. Sci., Washington, D.C., p. 224-252.

- Gausman, H. W., Escobar, D. E., and Knipling, E. B., 1977, Relation of Peperomia obtusifolias anomalous leaf reflectance to its leaf anatomy: Photogramm. Eng. Remote Sensing, Vol. 43, p. 1183-1185.
- Gausman, H. W., Escobar, D. E., Everitt, J. H., Richardson, A. J., and Rodriguez, R. R., 1978, Distinguishing succulent plants from crop and woody plants: Photogramm. Eng. Remote Sensing, Vol. 44, p. 487-491.
- Goetz, A. F. H., and Rowan, L. C., 1981, Geologic remote sensing: Science, Vol. 211, p. 781-791.
- Goetz, A. F. H., Rowan, L. C., and Kingston, M. J., 1982, Mineral identification from orbit: initial results from the shuttle multispectral infrared radiometer: Science, Vol. 218, p. 1020-1024.
- Goetz, A. F. H., Rock, B. N., and Rowan, L. C., 1983, Remote sensing for exploration: an overview: Econ. Geol., Vol. 78, p. 573-590.
- Goetz, A. F. H., Vane, G., Solomon, J. E., and Rock, B. N., 1985, Imaging Spectrometry for Earth Remote Sensing: Science, in press.
- Gonzales, R. C. and Wintz, P., 1979, Digital Image Processing, Addison-Wesley, Reading, MA.
- Horler, D. N. H., Barber, J., and Barringer, A. R., 1980, Effects of heavy metals on the absorbance and reflectance spectra of plants: Int. J. Remote Sensing, Vol. 1, p. 121-136.
- Horler, D. N. H., Dockray, M., Barber, J., and Barringer, A. R., 1983, Red edge measurements for remote sensing plant chlorophyll content: Proc. Comm. on Space Research Symp. on Remote Sensing and Mineral Exploration, Ottawa.
- Meissner, D., Laucht, H., Bodechtel, J., and Haydn, R., 1983, Modular optoelectronic multispectral scanner (MOMS) for earth observations: First results of STS-7 mission, Proc. 1983 Int'l Geoscience and Remote Sensing Symp, IEEE Cat. No. 83CH1837-4.
- Milton, N. M., Collins, W., Chang, S. H., and Schmidt, R. G., 1983, Remote detection of metal anomalies on Pilot Mountain, Randolph County, North Carolina: Econ. Geol., Vol. 78, p. 605-617.
- Rowan, L. C., Wellaufer, P. H., Goetz, A. F. H., Billingsley, F. C., and Stewart, J. H., 1974, Discrimination of rock types and detection of hydrothermally altered areas in south-central Nevada by use of computer-enhanced ERTS images: U. S. Geol. Survey. Prof. Paper 883, 355 p.
- Rowan, L. C., Goetz, A. F. H., and Ashley, R. P., 1977, Discrimination of hydrothermally altered and unaltered rocks in visible and near-infrared multispectral images: Geophysics, Vol. 42, p. 522-535.

Vane, G., Goetz, A. F. H., and Wellman, J. B., 1983, Airborne imaging spectrometer: a new tool for remote sensing: Proc. 1983 Int'l. Geoscience and Remote Sensing Symp., IEEE Cat No. 83CH1837-4.

Vane, G., Chrisp, M., Enmark, H., Macenka, S., and Solomon, J., 1984, The Airborne Visible/Infrared Imaging Spectrometer (AVIRIS): An advanced tool for Earth Remote Sensing: Proc. 1984 Int'l. Geoscience and Remote Sensing Symposium.

Wellman, J. B., Goetz, A. F. H., Herring, M., and Vane, G., 1983, An imaging spectrometer experiment for the shuttle: Proc. 1983 Int'l. Geoscience and Remote Sensing Symp., IEEE Cat. No. 83CH1837-4.

N86-11619

## MINERALOGICAL MAPPING IN THE CUPRITE MINING DISTRICT, NEVADA

ALEXANDER F. H. GOETZ and VINAY SRIVASTAVA, Jet Propulsion  
Laboratory/California Institute of Technology, Pasadena, California  
91109, U.S.A.

### INTRODUCTION

The Airborne Imaging Spectrometer (AIS) has provided for the first time, the possibility to map mineralogical constituents in the earth's surface and thus has enormously increased the value of remote-sensing data as a tool in the solution of geologic problems.

The question addressed with AIS at Cuprite was how well could the mineral components at the surface of a hydrothermal alteration zone be detected, identified and mapped? The question has been answered positively as discussed below, and perhaps more importantly a relatively rare mineral, buddingtonite, that could not have been detected by conventional means, was discovered and mapped by the use of AIS.

### SETTING

The Cuprite mining district straddles U.S. Hwy. 95 approximately 17 km south of Goldfield in southwestern Nevada. The eastern half of the district studied with AIS is an area of extensive hydrothermal alteration within a sequence of rhyolitic welded ash flow and air fall tuffs. The major unit is the 7 my-old Thirsty Canyon Tuff whose source is the Black Mountain Caldera, 50 km to the southwest (Ashley and Silbermann, 1976). The altered units consist of a central core of almost pure silica, a ring of opalized rocks containing alunite and kaolinite, and an outer argillized zone containing mainly kaolinite and montmorillonite as well as opal and some limonite (Abrams, et al., 1977).

### PREVIOUS STUDIES

The Cuprite area has been the focus of remote-sensing studies for the last decade. Because of its varied mineralogy and relatively sparse vegetation cover, a number of spectral remote-sensing studies have been carried out there (Abrams, et al., 1977; Kahle and Goetz, 1983; Goetz, et al., 1985). Abrams, et al. (1977) showed that broad-band multispectral imaging, including bands centered at 1.6 and 2.2 $\mu$ m, was far superior in mapping hydroxyl-bearing minerals than those restricted to the region short of 1.0 $\mu$ m, and provided the conclusive evidence that aided in the decision to include the seventh band (2.08-2.36 $\mu$ m) on the Landsat Thematic Mapper.

Abrams, et al. (1977) found that color ratio composites utilizing the 1.6 and 2.2 $\mu$ m bands, in combination with bands at shorter wavelengths, could be used to delineate the major boundaries in surface mineralogy very accurately. The mapping was verified by laboratory analysis of field samples. Although boundaries between units could be mapped accurately, it was not possible to identify the surface mineralogy without resort to in-situ measurements. Laboratory-like spectral reflectance measurements are required to identify mineral constituents in the surface directly. The AIS provides image data at 9.3-nm intervals throughout the

1.2-2.4 $\mu$ m spectral region and has sufficient spectral resolution to make direct mineral identification possible.

#### AIS DATA ACQUISITION

AIS data over Cuprite, Nevada were first acquired in August 1983. Two subsequent flights in 1984 covered the areas shown in Fig. 1. The 1983 flight covered a small area extending from south to north across the southern boundary of the alteration zone. Prominent features are a bright hill in the center of the coverage shown in Fig. 2a and a bulldozed area which shows up very brightly in the northern end of the coverage. During 1984 the area was reflighted, but in order to cover the same area exactly it was necessary to roll the aircraft approximately 5°. After overflying the bulldozed area, the horizontal attitude was resumed causing the dogleg seen in Fig. 1.

#### DATA REDUCTION

On-board data reduction consists of an automatic dark current subtraction before the data were recorded. On the ground the light transfer curve derived from laboratory calibration for each of the 1024 detector elements is applied to produce the so-called "raw" data. The resulting spectrum for each pixel has the general shape seen in Fig. 2b. The major features are a fall-off in signal toward longer wavelengths, a function of irradiance, and the two major atmospheric water absorption features centered at 1.4 and 1.9 $\mu$ m. The reduced curve shown in Fig. 2 was obtained by removing the solar spectrum and normalizing the data to an area overflown outside the Cuprite region, but during the same pass. The area was assumed to be spatially uniform and spectrally flat, or at least smoothly varying. All the data in one pass are normalized to this region. The normalization is important to remove residual stripping in the images caused by minor inaccuracies in the laboratory calibration data.

The resulting reduced curve is shown in Fig. 2b. The regions within the atmospheric water bands are very noisy because of the lack of energy reaching the surface at these wavelengths. Mineral spectral features can be seen beyond 2.0 $\mu$ m.

#### RESULTS

The results of the 1983 overflight can be seen in Fig. 2c and Fig. 3. Figure 2c shows images in 32 contiguous channels from 2.03-2.32 $\mu$ m to which an equal area normalization has been applied (Goetz, et al., 1985). The result is an enhancement of spectral differences and suppression of brightness differences associated with topography.

Figure 3 shows the result of extraction of spectra from individual 3-by-3 pixel areas. The bright hill exhibits an absorption doublet at 2.17 and 2.20 $\mu$ m that is diagnostic of the clay kaolinite while the bulldozed area exhibits a single, broad absorption minimum at 2.16 $\mu$ m, diagnostic of alunite. Laboratory spectra for samples collected in these areas are shown as dashed lines.

A ground traverse was carried out to identify the exact boundary of opalized and secondary quartz zones. Figure 1 shows the location of the traverse while Fig. 4 shows laboratory spectra of individual samples

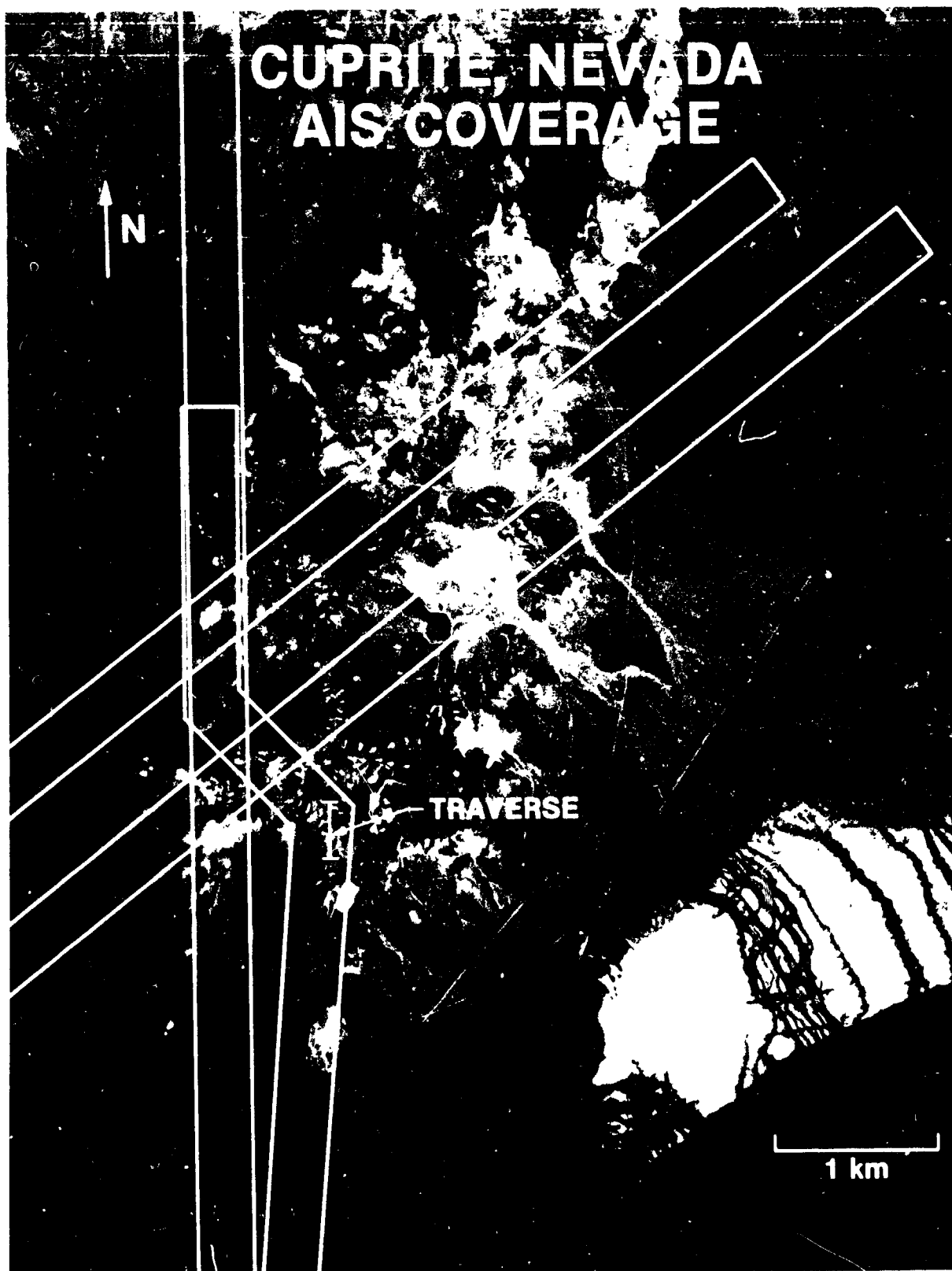


Figure 1. Airphoto of the Cuprite mining district showing the approximate AIS ground coverage.

ORIGINAL PAGE IS  
OF POOR QUALITY

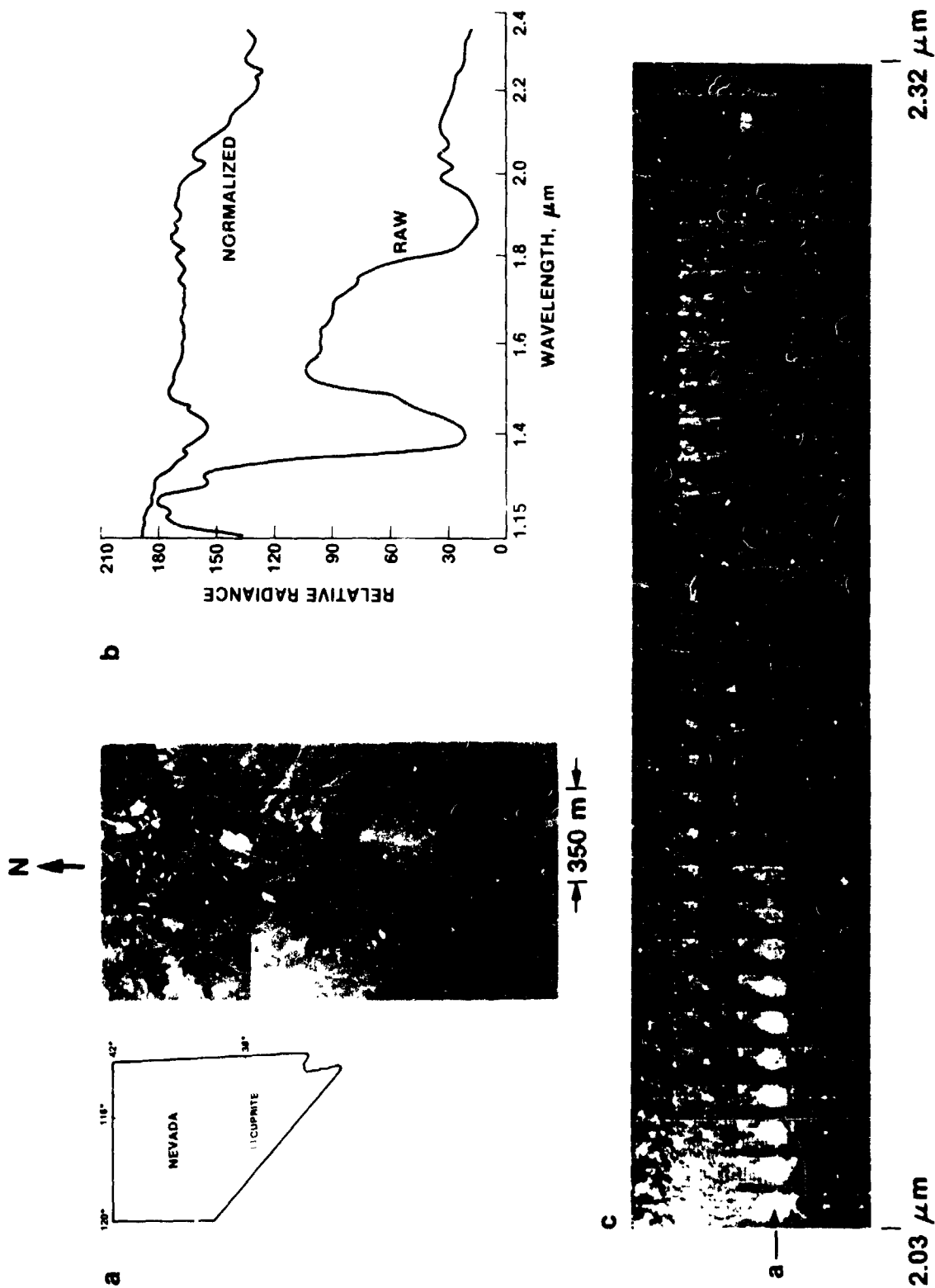


Figure 2. (a) Segment of an AIS ground track covering the southern portion of the Cuprite district. (b) Raw and normalized spectrum from a 3-by-3 pixel area. (c) Thirty-two AIS images covering the wavelength range 2.03-2.32  $\mu\text{m}$  normalized by the equal energy technique so that each pixel spectrum contains the same area under the curve.

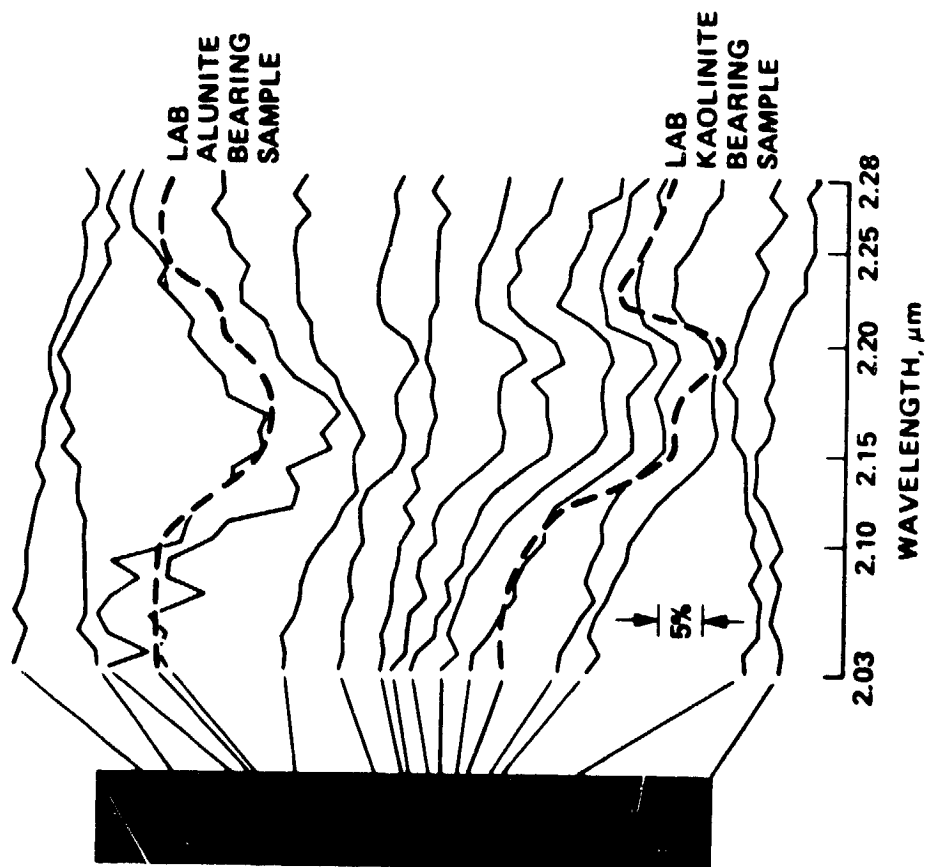


Figure 3 An AIS image at 2.03  $\mu\text{m}$  of the same area as shown in Figure 2(a). Shown here are 3-by-3 pixel spectra taken from the image and in two areas laboratory spectra from samples collected from the locations indicated. The laboratory spectra required 10 minutes to acquire, the AIS spectra 10 ms.

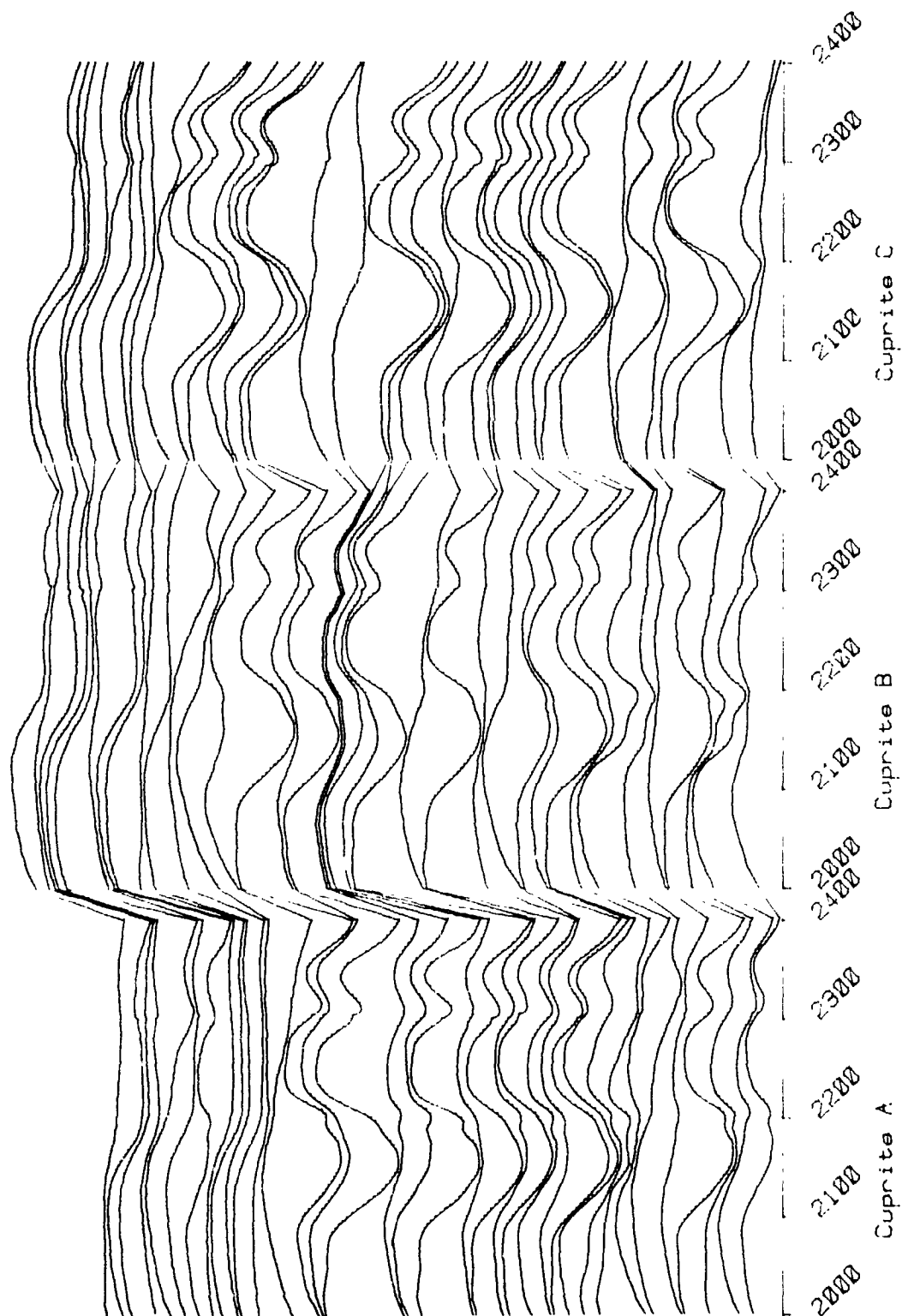


Figure 4. Laboratory spectra from 36 samples taken at 10 m intervals in each of three traverses spaced 10 m apart at the location shown in Fig. 1. The predominant mineral is alunite with absorption at 2.16 and 2.32  $\mu\text{m}$ . At the top of the traverse the flat curves indicate almost pure secondary quartz.

collected at 10-m intervals along the traverse. The traverses A, B and C were spaced 10 m apart in an east-west direction. The dominant features are the 2.16 and 2.32 $\mu$ m absorption features of alunite. Several samples contain kaolinite and a mixture of the two minerals is also seen. The secondary quartz spectra seen at the top of Fig. 4 are almost featureless as expected for quartz. However, a 2.25 $\mu$ m feature is seen and can be attributed to an Si-OH overtone (Podwysocki, personal communication). The boundaries seen in the traverse spectra are also identified in the AIS images.

The results of the July 1984 flight are seen in Fig. 5. The SPAM program (AIS User's Guide, 1985) was used to map mineral constituents that are plotted in red. In each case the upper spectrum is taken from the image and the lower is a laboratory spectrum of a sample collected in the mapped area.

The mineral buddingtonite, an ammonium feldspar, although not at first identified, was detected through a 2.12 $\mu$ m absorption feature in the image spectra and subsequently sampled in the field in the area shown in red. The field sampling was blind because buddingtonite is not identifiable in the field, and at the time the cause of the 2.12 $\mu$ m absorption feature was not known. The identification of the mineral was made by L. Rowan (personal communication) after samples were collected. Cuprite is now the fifth known location of buddingtonite in hydrothermal areas (D. Krohn, personal communication).

The AIS is the first modern, albeit modest, imaging spectrometer to be flown over earthly targets. As the results in Cuprite have shown, direct identification of surface mineralogy, and mapping thereof, is feasible. Proper calibration and normalization of the data are required to detect diagnostic absorption features and facilitate mineralogical mapping.

#### ACKNOWLEDGMENTS

This work was carried out at the Jet Propulsion Laboratory, California Institute of Technology, under a contract with the National Aeronautics and Space Administration.

#### REFERENCES

- Abrams, M. J., Ashley, R. P., Rowan, L. C., Goetz, A. F. H. and Kahle, A. B. 1977. Mapping of hydrothermal alteration in the Cuprite mining district, Nevada, using aircraft scanner imagery for the 0.46-2.35 $\mu$ m spectral region. Geology. vol. 5. pp. 713-718.
- AIS User's Guide - 1985, Jet Propulsion Laboratory, California Institute of Technology, Pasadena, California 91109.
- Ashley, R. P. and Silberman, M. L. 1976. Direct dating of mineralization of Goldfield, Nevada by potassium-argon and fission track method. Economic Geology. vol. 71. pp. 904-924.

ORIGINAL PAGE IS  
OF POOR QUALITY

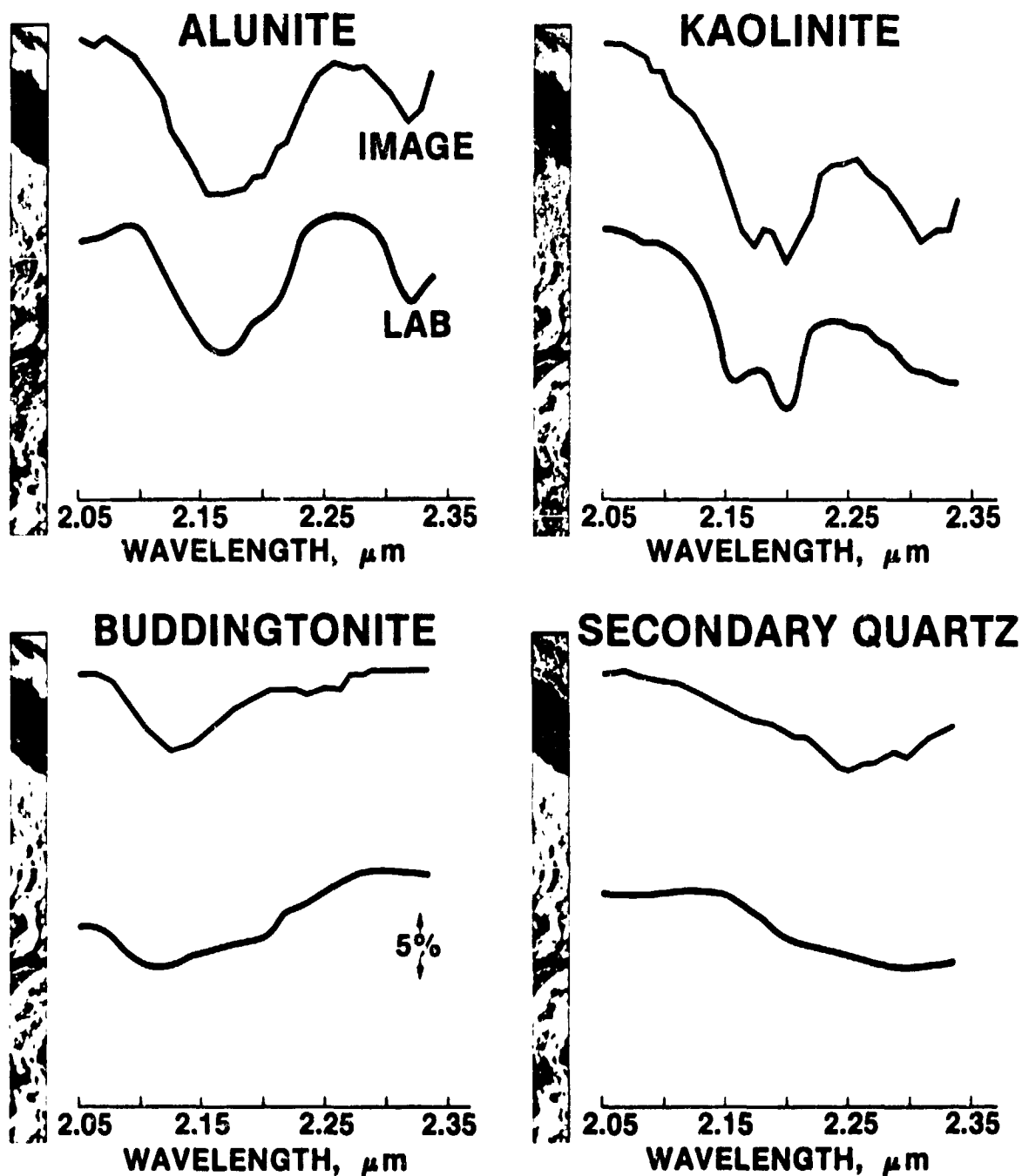


Figure 5. AIS coverage of Cuprite, with south at the top, covering the track with a "dogleg" shown in Fig. 1. The upper curves are the 3-by-3 pixel spectra of the red area in the respective images. The lower curves are laboratory spectra of samples collected in the red areas. The individual mineral maps were made using the SPAM program by selecting representative regions for the four spectral types shown and searching the images for similar spectral types. In each image, the regions of similar spectral types are shown in red.

Goetz, A. F. H., Vane, G., Solomon, J.E. and Rock, B. N. 1985. Imaging spectrometry for earth remote sensing. SCIENCE. in press.

Kahle, A. B. and Goetz, A. F. H. 1983. Mineralogic information from a new airborne thermal infrared multispectral scanner. SCIENCE. vol. 222. pp. 24-27.

PRECEDING PAGE BLANK NOT FILMED

REMOTE STRATIGRAPHIC ANALYSIS: COMBINED TM AND AIS RESULTS IN THE  
WIND RIVER/BIGHORN BASIN AREA, WYOMING

N86-11620

LANG, H.R., E.D. PAYLOR and S. ADAMS, Jet Propulsion Laboratory, California  
Institute of Technology\*, Pasadena, California 91109.

ABSTRACT

An in-progress study demonstrates the utility of AIS data for unraveling the stratigraphic evolution of a North American, western interior foreland basin. AIS data are used to determine the stratigraphic distribution of mineralogical facies that are diagnostic of specific depositional environments. After wavelength and amplitude calibration using natural ground targets with known spectral characteristics, AIS data identify calcite, dolomite, gypsum and montmorillonite-bearing strata in the Permian-Cretaceous sequence. Combined AIS and TM results illustrate the feasibility of "spectral stratigraphy", remote analysis of stratigraphic sequences.

SUMMARY

Prior to 1982, inadequate spatial resolution and spectral coverage limited the utility of multispectral image data for stratigraphic studies. Thematic Mapper (TM) and Airborne Imaging Spectrometer (AIS) data now provide improved spatial and spectral resolution, geometric fidelity and spectral coverage. Evaluation of the combined utility of these data demonstrates that they can complement conventional geological and geophysical information for stratigraphic studies in a typical North American foreland basin.

TM and AIS data were acquired in the Wind River/Bighorn Basin area of central Wyoming. Combined photogeologic, image processing and spectral analysis methods were used to: 1) map strata, 2) construct stratigraphic columns, 3) correlate strata, and 4) identify mineralogical facies.

Photogeologic interpretation of a 1:250,000 scale TM image identified an appropriate locality for constructing an image-derived stratigraphic column. This "type locality" encompasses exposures of homoclinal strata in the Deadman Butte area of the Casper Arch, eastern Wind River Basin. A 1:24,000 512 x 512 pixel TM image of the Deadman Butte area provided a photogeologic base for mapping spectral, textural and geomorphically defined photogeologic horizons. The TM image geometrically matched U.S.G.S. 7 1/2' topographic maps. Thus, standard geologic map interpretation methods could be used to construct a stratigraphic column incorporating TM spectral characteristics, true stratigraphic thickness and resistance of the photogeologic units. This column was correlated with a conventional surface section measured 6 miles to the west. Thus, 38 image units were assigned to 11 formations ranging from the Permian Phosphoria to the Cretaceous Cody Shale. The Deadman Butte TM stratigraphic column

\*Performed under contract with NASA.

~~PRECEDING PAGE BLANK NOT FILMED~~

was also correlated with a similarly constructed column from a structurally complex area in the southern Bighorn Basin and also with well logs from both the Wind River and Bighorn Basin.

Thirty-two channel, 2.1  $\mu\text{m}$ -2.4  $\mu\text{m}$ , AIS data acquired in October, 1983 were registered to the 1:24,000 scale Deadman Butte TM image to provide mineralogical information for TM defined stratigraphic units. Methods used to analyze the AIS data included: 1) empirical wavelength and amplitude calibration using natural ground targets with known reflectance spectra, 2) principal components analysis using 10 spectral bands selected on the basis of field and laboratory spectra of stratigraphically diagnostic minerals, 3) interactive sampling and mineralogical interpretation of image spectra, 4) automated mineralogical classification using a laboratory spectral library, and 5) along-track evaluation of spectral variability using residual processing.

Analyses revealed an approximate 4 channel wavelength shift from nominal and excessive noise in the last 5 channels. After correcting for these problems, AIS data revealed the stratigraphic distribution of dolomite (dolostones in the Phosphoria Formation), gypsum (anhydrites in the Dinwoody/Chugwater Formation transition), calcite (limestones in the Alcova Member of the Chugwater Formation), montmorillonite (bentonites in the Mowry Shale and Frontier Formation) and quartz (orthoquartzites throughout the section). This information was incorporated into the TM-defined stratigraphic column.

One hundred twenty-eight channel, 1.15  $\mu\text{m}$  - 2.34  $\mu\text{m}$ , AIS data were acquired on the same flightline in September, 1985. Comparison of image spectra to laboratory spectra (Fig. 1) confirmed results of the analysis of 1983 data. Residual processing of the data, using the same methods that were applied to the 1983 data, however, yielded unsatisfactory results. Refinement of the residual method is now in progress.

These results demonstrate the feasibility of using coregistered AIS and TM data for correlation of strata and for isopach and facies mapping. This stratigraphic information can be integrated with conventional surface, borehole and geophysical data for detailed stratigraphic studies of North American western interior sedimentary basins. When available, AVIRIS and SISEX data could provide images with sufficient spatial coverage and geometric fidelity to replace TM data as a photogeologic base for similar spectral stratigraphic studies.

#### REFERENCES

- Wolfe, W.L., and G.J. Zissis (eds), 1978. The Infrared Handbook (Ann Arbor, Michigan: Environmental Research Institute of Michigan), pp. 5-88.

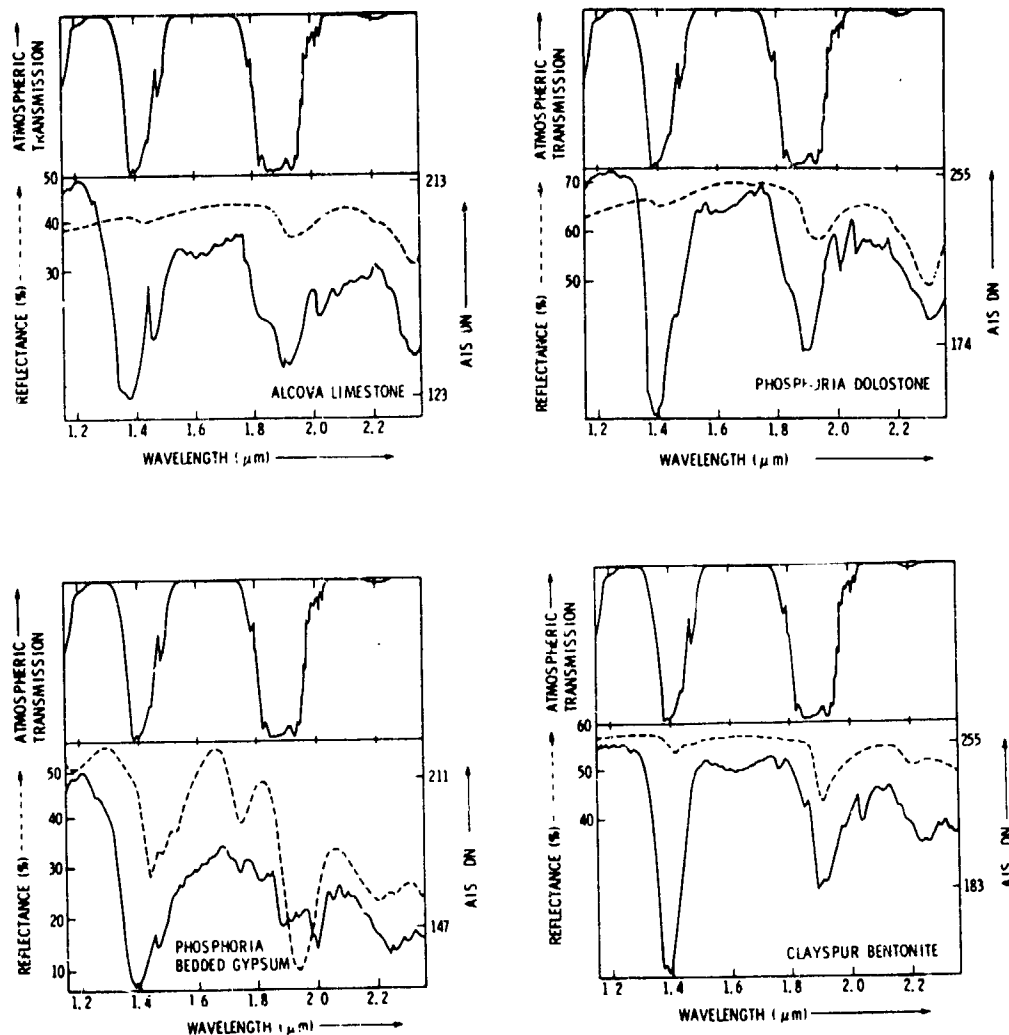


Fig. 1. Comparison of selected 3 x 3 pixel, flat-field corrected, AIS image spectra to laboratory spectra of samples obtained from same locations. Atmospheric transmission spectrum (after Wolfe and Zissis, 1978, pp. 5-88) is also shown. Data span 1.15  $\mu\text{m}$ -2.34  $\mu\text{m}$  wavelength interval. Absorption features include atmospheric  $\text{CO}_2$  bands near 1.45  $\mu\text{m}$  and 2.0  $\mu\text{m}$ , and bands near 2.33  $\mu\text{m}$  (calcite), 2.30  $\mu\text{m}$  (dolomite) and 2.2  $\mu\text{m}$  (gypsum and montmorillonite). Long wavelength shifts ( $\sim 4$  AIS channels) of 2.2  $\mu\text{m}$  gypsum and montmorillonite bands in AIS spectra as compared to laboratory spectra are probably due to along-track differences in wavelength interval sampled by fourth grating position.

FIELD UTILIZATION AND ANALYSIS OF AIS 128-CHANNEL IMAGERY USING  
MICROCOMPUTERS: APPLICATION TO YERINGTON, NV FIELD AREA

R.J.P. LYON, Department of Applied Earth Sciences, Stanford Univ., Stanford, CA, 94305; Kai LANZ, Remote Sensing Lab., AES Department, Stanford, CA, 94305

**ABSTRACT**

As geologists in exploration we need to be able to determine the mineral composition of a given outcrop, and then proceed to another in order to carry out the process of geologic mapping. Since April 1984 we have been developing a portable microcomputer-based imaging system (with a "grey-scale" of 16 shades of amber), which we demonstrated during the November 1984 GSA field trip in the field at Yerington, NV. We have recently also demonstrated a color-version of the same technology, at this AIS Workshop, at JPL. The portable computer selected is a COLBY 10-Megabyte, hard disk-equipped "repackaged-IRM/XT", which operates on either 110/220 VAC or on 12VDC from the cigarette lighter in a field vehicle. (See Figure 2: upper). A COMPAQ PLUS or an IBM Portable will also work on modified software.

Our software was internally developed and owes much to Dr. Andy Green, CSIRO, North Ryde, NSW, Australia, and follows his ideas of LOG-RESIDUALS (see associated paper in this issue by A. A. Green and M. D. Craig). The underlying concept is that the atmospheric transmission and surface albedo/slope terms are multiplicative, relating the spectral irradiance to the spectral "color" of the surface materials - the end result we wish to examine in the field. Thus the spectral color of a pixel remains after averaged log-albedo and log-irradiance have been estimated. All these steps can be carried out on the COLBY microcomputer, using 80 image lines of the 128-channel, 12-bit imagery.

Results are shown for such an 80-line segment, showing the identification of an O-H bearing mineral group (of slightly varying specific characters) on the flight line. (See Figure 2: lower.)

**GEOLOGY OF THE SITE (After Proffett & Dilles, 1984)**

The Jurassic plutonic rocks (granodiorite and quartz monzonite) and associated porphyritic quartz monzonite dikes were intruded as a 7-km deep section. This rock sequence was deeply eroded (2 km) in late Mesozoic to early Tertiary times, and left a high-relief terrain with 0.5 km (2000 ft) peaks. Upon this rough terrain were laid a thick series of Oligocene and early Miocene ash-fall tuffs (ignimbrites) with a total thickness of about 2 km (7500 ft). Rotational tilting of the whole area occurred continuously during this deposition, so that the originally-flat basal tuffs (Guild Mtn. member, Tgm) now have 70° west dips, while the uppermost (Miocene) hornblende andesite tuffs of Lincoln Flat (Tha) dip only 20-30° west (Proffett & Proffett, 1976).

Significantly for this remote-sensing application, south of the Singatse Fault, in the Ann Mason area, the originally vertical section through the porphyry-copper "plumbing" is now displayed in a near-horizontal outcrop. Top is to the WNW, the base is to the ESE, and over 5 km (16,000 ft) of almost continuous outcrop traverses the Singatse Range.

ORIGINAL PAGE IS  
OF POOR QUALITY

AIS IMAGERY, YERINGTON, NV, 28 JULY 1984

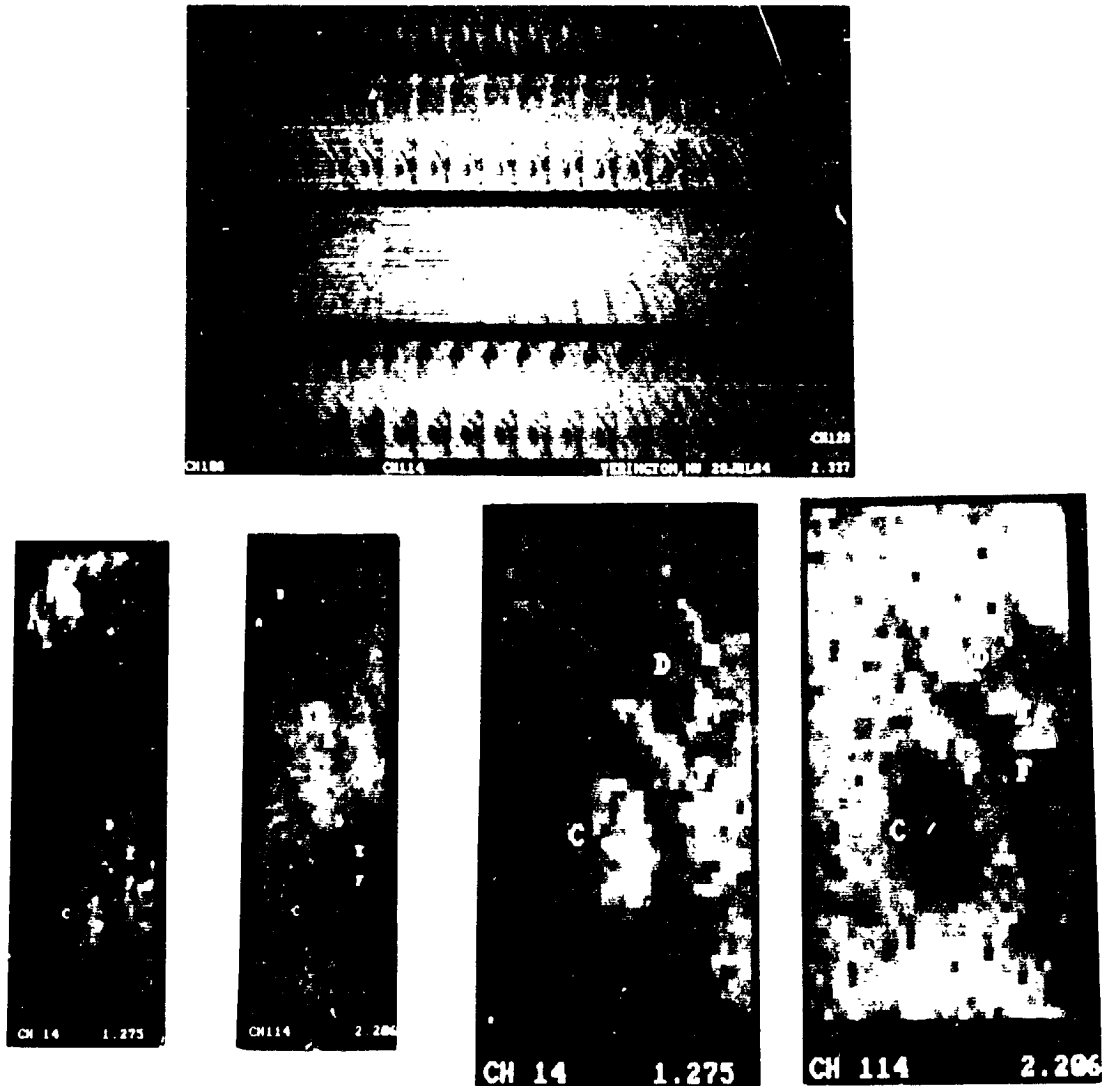


FIGURE 1. (Upper) Display of 80 channels, each of 80 flight lines, for Run 407, commencing at line 750. Top left is channel 48 ( $1.60\mu\text{m}$ ). Left to right covers 20 channels, each differing by  $9.3\text{nm}$ . Notice lower right set commences at CH108 ( $2.15\mu\text{m}$ ). Targets are blacker in CH110-118, reaching a maximum around CH 114 ( $2.206\mu\text{m}$ ). Flight data over Yerington, NV, taken 28 July, 1984

(Lower Left pair). Displays of 80 line segments, for channels 14 ( $1.275\mu\text{m}$ ) and 114 ( $2.206\mu\text{m}$ ), respectively, at 2x enlargement on the CRT. Notice specific pixels A-F.

(Lower right pair) 4x enlargements of the lower portion of the scene, showing localities C-F. Black on channel 114 is indicative of O-H absorptions, probably due to sericite alteration products.

ORIGINAL PAGE IS  
OF POOR QUALITY  
AIS IMAGERY, YERINGTON, NV, 28 JULY 1984

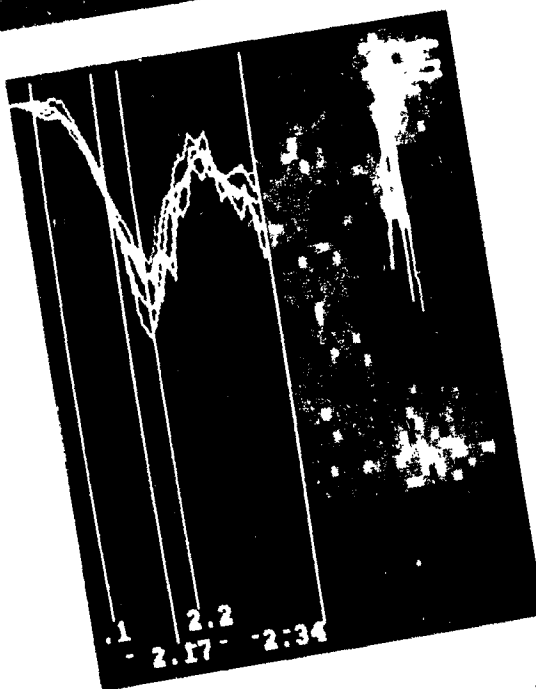
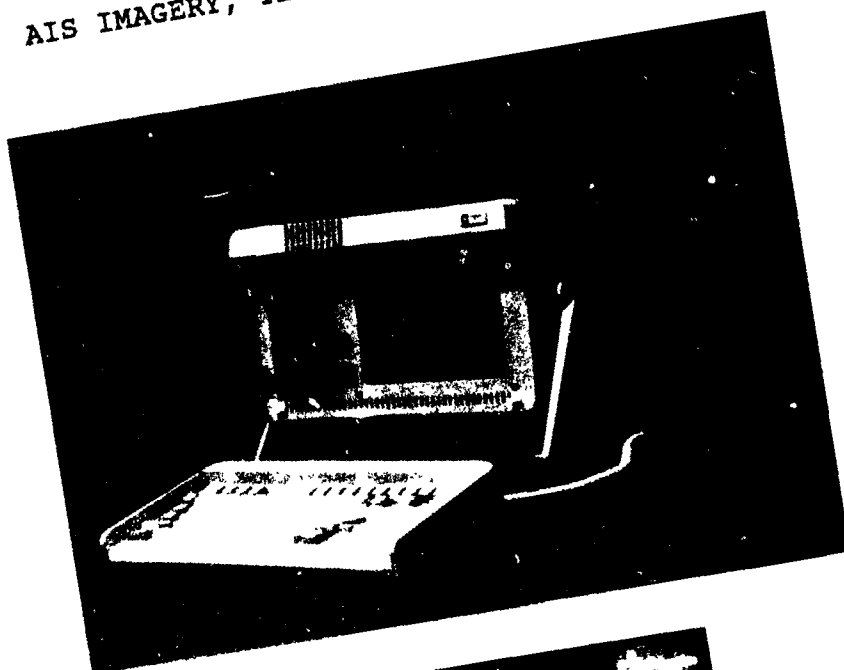


FIGURE 2. (Upper) COLBY Portable computer, as used for the field analysis of AIS flight data (Demonstrated at JPL AIS Workshop, 4/85). Present image on 16-level gray scale (Amber) is of a U-2 TMS image, over Yerington, NV. Black area is the water-filled old pit, white areas are the dumps of q.monzonite used for AIS calibration.

(Lower) AIS image of CH 114 ( $2.206\mu\text{m}$ ), wherein O-H absorptions are black, showing the pixel-by-pixel analysis, and their associated spectra. Originals are colored in seven colors. Notice the variability of the O-H absorptions, in detail.

### Ann Mason Area

M. Einaudi and his students (Einaudi, 1977; Carten, 1981; Harris and Einaudi, 1982) studied the area in great detail, during the period 1975-1982. The recent extensive mineralogical study of J. Dilles (Ph.D thesis, 1983), however, provides most of the background materials for the AIS flight-calibration mineralogies.

### U-2 TMS Flights - 1983-85

Although the Stanford Remote Sensing Lab (SRSL) has been studying these sites since 1972 (SKYLAB), the major breakthrough occurred with the acquisition of the 12-channel (TMS) digital imagery over the Singatse Ra., in April 1983. For the first time it was possible to locate "clay-alteration" areas (O-H bond absorptions, near 2.2  $\mu\text{m}$ ) in spatially-coherent patches with the expected locations and trends observed in our fieldwork. Both the Ann Mason (Singatse Peak) and the northern MacArthur areas were imaged in a single 30,000-wide strip down the length of the Singatse Ra.

These imaged data were shown to John Dilles in that month, as he was completing his Ph.D thesis research (Dilles, 1983). He confirmed that the 1.6/2.2- $\mu\text{m}$  "anomalies" indeed very closely mapped his "Late-Stage" alteration, identified from thin-section and XRD studies as tourmaline-sericite-pyrite assemblages. In addition we feel, that by careful matching of these, 1983 ratio-images showed the possible detection of this even-more subtle potassic (hydrothermal) alteration (chlorite-hydrobiotite) which occurred lower (deeper) into the original dike swarm, below the late-stage (geothermal) sericite-pyrite capping.

### AIS-Flight, 28 July 1984

After three clouded-out attempts the NASA/ARC C130 was able to gather 128-channel spectral images over five specially designed flight runs, each 700 ft wide, crossing the previously identified "clay anomalies". Two lines (407, 409) paralleled the WNW trend of the dike swarms, flying up the "plumbing system" of the mineralization, from the base to the top of the erosion surface. Another line (#410) crossed these at right angles over the sericite-pyrite zone, while (#408) traversed close to (but unfortunately not over) the MacArthur deposits to the north.

### Pre-Processing of the AIS Data

Our SRSL-AIS pre-processing package consists of three units;

AIS2 - a program which accesses the 1600 BPI, 9-track CCT tapes, images a 400-line segment, displaying 16 adjacent wavelength bands, so that one can identify locations on the left and right margins of the flight on the associated 35mm B/W photographs (roughly along the center third of the prints). In a second part of the program, files may be created for the any 80 lines of the scene, 128-channels deep, on to the COLBY (IBM/XT) 10-Mb hard disk. These files are given the extension \*.AIS.

ANDY - the next program which forms the main pre-processing step in the SRSL package. The program presently operates only on the 80-line segment (later to be the whole flight line of approximately 2000 lines), and performs the following steps;

- (i) Takes natural logarithms of all the imagery digital data
- (ii) AVERAGES all wavelengths for a given pixel, to yield a single scalar (A)
- (iii) AVERAGES all pixels for a given wavelength plane (80x32), for 128 planes, yielding a 128-element vector (H-bar)
- (iv) AVERAGES all the H-bars to give a single (global) scalar (G).

For each pixel of the image, the program takes its given LOG-DIGITAL NUMBER (Log-DN), subtracts in turn its H-BAR, subtracts A, and adds G-BAR. The resultant LOG RESIDUAL (R) is saved as the final "SPECTRAL-IMAGE" set, designated \*.NDY.

DESTAIS - cleans up the vertical striping, by forcing each of the 32 detector elements (vertical lines on the image displays) to have the same area-under-the-curve. This is performed 128 times, once on each image plane. The resultant file is designated \*.DES.

#### Display Programs for the AIS-Imagery

The AIS-display package consists of three units:

- a. MULTI - presents 80 channels, for 80 image lines, starting at channel N = 1,,43, in a single selected linear stretch for all 80 channels. (See Figure 1: upper, for 1X, and lower, for 2X and 4X enlargements, to show specific localities. Pixel size is 8X8 m.)
- b. TVAIS - (or CAIS, on the B/W field unit.) The user selects any one channel (N = 1,,128) for display at a 4X scale. ANY of the pixels are cursor selectable, and alongside the indicated pixel either a color-coded residual is shown as a horizontal "color-bar", or the spectrum of the log-residual is graphed in one of seven colors, as a graphics plot. (See Figure 2: lower.)
- c. ANDY - (or CANDY, on the B/W field unit.) A version of TVAIS to color-plot, or color-code, any digitized spectrum, for n = 128, or 256 data points, as from a published database, field spectra from the flight lines, etc.

#### STATUS

Results are shown for such an 80-line segment, showing the identification of an O-H bearing mineral group (of slightly varying specific characters) on the flight line. (See Figure 2: lower.) Active studies are in progress, the completion of which are entirely dependent upon available funding.

## REFERENCES

- Carten, R.B. 1981. Sodium-calcium metasomatism and its spacetime relationship to the potassium metasomatism in the Yerington porphyry copper deposit: Ph.D. dissertation, Stanford University, Stanford, California.
- Einaudi, M.T. 1977. Petrogenesis of the copper-bearing skarn at the Mason Valley mine, Yerington district, Nevada; Economic Geology, 72, pp. 769-795.
- Harris, N.B. and Einaudi, M.E. 1982. Skarn deposits in the Yerington district, Nevada-metasomatic skarn evolution near Ludwig: Economic Geology, 77, pp. 877-898.
- Proffett J.M., Jr. and Dilles, J.H. Geologic map of the Yerington district, Map 77; Nevada Bureau of Mines and Geology, Reno, Nevada.
- Proffett, J.M. and Proffett, B.M. 1976. Stratigraphy of the Tertiary ash-flow tuffs in the Yerington district, Nevada: Nevada Bureau of Mines and Geology Report 27.

N86-11622

PRELIMINARY ANALYSIS OF AIS SPECTRAL DATA ACQUIRED FROM SEMI-ARID SHRUB COMMUNITIES IN THE OWENS VALLEY, CALIFORNIA

SUSAN L. USTIN, Department of Botany, University of California, Berkeley, CA 94720, USA; BARRETT N. ROCK, Jet Propulsion Laboratory, Pasadena, CA 91109, USA

ABSTRACT

Spectral characteristics of semi-arid plant communities were examined using 128 channel AIS data acquired on October 30, 1984. Both field and AIS spectra of vegetation were relatively featureless and differed from substrate spectra primarily in albedo. Unvegetated sand dunes were examined to assess spectral variation resulting from topographic irregularity. Although shrub cover as low as 10% could be detected on relatively flat surfaces, such differences were obscured in more heterogeneous terrain. Sagebrush-covered fans which had been scarred by fire were studied to determine the effect of changes in plant density on reflectance. Despite noise in the atmospherically corrected spectra, these provide better resolution of differences in plant density than spectra which are solar-corrected only. A high negative correlation was found between reflectance and plant cover in areas which had uniform substrates and vegetation types. A lower correlation was found where vegetation and substrates were more diverse. Thus shadows caused by substrate roughness or plant canopies also appear to have an important effect on brightness, making predictions from spectral characteristics difficult. Spectra obtained during periods of active plant growth may be more useful in vegetation studies.

INTRODUCTION

High spectral resolution imaging spectrometers such as AIS have potential for identification of minerals and plants based on the unique absorption features of their spectra. For ecologists, this may lead to new ways of studying and monitoring ecosystem processes, detecting environmental stresses, and measuring plant productivity. These instruments are also of considerable interest to exploration geologists working in arid and semi-arid regions, since in such areas the interpretative problems arising from mixed spectral reflectances should be minimal, due to the relatively low vegetation cover.

The primary objectives of our study are to evaluate the importance of vegetation in mixed pixel AIS data from representative semi-arid shrub communities, to assess dynamic changes in spectral features of vegetation over the year, and to develop methods by which the spectra of vegetation and substrate may be separated.

Owens Valley, CA was chosen as a test site because it has a diverse combination of plant communities and substrate types. A creosote bush community, typical of the warmer Mojave desert, extends into the southern end of Owens Valley on alluvial fan skirts from the Sierra Nevada to the west and the Inyo Mountains to the east. Vegetation on fans farther north is more typical of the Great Basin sagebrush community. Saltbush communities are found on the valley floor and on other alkaline soils. Major geologic units in the surrounding areas are Mesozoic granitic intrusives, Tertiary volcanics (primarily basalts), and Paleozoic sediments. Differences in plant density and species diversity exist within the various substrate types, offering the opportunity to examine the impact of vegetation on spectral characteristics.

#### AIS DATA AND CALIBRATION PROCEDURES

At present, we have had three flights over our study sites, on July 10 and October 30, 1984 and April 2, 1985. All flights obtained 128 channel AIS data, most of them in the "rock" grating position mode, 1.21-2.40  $\mu\text{m}$  (Vane et al., 1983). For comparison, on some flights data from one line were recorded in the "tree" mode, ca. 0.85-2.10  $\mu\text{m}$ . Thematic Mapper Simulator (NS001) imagery, Nikon black and white photographs, Zeiss color infrared images, and ground track videotapes were collected simultaneously.

Data reported here are entirely from the October overflight. The data acquired in July are of questionable value due to a high concentration of smoke from a large brush fire in Sequoia National Park to the west of Owens Valley. However, preliminary examination of these data supports the observations and conclusions of this report.

The October 30, 1984 flight occurred at 1145-1245 hours PST, on a cloud-free day. Mean flight altitude was 5.25 km above the terrain, with an instantaneous field of view of about 10 m. Data were analysed on a VAX/IDIMS system using the SPAM (Spectral Analysis Manager) package developed by the Jet Propulsion Laboratory. Prior to data analysis, a solar irradiance correction was applied to compensate for brightness variation with wavelength in the solar spectrum. We compared results of this correction with those of two additional methods for removing atmospheric absorptance effects: a "flat field" method ratioing pixel reflectances by the mean reflectance obtained from a 32 by 50 pixel area judged to be spectrally and spatially homogeneous, and a theoretically based correction algorithm (J. Solomon, personal communication) which ratios each pixel reflectance by the mean reflectance along the flight line for each channel.

#### RESULTS AND DISCUSSION

Coinciding with the October overflight, we performed an experiment with a Collins Visible Infrared Intelligent Spectrometer (VIRIS) to examine the effect of spectral mixing at different distances above the plant and soil surfaces. When the spectrometer was close to the canopy, the spectral pattern was distinctively plant-shaped; however, this pattern was progressively damped out as distance increased (Ustin et al., 1985). This response appears to be due to shadows within the canopy branches and the increasing contribution of sand to the

spectra. From this we conclude that the influence of vegetation in October AIS data would be most evident in albedo effects.

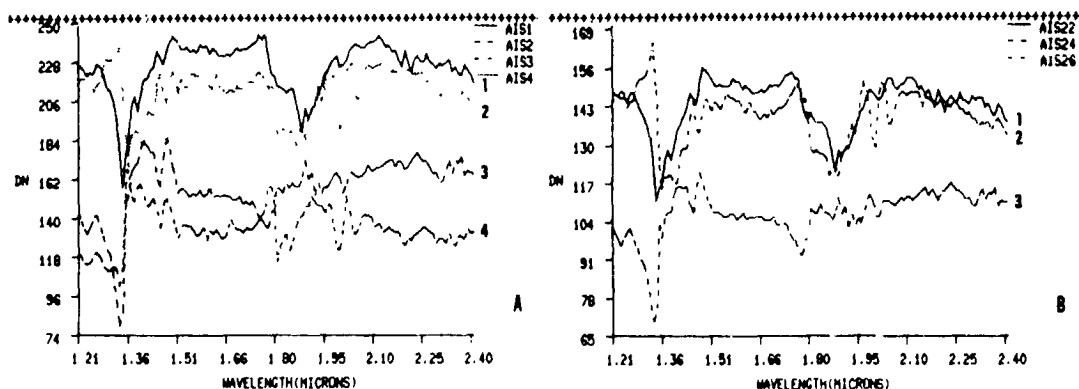


Fig. 1. AIS sand spectra with (a) flat field correction and (b) theoretically based atmospheric correction. Curve 1 is sunlit dune, 2 shaded aspect, 3 a flat surface.

Data from an unvegetated sand dune region show that topographic differences, such as changes in slope and aspect, confound interpretations of even atmospherically corrected spectra. Figure 1 shows data from the same 3-by-3 pixel areas using the flat field correction (1a) and the atmospheric correction (1b). Curve 1 is from the sunlit side of a dune, curve 2 from the shaded side, and curve 3 from a flat surface normal to the AIS (curve 4 in 1a, from the shaded side of another dune, is not shown on 1b). From these and other curves, it appears that both correction methods yield comparable results, although the digital number (dn) values depend on the method of correction. The curves are featureless and essentially flat or slightly increasing across the spectrum, as expected for quartz sands. At another area which was studied in detail, we could distinguish a saltbush vegetation cover of only 10% (based on ground transects) from a non-vegetated uniform sandy surface of similar slope, because of brightness differences. However, these differences were within the dn range seen in Figure 1 on the two aspects of the same sand dune. During spring, greater divergence in spectral response curves between vegetation and substrate may provide a less ambiguous basis for their distinction.

Spectral data in Figure 1 and in Figures 2 and 3, from the Symmes Creek and Division Creek sites on fans on the west side of the valley, all show considerable noise, making identification of absorption features difficult or impossible. We found that omitting the water absorptance bands and replotting portions of the spectra (e.g., 2.10-2.40  $\mu\text{m}$ ) reduced the apparent noise in the atmospherically corrected spectra. Still less noise is evident in data to which only the solar correction was applied (Figure 2a), but the differences between spectra from different areas within sites are less than in spectra corrected for both solar and atmospheric effects (Figure 2).

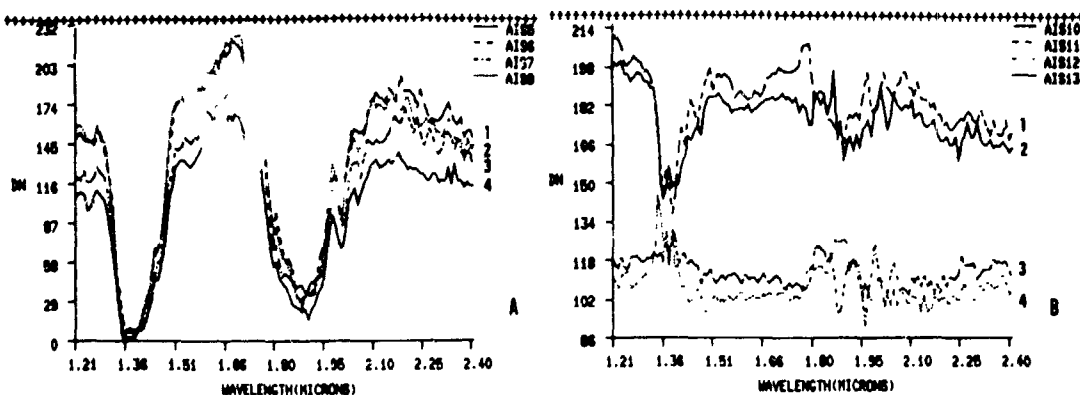


Fig. 2. AIS spectra (a) without atmospheric correction and (b) with atmospheric correction. Spectra 1 and 2 are from an area which had been burned, spectra 3 and 4 the non-burned vegetation.

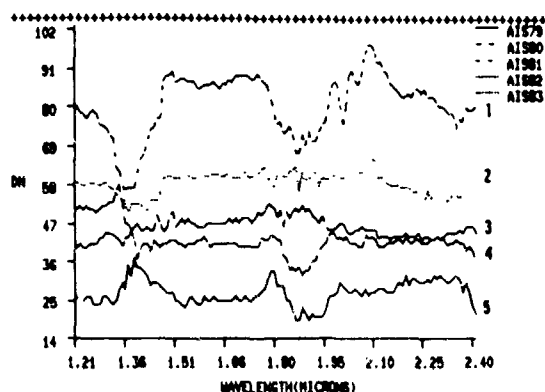


Fig. 3. AIS spectra from surfaces which differ in plant cover and substrate. Spectrum 1 is from burned alluvium, 2 burned basalt, 3 non-burned alluvium, 4 non-burned basalt, and 5 non-vegetated basalt.

Despite the greater noise in data with the atmospheric correction, they show clear differences related to vegetation cover. At Symmes Creek (Figure 2), alluvial substrates are essentially homogeneous and spectral differences relate to an abrupt change in vegetation density due to a brush fire which removed the plant cover in 1977. The upper two curves in 2a and 2b are from the burned area, which has a total plant cover of 23% including litter. The lower two curves are from the surrounding undisturbed sagebrush community, which has 46% cover. Reflectance differences between these two areas, assuming the curves are flat and using the dn value at 1.21  $\mu\text{m}$  from randomly chosen 3-by-3 pixels ( $n=18$  and 15 on and off the burn, respectively), are statistically significant (ANOVA,  $p<.0001$ ).

We also measured plant density on and off burns at two other sites near Symmes Creek. Burns at these sites were much older (pre-1947) and had greater plant densities, but adjacent unburned areas did not vary significantly in cover. Twelve to 15 spectral curves were obtained from randomly chosen 3-by-3 pixels within each of these areas. As described above, curves from each area were averaged and compared with plant cover, which ranges from 23 to 48 %. A linear regression of mean dn from all three sites with mean total plant cover produced a negative correlation coefficient of 95 % (n=6). Thus, shrub cover has a consistent effect in lowering substrate albedo, and the amount of change is related to plant density.

At Division Creek, a similar sagebrush community occurs on both a granitic alluvial substrate and a basalt flow. In 1982, a fire removed the vegetation across both substrates. Curves in Figure 3 are representative of 12-16 reflectance spectra from each of these surfaces. The upper curve (1) is from the burned alluvial surface, which has a 9 % plant cover, nearly all of which consists of herbaceous dicot litter at this season. The next curve (2) is from the burned basalt, which has a surprisingly high reflectance. It has a high cover, 52 %, almost all of which is grass litter. Curves 3 and 4 are from the non-burned areas on the alluvial and basalt substrates, which support a similar shrub community with covers of 64 % and 45 %. The lowest curve (5) is from a non-vegetated basalt outcrop. Although there is a good correlation of dn with cover (71 %), it is lower than that from the other burns. This probably reflects the greater substrate roughness on the basalt flow and differences in physiognomy (shrub vs. herbaceous). Thus, although the amount of plant cover is clearly the major determinant of reflectance, shadows caused by plant canopies and substrate roughness may also be an important source of albedo variation. The presence of vegetation reduces the differences in reflectance between the two substrates, thus masking any geologic absorption features. Although this feature is somewhat difficult to detect in curve (1), other curves from the burned alluvial surface clearly show a hydroxyl absorbance of presumed substrate origin, at 2.19  $\mu$ m, and which was confirmed by field VIRIS spectra. This feature is absent in all AIS data from surfaces with greater plant cover.

#### REFERENCES

- Ustin, S.L., Rock, B.N., and Woodward, R.A. 1985. Analysis of substrate and plant spectral features of semi-arid shrub communities in the Owens Valley, California. Proc. Int. Symp. on Remote Sensing of Environment. Fourth Thematic Conference: Remote Sensing for Exploration Geology (in press)
- Vane, G., Goetz, A.F.H., and Wellman, J.B. 1983. Airborne imaging spectrometer: a new tool for remote sensing. Proc. 1983 International Geoscience and Remote Sensing Symposium. pp. FA-4, 6.0-6.5

## AIS SPECTRA FOR STRESSED AND UNSTRESSED PLANT COMMUNITIES IN THE CAROLINA SLATE BELT

DIANE E. WICKLAND, Jet Propulsion Laboratory, California Institute of Technology, USA

## ABSTRACT

Airborne imaging spectrometer (AIS) data were collected over a number of derelict heavy metal mine sites in the Carolina slate belt of North Carolina. A 32 channel (1156 - 1456 nm) data set was acquired in October, 1983 at the time of peak fall foliage display, and a 128 channel (1220 - 2420) data set was acquired near the end of the spring leaf flush in May, 1984. Spectral curves were extracted from the AIS data for differing ground cover types (e.g., pine forests, mixed deciduous forests, mine sites, and pastures). Variation in the width of an absorption feature located at approximately 1190 nm has been related to differences in forest type. Small differences in the location and shape of features in the near infrared plateau (1156 - 1300 nm) and the region 2000 - 2420 nm have yet to be evaluated. Because these variations were subtle, and because atmospheric effects were apparent in the data, high priority must be assigned to devising a means of removing atmospheric effects from AIS spectra.

## INTRODUCTION

Extensive ecological studies of vegetation on and near derelict heavy metal mine sites in the Carolina slate belt of the North Carolina Piedmont (Wickland, 1983) prompted a remote sensing study of the area (Wickland, 1984). The main objective of the remote sensing study was to attempt to identify spectral characteristics of vegetation related to the type of stress the vegetation was experiencing. Airborne imaging spectrometer (AIS) data were acquired as part of this study because high spectral resolution data seemed to have great potential for uniquely identifying stress factors. Two AIS data sets were acquired. In October, 1983, at the time of peak fall foliage display, a 32 channel (1156 - 1456 nm) data set was acquired for 6 flightlines. In May, 1984, near the end of the spring leaf flush, a 128 channel data set (1220 - 2420 nm) was acquired for 4 flightlines.

## METHODS OF DATA ANALYSIS

For the 32 channel fall data set, raw, logged data (i.e., neither atmospheric nor solar irradiance corrections were applied) were subjected to the Walsh-Hadamard transformation and Principal Components analysis. Color composites of the first three components from both transformations provided essentially the same information, but the color contrast in the principal components image was somewhat more pleasing. Spectra were extracted from the raw data using the program ISCAN. Vertical striping was evident in the fall imagery, and the imagery

lacked crispness due to hazy skies at the the time of acquisition.

For the 128 channel spring data set, the raw, logged data were subjected to a correction for the solar spectral irradiance. Again, atmospheric effects were not removed. Ground reflectance data were acquired at the time of the overflight for the purpose of flatfield correction, but the flightline involved could not be logged properly. Spectra were extracted from other flightline data sets using the program SPAM. There was little haze at the time of the spring overflights, and the AIS imagery was much crisper. Horizontal data loss bands due to interference by the Nikon camera were visible in the images.

## RESULTS AND DISCUSSION

### Fall Imagery

All ground cover types discernible in color infrared photography and Thematic Mapper Simulator imagery were clearly distinguishable in the fall AIS imagery. Farm ponds in the image for a flightline in the Virgilina area did not have the low, flat spectra expected of water in the near infrared. Although algae or sediments in the ponds could have been responsible for this difference, it seems more likely that atmospheric absorption and scattering were responsible.

A large plantation of loblolly pine (Pinus taeda L.) and the upper and mid-slope portions of a small ridge covered by mixed deciduous forests were imaged in the Virgilina flightline. The top of the ridge supported a mixed oak-hickory-pine (Quercus spp.-Carya spp.-Pinus spp.) forest and the mid-slope area supported a white oak-tulip poplar-sweet gum (Quercus alba L.-Liriodendron tulipifera L.-Liquidambar styraciflua L.) forest. All spectra extracted from the pine plantation had a broader absorption feature at approximately 1190 nm than did spectra from the two deciduous forests. This absorption feature is in the wavelength region of a minor water absorption band, and it is not clear whether the differences seen are due to atmospheric or plant water content or to something else. Spectra from the mixed oak-hickory-pine forest often had characteristics intermediate to spectra from the pine plantation and the pure hardwoods stands. Typical spectra from these forests are shown in Figure 1.

It was readily apparent that the starting and ending wavelengths for this AIS data set were not the nominal 1200 and 1500 nm. Vegetation spectra from this data set were compared with laboratory spectra, and the starting and ending wavelengths were estimated as 1156 and 1456 nm. The exact position of the absorption feature described above has not been specified because of uncertainty about the exact wavelengths imaged.

The edge of the Silver Valley lead-zinc mine was imaged in a north to south flightline. There was a halo of slightly different color and texture surrounding the mine site in the principal components transformed AIS image. Spectra extracted from this area were not appreciably different from those from surrounding forests of similar composition. The spectra from the halo area had slightly higher overall reflectance; this could be an indication that the vegetation near the mine was drier than the surrounding vegetation on normal soils.

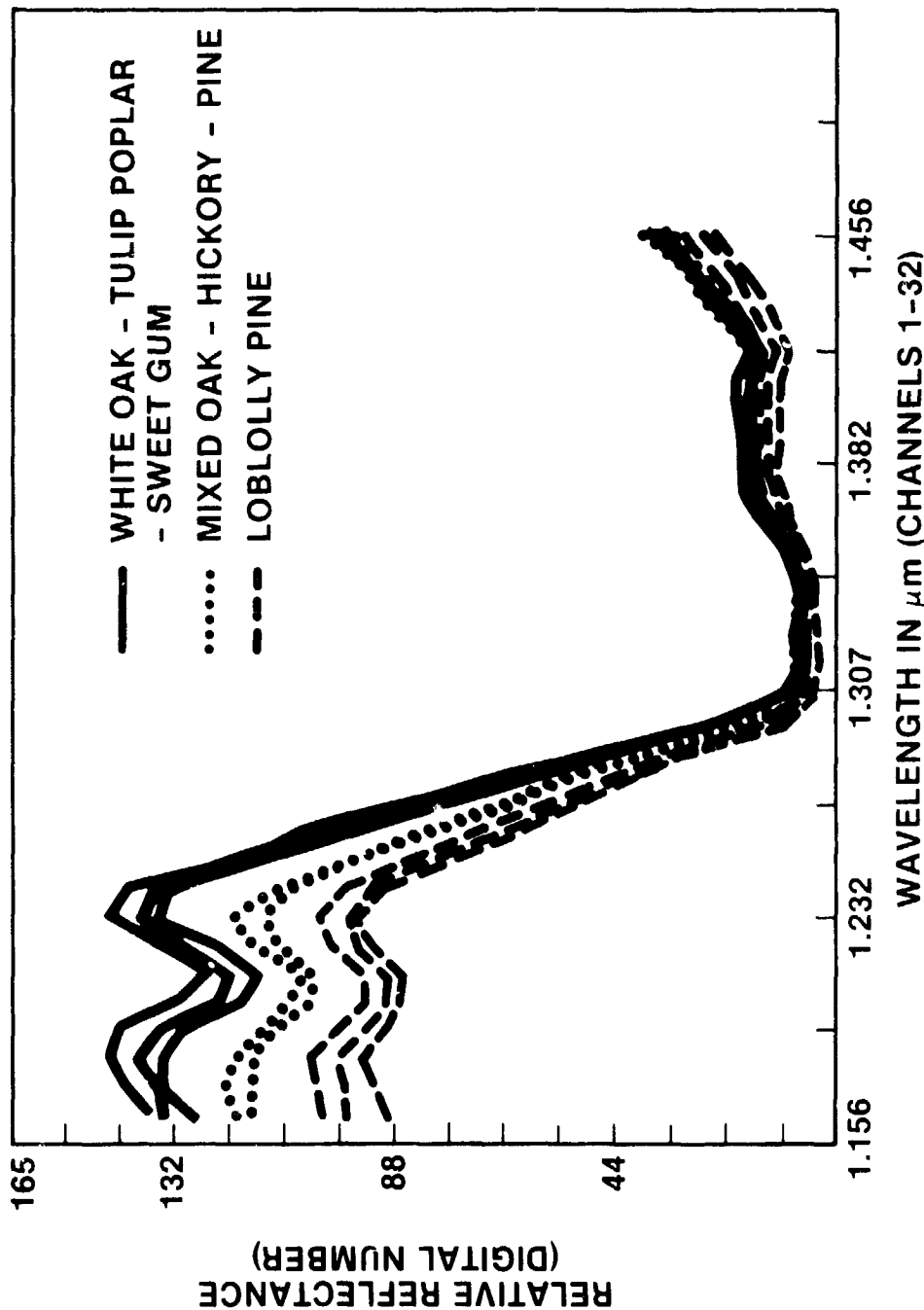


Fig. 1. Typical relative reflectance spectra for forests in the Virgilina area on October 18, 1983. The spectra have been averaged for 3 x 3 pixel areas. The deciduous forests have higher overall reflectance and a narrower absorption feature at approximately 1190 nm than do the evergreen pine forests. The mixed forests have intermediate spectral characteristics.

### Spring Imagery

Several small absorption features were noted in vegetation spectra when previewing the spring 128 channel data. Schematic transmission spectra of water vapor and carbon dioxide were superimposed on these plant spectra to identify those atmospheric absorption features which coincided with features in the plant spectra. Carbon dioxide bands at 1575, 1613, 1961, 2020, and 2062 nm and minor water bands at 1190, 1538, 1667, and 2198 nm were evident in the plant spectra. The major water absorption bands at 1400 and 1900 nm matched almost exactly on these superimposed spectra. The water bands for water and vegetation spectra were aligned with the schematic water bands, and the beginning and ending wavelengths were calculated to be 1220 and 2420 nm. Thus, the absorption feature at about 1900 nm noted in the fall AIS data set could not be evaluated in the spring data set.

Two of the spring AIS flightlines included sites imaged in the fall. The pine plantation and mixed deciduous forests in the Virgilina area were imaged; and the edge of the Silver Valley lead-zinc mine site was included, this time on an east to west flightline. The main differences noted among the various vegetation cover types were all related to relative reflectance. Bare fields were most reflective, deciduous forests were intermediate, and pine forests were the least reflective. This was also the pattern for the 1156-1456 nm fall data set. Again, the halo area around the Silver Valley mine site had a slightly higher overall reflectance than surrounding vegetation of the same type. It was not possible to evaluate small differences in plant spectra; they could have been due to atmospheric phenomena, noise, or actual plant differences.

### CONCLUSIONS

The width of an absorption feature at approximately 1900 nm was related to differences between evergreen and deciduous forest types in the fall AIS data set. Because atmospheric effects have not been removed from the data, no further conclusions could be made. Removal of atmospheric effects, due to both gases and particulates, must be an important priority for future analysis of AIS data sets.

To successfully evaluate differences in vegetation spectra, which are often small and subtle, new techniques for spectral analysis are needed. Those which have been successfully applied to mineral spectra do not work with vegetation spectra. Clever use of absolute reflectance could be useful. A library of plant reflectance spectra should be prepared. Spectra for plant chemical constituents, such as cellulose, lignin, proteins, and oils, should be included. Mixing models using some of these spectra could yield insights about the nature of vegetation spectra. Also, more study of plant spectral response in the laboratory and the field seems to be necessary before understanding of remotely sensed vegetation spectra will be achieved.

### ACKNOWLEDGEMENTS

The research described in this paper was performed while the

author held a National Research Council-NASA Research Associateship at the Jet Propulsion Laboratory, California Institute of Technology, under contract with the National Aeronautics and Space Administration. Barrett N. Rock made substantial contributions to this work, and Alex Zak, Deanne Tucker, and Jerry Solomon provided useful advice.

#### REFERENCES

- Wickland, Diane E. 1983. Vegetation patterns on derelict heavy metal mine sites in the North Carolina Piedmont. Ph.D. Dissertation. University of North Carolina, Chapel Hill. 623 pp.
- Wickland, Diane E. 1984. Remote sensing of stressed vegetation in the Carolina slate belt. p. 609-614. In: Proceedings, International Symposium on Remote Sensing of Environment, Third Thematic Conference, Remote Sensing for Exploration Geology, Colorado Springs, Colorado, April 16-19. Volume II.

SPECTRAL CHARACTERIZATION OF SUSPECTED ACID DEPOSITION DAMAGE IN RED SPRUCE (*PICEA RUBENS*) STANDS FROM VERMONT

JAMES E. VOGELMANN and BARRETT N. ROCK, Jet Propulsion Laboratory, California Institute of Technology, Pasadena, CA 91109, USA

## ABSTRACT

In an attempt to demonstrate the utility of remote sensing systems to monitor sites of suspected acid rain deposition damage, intensive field activities, coupled with aircraft overflights, were centered on red spruce stands in Vermont during August and September of 1984. Remote sensing data were acquired using the Airborne Imaging Spectrometer, Thematic Mapper Simulator, Barnes Model 12-1000 Modular Multiband Radiometer and Spectron Engineering Spectrometer (the former two flown on the NASA C-130; the latter two on a Bell UH-1B Iroquois Helicopter). Field spectral data were acquired during the week of the August overflights using a high spectral resolution spectrometer and two broad-band radiometers. Preliminary analyses of these data indicate a number of spectral differences in vegetation between high and low damage sites. Some of these differences are subtle, and are observable only with high spectral resolution sensors; others are less subtle and are observable using broad-band sensors.

## INTRODUCTION

Since 1965, red spruce (*Picea rubens* Sarg.) has shown a marked decline in vigor in the high elevation spruce-fir forests of northeastern United States (Siccama, et al., 1982; Vogelmann, et al., 1985). Other members of the montane forest, including sugar maple (*Acer saccharum* Marsh.), mountain maple (*A. spicatum* Lam.), striped maple (*A. pensylvanicum* L.), white birch (*Betula papyrifera* Marsh. var. *cordifolia* (Regel) Fern.) and balsam fir (*Abies balsamea* (L.) Mill.) have experienced less dramatic declines throughout this time period (Vogelmann, et al., 1985). Although the specific cause of the forest decline has been disputed, there is mounting evidence that high inputs of air pollutants into high elevation forests are a significant factor.

Camels Hump Mountain, located in the Green Mountains of northern Vermont, was chosen as a study area for the current investigation because of (a) the presence of an extensive data base (Siccama, 1974), (b) the marked vegetational damage symptoms apparent, especially in red spruce (Siccama, et al., 1982; Vogelmann, et al., 1985), and (c) the influx of high levels of air pollutants into the region (Scherbatskoy and Bliss, 1984). In addition, Mount Ascutney, located in the Taconic Mountains of southeastern Vermont, and sites in Ripton, Vermont were included in the study.

The overall objective of this study is to correlate various levels of forest decline (presumably caused or exacerbated by the influx of pollutants into the high elevation ecosystem) with remote sensing data. Some specific goals are as follows: (a) determine what levels of forest

damage can be detected using spectral data; (b) determine which remote sensing systems are most useful/appropriate for continuing study of the problem; (c) determine the feasibility of using remote sensing to monitor forests through time, and d) determine if spectral data will provide insight into the nature of the forest decline (e.g. heavy metal stress, water stress).

## MATERIALS AND METHODS

**Study Sites:** A total of 12 spruce stands, including seven from Camels Hump Mountain, three from Mount Ascutney, and two from Ripton are included in this study. These represent a gradient from low to high levels of damage. A "high damage" site and a "medium damage" site on Camels Hump and a "low damage" site from Ripton were selected for more extensive study using Scholander pressure bombs and portable field spectrometers and radiometers.

**Damage Level Evaluation:** Percentage red spruce and balsam fir damage and mortality estimates were calculated separately at each site. Damage estimates were based upon the amount of red spruce foliar damage (i.e. percentage of needles missing from the live crown) visually apparent.

**Field Measurements:** Field spectral data were acquired from clipped sunlit branches with needles from a high damage site and a low damage site using the Visible/Infrared Intelligent Spectrometer (VIRIS). This is a high spectral resolution sensor with spectral coverage from 0.4 to 2.5 microns. Simultaneous with field spectral data acquisition, xylem water column tension was measured using Scholander pressure bombs.

**Aircraft Data Collection:** The sensors onboard the C-130 included the JPL Airborne Imaging Spectrometer (AIS), the NS-001 Thematic Mapper Simulator (TMS) and aerial photographic cameras. Study sites on Camels Hump Mountain and Mount Ascutney were flown on August 17, 1984 about 4.8 km above the ground. Sites were reflown on September 8, 1984 due to a malfunction of the AIS instrument during the earlier overflight. AIS data were acquired using the "tree mode" with spectral coverage ranging from approximately 0.9 to 2.1 microns.

On August 17, 1984, a Bell UH-1B Iroquois helicopter was used to collect spectral data over four sites on Camels Hump. The instrument package onboard included a Spectron Engineering spectrometer (SE-590), a Barnes Model 12-1000 MMR radiometer, and various cameras.

See Rock, et al. (1985) for more discussion regarding the above procedures/instrumentation.

## RESULTS AND DISCUSSION

**Damage Level Evaluation:** Spruce stands showed marked differences in levels of foliar damage (see Rock, et al., 1985, for numerical estimates of damage). At Camels Hump, percentage mortality closely paralleled damage values, ranging from 0.6 to 31.1%. The damage levels for the Camels Hump sites are highly correlated with elevation ( $r^2=0.90$ ), with the most damaged sites located at relatively high elevations, and the least damaged sites located at relatively low elevations.

Balsam fir damage also showed marked differences in levels of damage (see Rock, et al., 1985). There is a good correlation between fir damage and spruce damage ( $r^2=0.88$ )--those sites with the highest spruce damage values also have the highest fir damage values; those sites with the lowest spruce damage values also have the lowest fir damage values.

Spectral Data: VIRIS and SE590: Field spectral curves from representative spruce samples from high and low damage sites (acquired by the VIRIS) indicate the following: 1) A slightly reduced absorption at approximately 0.68 microns characterizes spectral curves from the high damage site. 2) The chlorophyll absorption maximum located at about 0.67 to 0.68 microns is at a slightly shorter wavelength for the high damage site (i.e., the "blue shift"). 3) Spectra from the high damage site have a reduced reflectance along the NIR plateau. 4) Ratios of the amplitudes of spectral reflectance maxima between near 1.26 and 1.65 microns are different for the two sites (see below).

Helicopter SE-590 data from a high damage site and a medium damage site independently confirmed the reduced absorption and the "blue shift" of the chlorophyll absorption feature at 0.68 microns for vegetation at the more highly damaged site. However, in contrast to the field spectral data, helicopter-acquired spectra from the more highly damaged site had an increased reflectance along the NIR plateau. This apparent discrepancy is thought to be a function of the increased presence of highly reflective broadleaved species which invade the high damage sites as the canopy becomes more open.

The above information indicates that broad-band sensors such as TM/TMS are most appropriate for detecting certain vegetative spectral differences between sites of different damage levels. However, high spectral resolution sensors such as AVIRIS will be needed to detect the subtle shift to shorter wavelengths in the chlorophyll absorption feature (0.68 microns) in stressed vegetation.

IMS Data--Use in Estimation of Water Stress: The relative heights of spectral reflectance maxima near 1.26 and 1.65 microns provide an accurate indication of leaf water content (Rohde and Olson, 1971; Goetz, et al., 1983). The ratio of the the 1.65 micron reflectance divided by the 1.26 micron reflectance is herein referred to as the Moisture Stress Index (MSI). As vegetation dries, this ratio increases and approaches 1.0.

NS-001 TMS bands 6 and 5 contain the 1.65 and 1.26 micron regions, respectively. Thus, TMS 6/5 ratios are the broad-band equivalent of the MSI ratios. TMS 6/5 ratios were obtained from approximately 100 pixels at each of the seven Camels Hump sites using the September data set. Suspected rocky and/or deciduous areas were excluded from this analysis, such that comparisons are among mostly coniferous areas. Results from this analysis indicate that TMS 6/5 ratios correlate well with site damage values ( $r^2=0.90$ --as damage increases, site 6/5 ratios also increase (see Figure 1)).

AIS Data Analysis: AIS data were acquired from four study sites from Camels Hump and two from Mount Ascutney. As expected, spectra from coniferous areas had markedly lower DN values than those from deciduous areas (see Figure 2). No obvious spectral differences were seen between high damage and low damage sites. Attempts to atmospherically

correct the data using a program developed by Jerry Solomon (JPL) did not appear to work since it dramatically decreased the already low coniferous DN values such that interpretation of spectra became difficult.

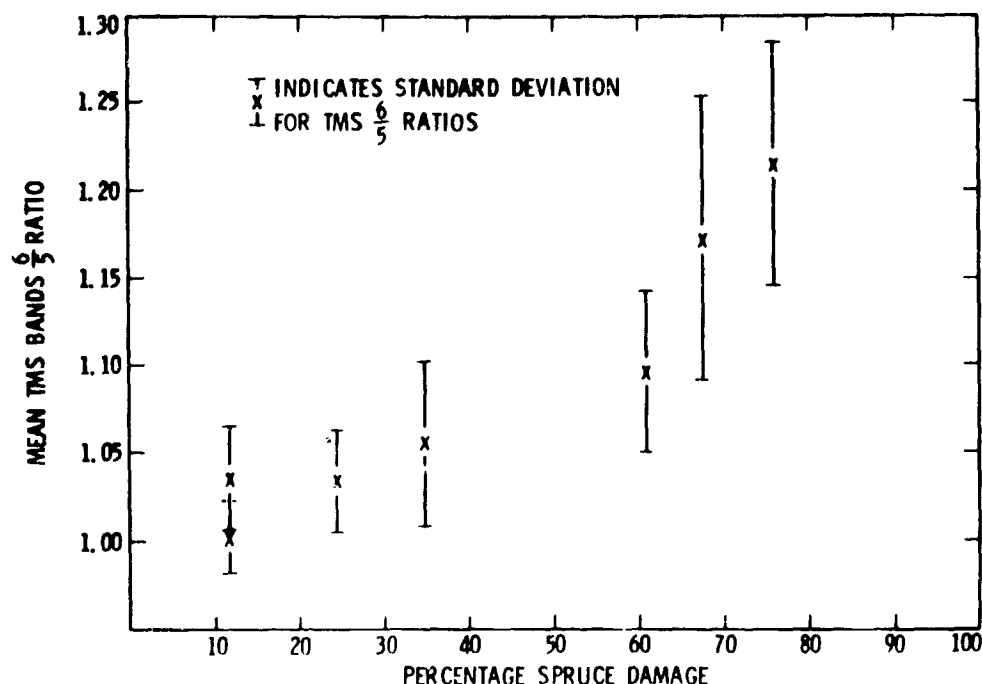


Figure 1. Red spruce damage versus ratios of TMS bands 6/5 for seven sites on Camels Hump Mountain, Vermont.

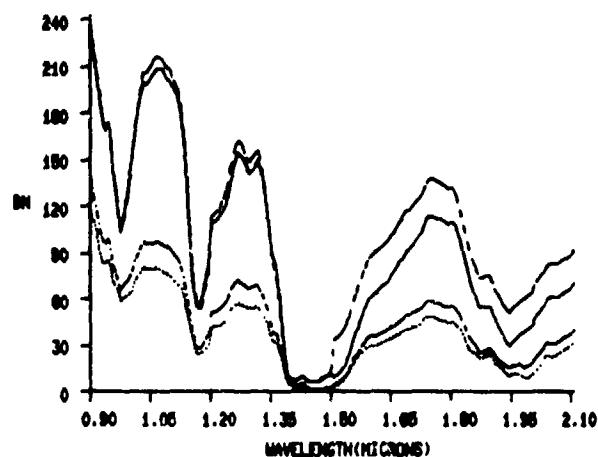


Figure 2. AIS spectra for deciduous areas (top two spectra) versus coniferous areas (bottom two spectra) from Camels Hump Mountain, Vermont. Each spectrum represents an average of 400 pixels.

Using AIS data, MSI values were calculated from spectra of 2x2 pixels from each study site. Results from the four Camels Hump sites were compared with site damage levels and TMS 6/5 ratios (Table 1). The site with the lowest TMS 6/5 ratio (i.e., the one showing the least amount of water stress) also has the lowest MSI value. Similarly, the

site with the highest TMS 6/5 ratio (i.e., the one showing the highest amount of water stress) also has the highest MSI value. However, the two sites with medium low and medium high TMS 6/5 ratios (Camels Hump 2 and 5, respectively) have very similar MSI values. Thus, there is some, but not complete agreement between TMS and AIS results.

Table 1. Comparison of forest damage, TMS 6/5 ratios, and AIS 1.65 micron/1.26 micron (MSI) ratios for four sites from Camels Hump Mountain, Vermont.

SITE	PERCENTAGE SPRUCE DAMAGE	RATIO OF TMS BANDS 6/5	RATIO OF AIS 1.65 $\mu$ m PEAK DN / 1.26 $\mu$ m PEAK DN
CAMELS HUMP 1	11.8	1.004 $\pm$ 0.022	0.787 $\pm$ 0.059
CAMELS HUMP 2	11.9	1.036 $\pm$ 0.030	0.819 $\pm$ 0.040
CAMELS HUMP 5	61.2	1.097 $\pm$ 0.047	0.815 $\pm$ 0.029
CAMELS HUMP 7	76.0	1.216 $\pm$ 0.069	0.856 $\pm$ 0.049

AIS data were also analysed using a cross-band correlation analysis. This technique is discussed by Vern Vanderbilt elsewhere in these proceedings. No evidence was found for subtle differences existing between high damage and low damage sites using this method. However, it is felt that this approach will have much potential in detecting subtle spectral differences when they exist in future studies, especially when AIS instrument noise problems become mitigated.

#### REFERENCES

- Goetz, A.F.H., Rock, B.N., and Rowan, I.C. 1983. Remote sensing for exploration: an overview. *Economic Geology* 78: 573-590.
- Scherbatskoy, T., and Bliss, M. 1984. Occurrence of acidic rain and cloud water in high elevation ecosystems in the Green Mountains of Vermont: *The Meteorology of Acidic Deposition*. Proceedings of the APCA specialty conference, Oct 16-19, 1983, in press.
- Siccama, T.G. 1974. Vegetation, soil and climate on the Green Mountains of Vermont. *Ecological Monographs* 44: 325-349.
- Siccama, T.G., Bliss, M., and Vogelmann, H.W. 1982. Decline of red spruce in the Green Mountains of Vermont. *Bulletin of the Torrey Botanical Club* 109: 162-168.
- Rock, B.N., Williams, D.L. and Vogelmann, J.E. 1985. Field and airborne spectral characterization of suspected acid deposition damage in red spruce (*Picea rubens*) from Vermont. 11th Symposium on Machine Processing of Remotely Sensed Data, Laboratory for Applications of Remote Sensing, in press.
- Rohde, W.G., and Olson, C.E. Jr. 1971. Estimating foliar moisture from infrared reflectance data. *Third biennial workshop on color aerial photography in the plant sciences*, Falls Church, American Society of Photogrammetry, pp.144-164.
- Vogelmann, H.W., Bliss, M. and Badger, G. 1985. Deterioration of forest ecosystems on Camels Hump, Vermont: submitted to *Bulletin of the Torrey Botanical Club*.

A FIRST LOOK AT AIRBORNE IMAGING SPECTROMETER (AIS) DATA IN AN AREA OF ALTERED VOLCANIC ROCKS AND CARBONATE FORMATIONS, HOT CREEK RANGE, SOUTH CENTRAL NEVADA

SANDRA C. FELDMAN, Mackay School of Mines, University of Nevada, Reno, NV, USA; JAMES V. TARANIK, Mackay School of Mines, University of Nevada, Reno, NV, USA; DAVID A. MOUAT, Department of Applied Earth Sciences, Stanford University, Stanford, CA, USA

ABSTRACT

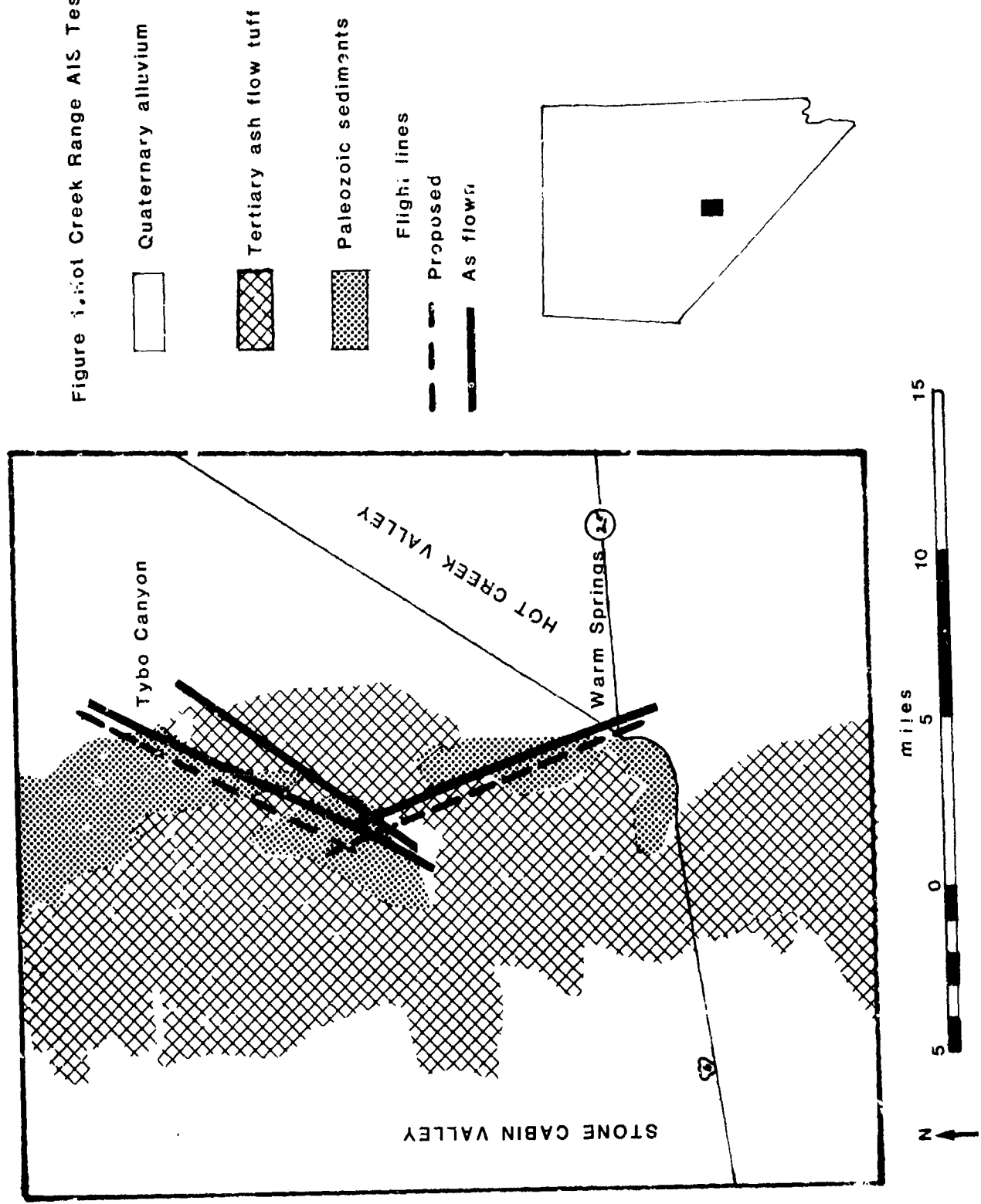
Three flight lines of Airborne Imaging Spectrometer (AIS) data were collected in 128 bands between 1.2 and 2.4  $\mu\text{m}$  in the Hot Creek Range, Nevada on July 25, 1984. The flight lines are underlain by hydrothermally altered and unaltered Paleozoic carbonates and Tertiary rhyolitic to latitic volcanics in the Tybo mining district.

The original project objectives were to discriminate carbonate rocks from other rock types, to distinguish limestone from dolomite, and to discriminate carbonate units from each other using AIS imagery. Because of high cloud cover over the prime carbonate flight line and because of the acquisition of another flight line in altered and unaltered volcanics, the study has been extended to the discrimination of alteration products.

In an area of altered and unaltered rhyolites and latites in Red Rock Canyon, altered and unaltered rock could be discriminated from each other using spectral features in the 1.16 to 2.34  $\mu\text{m}$  range. The altered spectral signatures resembled montmorillonite and kaolinite. Field samples were gathered and the presence of montmorillonite was confirmed by x-ray analysis.

INTRODUCTION

Three flight lines of Airborne Imaging Spectrometer (AIS) data between 1.2 to 2.4  $\mu\text{m}$  wavelengths were acquired in the Hot Creek Range in south central Nevada (Figure 1) from a NASA C-130 aircraft on July 25, 1984 at an average of 19,000 feet above mean terrain. Thematic Mapper Simulator (NS001) imagery, Nikon black and white photographs, and Zeiss color photographs were collected simultaneously. The proposed flight lines are shown as dashed lines in Figure 1 and the actual flight lines are shown as solid lines. The flight lines were designed to include as many different carbonate formations as possible. Four limestone formations, three dolomite formations, two shale/argillite formations, one quartzite, one siltstone and three volcanic units ranging in composition from rhyolite to dacite were represented on the proposed flight lines. The primary objective was to use the AIS imagery to discriminate between carbonate units and other rock types, to distinguish limestone from dolomite, and limestone formations from each other.



## GEOLOGY OF THE HOT CREEK AIS SITE

In the southern Hot Creek Range approximately 7,500 feet of Paleozoic marine carbonates, sandstones and shales are overlain by 15,000 feet of Tertiary volcanics and volcanoclastics. Seventy-five percent of the Paleozoic section consists of carbonates (Cook, 1966; Quinlivan and Rogers, 1974). During the Devonian-Mississippian Antler orogeny, western assemblage eugeosynclinal rocks were thrust over eastern assemblage miogeosynclinal carbonates and clastics.

The major structural elements of the Hot Creek Range were formed in Cenozoic time and they consist of a broad anticlinal arch and normal faults. Normal faulting occurred concurrent with, and subsequent to, the eruption of large volumes of rhyolitic ash flow tuffs and minor amounts of intermediate lava.

The Cenozoic normal faulting has juxtaposed Paleozoic structural blocks adjacent to each other and to the Tertiary volcanics, and this juxtaposition enables the collection of AIS imagery over many of the carbonate and volcanic units in a short flight distance.

The project area is located in the Tybo mining district, a large producer of silver, lead, gold and zinc prior to 1940 (Kleinhampl and Ziony, 1984) with Paleozoic carbonates being the primary host rocks for mineralization. Alteration has locally affected both the carbonates and the volcanics. The carbonate units have been dolomitized, silicified and stained by ferric iron minerals, while the volcanics have been subject to bleaching, silicification and argillic and propylitic alteration.

## AIS AND ANCILLIARY DATA DESCRIPTION, QUALITY AND ANALYSIS PROCEDURE

The proposed AIS flight lines (Figure 1) were designed to include as many Paleozoic carbonate formations as possible, with the highest concentration of carbonate units on the proposed northern line which extends from Tybo Canyon to Rawhide Mountain.

As flown, one northern line passes over almost entirely altered and unaltered volcanics and is cloud-free. The second northern line which passes over a high concentration of carbonate units contains 25% cloud cover and cloud shadows. The southern AIS flight line as flown, extends from just east of Rawhide Mountain southeast to Warm Springs and contains 17% cloud and cloud shadow cover. It passes over Tertiary volcanics, Paleozoic clastic units and some carbonates. Taking into consideration the change in the location of the flight lines and the weather conditions, it was decided to extend the Hot Creek AIS study to include alteration in both volcanics and carbonates in addition to discriminating between carbonate formations.

Thematic Mapper Simulator (TMS) data tapes were analyzed on a VAX/IDIMS system to locate areas of alteration as well as to enhance carbonate formations prior to processing the AIS tapes.

On July 25, 1984 at 1300 hours, 128 bands of AIS imagery in the Hot Creek Range were collected in the scan mode by the sensor over four grating positions. The calibrated wavelength range was 1.16 to 2.34  $\mu\text{m}$  and the band width was approximately 9 nm. Flight lines average about 19,000 feet (5.8 km) above mean terrain; AIS swath width is 1200 feet (370 m); and ground instantaneous field of view or pixel size is about 38 feet (12 m).

For a first look at AIS imagery and ancillary data, an area of altered rhyolitic and latitic ash flow tuffs in Red Rock Canyon was chosen. The 5x7 Nikon prints taken on the flight and as received from JPL were printed low contrast. We enlarged these to 8x10 and printed them high contrast as suggested by R.J.P. Lyon (personal communication). A mask for the Nikon photos, the width of the flight line (approximately 1200 feet), was produced. The high contrast Nikon enlargements with the mask overlay made it relatively easy to locate position on the AIS imagery when used in conjunction with color aerial photographs.

All 128 AIS bands in the Red Rock Canyon area were examined in strips of 32 by 512 pixels. Raw data and data to which a sun radiance and an atmospheric correction (Solomon, 1984) had been applied, were compared. Both in the raw bands and atmospherically corrected bands, across-track striping is pronounced in the shorter wavelength bands but not in the longer wavelength bands. Along-track striping is prominent in all wavelengths of raw data as a result of uneven detector response. The along-track striping is not present in the atmospherically corrected data and has been removed by the atmospheric correction algorithm.

AIS data were analyzed using SPAM (Spectral Analysis Manager) developed by the Jet Propulsion Laboratory (JPL). Figures 2 and 3 show spectra of the last 32 AIS bands (2.05 to 2.34  $\mu\text{m}$ ) of altered and unaltered rhyolitic and quartz latitic ash flow tuffs from the Red Rock Canyon area. The spectra in Figure 2 are not atmospherically corrected while those in Figure 3 are. An absorption feature near 2.2  $\mu\text{m}$  can be seen in the spectra of altered volcanics and becomes much more distinctive after the atmospheric correction has been applied.

A SPAM unsupervised classification function called FIND PLOT searches for pixels with spectra in all 128 bands similar to those of a specified pixel and color codes all such similar pixels on the image. When FIND PLOT is applied to raw AIS data and asked to find pixels similar to those in altered or unaltered rhyolite, the result is colored bands coincident with the along track striping previously discussed. This implies that there is greater similarity among pixels from individual detectors than among pixels from similar geologic entities. However, when the FIND PLOT function is applied to atmospherically corrected AIS data, a correct classification of altered and unaltered volcanics results.

Since altered volcanics can be distinguished from unaltered volcanics in Red Rock Canyon, SPAM library spectra of different minerals with absorptions near 2.2  $\mu\text{m}$  were compared with altered rock spectra (Figure 4) and field and laboratory data were gathered. Some AIS spectra in the 2.2  $\mu\text{m}$  region had signatures that resembled kaolinite and others had signatures that resembled montmorillonite. Although AIS spectra were examined over the entire altered area, only a limited number of samples of altered and unaltered rock along the AIS flight line were collected, examined and x-rayed. A location which appeared to consist of unaltered rock on AIS imagery proved to be a densely welded tuff composed of quartz, plagioclase, K-feldspar and biotite. From x-ray analysis, one sample from the altered area consisted of pure montmorillonite and two others proved to contain the same minerals as the unaltered tuff with the addition of some montmorillonite.

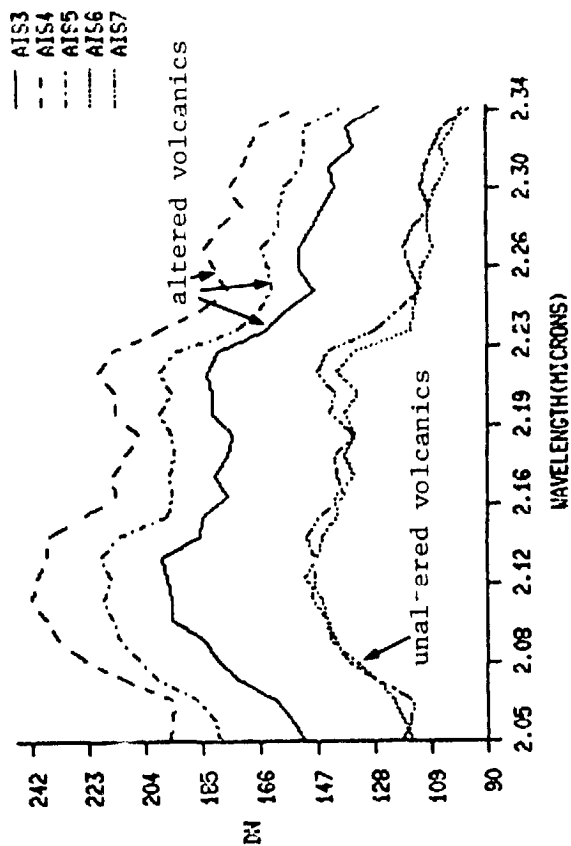


Figure 2. AIS spectra without atmospheric correction.

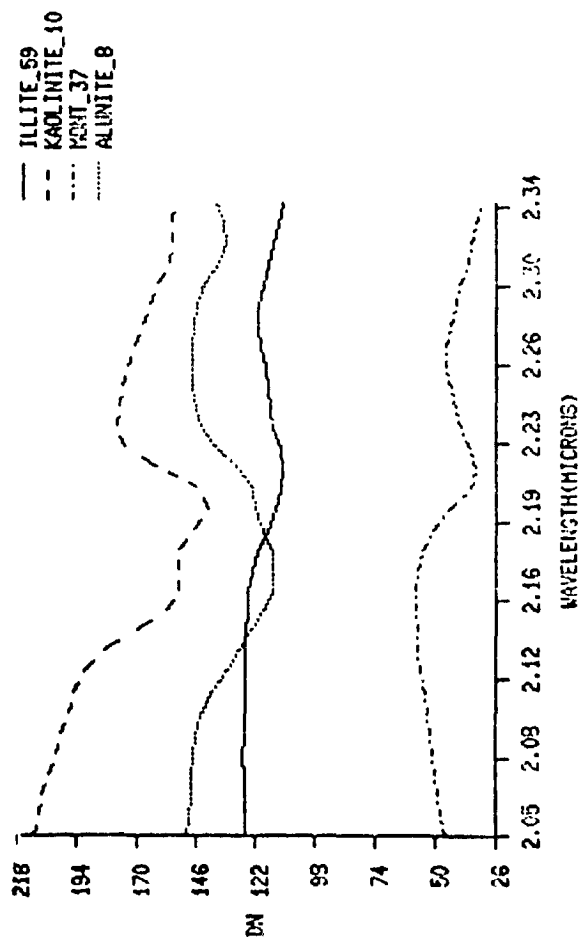
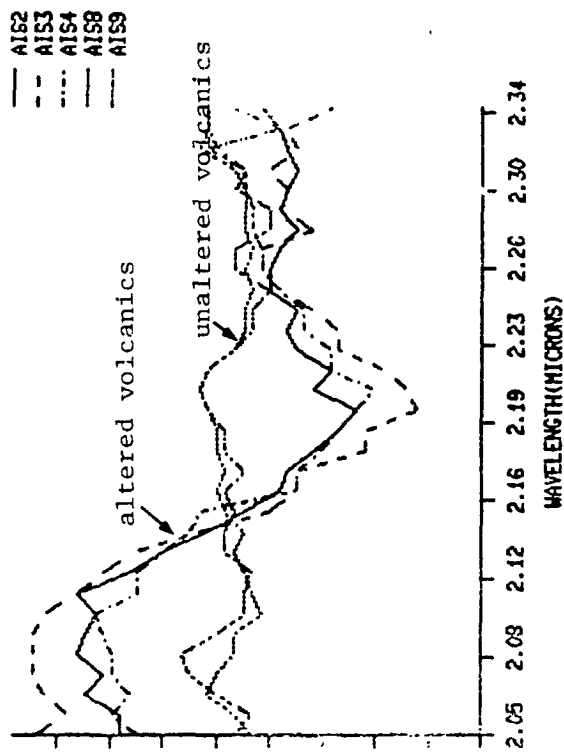


Figure 3. AIS spectra with atmospheric correction.



## CONCLUSION

AIS spectra of altered and unaltered ash flow tuffs, with and without atmospheric corrections applied, have been examined in the Red Rock Canyon area. It was possible to distinguish unaltered volcanics from altered volcanic rock with AIS spectra. Based on comparison with library spectra, montmorillonite and kaolinite could be present and montmorillonite was found to be present from x-ray analysis.

Flight lines as flown, as compared to flight proposed, contain a lower concentration of carbonate units than expected because of high cloud cover. The Hot Creek AIS study has therefore been extended to include hydrothermal alteration as well as carbonate formations.

Over the next two years we look forward to more detailed studies dealing with both carbonate formations and altered rock in the Hot Creek Range using AIS imagery.

## REFERENCES

- Cook, H.E. 1966. Geology of the southern part of the Hot Creek Range, Nevada. Unpubl. Ph.D. dissertation, University of California, Berkeley, 115 p.
- Kleinhampl, F.J., and Ziony, J.I. 1984. Mineral resources of northern Nye County, Nevada. Nevada Bureau of Mines and Geology, Bull. 998, 243 p.
- Quinlivan, W.D., and Rogers, C.L. 1974. Geologic map of the Tybo quadrangle, Nye County, Nevada. U.S. Geological Survey, Misc. Invest. Map I-821.
- Solomon, J. 1984. Some thoughts on atmospheric "corrections" for AIS imagery. JPL Interoffice Memorandum.
- Vane, G., Goetz, A.F.H., and Wellman, J.B. 1983. Airborne Imaging Spectrometer: A new tool for remote sensing. Proc. 1983 Int'l Geoscience and Remote Sensing Symposium, 5 p.

INTERPRETATION OF AIS IMAGES OF CUPRITE, NEVADA USING CONSTRAINTS  
OF SPECTRAL MIXTURES

N86-11626

Milton O. Smith and John B. Adams  
Department of Geological Sciences  
University of Washington, Seattle, WA. 98195

ABSTRACT

A technique is outlined that tests the hypothesis that AIS image spectra are produced by mixtures of surface materials. This technique allows separation of AIS images into concentration images of spectral endmembers (e.g., surface materials causing spectral variation). Using a spectral reference library it was possible to uniquely identify these spectral endmembers with respect to the reference library and to calibrate the AIS images.

INTRODUCTION

A primary objective for interpretation of multispectral images is to identify the direct physical factors causing spectral variation on the ground. We demonstrate in this paper that a spectral mixture model makes possible the identification of image spectra, assuming that there is a linear relationship between image spectra and a library of reference spectra. Modeling spectral mixtures reduces the dimensionality of the spectral data and leads to inferences regarding the spatial interrelation of spectral classes that have been delineated using conventional classification techniques.

Two AIS image scenes from Cuprite, Nevada were analyzed against a reference library of laboratory spectra. The first image is from August 1983 (RUN ID101) and the second July 1984 (RUN ID403). All analyses were limited to the wavelength range of 2.1  $\mu\text{m}$  to 2.4  $\mu\text{m}$  comprising 32 spectral channels. The reference library spectra were obtained from field samples collected from the Cuprite area. They included a variety of altered rhyolites containing opaline silica, kaolinite, and alunite, and samples of soils, playa, desert varnish, and green and dry vegetation. The laboratory spectra were taken using a Beckman DK2-A spectrophotometer.

An initial objective of our analysis was to determine the spectral endmembers and their abundances among the laboratory samples, using the method described by Smith *et al.* (1985). The endmembers are defined as those spectra from the reference library that when linearly combined (linear mixture model) can form all other spectra. Endmembers must have an abundance of 1 and the computed endmember abundances for all other spectra must be between 0 and 1. Based on the eigenvalues of spectra in the 2.1 to 2.4  $\mu\text{m}$  region there are six potential endmembers among the Cuprite samples: opaline silica, desert varnish, alunite, kaolinite, and playa, and green vegetation. A plot of the transformed spectra by the two primary eigenvectors is depicted in Fig. 1. These plots indicate the compositional trends for the reference samples. A major objective is to determine to what extent the variation observed in the reference spectra is present in the image spectra.

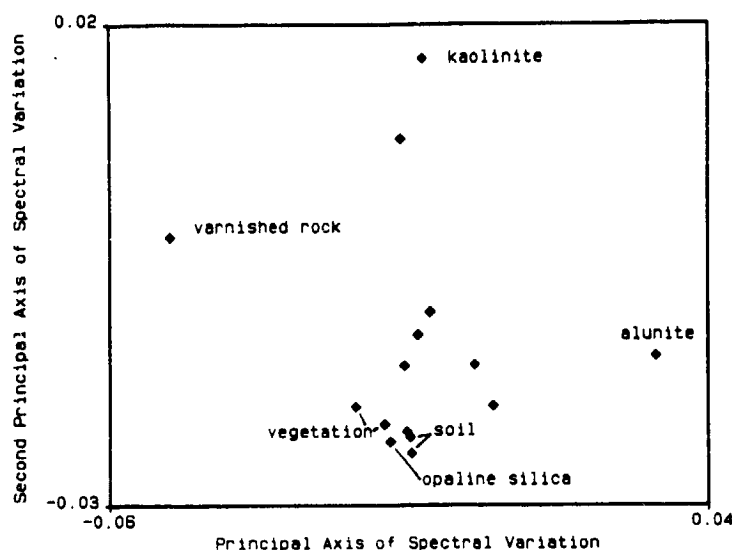


Fig. 1. The linear transformation of laboratory spectra of field samples onto the first two principal axes of variation. Prospective endmember spectra are those nearest the outside boundaries.

#### COMPARISONS OF NORMALIZED SPECTRA

For the image spectra we also determine how many endmembers are required to predict all other image spectra given the previously stated constraints. However, unlike the laboratory spectra, the image spectra include variation from the surface orientation, atmospheric absorption, etc. Thus, some of the endmember spectra resolved from the image may represent factors that are not associated with mixing of the spectra of the surface materials. Three unknown spectral endmembers were found for the 32 wavelength bands of 2.1 to 2.4  $\mu\text{m}$  using the calibrated energy normalized image of August 1983. Here, normalized spectra are computed by dividing each reflectance by the sum of the reflectances over the wavelength interval of analysis. Mixtures of these image-derived endmembers model all image spectra to nearly within the instrumental error. Further comparisons need only consider these endmember spectra and their uniqueness in causing the observed spectral variation. To compare the image spectra with the reference spectra it is necessary to calibrate the image data.

To first order, we select a linear model that maps flux density measurements of the surface to reflectance measurements from a laboratory spectrophotometer, i.e.,

$$G_b (DN_b + A_b) = \sum_{i=1}^n (f_n R_{nb}) \quad (1)$$

where  $G_b$  is the gain for band  $b$ ,  $A_b$  the offset for band  $b$ ,  $DN_b$  is the image brightness value for band  $b$ ,  $f_n$  the fraction of endmember  $n$ , and  $R_{nb}$  the reflectance of endmember  $n$  for band  $b$ . The  $G_b$ 's can be different for each wavelength band. If the image is correctly calibrated the  $G_b$  coefficients can be reduced to one by normalizing both image and reference spectra by the sum of flux densities or reflectances over the

32 wavelengths. Using the 32 channels from 2.1  $\mu\text{m}$  to 2.4  $\mu\text{m}$  of Cuprite (August, 1983 image) an optimal solution of spectral mixtures providing correspondence in spectral variation between the image and the reference library was determined to include alunite, kaolinite, and playa silt. Using normalized spectra we could not differentiate between the playa silt, opaline silica, or vegetation in the 2.1 to 2.4  $\mu\text{m}$  range.

The use of normalized spectra with a simple calibration model does support the hypothesis that image spectra are produced by mixtures of surface materials. The disadvantages of this approach are that if the attenuations are poorly corrected due to instrument-calibration errors and/or atmospheric uncertainties, then solutions based on the spectral library may be wrong. Also, much of the spectral variation is lost from normalizing the spectra by whatever method, and thus may result in more than a single physical explanation (i.e., reduce the uniqueness) of the source of spectral variation. Optimally, it is desired to have a technique that validates the atmospheric corrections and instrumental calibration assumptions as well as providing a unique solution to the source of spectral variation.

#### ABSOLUTE SPECTRAL COMPARISONS CALIBRATED TO TWO OR MORE REFERENCE AREAS

Given laboratory measurements of representative samples, the gains and offsets expressed in Equation 1 could be calculated directly by hypothesizing analogous image and laboratory spectra. This requires that pixels exist in the image that encompass spectrally pure and homogeneous areas on the ground (training areas) and that such spectra also exist in the reference library. To determine the gains in Equation 1, we perform a linear search of the reference library solving for the attenuations ( $G_p$ ) for each spectrum. For a given mixture model of  $n$  spectral endmembers in an image, the validity of the attenuations is determined from the compositional abundances and rms errors and should ideally appear as in Table 1. Note that at this point we introduce illumination intensity (shade) as a spectral endmember (Adams *et al.*, 1985).

Table 1. The optimal pattern of reference and library endmember abundances if the calculated attenuations ( $G_p$ ) are valid.

Abundance of Reference Spectra	Abundances of Image		Endmember: Illumination	rms error
	Spectrum A	Spectrum B	Intensity	
Sample A	1.0	0.0	0 - 1	0
Sample B	0.0	1.0	0 - 1	0
Sample C . . .	0 - 1	0 - 1	0 - 1	0

For the July, 1984 uncalibrated AIS image two training areas were selected representing a fan containing varnished rhyolites (varnished spectrum) and "kaolinite hill" (kaolinite spectrum). Searching the spectral reference library for the optimum calibration, as defined above, resulted in a single solution (Table 2) that matches the above matrix pattern. The search through the reference library included

140 reference spectra of minerals and vegetation in addition to the spectra of samples collected from Cuprite. Abundances that are less than zero and greater than one indicate spectral variation that is greater than that of the sample for which the attenuation coefficients were computed. The model could be changed to incorporate the reference spectrum endmember having the greatest degree of variance, which would result in all positive fractions with values between zero and one, similar to the ideal pattern of Table 1.

Table 2. An Optimal mixture model fit of the Cuprite, Nevada (July, 1984) uncalibrated AIS image. This model provided the best fit for the major source of spectral variation in the image.

Abundance of Reference Spectra	Abundance of Image Spectra: Illumination			rms error
	Varnished	Kaolinite	Intensity	
Varnished Rhyolite #1	1.0	0.0	0.0	0.00
Kaolinite #2	0.0	0.6	0.4	0.01
Kaolinite #1	0.0	0.9	0.1	0.02
Varnished Rhyolite #3	1.6	-0.4	-0.2	0.01
Varnished Rhyolite #2	1.1	0.2	-0.3	0.02

Unlike the example using normalized spectra, the above procedure provides a means of calibrating an image absolutely with respect to illumination intensity, and thus resolves the effects due to both surface orientation and self-shading of surface materials. The illumination intensity is a spectral endmember analogous to the endmembers of the surface materials. An image of the illumination intensity provides qualitative evidence of the validity of the model by depicting topographical features. From this calibration, it was possible to determine that the albedo of the most likely spectral reference endmember was associated with the playa silt. The opaline silica and vegetation spectra that were similar to the playa when normalized are distinct and separable when spectral variation due to illumination intensity was removed and comparisons made on non-normalized spectra.

Vertical striping occurred in the endmember abundance images, and is a result of assuming that all vertical lines had equal attenuation coefficients ( $G_b$ ). This is true to a first approximation, but for extraction of the minor absorption features characteristic of minerals such as alunite and kaolinite these differences in gain must be exact. The presence of the vertical striping indicates the calibration proposed by Equation 1 is not valid in the case of the AIS images, where each vertical line can have a different gain and offset as well as each wavelength band.

#### ABSOLUTE SPECTRAL COMPARISONS CALIBRATED TO MIXTURES OF ENDMEMBERS

Reference (training) areas of spectrally pure materials do not always exist on the pixel scale in an image. More typically all pixels contain spectral mixtures. A more generalized approach requires only that the mixture space in the spectral library exist in the image. For

the simple case of two mixture components in an image the following equations are applicable:

$$G_s G_b DN_{e1b} = f_{1a} R_{e1b} + (1 - f_{1a}) R_{e2b} \quad (2)$$

$$G_b DN_{e2} = f_{1b} R_{e1b} + (1 - f_{1b}) R_{e2b} \quad (3)$$

$G_b$  is the gain for band b,  $G_s$  a gain due to differential illumination of the image endmembers,  $DN_{e1b}$  and  $DN_{e2b}$  are the 16-bit image brightness values for two spectral endmembers e1 and e2 in the raw data AIS image,  $f_{1a}$  and  $f_{1b}$  are the fractions of reference spectra that mix to form the image spectra, and  $R_{e2}$  and  $R_{e1}$  are the library reflectances of two reference spectra at band b. Our objective is to identify those combinations of spectra in the reference library that provide a solution to the fractions in Equations 2 and 3 and to determine how unique the solution is with respect to the reference library. The example is based on two spectra for simplicity; however, multiple spectra were actually used. By algebraic manipulation of Equations 2 and 3, one can solve for the mineral abundances ( $f_{1a}$  and  $f_{1b}$ ) independent of the gains  $G_b$ . Since the fractions should be constant at each wavelength for a given mixture of materials, the 32 wavelength bands from the AIS image allow a least squares fit (or coefficient of variation) to be determined for each fraction from any combination of two library reference spectra. By searching the spectral library using all combinations of two spectra in the reference library we can rank solutions by their fit to all 32 bands. For the Cuprite images this search procedure also led to the spectra of kaolinite and varnished rhyolite.

It is also possible to use Equations 2 and 3 to test the assumption that the calibration gains and offsets are spatially equal as well as to compute them. In the previous example we found that this assumption was not valid. Spatial gains and offsets can be calculated by identifying the spectral endmembers in each line independently. For an image with two spectral endmembers Equations 2 and 3 can then be applied to solve for the gains  $G_b$  between each line rather than between the image and the reference library. It is not necessary that all endmembers be represented in the image spectra from line to line, but at least two of the endmembers must be present.

## CONCLUSIONS

We have demonstrated an approach using spectral mixture models and a spectral reference library that identifies the origin of spectral variation in AIS images. To make use of the spectral library it was necessary to separate the effects of spectral variation in the image that were not due to surface materials, e.g., illumination intensity, atmospheric attenuation, and instrument calibration. The Cuprite image was modeled successfully as spectral playa silt, kaolinite, alunite, and shade. These materials form spectral endmembers in the 2.1 to 2.4  $\mu m$  range, whereas other samples are spectral endmembers in other wavelength regions (e.g., green vegetation in the 0.4 to 1.1  $\mu m$  range).

The alignment of image and reference library spectral endmembers provides evidence that linear spectral mixtures are applicable to organizing the high spectral-spatial resolution of AIS images. The inverted approach to calibration presented here does not rely on

statistical assumptions or local parameter uncertainties in removing effects due to atmospheric attenuation and instrumental calibration, and so provides an independent test on the applied calibrations.

#### REFERENCES

- Adams, J. B., M. O. Smith, and P. E. Johnson, Viking Lander 1: A new map of rock and soil types, Abst. Proc. Lunar Planet. Sci. Conf. 16th.
- Smith, M. O., P. E. Johnson, and J. B. Adams, Quantitative determination of mineral types and abundances from reflectance spectra using principal components analysis, Proc. Lunar Planet. Sci. Conf. 15th, C797-C804, 1985.

## EVALUATION OF AIS DATA FOR AGRONOMIC AND RANGELAND VEGETATION: PRELIMINARY RESULTS FOR AUGUST 1984 FLIGHT OVER NEBRASKA SANDHILLS AGRICULTURAL LABORATORY

BLAINE L. BLAD, PATRICK J. STARKS, CYNTHIA HAYS, University of Nebraska, Lincoln, Nebraska, USA; BRONSON R. GARDNER, Standard Oil of Ohio, Cleveland, Ohio, USA

### ABSTRACT

Since 1978 scientists from the Center for Agricultural Meteorology and Climatology at the University of Nebraska have been conducting research at the Sandhills Agricultural Laboratory on the effects of water stress on crop growth, development and yield using remote sensing techniques. We have been working to develop techniques, both remote and ground-based, to monitor water stress, phenological development, leaf area, phytomass production and grain yields of corn, soybeans and sorghum. Because of the sandy soils and relatively low rainfall at the site it is an excellent location to study water stress without the necessity of installing expensive rainout shelters.

The primary objectives of our research with the AIS data collected during an August 1984 flight over the Sandhills Agricultural Laboratory are to evaluate the potential of using AIS to: (a) discriminate crop type; (b) to detect subtle architectural differences that exist among different cultivars or hybrids of agronomic crops; (c) to detect and quantify, if possible, the level of water stress imposed on the crops; and (d) to evaluate leaf area and biomass differences for different crops.

### MATERIALS AND METHODS

AIS data were collected at approximately 1500 h solar time on August 7, 1984. In 1984 we conducted experiments on several different agronomic crops including six different corn hybrids, some of which were architecturally quite different. Other vegetative surfaces included soybeans, alfalfa, corn grass (corn planted into grass rather than bare soil), rangeland and a recently harvested oat field.

Different water stress levels were achieved by means of sprinkler irrigation. At various times during the growing season moderate to severe levels of water stress were established on some plots. Unfortunately, about 1.2 cm of rain were received the night preceding the AIS flight so only minor differences in water stress levels between the different plots were present at the time of the overflight.

After narrowing the AIS data to include only that portion of the AIS data set in the general vicinity of the research plots, frequency distribution curves were obtained for each AIS channel. Two types of frequency distribution curves were observed--one was single peaked and the other showed a bimodal distribution. Gray maps were produced using a channel representing each curve type. The gray map produced with the bimodal type curve was much more useful than the single peaked curve in pinpointing the locations of the various plots. Some difficulty due

in large measure to an adjustment in the flight path over the plots, was encountered in locating the plots on the gray map.

Once the research plots and surrounding features were identified from the gray map, 10 pixels from each of six different vegetation types on the imagery were selected for the discriminant analysis procedures. Also one pixel from each vegetation type was selected to produce spectral curves. The data reported on here were not calibrated except for making the radiometric corrections.

In our study we attempted to discriminate between the six vegetative types using data from the 128 AIS channels as the discriminating variables. We first used all 128 channels of data via the direct method, i.e., all variables were tested to meet a default tolerance test. Those variables which met the requirements were then used in the construction of discriminant functions to classify each of the six groups. Next we used the direct discriminant analysis procedure on each group of 32 channels (i.e., 1-32, 33-64, 65-97 and 98-128). Lastly, we employed a stepwise discriminant analysis procedure which selects independent variables for entry into the analysis based on their discriminating power (Kleeka, 1975). Of the five selection criteria available we selected the Wilk's method. This method employs the overall multivariate F ratio for the test of differences among group centroids. The variable which maximizes the smallest F ratio between pairs of groups also minimizes the Wilk's lambda, a measure of the group discrimination (Kleeka, 1975).

## RESULTS AND DISCUSSION

An examination of the spectral curves for the different vegetative surfaces suggests the following: (1) The curves for the corn - corn grass are almost identical in shape and magnitude except that the corn grass shows slightly higher reflectance in the 1160-1307 nm range and some variability in the shape of the two curves in the region from about 1600-1710 nm. (2) The reflectance from corn was slightly less than for soybeans or alfalfa for almost all channels. Some features in the curves of the three crops between 1185 and 1310 nm and from 1605 to 1775 nm suggest that fine spectral resolution data in these regions may be useful in discriminating between these three crops. (3) The magnitude of the reflectance from the oat stubble is consistently higher than from any other surface throughout the entire range of the AIS. This may result from a greater contribution of soil reflectance due to reduced vegetative cover. High reflectance from this soil in TM5 and TM7 has been previously observed. (4) Compared to the corn the magnitude of the reflectance from the rangeland in the wavebands from 1150 to 1310 nm is less but from 1450-1760 nm and from 2000-2340 nm it is higher. Features of the curves in the 1185-1310 and 1605-1710 nm regions of the spectrum should be examined in greater detail for their use in discriminating rangeland and oat stubble from corn.

To this point, we have only been able to analyze the AIS data to meet objective (a). Future analysis is planned to meet the remaining objectives. For the discriminant analysis procedure using all 128 AIS channels we found that channels 1-50, 53 and 116 passed the tolerance test. Using the data from these channels we achieved a 100% classification accuracy with good separation of the different vegetative types.

When we used only the first 32 channels we achieved a classification accuracy of about 98% with good separation of all types except for the corn from the corn-grass. With channels 33-64 we had a classification accuracy of 100% and very good type separation. For channels 65-97 we had a classification accuracy of only 72% and all except channels 65, 66, 68, 71, 74 and 83 failed the tolerance test. We achieved a 100% classification accuracy using channels 98-128 but the separation was not particularly good.

Using the stepwise discriminant procedure twenty-six channels were selected to construct the five discriminant functions. The twenty-six channels selected were 2, 8, 9, 16, 23, 25, 30, 32, 34, 36, 42, 44, 49, 51, 61, 62, 63, 64, 65, 91, 99, 102, 113, 116, 117 and 127. The classification accuracy was 100% and the separation between vegetative types was very good--the best of all the procedures.

In conclusion, it should be emphasized that the results of this study are very preliminary and further analysis is required before definitive statements about the true value of AIS data for monitoring agronomic and rangeland vegetation can be made. Nevertheless, the results thus far suggest that AIS data does an excellent job of discriminating between the various types of vegetation examined at this site and that there are some features in certain AIS wavebands that may be useful in discriminating vegetation type.

#### REFERENCE

Kleeka, Wm. R. 1975. Discriminant analysis. In Statistical Package for the Social Science, 2nd Edition. Nie et al. (ed.), McGraw Hill, NY. Chapter 23, pp. 434-467.

SITE DESCRIPTION FOR THE UNIVERSITY OF NEBRASKA'S SANDHILLS  
AGRICULTURAL LABORATORY

B. R. GARDNER, Standard Oil of Ohio, Cleveland, Ohio, USA; BLAINE L.  
BLAD, University of Nebraska, Lincoln, Nebraska, USA

## ABSTRACT

The Sandhills Agricultural Laboratory is operated by the University of Nebraska. The laboratory is located in the south-central part of the Nebraska Sandhills near Tryon, Nebraska (41° 37' N; 100° 50' W). The laboratory is surrounded on the west and south by native rangeland vegetation, on the south by a large field of corn irrigated by a center pivot, and on the east by wheat stubble. This site is appropriate for moisture stress studies since rainfall is almost always inadequate to meet evaporative demands of agricultural crops during most of the growing season and the sandy soils (Valentine fine sand) at the site do not store large quantities of water. Various levels of water stress are achieved through irrigation from solid set sprinklers.

## HISTORICAL SUMMARY

Remote sensing research began at the laboratory in 1978 with a canopy temperature study designed to determine relationships between crop water use, grain yield and canopy temperatures of corn and sorghum. In 1979, a study was conducted to demonstrate the feasibility of using canopy temperatures to schedule irrigation in corn. In 1980 a pilot study was conducted to determine the feasibility of growing soybeans in the Sandhills and to evaluate the use of canopy temperatures in monitoring crop water stress.

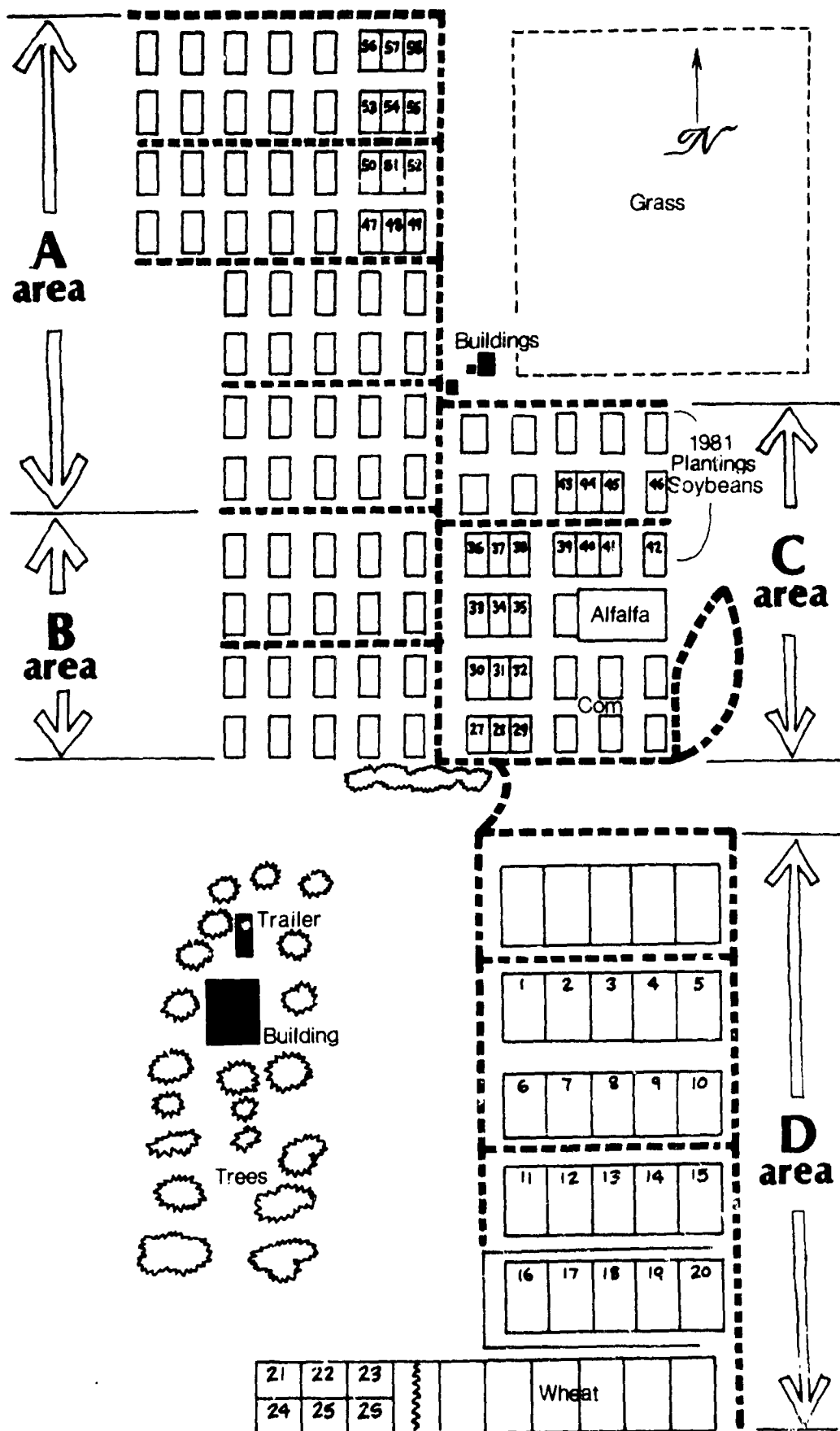
In 1981, the laboratory became involved in AgRISTARS research using the eight-band Barnes radiometer, which simulates the Thematic Mapper wavebands. Experiments have been conducted on corn and soybeans. These experiments have addressed techniques for remote estimates of biomass, leaf area and yields and water stress, canopy geometry and hybrid effects on canopy reflectance. Although the AgRISTARS program no longer exists, research in this area has continued.

The laboratory has been involved in a broad range of agricultural research in addition to its remote sensing efforts. Studies have been conducted on nitrogen levels in corn, corn-grass inter-cropping systems, variety testing, wheat, sorghum and soybean agronomic studies. In addition, studies have been conducted on the inter-actions between irrigation and spider-mite populations. Physiological studies of leaf-water potential, stomatal resistance, photosynthesis and transpiration are also conducted. In short, the laboratory has been the site of a wide range of studies of importance to agricultural scientists.

## 1984 STUDY

The areas of primary interest in 1984 were located in the south portion of the lab, known as D area and in C area (see figure). There were sixty plots used in this study. Each plot measured approximately 18 meters E to W and 9 meters N to S. Twelve plots were planted to soybeans (cultivar, Corosoy). The remaining 48 plots were planted in a completely randomized design to five hybrids of corn. Four of these plots contained a population study of Pioneer 3901, wherein the populations ranged between 15000 and 30000 plants/ha. The remaining 44 plots of corn were planted to Pioneer 3901, B73xMol7, and three experimental hybrids designated: S3, S6 and S12. Two irrigation treatments were used: 1. full irrigation and 2. 33% of full irrigation.

Phenology and plant height measurements were made weekly. Wet and dry weights of leaves, ears and stalks were obtained every two weeks. Canopy temperatures were measured several times weekly between 1400 and 1600 local time. Canopy reflectances were measured in the Thematic Mapper wavebands approximately weekly, or whenever conditions permitted. Diurnal studies of canopy temperature, photosynthesis and stomatal resistance were conducted on selected days. Sixty feet of row were harvested per plot for grain-yield estimates at the end of the season. Soil moisture contents were measured with a neutron probe on a weekly basis. Phenological data were collected at least twice weekly and on a daily basis during the pollination period.



**University of Nebraska  
Sandhills Ag. Lab. Solid Set Irrigation 1982**

N86-11629

PRELIMINARY EVALUATION OF AIS SPECTRA ALONG A TOPOGRAPHIC/MOISTURE  
GRADIENT IN THE NEBRASKA SANDHILLS

DONALD C. RUNDQUIST, Remote Sensing Center, Conservation and Survey  
Division, Institute of Agriculture and Natural Resources, University of  
Nebraska, Lincoln, Nebraska, USA.

ABSTRACT

Six spectral plots, each summarizing single-pixel reflectance for 128 channels of AIS data, were examined. The six sample pixels were located along a topographic/moisture gradient from lake surface to dune top in the Nebraska Sandhills. AIS spectra for various moisture regimes/vegetative zones appear quite logical, with a general positive relationship between increasing elevation (i.e., decreasing access of plant roots to water) and increasing reflectance in the spectral regions diagnostic of leaf-water content (i.e., bands centered on 1.65 and 2.20  $\mu\text{m}$ ).

INTRODUCTION

The importance of moisture content in plant leaves as a factor in spectral reflectance is well known and widely accepted in remote sensing. Close examination of one spectral region, the middle-infrared, underscores the water-content/reflectance relationship since reflectance measurements at 1.65 and 2.20  $\mu\text{m}$  are significantly related to the total amount of water in the leaf and to the leaf-moisture deficit (Myers et al, 1970).

The intent of the present research activity was to provide a cursory evaluation of the utility of AIS spectral data for detecting variations in vegetative water status along a topographic/sub-surface moisture gradient in the Nebraska Sandhills. The availability of water is a primary determinant in the composition of plant communities that cover the sand dunes and inter-dunal valleys (IANR, 1983).

The study area for the research was the Crescent Lake National Wildlife Refuge, Garden County, Nebraska. This 46,000 acre unit is located in the western portion of the Nebraska Sandhills. The landscape consists of sand dunes stabilized, for the most part, by range grasses. Lakes and wetlands are numerous due to a large underground water reserve and minimal depth to that ground water. Many of the lakes in and around the Crescent Refuge are alkaline; summer temperatures exceed 100 degrees F and total annual rainfall is only about 16 inches.

The specific site selected for detailed examination is along a line extending from (and including) the northwestern portion of Gimlet Lake to a dune field beginning approximately one-fourth mile northwest of the lake. Relief from the lake to the dune tops is on the order of 100 feet.

The rationale for the analysis is based upon a simple inverse relationship between the elevation of selected locations along a Sandhills transect and the access of vegetation at those locations to

moisture, whether at the surface or in sub-surface storage. In the Sandhills, the densest, most productive vegetation (by weight) occurs in the shallow lowland marshes and subirrigated meadows while the least productive is found on the dunes (IANR, 1983; Novacek, 1984).

Spectral data were acquired at the Crescent Refuge by the NASA Ames C-130 flight crew on August 6, 1984 for AIS grating positions 1-4. The flight corridor, five miles in length, began over Crescent Lake and terminated about two miles north and west of Gimlet Lake. Ground resolution elements are approximately ten meters on a side. Simultaneous 35mm black-and-white aerial photography, color-infrared aerial photography, and airborne Thematic Mapper digital data were obtained. A small subset of the Sandhills AIS dataset was analyzed for the present research. The dataset received the standard NASA JPL radiometric correction, but was neither calibrated for solar irradiance nor the atmosphere because of the short time span between data receipt and preparation of this preliminary report.

#### ANALYSIS

Six pixels were selected for analysis along the transect described above. Each of these six AIS elements was located within the study site through comparison of the digital dataset with the concurrent aerial photography, 35mm oblique air photos of the area taken during previous projects, on-site ground-level photos, and the relevant USGS map quadrangle (Mumper, Nebraska, 15-minute). Unfortunately, a short lead time prior to the execution of the flight negated in-field vegetation sampling at the time of the mission. However, the on-site characteristics of each sample pixel (from wettest to driest position) can be summarized.

The first element ("lake surface") was comprised of open surficial water, for the most part, although some floating vegetation was present at the time of the AIS data collection and is discernible on the color-infrared photos taken during the mission. The location of the second element ("lake margin") was also offshore, although it was in close proximity to the shoreline. The vegetative mat was relatively thick, as evidenced on the aerial photography, with some emergents associated with floating types. Such a Sandhills location is typified by Cattails (*Typha*), Bulrushes (*Scirpus*), and Reeds (*Phragmites*) (U.S. Department of Agriculture, 1975). The third sample pixel ("shoreline") was located on shore, but very close to the lake proper. Thick emergent vegetation characterizes such a site with Cattails and Bulrushes being colocated with vegetation such as Arrowhead (*Sagittaria*), Smartweed (*Polygonum*), and some Sedges (*Carex*) (U.S. Department of Agriculture, 1975). The location of the fourth element ("lowland meadow") is in a Sandhills subirrigated meadow consisting typically of Sedges plus Prairie Cordgrass (*Spartina*), Reedgrass (*Calamagrostis*), Reed Canarygrass (*Phalaris*), Switchgrass (*Panicum*), some Big Bluestem (*Andropogon*), and various shrubby plants (U.S. Department of Agriculture, 1975; Nichols, 1984). The fifth element ("dune slope") is located on a southeast-facing slope just above the meadow/dune transition. Such a Sandhills range site contains mostly warm-season grasses including Blue Grama (*Bouteloua*), Porcupinegrass (*Stipa*), and Little Bluestem (*Schizachyrium*) (U.S. Fish and Wildlife Service, 1969; Nichols, 1984).

The last element in the transect ("dune top") is located high on a dune and consists of warm-season grasses such as Sand Bluestem (Andropogon), Hairy Grama (Bouteloua), Prairie Sandreed (Calamovilfa), and Soapweed (Yucca) (U.S. Fish and Wildlife Service, 1969; Nichols, 1984).

Three spectral plots along the topographic/moisture gradient are shown as Figures 1-3. As expected, the variations in the curves tend to occur in the three portions of the AIS spectrum separated by the atmospheric water-absorption bands centered on 1.45  $\mu\text{m}$  (Channel 33) and 1.93  $\mu\text{m}$  (Channel 85). Even though some variation in the spectra is apparent in the range from Channel 1 (1150.68 nm) to approximately Channel 20 (1334.9 nm), this area of the spectral plot is not important with regard to the present analysis since spectral response in this region is due primarily to cell structure rather than water content (Hoffer, 1978). However, the spectra centering on 1.65  $\mu\text{m}$  (Channel 54) and 2.20  $\mu\text{m}$  (Channel 113) are significant to the purpose of this research since, as noted earlier, these spectra are diagnostic of water content in the leaf.

Reference to the spectra illustrated as Figures 1-3 allows for some preliminary inferences. The "flat" curve associated with the "lake-surface" element (not shown) is as expected, although some minor amounts of reflectance from the floating vegetation were seen. A noticeable increase in reflectance at all wavelengths is apparent in the "lake-margin" element (Figure 1), but the curve remains relatively flat due to the influence of standing water beneath the canopy of emergent and floating vegetation. The spectra for the "shoreline" pixel (not shown) was noticeably different from the first two examples. Presumably, the effect of greater canopy development and little or no standing water caused increased reflectance in the three spectral "zones" adjacent to the two water-absorption regions. The slope of the curve from approximately Channel 40 to Channel 60 (1513.2 - 1707.6 nm) may be of diagnostic value, but the cause of that slope is as yet unknown to the writer. The most interesting spectral plot of those presented may well be that for the "lowland-meadow" pixel (Figure 2) where both a pronounced increase in reflectance and a very steep slope can be seen for the peak vegetative-reflectance bands centering on 1.65  $\mu\text{m}$  (Channel 54). Again, I am uncertain about the cause for the change in slope, but the increased reflectance appears to be diagnostic of a decrease in leaf-water content relative to the previous pixel ("shoreline"). The spectral plot labelled "dune slope" (not shown) not only exhibits reduced reflectance in the "cell-structure" region (Channels 1-20), presumably because of reduced density of vegetation as compared to the wetland locations of pixels 1-4, but also exhibits a noticeable flattening of the curve in the area centering on 1.65  $\mu\text{m}$  (Channel 54). Interestingly enough, the plot for the pixel located at the highest elevation ("dune top") also displays a "flattish" characteristic for the spectral zone centering on 1.65  $\mu\text{m}$  with what appears to be a slight tendency toward a "negative" slope (Figure 3). Some exposed sand may contribute to reflectance from the "dune-slope" and "dune-top" pixels, but further research is needed to evaluate that phenomenon.

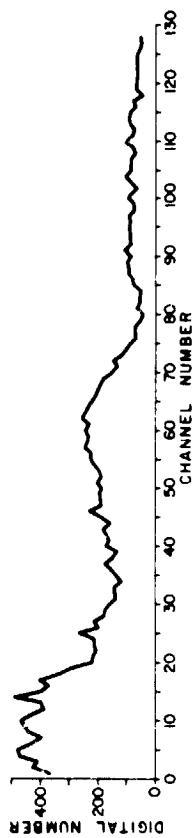


Fig. 1. Raw AIS data for lake-margin location

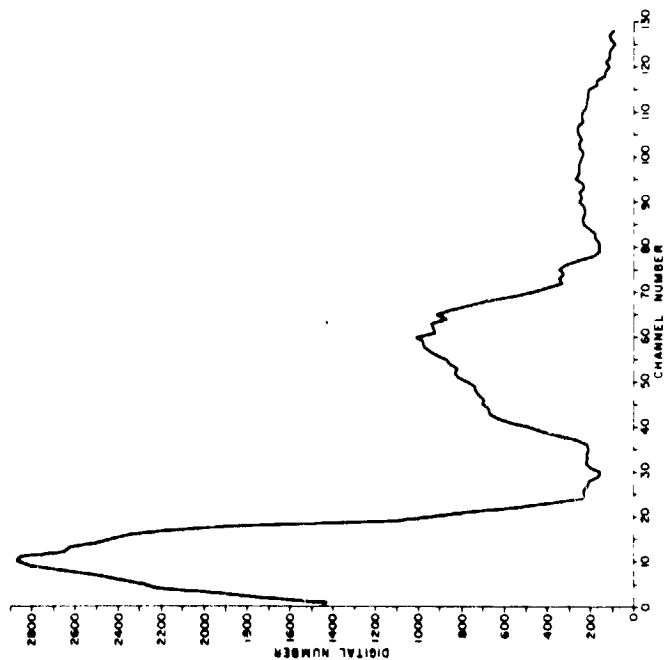


Fig. 2. Raw AIS data for lowland-meadow location

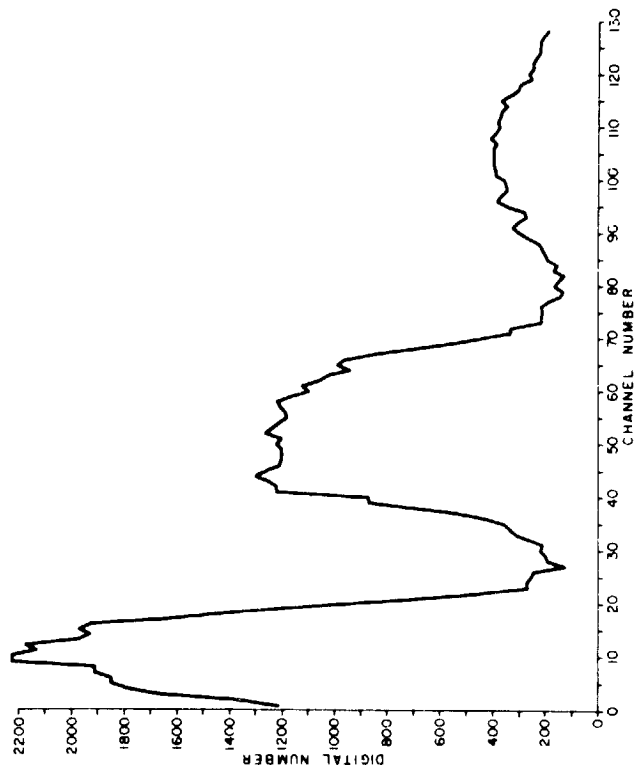


Fig. 3. Raw AIS data for dune-tun location

## CONCLUSION

Despite use of essentially uncorrected AIS data, the plotted raw spectra are deemed useful for comparing and analyzing vegetative sites in the Sandhills. Examination of data for the peak vegetative-reflectance region centering on 1.65  $\mu\text{m}$  (Channel 54) produced the expected result: a positive relationship between increasing elevation (i.e., decreasing access of plant roots to water) and a general increase in reflectance. It seems certain that variations in the slope of the curve in this spectral region are diagnostic of some condition related to the plants themselves or materials within their root zone, but the exact cause of slope variability is unknown at present. Some variation is evident in the spectral region centering on 2.20  $\mu\text{m}$  (Channel 113), a secondary vegetative reflectance peak in the middle-infrared, but the overall visual impact of variability is not as pronounced as that for the 1.65  $\mu\text{m}$  peak.

## REFERENCES

- Hoffer, R. M., 1978. Biological and physical considerations in applying computer-aided analysis techniques to remote sensor data. Remote Sensing: The Quantitative Approach, P. H. Swain and S. M. Davis, eds. (New York: McGraw-Hill), pp. 228-289.
- IANR, 1983. Report of the IANR Sandhills Task Force. Institute of Agriculture and Natural Resources, University of Nebraska-Lincoln, 67 pp.
- Myers, V. I. et al, 1970. Soil, water, and plant relations. Remote Sensing with Special Reference to Agriculture and Forestry. (Washington D.C.: National Academy of Sciences), pp. 253-297.
- Nichols, J. T., 1984. Physical characteristics of the Sandhills: vegetation. Proceedings, Water Resources Seminar Series, Nebraska Water Resources Center, University of Nebraska-Lincoln, pp. 74-79.
- Novacek, J. M. 1984 Report on Eastern Sandhills Wet Meadow Productivity and Species Composition in Wheeler County, Nebraska. Center for Rural Affairs, Walthill, Nebraska, and Nebraska Natural Resources Commission, Lincoln, Nebraska, 47 pp.
- U.S. Department of Agriculture, 1975. Wetland types in Nebraska. Attachment to Biology Technical Note #29, Soil Conservation Service, Lincoln, Nebraska. 10 pp.
- U.S. Fish and Wildlife Service, 1969. Native Sandhills grasses. Pamphlet #1L 3-2, Bureau of Sport Fisheries and Wildlife, 8 pp.

## THE USE OF AIS DATA FOR IDENTIFYING AND MAPPING CALCAREOUS SOILS IN WESTERN NEBRASKA

SCOTT A. SAMSON, Department of Agronomy, University of Nebraska-Lincoln, Lincoln, Nebraska, USA.

### ABSTRACT

The identification of calcareous soils, through unique spectral responses of the vegetation to the chemical nature of calcareous soils, can improve the accuracy of delineating the boundaries of soil mapping units over conventional field techniques. The objective of this experiment is to evaluate the use of the Airborne Imaging Spectrometer (AIS) in the identification and delineation of calcareous soils in the western Sandhills of Nebraska. Based upon statistical differences found in separating the spectral curves below 1.3 microns, calcareous and non-calcareous soils may be identified by differences in species of vegetation. Additional work is needed to identify biogeochemical differences between the two soils.

Conventional methods for the identification of homogeneous soil mapping units rely upon selective soil sampling and landscape interpretation. While the former approach is a relatively quantitative method, the latter is dependent upon the soil surveyor's experience to accurately identify the boundaries of a soil unit (i.e., a qualitative judgement). The mapper relies upon his ability to separate soils, partly based on geobotanical observations and limited biogeochemical analysis.

Aerial reconnaissance techniques have historically assisted in delineating soil boundaries based on the ability to distinguish between relatively homogeneous vegetation communities and the identification of changes in the topography. However, subtle changes in vegetation are not always apparent on panchromatic or color-infrared aerial photography because of spectral limitations found in the visible and near-infrared portions of the electromagnetic spectrum. These variations in vegetation may be attributed to many factors, such as differences in species, moisture availability or content of the vegetation, or chemical stress.

The purpose of this experiment is to undertake a preliminary examination of the feasibility of using the Airborne Imaging Spectrometer in the identification and delineation of calcareous soils in the western Sandhills of Nebraska.

### MATERIALS AND METHODOLOGY

Two soil series were selected for this experiment (Map 1). An Els-Tryon complex, 0 to 3% slopes, was selected as the non-calcareous soil, and a Els calcareous-Wildhorse fine sands, 0 to 3% slopes, to represent the calcareous soils. Both locations are similar in range site and type of vegetative cover (e.g., short meadow grass). These soils were identified and mapped by the Soil Conservation Service recently, and laboratory data on the chemical and mineralogical

composition of the soils were not available at the time of this study.

A flight by the Airborne Imaging Spectrometer was made over the study site on August 6, 1984, at approximately noon. The sky at the time of the flight was free from clouds or apparent atmospheric haze. Spectral data were collected under the "rock" mode (GPOS 1-4) and were obtained at a spatial resolution of approximately ten meters.

Processing of the spectral data collected by the scanner was initially made on a Harris 700 computer, with an IBM/PC microcomputer used to analyze data subsets and generate graphics. Statistical analysis was made through the Statistical Analysis System (SAS) software on an IBM 3081 mainframe computer. All software, except for the multivariate statistical programs, were developed and implemented locally at the University of Nebraska-Lincoln.

Six locations (pixels) were selected for an area covered by the Els-Tryon complex (non-calcareous) soils, and three locations to represent the Els calcareous-Wildhorse fine sands (Figure 1). All one hundred and twenty-eight channels were extracted for each of the nine samples. The raw data were used for all analyses and were not adjusted for atmospheric corrections.

Cluster analysis was used to test for statistical separation ( $p < .05$ ) between the two training sites to insure that spectral differences were present. Dimension reduction of the one hundred and twenty-eight channels was accomplished after the cluster analysis through a t-test ( $p < .05$ ).

## RESULTS

Figure 2 shows the spectral curves for the average of the six pixels from the non-calcareous soil and the three pixels from the calcareous soil. Except for channels one through fifteen (1150.7 - 1288.8 nm), the curves are almost superimposed upon one another.

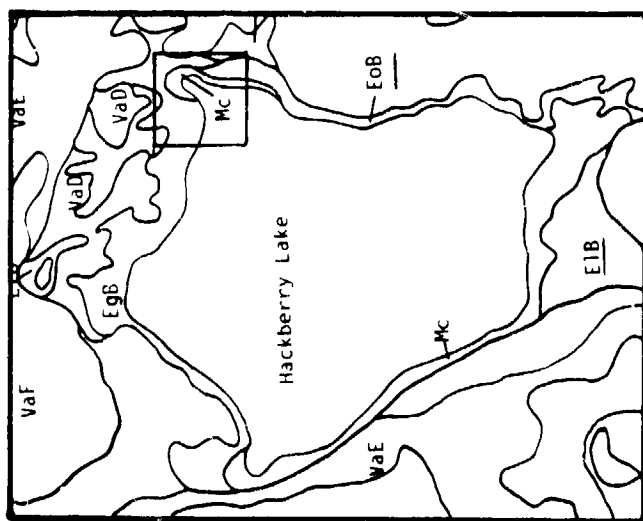
FASTCLUS, from the SAS cluster analysis set of programs, verified that the two locations contained spectral curves which were more similar within the training sites than between the two training sites.

With this test of separability providing evidence that the two test sites are probably spectrally distinct from one another, T-TEST was used to reduce the number of dimensions down to those wavelengths which explained statistically where the greatest difference between the two sets (locations) of spectral curves occurred.

According to the results obtained from the t-test, channels one through fifteen (1150.8 - 1288.8 nm), thirty-three (1448.4 - 1457.6 nm), eighty-one (1892.0 - 1901.3 nm), and one hundred and six (2127.2 - 2136.5 nm) were statistically different between the calcareous and non-calcareous soils. Figure 3 shows the same curves as were shown in Figure 2 except for the removal of the curve segments which were determined to be statistically similar to one another.

Possible explanation for the observed differences may be found in channels one through fifteen. Empirical evidence has shown that this region in the spectrum is associated with morphological features of vegetation, indicating that the two curves may represent two different types of vegetation (no field data has been collected to confirm this supposition; however, the difference in the pH between the two soils may influence the type of vegetation found at the two

ORIGINAL PAGE IS  
OF POOR QUALITY



Map 1. Soils map around the study site (boxed area). The calcareous soil in this study is represented by EoB and the non-calcareous soil by EgB.

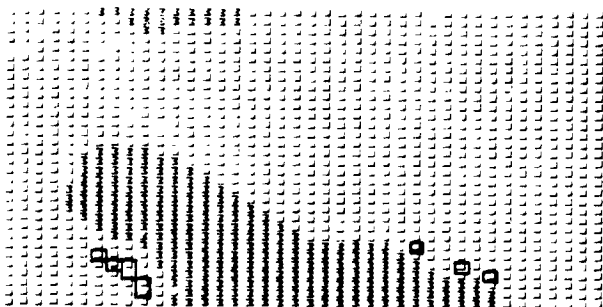


Fig. 1. Location of the sampled pixels (water body corresponds to the upper right inlet of Hackberry Lake in Map 1). L = land surface, W = water

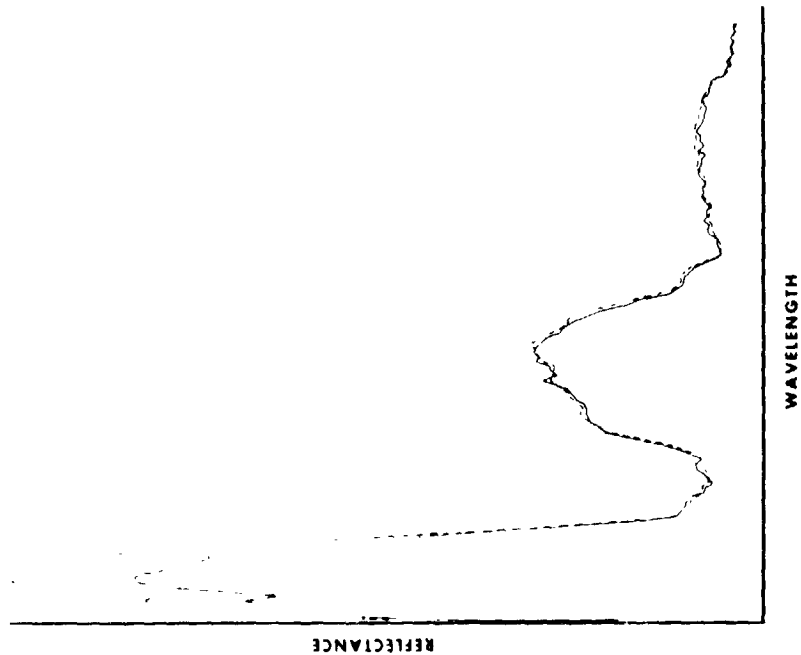


Fig. 2. Averaged spectral curves for non-calcareous soil (dash line) and calcareous soil (solid lines).

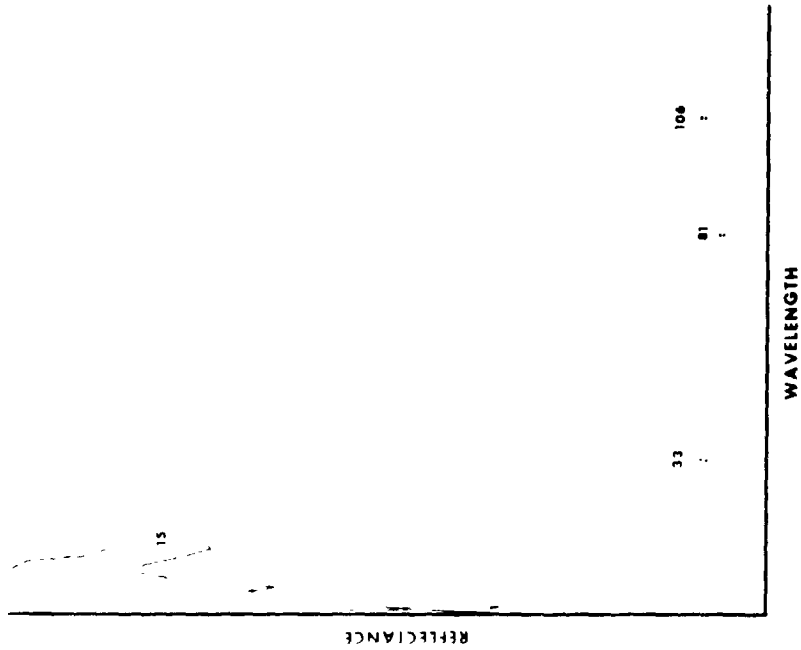


Fig. 3. Figure 2 after running a t-test against the raw spectral data. The line segment and the three discrete points indicate wavelengths where statistical differences occur between the two curves.

sites). Explanation for the effect the three discrete spectral (channels thirty-three, eighty-one, and one hundred and six) has not been investigated at this time.

#### CONCLUSIONS

With the limited ground truth available at the time of this study, it appears that a separation between a calcareous and a non-calcareous soil can be made based upon geobotanical differences between the two soils is not readily apparent, but may possibly be found in one of the three discrete channels not analyzed in this study. It may also be beneficial to pre-process the raw data to remove atmospheric interferences as well as investigate additional signal processing and statistical techniques.

## CALIBRATION OF AIS DATA USING GROUND-BASED SPECTRAL REFLECTANCE MEASUREMENTS

JAMES E. CONEL, Jet Propulsion Laboratory, California Institute of Technology, Pasadena, California, USA

## ABSTRACT

Present methods of correcting airborne imaging spectrometer (AIS) data for instrumental and atmospheric effects include the flat- or curved-field correction and a deviation-from-the-average adjustment performed on a line-by-line basis throughout the image. Both methods eliminate the atmospheric absorptions, but remove the possibility of studying the atmosphere for its own sake, or of using the atmospheric information present as a possible basis for theoretical modeling. The method discussed here relies on use of ground-based measurements of the surface spectral reflectance in comparison with scanner data to fix in a least-squares sense parameters in a simplified model of the atmosphere on a wavelength-by-wavelength basis. The model parameters (for optically thin conditions) are interpretable in terms of optical depth and scattering phase function, and thus, in principle, provide an approximate description of the atmosphere as a homogeneous body intervening between the sensor and the ground.

## SUMMARY

AIS and Thematic Mapper Simulator (TMS) data flights were obtained under clear atmospheric conditions at Mono Lake, California, on October 31, 1984. The planned AIS flight lines were oriented in a north-south direction, extending 22 miles from north of Mono Lake, south across Mono and Inyo Craters; the approximate flight elevation was 20,000 feet above terrain. Both morning (solar elevation = 15 degrees) and noon (solar elevation = 43 degrees) observations were taken. All of the planned flights were carried out, excepting the northernmost (crucial) segment of the noontime series which was interrupted by failure of the Thematic Mapper Simulator.

The north shore of Mono Lake is characterized by broad contiguous beaches of (seasonal) bright evaporite crust and dark basalt pebbles that extend with more or less lateral continuity an arcuate distance of 10 miles in an east-west and northwest-southeast direction. Both AIS and TMS flight lines were laid out to cross the beaches orthogonally and with bright and dark swaths extending transversely across the image width. The bright and dark beach deposits, together with asphalt roads and other rock and volcanic deposits, provide a series of calibration targets for the construction of reflectance scatter plots. The bright and dark interface between beach deposits is an extremely sharp boundary that may be useful for study of the

atmospheric/instrumental modulation transfer functions. This boundary, together with the evaporite-water interface, may be useful in obtaining estimates of atmospheric parameters by yet another technique known as the two-halves method. The lateral continuity of uniform dark beach deposits provides multiple estimates of the atmospheric optical depth (for TMS data) which may also be used for comparison with estimates provided by the curve fitting and two-halves methods. The surface of Mono Lake provides a large uniform target for flat-field corrections.

An intercomparison of all the methods described plus experiments with TMS data on separation of directional effects of atmospheric and of surface origin, model studies on correction of the data for atmospheric effects, and geologic studies of the area will, to the extent possible, be worked out with these data.

N86-11632

ANALYSIS OF AIS DATA OF THE RECLUSE OIL FIELD, RECLUSE, WYOMING

Jon D. Dykstra and Donald B. Segal, Earth Satellite Corporation, Chevy Chase, MD 20815; (301)951-0104

ABSTRACT

AIS data were flown over the Recluse, Wyoming oil field on September 9, 1984. Processing software has been developed at Earth Satellite Corporation (EarthSat) for interactive analysis of the AIS data. EarthSat's AIS processing capabilities include destripping, solar irradiance corrections, residual calculations, geometric resampling, equal energy normalization, interactive spectral classifications and a variety of compressive algorithms to reduce the data to 8-bit format with a minimum of information loss. The in-house photolab facilities of EarthSat can routinely produce high-quality color renditions of the enhanced AIS data. EarthSat's AIS processing capabilities are available to fellow investigators through our Chevy Chase, Maryland office.

A total of 80 lithologic samples were collected under the AIS flight lines. Correlation (within the atmospheric windows) between the laboratory and the AIS spectra of sample sites was generally poor. Reasonable correlation was only possible in large, freshly plowed fields. We believe mixed pixels and contrast between the natural and sample's surfaces are mainly responsible for the poor correlation. Finally, a drift of approximately three channels was observed in the diffraction grating position within the 1.8 - 2.1 micron quadrant. The drift appears to be sinusoidal in nature.

AIS DATA

Four flight lines of AIS data, and contemporaneous TMS data, were flown over the Recluse, Wyoming oil field. The Recluse oil field is located along the northeastern flank of the Powder River Basin. Figure 1 is a location map for the Recluse oil field and gives the approximate position of the four flight lines. For this flight, the AIS spectral range extended from 1.155 to 2.337 microns.

AIS DATA PROCESSING

A flow diagram of EarthSat AIS processing software is shown in Figure 2. On this figure, EarthSat's processing begins at the DESTRIPE position.

Destripe

The corrected data, as provided by JPL, still contains a residual banding (or striping) along the flight direction. The banding is apparently caused by imbalances in the dark current (DC bias) of the detectors across the pixel direction of the detector. If a sufficiently large area of homogeneous, spectrally flat material is

present along the flight line it is possible to use the average radiance values, collected over several along-track pixels, to adjust the bias differences between the cross-track elements of the array. This is the approach commonly used by JPL, and one which produced the "flat field corrected" data for the Cuprite, Nevada scene described in the AIS User's Guide.

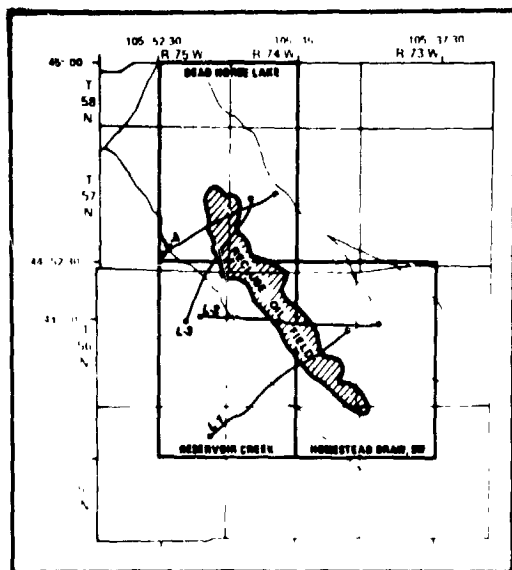


Fig. 1 Location Map

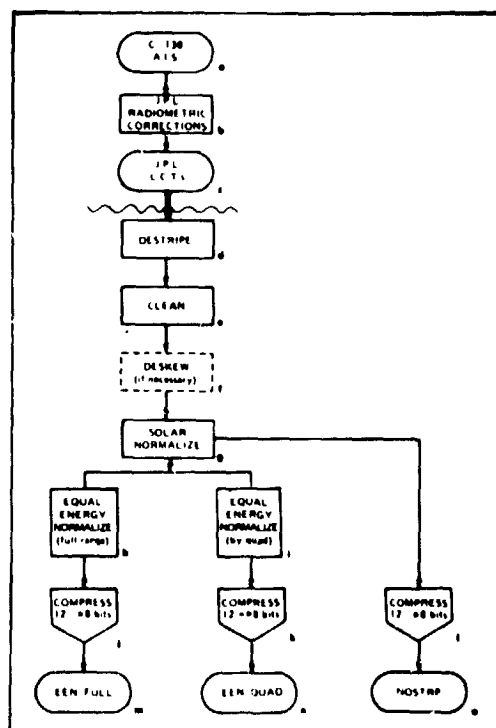


Fig. 2 Flow diagram of EarthSat's AIS processing

Unfortunately, no such area was found on any of our four flight lines. Therefore, we used a different approach for the destripping. Our approach is based on histogram matching. The assumption is that, over the course of a complete flight line, each of the 32 cross-track detectors has covered, on the average, very similar surface materials. As long as the individual detectors are reasonably well behaved, this technique works extremely well in removing intra-band striping. By way of example, Figures 3 and 4 show several AIS channels before and after destripping.

This method however can induce serious problems in terms of the inter-band radiometrics. Within a given band (i.e., one of the 128 spectral channels) matching of the 32 AIS detectors is totally dependent upon the shape of each bands' unique reference histogram. If there are fundamental differences between any two bands' reference histograms, these differences will be expressed in the output (destriped) data.

In our first attempt to describe the AIS data we chose a single detector within each band from which to collect the reference histogram. The criteria for selecting the reference detector were

ORIGINAL PAGE IS  
OF POOR QUALITY

that it show a low variance and appear, in other ways, to be well behaved. However, a problem arose because of the presence of an inaccurate "dark current correction" applied during data collection. The net effect of the erroneous dark current correction was to add random DC bias values to the individual detectors. Thus, during our original destriping process, a false bias was applied to each band; the magnitude of the bias was proportional to the level of the random noise at the detector for which we collected the reference histogram. The final result was 128 well-destriped bands; however, in many cases each of these bands had biases which were equal to or greater than the absorption features comprising the desired spectral information. Figure 5 is a strongly stretched version of the normalized destriped data showing the obvious DC bias differences between the spectral channels. To prevent the undesirable effects induced by the random DC biases, we have modified the destriping program to collect an average reference histogram as an average of all detectors, rather than for a single detector. The results (Figure 6) produce much more uniform inter-band radiometrics.



Fig. 3 Data as received from JPL

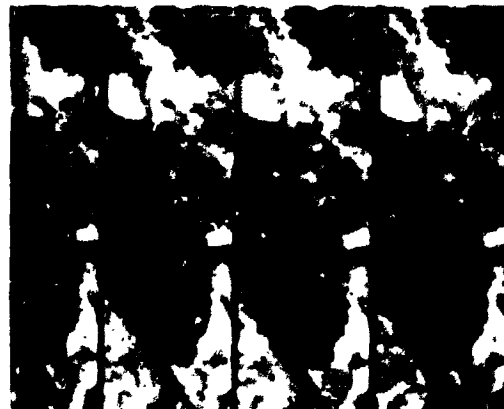


Fig. 4 Data after EarthSat's destriping

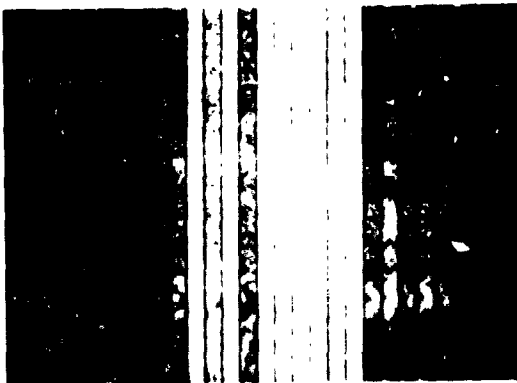


Fig. 5 Erroneous bias effects when destriping based on single detector

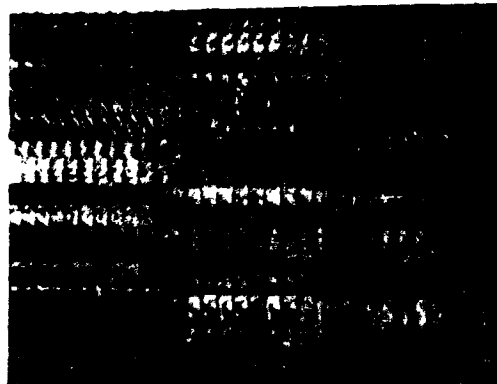


Fig. 6 Results of destriping based on all available detectors

### Clean

This procedure was written to interactively remove bad data lines. Bad lines appear as cross-track lines of fully saturated (DN 4095) or anomalously low DN values. Single lines are replaced by the average of the two adjacent lines on a pixel-by-pixel basis. Multiple line corrections are performed by a weighted average of the next adjacent good data lines. If these bad data lines are not removed they can adversely affect the later compression of the AIS data from 16 to 8 bits.

### Skew

The AIS sensor is fixed orthogonal to the longitudinal axis of the aircraft fuselage. Therefore, when the aircraft must crab (point into the wind in order to maintain its heading) the resulting yaw induces a skew in the geometry of the AIS data. The degree of skew is proportional to the yaw angle.

We have made a first order skew correction for those flight lines with yaw angles greater than 10 degrees. The correction is based on a nearest neighbor resampling along the flight path direction. The correction can be likened to looking edgewise at a deck of cards and sloping the top edge to the left or right to the appropriate number of degrees depending upon the sign and magnitude of the yaw angle.

### Solar Normalize

The incident energy at the top of the atmosphere drops off rapidly within the spectral range of the AIS sensor (approximately 1.2 to 2.4 microns). Using the LOWTRAN program for atmospheric calculations, the incident solar radiation was found to range between approximately 530 watts/square metre at 1.2 microns down to approximately 62 watts/square metre at 2.4 microns. Therefore, with increasing wavelength, each consecutive AIS spectral channel is receiving a decreasing intensity of incident light. In order to compensate for this imbalance, the pixels of each spectral channel are multiplied by a factor proportional to the inverse of the solar radiance for the channel. This effectively normalizes the 128 spectral channels to a common incident solar baseline.

### Equal Energy Normalize (Full-Range)

The purpose of the Equal Energy Normalize (EEN) calculation was to remove the effects of differing overall brightness and, thereby, accentuate the spectral, band-to-band, information. The algorithm used was identical to that described in the AIS User's Guide.

### Equal Energy Normalize (By Quad)

Within the spectral range of the AIS sensor there are two major atmospheric absorption regions, one around 1.4 microns and the other around 1.9 microns. The major portions of these features fall almost entirely within grating positions 1 and 3, respectively. When calculating the EEN data using all 128 channels, these major features tend to dominate the calculations; greatly decreasing the ability to detect smaller scale features in the other grating positions. Therefore, a procedure was developed which calculates the EEN separately for each of the four grating positions.

The algorithm used is the same as the EEN for the full-range. However, instead of basing the calculation on all 128 spectral channels, the calculations are performed four times, once for each of the 32 channel grating positions. Clearly, this procedure produces strong discontinuities at the grating boundaries. However, the presence of the discontinuities are well worth the greatly enhanced signal-to-noise ratio of the data, particularly within the 2.1 to 2.3 micron grating position.

#### Compress 12->8-bits

This was the final step in the digital data enhancement. The objective was to compress the 12-bit AIS data (contained in a 16-bit I\*2 format) into an 8-bit word which is then compatible with standard image display and printing devices. The compression algorithm was carefully designed to minimize the amount of information lost during the data compression.

Several data compression approaches have been used during this project. The most common was to calculate the mean and standard deviation for each of the spectral bands of a given flight line. Using the average of the means and three times the standard deviation of the channel with the largest calculated standard deviation, a minimum and maximum input value are calculated: minimum equals the average mean minus three times the largest standard deviation, the maximum equals the average plus three times the standard deviation. A linear lookup table is defined into which these minimum and maximum values are mapped to 0 and 255, respectively. This lookup table is then applied to all the pixels within each of the 128 spectral channels.

## RESULTS

### Correlation Between AIS and Lab Spectra

During the course of this study 80 lithologic samples were collected under the AIS flight lines. The samples were analyzed using X-ray diffraction, elemental analysis and laboratory spectral reflectance measurements. In open homogeneous areas, such as freshly plowed fields, it was possible to achieve reasonable correlations (within the atmospheric windows) between the AIS spectra and those measured in the laboratory. However, for the less disturbed areas it has been difficult to achieve much correlation between the lab and AIS spectra. We believe that this is largely due to the two phenomena: 1) The mixture of surface materials within a given pixel, and 2) natural vs. sample (laboratory) reflectance surfaces. The mixture problem is location dependent. Recluse is particularly bad in this regard. The problem of providing the laboratory spectrometer with a "natural" weathered surface is a more universal problem.

In a heterogeneous region, such as the Recluse study area, it is impossible to sample all the surface materials that fall within any given AIS pixel. Therefore, the only possible approach is to collect a hand sample at a given site which is characteristic of the general area. The approximately 100-square-metre AIS pixel will almost always contain many more different types of surface materials than are able to be represented in a hand sample. The only sites where this was not the case were in large, homogeneous, freshly plowed

ORIGINAL PAGE IS  
OF POOR QUALITY

fields. Not surprisingly, it was within these areas that we have the best correlations between the laboratory and AIS spectra.

The second, and equally difficult problem to control, is the unavoidable fact that the AIS data is measuring sunlight reflected from the upper few microns of naturally weathered surfaces. When unconsolidated samples reach the laboratory, these weathering surfaces have been lost. The degree to which the natural chemical and physical weathering environments have modified the mineralogy and reflective properties of the surface types will adversely affect the correlation between AIS and laboratory spectra.

#### Grating Drift

An important observation that came from our interpretation of specially processed imagery of the AIS data is an apparent sinusoidal drift in the wavelength position of the diffraction grating. Figure 7 is a photograph of the last sixty or so juxtaposed AIS spectral channels. The flight direction is from the top to the bottom of the picture. Note the wavy zone (arrow on Figure 7), approximately 3



Fig. 7 Approximately 60 AIS channels between 1.8 and 2.4 microns. Arrow locates 2.0 absorption of carbon dioxide. Note wavy pattern along flight line.

channels wide, which moves down the flight line in a sinusoidal nature with an amplitude of approximately three channels. This is marking the location of the 2.0-micron absorption band due to atmospheric carbon dioxide. Clearly, the channel number of this absorption ought to be constant. Its wavy appearance on the AIS imagery suggests that the electronics controlling the precise wavelength position of the diffraction grating are possibly being affected by a signal of the observed period and amplitude. There is not, to date, enough information to say whether or not this same phenomenon is affecting each of the other three grating positions; however, a similar effect, although less apparent, is observable in the second grating position (1.5 - 1.8 microns). Before more detailed analyses of absorption band placements can be performed, these apparent band shifts need to be further understood.

N86-11633

HIGH RESOLUTION SPECTROMETRY OF LEAF AND CANOPY CHEMISTRY  
FOR BIOGEOCHEMICAL CYCLING

MICHAEL A. SPANNER, Technicolor Government Services,  
NASA/Ames Research Center, Moffett Field, CA, USA; DAVID L.  
PETERSON, NASA/Ames Research Center, Moffett Field, CA, USA;  
WILLIAM ACEVEDO, Technicolor Government Services, NASA/Ames  
Research Center, Moffett Field, CA, USA; PAMELA MATSON,  
NASA/Ames Research Center, Moffett Field, CA, USA.

ABSTRACT

High-resolution laboratory spectrophotometer and Airborne Imaging Spectrometer (AIS) data were used to analyze forest leaf and canopy chemistry. Fundamental stretching frequencies of organic bonds in the visible, near infrared and short-wave infrared are indicative of concentrations and total content of nitrogen, phosphorous, starch and sugar. Laboratory spectrophotometer measurements showed very strong negative correlations with nitrogen (measured using wet chemistry) in the visible wavelengths. Strong correlations with green wet canopy weight in the atmospheric water absorption windows were observed in the AIS data. A fairly strong negative correlation between the AIS data at 1500 nm and total nitrogen and nitrogen concentration was evident. This relationship corresponds very closely to protein absorption features near 1500 nm.

INTRODUCTION

Remote sensing data are being used to study and to model processes in the biogeochemical cycling of carbon, nitrogen, and phosphorus for forest ecosystems. Based on recent insights (Melillo and Gosz, 1983) regarding nutrient availability and its interaction with the biochemical content of the canopy, a process level model (Fownes and Aber, 1985, this volume) is being developed. This model predicts productivity, gas exchange, nutrient transformations and fluxes using information about climate and the biochemical content of the canopy. The three canopy variables under investigation using remote sensing are leaf area index (LAI), foliar biomass, and biochemical composition. This paper describes preliminary analysis using a laboratory spectrophotometer and the Airborne Imaging Spectrometer to determine leaf and canopy biochemical composition.

## BACKGROUND

Various organic compounds present in foliage absorb infrared (IR) radiation in a manner analogous to the mineralogical features used in geology. The absorption features correspond to the fundamental stretching frequencies of organic bonds. The harmonics and overtones of these fundamentals are often found in the visible, near infrared and short wave infrared. Unlike feature identification used for mineralogical discrimination, the same organic compounds are generally always present in all vegetation types, but in different concentrations and total contents. Thus, a primary goal of infrared spectroscopy for plants should be quantification of these contents rather than discrimination of specific features. These organic compounds are of equal importance to nutrient cycling because they are composed of the key nutrients (carbon, nitrogen, phosphorous, etc.) that are required for plant growth.

Nitrogen is bound up in leaves primarily in various proteins, enzymes, amino acids, chlorophylls, alkaloids, and cyanogenic compounds. The absorption features for the proteins and chlorophylls are shown in Figures 1-a and 1-b, respectively. Nitrogen concentration usually varies between 0.5 to 3 percent by weight. Phosphorus content is typically lower than nitrogen (less than one percent) and is bound up in phospholipids, ATP, and other organic molecules. Carbon is ubiquitous in organic material; the forms most important to nutrient cycling are structural carbon (lignin and cellulose) and mobile carbon (starches (Figure 1-d) and sugars). Important features for lignin occur at 1148 and 1685 nm, and for cellulose at 2100 nm. Water is abundant in leaves and its spectrum is shown in Figure 1-c. The role of other constituents of leaves (oils, carotenoids, cuticular waxes) may not be as significant for nutrient cycling, but the fact that they also absorb IR radiation and may not co-vary with the other compounds, means that they contribute to the overall IR signature of the leaf and introduce variation in the reflected radiation.

Together with the multiple scattering properties of leaf structural interfaces, the biochemical constituents of leaves determine their infrared absorption characteristics in proportion to their concentration. Thus, at any one wavelength, the reflected radiation will be a composite dominated by the strength of the absorption feature of each compound so that multiple wavelengths are required to estimate any one constituent while accounting for the interference of other compounds. A goal of this research is to determine these predictive wavelength regions.

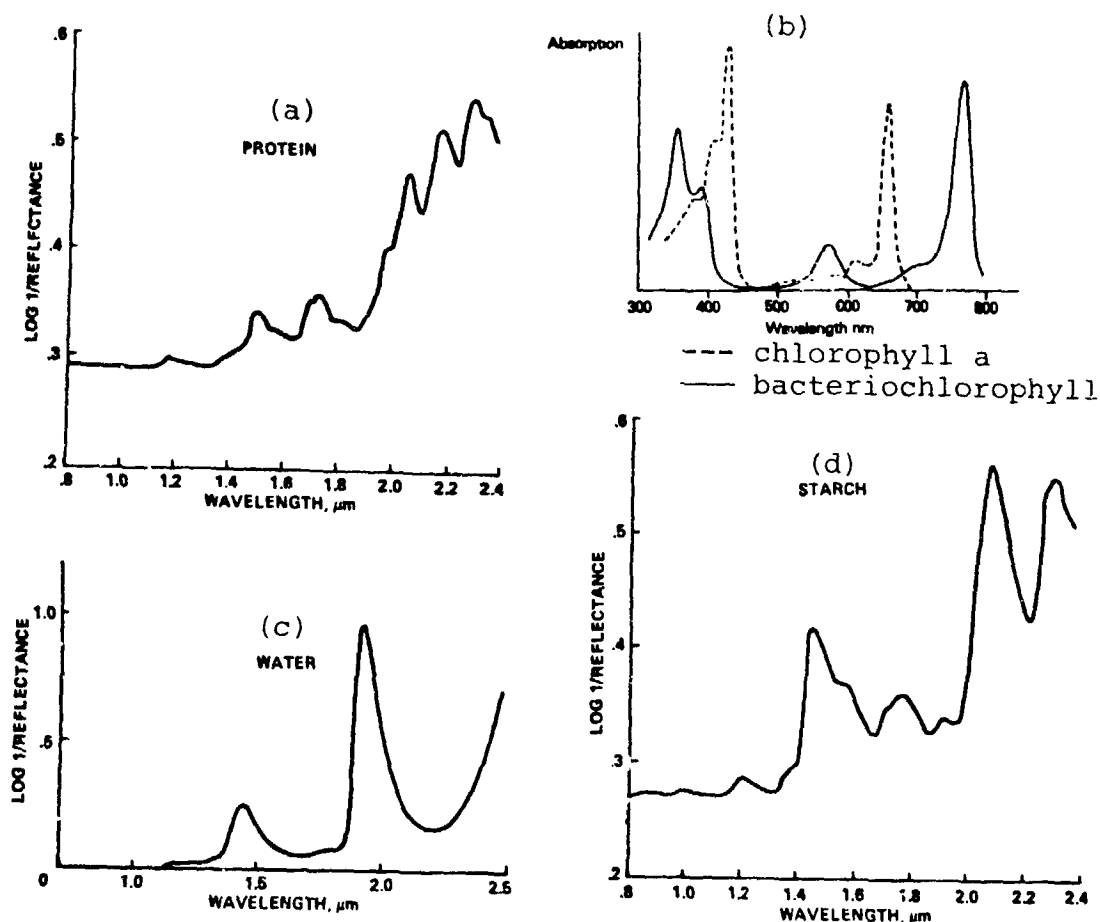


Figure 1. Absorption spectra for four organic compounds in the visible and shortwave radiation regions

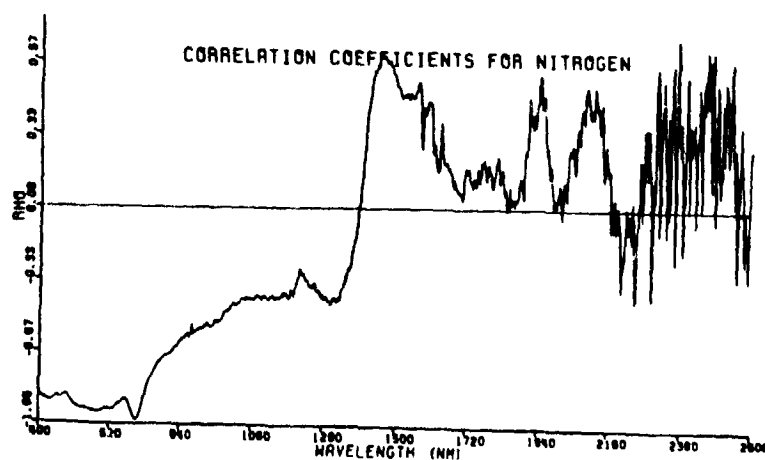


Figure 2. Correlogram for percent nitrogen versus total hemispherical reflectance for ground needles from seedlings of *Tsuga mertensiana* measured in a laboratory spectrophotometer

## LABORATORY TECHNIQUES AND RESULTS

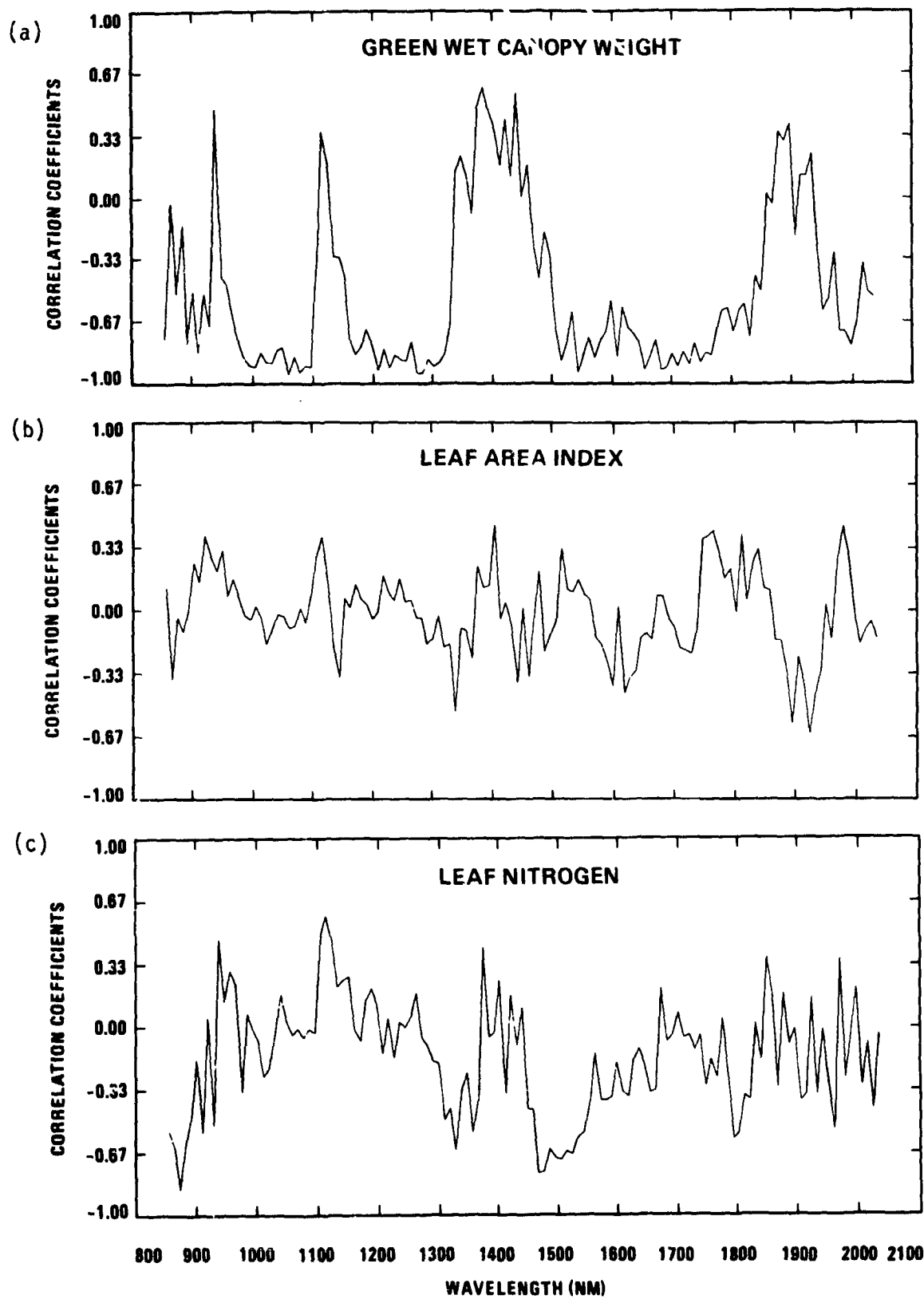
Our research is attempting to understand spectra of forest leaves and canopies as we proceed from laboratory to field to airborne spectroscopic techniques. Presented here are laboratory analyses of seedlings of Mountain hemlock (*Tsuga mertensiana*) grown in a phytotron under several treatments to vary the canopy chemistry. The treatments were: a control; fertilized with N, P, S; sugar addition; and fertilized and shaded. These seedlings were part of research by Dr. Matson who provided freeze-dried, ground leaf samples from each treatment for spectral analysis. These samples were analyzed in a wet chemical lab to determine the nitrogen, phosphorus, starch, and sugar content to correlate with the spectra. The ten samples were spectrally measured in a Perkin-Elmer spectrophotometer for percent reflectance between 400 and 2600 nm.

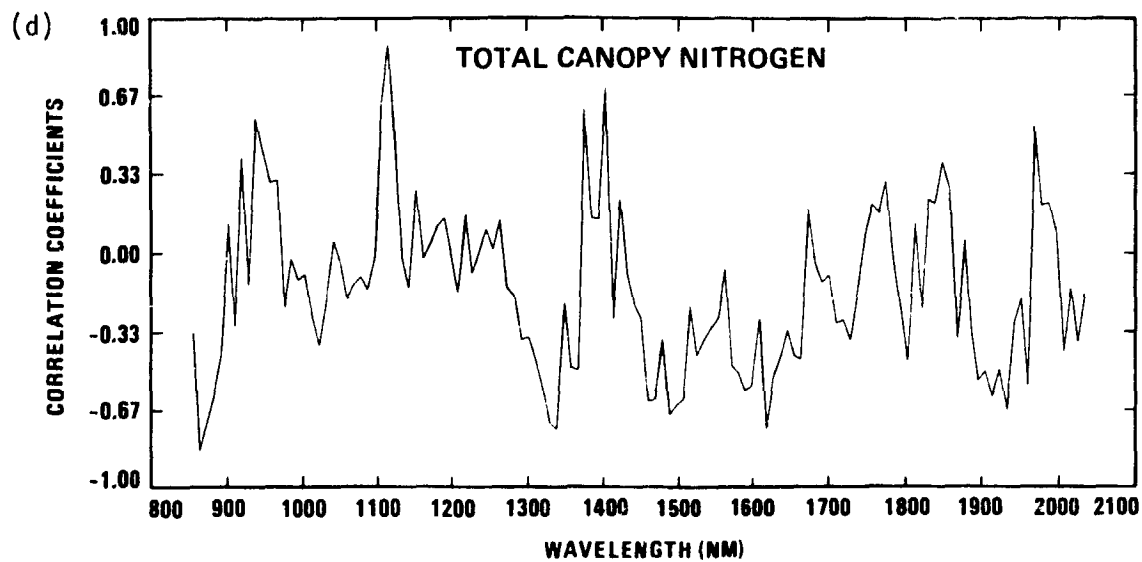
Correlation coefficients were calculated for each wavelength against the chemical analyses and are displayed as a correlogram. An example for percent nitrogen is shown in Figure 2. As expected, strong inverse correlations exist in the visible region due to the strong absorption effects of chlorophyll and associated proteins. Positive correlations are due most likely to other compounds which vary inversely with nitrogen (starch in this case) which corresponds to the correlation at about 2100 nm. Another absorption feature relating to protein begins to appear at about 2180 nm, but increasing instrument noise, small sample size, and small absolute differences in reflectance at these wavelengths may be obscuring this information.

We are in the process of investigating the use of smoothing functions and derivatives to identify and measure concentrations at specific spectral regions which may overcome some of these difficulties. The peak at about 1450 to 1500 nm is probably due to the presence of water reabsorbed by the samples during handling which masks the protein feature, thereby modifying the correlogram near 1500 nm and above. Similar correlograms were calculated (not shown) for phosphorous, starch and sugar, and indicate an inverse relationship between starch and nitrogen. The presence of a number of positive and negative peaks in the correlograms can be used to investigate multiple linear regressions for each constituent. This work is in progress and the present interpretations are still tentative due to the early stage of our investigations.

## AIRBORNE IMAGING SPECTROMETER DATA ANALYSIS

The Airborne Imaging Spectrometer onboard a C-130 aircraft acquired imagery over Blackhawk Island, Wisconsin on September 9, 1984. The AIS data were acquired in grating positions 0-3 (vegetation mode), covering wavelengths from





Figures 3(a) to 3(d). Correlograms for green wet canopy weight (tons/hectare), leaf area index (one-sided), nitrogen concentration ( $\text{mg}/\text{cm}^2$ ) and total nitrogen ( $\text{kg}/\text{hectare}$ ) of the Blackhawk Island plots measured by the Airborne Imaging Spectrometer.

855 to 2036 nanometers. The spatial resolution of these data was approximately ten meters. No preprocessing algorithms were applied to the AIS data. There are four atmospheric water absorption regions within the vegetation grating position. Minor ones are centered at .94 nm and 1.13 nm, with major ones centered at 1.4 nm and 1.9 nm. The AIS data are of fairly good quality, with minor vertical striping in some bands.

Analysis of the AIS data was performed on a VAX 11-780 using IDIMS image processing software and software modified and developed specifically for the analysis of AIS data. The location of the six Deciduous Forest sites on Blackhawk Island (Fownes and Aber, 1985, this volume) were delineated on the AIS digital imagery using an interactive display. A two-by-two pixel region for each site was extracted and the mean and standard deviation for the 128 channels were calculated and plotted. A residual image was generated by defining a three-pixel wide transect along a fertility gradient across Blackhawk Island. The mean reflectance for each channel along the gradient was calculated and subtracted from the raw reflectance for the Blackhawk Island AIS scene. The residual reflectance was plotted for each of the six sites. Locations of low reflectance displayed negative residuals and areas of high reflectance had positive residuals. The residual plots allowed for improved discrimination of the six sites. A visual assessment of the fertility gradient was performed using the residual image.

The correlogram program calculated the correlation coefficients for each of the measured canopy parameters of the six sites at each independent AIS wavelength. The canopy parameters analyzed were green wet canopy weight (tons/hectare), total nitrogen (kg/hectare), nitrogen concentration (mg/cm<sup>2</sup>), and leaf area index (one-sided). The correlograms are presented in Figures 3a-3d.

#### AIS RESULTS AND DISCUSSION

Very strong correlation was observed between green wet canopy weight and AIS data at wavelengths other than the atmospheric absorption bands. Correlations exceeded .85 for many of these wavelengths, indicating the sensitivity of the AIS data to total mass (water and foliage) of the canopy. As expected, these relationships did not exist in the atmospheric water absorption bands. The correlation occurs across a broad range of wavelengths indicating relatively slowly varying absorption.

There were no wavelengths that displayed high correlations to leaf area index. This was not surprising because wavelengths on the AIS are not the same as those used for leaf area index estimation. Leaf area index estimations generally make use of ratios or transforms of

red (.63-.69 $\mu$ m) and near infrared (.76-.90 $\mu$ m) portions of the electromagnetic spectrum. The Airborne Visible Infrared Imaging Spectrometer (AVIRIS) will provide spectral information in these shorter wavelengths and should be of significant value for leaf area index determinations when these data become available and are analyzed as ratios.

Analysis of the total nitrogen and nitrogen concentration correlograms reveals that there are strong negative correlations near 1500 nm, corresponding to a strong protein absorption feature at that wavelength. This result is very encouraging and shows the promise of a high spectral resolution imaging spectrometer. Another important protein absorption feature exists at 2180 nm; unfortunately, this wavelength is out of the range of the vegetation mode grating position of the AIS instrument.

Another observation from the correlograms is that when comparing the green wet canopy weight correlogram with the leaf nitrogen plot, different information from each plot emerges. The AIS is sensitive to specific canopy parameters at different wavelengths, providing unique information at each wavelength. At wavelengths between 1500 and 1600 nm especially, the plots trend in opposite directions. These dissimilar trends can be used to investigate multiple linear regressions for each constituent.

We plan to expand our research efforts in Wisconsin next summer. We hope to obtain 20-25 plots with additional canopy information including canopy lignin. We are very encouraged by these preliminary results and we are excited about upcoming analyses of high spectral resolution remote sensing data.

#### REFERENCES

- Danks, S.M., E.H. Evans, and P.A. Whittaker, 1983, Photosynthetic Systems: Structure, Function and Assembly, p. 37, John Wiley and Sons, New York.
- Fownes, J. H. and J.D. Aber, 1985, "Forest Canopy Chemistry From Blackhawk Island", Wisconsin, JPL Airborne Imaging Spectrometer Data Analysis Workshop, This Volume, Pasadena, California.
- Melillo, J.M. and J. R. Gosz, 1983, Interactions of Biogeochemical Cycles in Forest Ecosystems, Chapter 6, The Major Biogeochemical Cycles and Their Interactions, SCOPE 21, Bolin and Cook (ed.), pp. 177-221, John Wiley and Sons, New York.
- Rotolo, P., 1979, Near Infrared Reflectance Instrumentation, Cereal Foods World, 24:94-98.

N86-11634

FOREST CANOPY CHEMISTRY FROM BLACKHAWK ISLAND, WISCONSIN

FOWNES, JAMES H. and JOHN D. ABER, Department of Forestry, University of Wisconsin, Madison, WI 53706, USA.

ABSTRACT

Our ongoing project attempts to develop process-oriented models of forest productivity, which are driven by canopy spectral data. Concurrent with AIS flyover, we sampled a series of mixed-species hardwood forests for leaf morphological characteristics; total leaf mass, area, and vertical distribution; and overall average canopy nitrogen and lignin. Within a canopy, leaf specific weight (dry weight per unit area) varied significantly with height and between species. Species are separated ecologically by percent nitrogen and lignin. Mean total canopy percent lignin correlates well with previously published field estimates of soil nitrogen availability and total annual net primary productivity, which augurs well for the model, subject to identification of unambiguous spectral signals.

INTRODUCTION

In order to estimate large-scale patterns and changes in terrestrial productivity, we hope to sense remotely the attributes of ecosystem function which control annual net primary production (NPP). This hope is founded on results from field research indicating that two major feedbacks between forest canopy characteristics and NPP may allow extrapolation from sites of intensive measurement to other areas within a climatic region. The first control (Fig. 1, upper left circle) is that leaf characteristics constrain both photosynthesis and transpiration by leaf size, thickness, and enzyme (nitrogen) content. The second control (Fig. 1, bottom left circle) is that leaf chemistry predictably determines the release of nutrients through decomposition and consequently uptake by plants. Furthermore, the release of nitrogen from soil organic matter (termed N mineralization) controls allocation patterns between wood and roots (Fig. 1, circles on right; Aber et al. 1985). To discern differences in NPP, we must therefore sense not only total leaf mass, but subtler features such as nitrogen and lignin content of the leaves. We will need detailed spectral information such as that

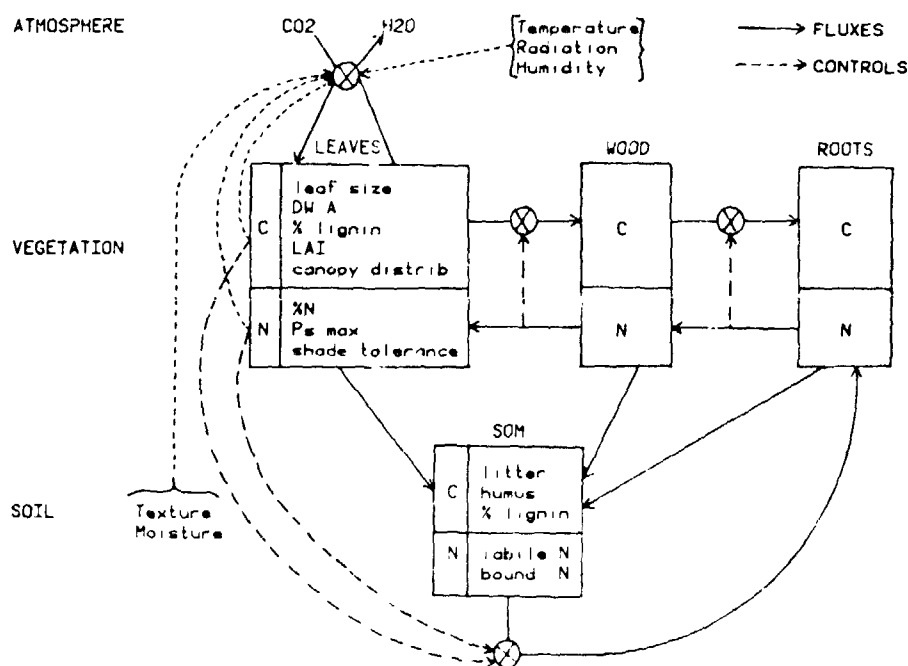


Fig.1 Canopy Controls on NPP

provided by the AIS, and also careful characterization of the canopies themselves. In this preliminary report we are concerned with the latter.

#### SITES AND METHODS

Our field sites are on Blackhawk Island, located in the Wisconsin River north of Wisconsin Dells (lat. 43°40' N, long. 89°45' W). The top of the island is relatively flat and soil depth and fineness increases from west to east. The hardwood forest changes in parallel from red oak and white oak in the west to sugar maple, red oak, and basswood in the east. Leaf litter quality and consequently N mineralization rates increase along the gradient as oaks are replaced by more mesic species (Pastor et al. 1984, Aber et al. 1985; Table 1).

We sampled green leaves by shooting down small branches with a shotgun. Leaves for the major species at each site were taken at four height levels: emergent or dominant, upper codominant, lower codominant, and suppressed. Green leaf area, fresh weight, dry weight (70°C), percent N and percent lignin were determined for several pooled samples of 5 to 10 leaves each.

Foliage height profiles were measured using a camera with a calibrated telephoto lens as a range-finder. A grid on the focal screen of the camera provided 15 sampling points within a single field of view. The leaf area index (LAI) in each height interval must be corrected for obstruction of upper leaves by lower leaves (MacArthur and Horn 1969, Aber 1979).

Litterfall was collected weekly from five 0.25 m<sup>2</sup> traps at each site, sorted by species, dried at 70°C, and pooled for all dates. Total canopy properties were calculated by weighting the green leaf data by the proportion of leaf area within each height class and multiplying the weighted averages by total leaf mass (litterfall).

AIS spectra from 850 to 2000 nm were taken over the island along the gradient on 7 Sep. 1984, one month after the green leaf sampling. The leaves were mature but not senescent at both times. By comparison with a detailed ground survey (Aber et al. unpub.), we located a transect of pixels corresponding to the gradient and selected those situated over field sites.

## RESULTS

Strong differences in leaf morphology (dry weight per unit area, DW:A) exist within the canopy and between species (Fig. 2). No differences appeared between congeners, so the observations for species groups were combined (e.g. 'oaks'). Because each "observation" is really the mean of several pooled subsamples for each site, species, and canopy position, the variance within a height class (Fig. 2) is that among different sites. Between site variation is clearly less than that between heights or species.

There was no trend in N concentration with canopy height. Increased DW:A at the top of the canopy is sufficient to explain an increase in N per unit leaf area. The lignin analyses are incomplete, but oak leaves generally have more lignin (20.4%, sd = 4.3%) than sugar maple (8.9%, sd = 1.8%). We detect no difference in lignin content between green and senesced leaves. Different species or groups of species fall out into distinctive groups based on leaf weight per area and percent N in green leaves (Fig. 3).

Canopy profiles for two contrasting sites on the gradient show the clustering of leaf area near the top of the mesic canopy due to domination by shade-tolerant species (Fig. 4a). The bimodal curve for the other site (Fig. 4b) is typical of drier sites dominated by shade-intolerant species (Aber et al. 1982).

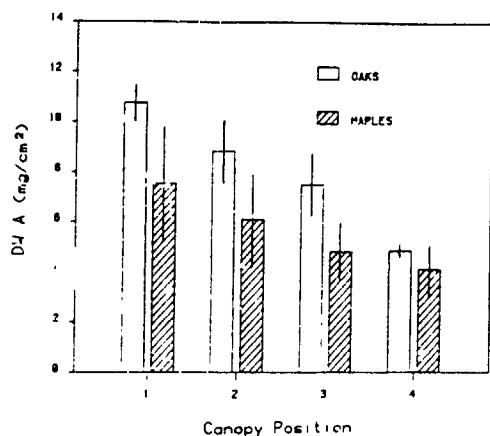


Fig. 2. Leaf weight per area from canopy top (1) to suppressed (4)

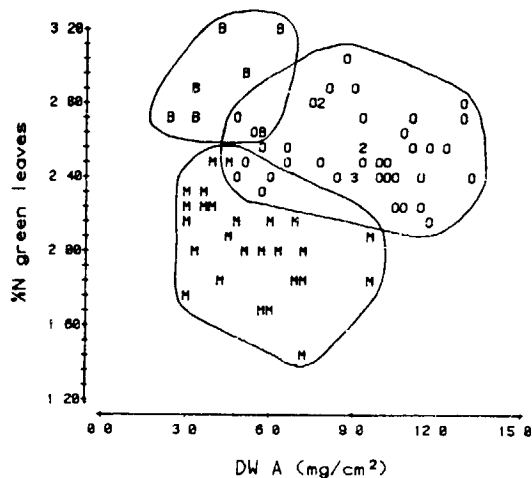


Fig. 3. Oak (O), maple (M) and basswood (B) green leaf data

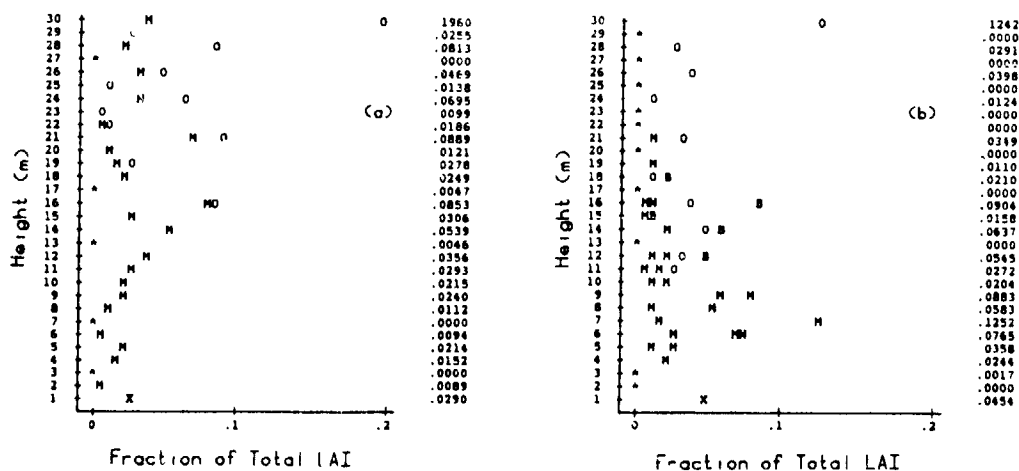


Fig. 4. Foliage height profiles for (a) SM2 and (b) R01. Species are red oak (O), sugar or red maple (M), white oak (W), basswood (B), understory (X).

Total canopy properties are influenced strongly by total leaf mass as given by litterfall (Table 1). Especially strong correlations exist between canopy mass and total green canopy N ( $r = .97$ ) and mass and total canopy lignin ( $r = .78$ ). Nitrogen uptake by vegetation (Table 1) is calculated from field data from Pastor et al. (1984) and Aber et al. (1985) and is correlated with the weighted percent lignin in the canopy ( $r = -.94$ ).

Table 1. Total canopy pools and fluxes for sites at Blackhawk Island.

Properties	Sites					
	R01	W0	R02	R03	SM1	SM2
NPP T/ha/yr	11	12	-	12	14	16
N uptake kg/ha/yr	86	92	-	94	106	133
LAI	4.5	3.7	3.8	5.0	6.0	5.1
Litterfall T/ha/yr	3.8	3.5	3.0	3.5	4.2	3.3
Canopy N kg/ha	90	81	58	85	103	76
Canopy lignin T/ha	.80	.74	.46	.62	.73	.43
% Lignin	21	21	15	18	17	13

#### REFERENCES

- Aber JD. 1979. A method for estimating foliage-height profiles in broad-leaved forests. J. Ecol. 67:35-40.
- Aber JD, JM Melillo, J Pastor, KJ Nadelhoffer, CA McClaugherty, and JM Lennon. 1985. Carbon-nitrogen interactions in the plant component of northern temperate forest ecosystems. Submitted to Geoderma.
- Aber JD, J Pastor, and JM Melillo. 1982. Changes in forest canopy structure along a site quality gradient in southern Wisconsin. Amer. Midl. Natur. 108:256-265.
- MacArthur RH and HS Horn. 1969. Foliage profile by vertical measurement. Ecology 50:802-804.
- Pastor J, JD Aber, CA McClaugherty, and JM Melillo. 1984. Aboveground production and N and P cycling along a nitrogen mineralization gradient on Blackhawk Island, Wisconsin. Ecology 65:256-268.

# ANALYTICAL TECHNIQUES FOR EXTRACTING MINERALOGICAL INFORMATION FROM MULTICHANNEL IMAGING SPECTROMETER DATA

FRED A. KRUSE, GARY L. RAINES, and KENNETH WATSON, United States Geological Survey, P.O. Box 25046, MS 964, Denver Federal Center, Denver, CO 80225 USA

## ABSTRACT

We are developing an analytical approach to airborne imaging spectrometer (AIS) data interpretation that can be used with knowledge of the spectral characteristics of minerals to identify and map their spatial distribution without a priori knowledge of their presence.

## SUMMARY

The general techniques we are using are (1) normalization of AIS spectra to remove albedo effects, and (2) calculation of "relative reflectance" AIS spectra to identify minerals. We have compared two methods of normalization -- normalization to one channel, and equal energy normalization. Relative reflectance spectra were computed by dividing a raw or normalized spectrum by a standard curve; standard curves were formed by (1) calculating the simple average of each channel along the flightline, and (2) using the low order terms of a discrete Fourier series representation employing a fast Fourier transform (FFT) method. These techniques allow us to map the occurrence of specific minerals but we cannot yet draw any conclusions regarding mineral abundance.

Interpretation of the relative reflectance spectra and AIS relative reflectance images is not altogether straightforward. Each type of relative reflectance image does contain artifacts of which the interpreter must be aware. To accurately identify minerals the interpreter must have a thorough knowledge of the data and the spectral characteristics of minerals, understand what the techniques used have done to the data, and be careful not to attach mineralogical significance to artifacts.

## SPECTROSCOPY OF MOSES ROCK KIMBERLITE DIATREME

CARLE M. PIETERS and JOHN F. MUSTARD, Department of Geological Sciences, Brown University, Providence RI 02912

**ABSTRACT:** Three types of remote sensing data (AIS, NS001, Zeiss IR-photographs) were obtained for the Moses Rock kimberlite dike in southern Utah. Our goal is to identify and characterize the mantle derived mafic component in such volcanic features. The Zeiss and NS001 images provide information on the regional setting and allow units of the dike to be distinguished from surrounding material. A potential unmapped satellite dike was identified. The AIS data provide characterizing information on the surface composition of the dike. Serpentinized olivine-bearing soils are (tentatively) identified from the AIS spectra for a few areas within the dike.

## Introduction

A number of small kimberlite-bearing diatremes of Tertiary age occur on the Colorado Plateau. The origin of these unusual volcanic features is not well understood, but is believed to be associated with mantle processes that result in a rapid rise of material from the mantle through the continental crust. Although such an event (presumably explosive) has never been directly observed, kimberlite-bearing volcanic features are a valuable source of otherwise inaccessible mantle and crustal rocks of great interest to the geochemist (and sometimes a source of diamonds for the investor). Kimberlite-bearing features have not been explored extensively with remote sensing techniques primarily because of their small size and because their identifying characteristics have not been well documented.

The Moses Rock dike in southern Utah was chosen for analysis with the Airborne Imaging Spectrometer (AIS). Rocks, breccias, and deposits of the dike have been mapped in detail (1:12000) by McGetchin (1968, unpublished). A schematic geologic map of Moses Rock dike and observed rock types were presented by McGetchin and Silver (1970, 1972) with a discussion of the mineralogy, petrology and geochemistry of the mantle-derived materials (summarized in Geology section below).

Our goal in studying Moses Rock Dike with AIS data is to identify and characterize the mantle-derived mafic and ultramafic material. These types of rocks and minerals are known to exhibit characteristic absorption bands near 1  $\mu\text{m}$  as well as bands between 1.6 and 2.5  $\mu\text{m}$  due largely to iron and other transition metals in their crystal structure (eg. Adams 1974, 1975; Hunt and Salisbury, 1970). If successful, this type of data will provide a significant exploration tool to be used not only in identifying these unusual volcanic structures, but also for unraveling the normally complex distribution of material within them.

The flight over the Moses Rock target area in Monument Valley was flown July 20, 1984. Data collected included Zeiss color infrared photographs, NS001 (TM simulator) multispectral images, and AIS data. The day was clear and cloudless. Analysis of these data commenced January 1985, and a preliminary discussion of results is presented below. A few system problems occurred on our flight: the navigation system (INS) was not functioning properly and could not provide accurate positioning of the aircraft, the Nikon camera was inoperative, and the clocks on the Zeiss and NS001 were either inoperative or inaccurate.

## Geology of the Moses Rock Dike

(from McGetchin, 1968; McGetchin and Silver 1970, 1972)

Moses Rock dike is a breccia-filled, kimberlite-bearing diatreme located in the Colorado Plateau of south-eastern Utah. It is hooked-shaped in plan and about 6 km in length. It intrudes the undeformed and unmetamorphosed sandstone, siltstone and limestone of the Permian Cutler formation. The dike contact is sharp and the walls are steep. A system of joints extends out into the host rocks parallel to the dike contact. Moses Rock dike occurs in a cluster of diatremes southeast of the Monument uplift (a large regional anticline) and along the axis of the Comb Ridge monocline. Superimposed on the regional structure are a series of north-south trending anticlines and synclines. Total structural relief does not exceed 1500 meters and is concentrated along the Comb Ridge monocline.

The majority of the dike consists of large blocks up to several hundred meters across derived from the Cutler formation of sandstones exposed in the vent walls. The interstices between the large blocks are filled with a matrix of unconsolidated breccia. This matrix is composed of fragments from the large blocks, limestone fragments, crystalline rock fragments, and mafic and ultramafic constituents.

Kimberlite, which constitutes about 1% of the dike, occurs as small bodies not larger than 10 meters in diameter. It is a highly serpentinized, ultramafic microbreccia containing olivine, pyroxene, garnet, phlogopite and spinel. Most of the primary mineralogy is relict after serpentine and chlorite. These mineral constituents and alteration products are found dispersed throughout the breccia matrix. Material derived from kimberlite constitutes about 12% of the breccias. About 3% of the breccia consists of igneous, altered igneous, and foliated metamorphic rocks derived from the basement. Dense ultramafic mantle-derived fragments, which include eclogite, lherzolite, websterite, and jadeite-pyroxenite, are rare. The distinctly comminuted texture, the absence of silicate melt, and the dispersion of kimberlite material throughout the breccia indicates that the dike was emplaced as a fluidized volatile and solid particle system driven by H<sub>2</sub>O and CO<sub>2</sub>. The source of the kimberlite magma has been estimated to have been at a depth in excess of 100 km.

## Zeiss Infrared Photographs

The Zeiss camera used color infra-red film with a spectral range of 510-900 nm. The field of view is approximately 7 kilometers with a ground resolution of about 1-2 meters. These high-quality stereo images provide a regional perspective of the flight lines and facilitate mapping of fine structural features. These images were our primary data for locating the ground tracks of both the NS001 and AIS data. The high-resolution and stereo viewing allow the influences of topography and texture to be assessed.

East and South of Moses Rock the Permian beds dip moderately away from the dike towards an area of flat-lying Triassic and Jurassic sandstones. Where the Navajo sandstone is exposed a prominent set of parallel joints is visible. They are oriented approximately ESE/WNW and are regularly spaced at 50 to 100 meter intervals with no apparent offset along the joints. The orientation of the joints is orthogonal to the axis of the Monument uplift and Comb Ridge which implies the joints are a result of the regional stresses that existed during the formation of the uplift and monocline. There are also scattered lineations oriented about 60 degrees to the joints and localized circular and curvi-linear fracture patterns in the same formation. These are attributed to local structural response due to stratigraphic irregularities in the regional stress environment.

On the basis of texture and color in the Zeiss images, Moses Rock dike is divided into three units; the head, the body, and the tail. The apparent color of each unit is distinctive in the IR

photographs: pale blue, green, and grey to blue-grey. The head is complex and coarsely textured. On the east margin of the head a long linear feeder dike intersects two elliptical mounds of uniform debris. In the body, large locally derived breccia blocks are surrounded by a mottled, bright matrix. The tail is characterized by a uniform fine-grained texture and an absence of breccia blocks. 900 meters east of the tail is a small elliptical zone about 300 meters in length with the long axis oriented parallel to the bedding. It is similar in texture and apparent color to the tail, and may be a previously undetected satellite dike.

### NS001 (TM Simulator)

Airborne simulated thematic mapper (NS001) digital data were examined to quantify the qualitative observations from the Zeiss images. Ratio images were prepared and principal component analysis (PCA) images were studied in this preliminary examination to better define the general nature of Moses Rock dike as well as potential satellite dikes.

It is apparent by visual inspection that the units of the dike show the greatest spectral variation in the first five TM bands. Many ratios were examined and it was found that the ratios of bands 2 (0.53-0.60  $\mu\text{m}$ ) to 5 (1.00-1.35  $\mu\text{m}$ ) and bands 3 (0.63-0.69  $\mu\text{m}$ ) to 5 (1.00-1.35  $\mu\text{m}$ ) best differentiate the dike units. In both images the tail has a uniformly high ratio while the head and body show an irregular distribution of regions with a high ratio. Comparisons of these regions to the Zeiss images show that they occur in the interstices between breccia blocks. Kimberlitic mineral components and alteration products are found dispersed throughout the matrix (see Geology section), and may account for the observed distinction in the ratio images. Further comparison with the geologic map of Moses Rock (McGetchin, 1968) shows that the regions with the highest ratios correspond very well with the units mapped as containing the most serpentine in the matrix. Some beds within the Cutler formation, however, exhibit comparable ratio values and may also be a significant component of the matrix. The potential satellite dike unfortunately lies along one of these beds and was unresolvable in the ratio images.

PCA of the first six thematic mapper bands was done to further classify the dike. The program used accepts up to six input images and by a linear transformation of the variables produces images of the first three principle components. Although the results of the PCA are at the moment preliminary and qualitative, the third principle component image clearly shows that the "satellite dike" is similar in nature to the tail and different than the sedimentary units surrounding it. With further analysis of the principal component images in conjunction with the ratio images, we expect to obtain a better understanding of unit distinctions within the Moses Rock area.

### Airborne Imaging Spectrometer (AIS)

Six of seven short AIS swaths did cross the Moses Rock dike target. Five of these were in the 'rock' mode (about 1.15 to 2.35  $\mu\text{m}$ ); one was in the 'tree' mode (about 0.86 to 2.04  $\mu\text{m}$ ). Data processing was performed at JPL using the specialized, but versatile, software package 'SPAM' developed by J. Solomon. When this useful package is incorporated into the VAX-based VICAR2 package, we will continue AIS analysis using our facilities at Brown.

#### AIS Data Assessment

Although the data from this flight were adequate to determine that useful spectroscopic information is indeed obtainable for kimberlite-bearing surfaces (see below), there were a number of undetermined instrumental or calibration problems that made the precision, and possibly accuracy, of the data lower than it should be. Serious line-to-line (spatial) banding was

observed for about half the spectral channels. Banding in one channel was correlated with banding in neighboring channels. For a few channels along-track stripping was also present. These effects added considerable noise to the spectroscopic measurements of pixel groups and could not be removed without destroying most spatial information.

#### AIS Data Processing

Data analysis dealt largely with 'relative reflectance spectra' produced by ratioing the spectrum of an area of interest to the spectrum of a standard area (chosen as representative of local soil around the dike). This process has the advantage of allowing instrumental and atmospheric effects to be cancelled (except in saturated water bands). To obtain true reflectance spectra, the standard area needs to be calibrated independently. For these preliminary analyses we have assumed that the spectral character of the standard soil is relatively featureless. (Anticipated field work this summer will check this.)

Once distinctive spectroscopic areas were identified (see below), the SPAM 'find' function was employed on the type spectrum (original, not ratioed) to estimate areal extent of a unit within the AIS swath.

#### AIS Data Analysis

Within the limits of this flight of data, two distinct units with well-defined spectroscopic features were identified in addition to the more spatially extensive local standard. The vast majority of surface material covered in the AIS swath is not greatly different from our chosen standard.

The first of the spectroscopic units is in the dike and is what we have tentatively called Moses Rock 'kimberlite'. The type area was chosen based on the unpublished map of McGetchin (1968). This type area was crossed by AIS swaths of both spectroscopic modes allowing its spectral character to be examined from 0.86 to 2.35  $\mu\text{m}$ . The 'kimberlite' area exhibits two spectral features: 1) a band that begins relatively sharply at about 2.25  $\mu\text{m}$  and increases in absorption (up to about 25%) toward 2.35  $\mu\text{m}$ ; and 2) a broad band of similar strength between 0.86 and 1.50  $\mu\text{m}$  with an apparent center near 1.15  $\mu\text{m}$ . These features are consistent with serpentinized olivine-bearing rocks or soil, currently our preferred interpretation. For comparison our "kimberlite" relative spectrum is presented in Figure 1, and a serpentinized olivine reflectance spectrum from Hunt and Salisbury (1970) is presented in Figure 2.

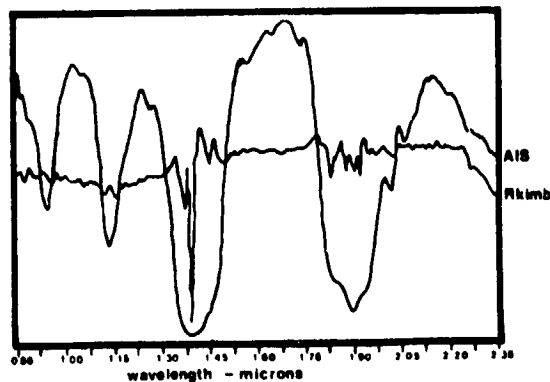


Figure 1. AIS spectra from combined 'rock' and 'tree' modes for our standard area (AIS, raw calibrated spectrum) and the 'kimberlite' area (Rkimb, reflectance spectrum relative to the standard area spectrum).

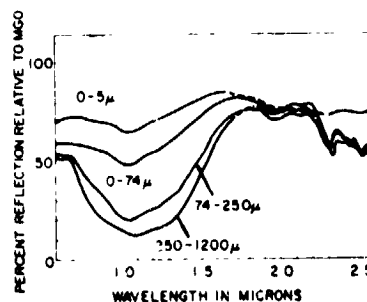


Figure 2. Reflectance spectra of serpentinized olivine (from Hunt and Salisbury, 1970)

The second spectroscopic unit occurs as a local soil type east of the dike that exhibits a weak band (about 7%) between 2.1 and 2.35 $\mu$ m, centered near 2.2 $\mu$ m [and perhaps another feature hidden by the 1.9 $\mu$ m atmospheric water band]. We interpret this as soil containing an abundance of a hydrated mineral (currently undefined).

## Summary of Results

Although we have not yet thoroughly analyzed the interrelation between the AIS, NS001, and Zeiss data, it is clearly important to have coordinated data: one type of data is needed that is optimized for *mapping* surfaces (such as the NS001 and Zeiss) and allows material of generally similar characteristics to be identified and mapped over large areas; and another type of data is needed that is optimized for *characterization* of surface material (such as AIS) and allows specific compositional information to be determined. The AIS data has produced spectra that can be interpreted directly in terms of mineral components. Mafic material at Moses Rock dike has tentatively been identified and interpreted as serpentized olivine-bearing soils (confirmation awaiting field work). The NS001 images have not only allowed the necessary regional overview, but have also identified additional areas in the region that may be associated with the dike. Additional AIS flights and/or field work for these areas will clarify the association.

## Recommendations

High-spectral resolution mapping spectrometers provide important information about the composition of surface materials. The AIS is a good, if not excellent, prototype of such instruments. Major areas of improvement that would strongly enhance and enable science applications include: 1) more complete spectral coverage [eg. 0.5 to 2.5 $\mu$ m], 2) higher accuracy and precision [largely a function of instrument calibration and noise control], 3) wider swath width [or at least continuation of coordinated multispectral imaging over a wider area].

## References:

- Adams J. B. (1974) Visible and near-infrared diffuse reflectance spectra of pyroxenes as applied to remote sensing of solid objects in the solar system, *J. Geophys. Res.*, 79, 4829-4836.
- Adams J. B. (1975) Interpretation of visible and near-infrared diffuse reflectance spectra of pyroxenes and other rock-forming minerals. In: *Infrared and Raman Spectroscopy of Lunar and Terrestrial Materials* (C. Karr, Ed.) Academic Press, New York, 91-116.
- Hunt, G. R. and Salisbury, J.W. (1970) Visible and near-infrared spectra of minerals and rocks: I Silicate minerals. *Modern Geology*, Vol. 1, 283-300.
- McGetchin T. R. (1968) The Moses Rock dike: Geology, petrology, and mode of emplacement of a kimberlite-bearing breccia dike, San Juan County, Utah, Ph.D. thesis, 405 pp., Calif. Inst. of Technol., Pasadena.
- McGetchin T. R. and Silver L. T. (1970) Compositional relations in minerals from kimberlite and related rocks in the Moses Rock Dike, San Juan County, Utah. *The American Mineralogist*, Vol. 55, 1737-1771.
- McGetchin T. R. and Silver L. T. (1972) A crustal-upper mantle model for the Colorado Plateau based on observations of crystalline rock fragments in the Moses Rock Dike. *J. Geophys. Res.*, 77, 7022-7037.

## ANALYSIS OF AIRCRAFT SPECTROMETER DATA WITH LOGARITHMIC RESIDUALS

A.A. GREEN and M.D. CRAIG, CSIRO Division of Mineral Physics, Sydney, Australia

## ABSTRACT

Spectra from airborne systems must be analysed in terms of their mineral-related absorption features. The first part of this paper discusses methods for removing backgrounds and extracting these features one at a time from reflectance spectra. The second part discusses methods for converting radiance spectra into a form similar to reflectance spectra so that the feature extraction procedures can be implemented on aircraft spectrometer data.

## INTRODUCTION

Aircraft and spacecraft based spectrometer data pose fundamentally different analytical problems to those we have found when working with multispectral imagery. These new problems are associated with the analysis of curve shape. The overall brightness variability which is the dominant feature in multispectral imagery is now taken for granted and we are interested in the detailed shape of the reflectance curve as a function of wavelength. In this paper we shall deal with spectra in the SWIR region 1.9-2.5  $\mu\text{m}$  and treat the problems involved in analysing both reflectance curves, such as those obtained in the laboratory, and the more difficult problem of radiance curves acquired by remote sensing systems.

## ANALYSIS OF REFLECTANCE SPECTRA

Reflectance spectra in the SWIR region are usually composed of a flat or generally convex background with superimposed sharper absorption features due to the chemical groups which are of interest for remote sensing. The information content of these curves lies primarily in the wavelength position of these absorption minima and to a lesser extent in the relative intensity and shape of the absorption features. The extraction and parametrization of absorption features in a spectrum is the first step in the recognition of the chemical species which are causing the absorption spectrum. In order to extract these features we must first remove the overall convex background.

This may be done by ratioing the spectrum to its "upper convex hull (or envelope)", defined as the lowest convex curve lying above the given spectrum. The resulting curve - called the "hull-quotient" of the input curve - appears as a horizontal line of height unity interrupted by absorption features extending down towards the horizontal axis. Figure 1 illustrates a raw spectrum, its hull, and hull-quotient. Note especially the enhancement of features beyond 2.2  $\mu\text{m}$ , where removal of the sloping background has brought out sharp minima not identifiable in the raw data.

The technique is easily extended to permit the isolation and extraction of individual features. Thus, the "first featuregram" is obtained as the union of hulls for the parts of the hull-quotient to

left and to right of the lowest point on that curve. The ratio of hull-quotient to first featuregram is a curve coinciding with the hull-quotient, except for the absence of its dominant feature. Remaining features may be extracted successively until the residual spectrum is reduced to mere noise fluctuation of no significance.

If implemented as described above the algorithm produces V-shaped absorption features which do not match well with the usual inverted Gaussian shape of most absorption features. Improved performance is obtained by making the featuregram coincide with the curve (from which it is to be removed) between the points of inflection closest to the minimum and on either side of it. The rest of the featuregram is made up of the two hulls computed beyond those points. Figure 2 illustrates the features extracted from a simple reflectance spectrum.

Feature extraction can provide the basis for automatic classification of spectra. Classification of two types is possible.

The first type compares the wavelength position, relative depth and shape of each extracted feature with a list of characteristics of reference materials, and makes an assignment in much the same way as would a human interpreter.

The second type of classifier relies on the signs of first and second derivatives of hull-quotients. The second derivative of a convex curve is always non-positive. On the other hand, the slope of a featuregram will be negative to the left of the feature-minimum, positive to the right. The ratio of a hull-quotient to its residual noise-spectrum equals the product of extracted features and so is characterized by long runs of channels with the same sign for the first or second derivative.

By encoding the sign as 0 or 1, and concatenating the strings for first and second derivative, we obtain the 2N-channel "binary signature" of an N-channel spectrum. The Hamming distance (equal to the number of mismatches in corresponding channels) between two such signatures provides an effective measure of their similarity. Input spectra could then be classified by comparison with stored, library spectra.

## RADIANCE SPECTRA

Radiance spectra acquired in airborne systems bear little resemblance to the laboratory reflectance spectra that would result from sampling the surface materials along the flight path. Apart from the ambiguity introduced by the heterogeneous composition of each pixel, the difficulties are of two kinds. First, topographic effects, such as different inclination, affect the apparent brightness of different occurrences of the same material. Secondly, the solar illumination curve, unlike a laboratory light source, varies considerably in accordance with prevailing atmospheric conditions.

Using a very simple model we relate the radiance measurement  $X_{i\lambda}$  to the reflectance  $R_{i\lambda}$  in sample i, wavelength  $\lambda$ , by means of a multiplicative formula

$$X_{i\lambda} = T R_{i\lambda} I_{\lambda} \quad (1)$$

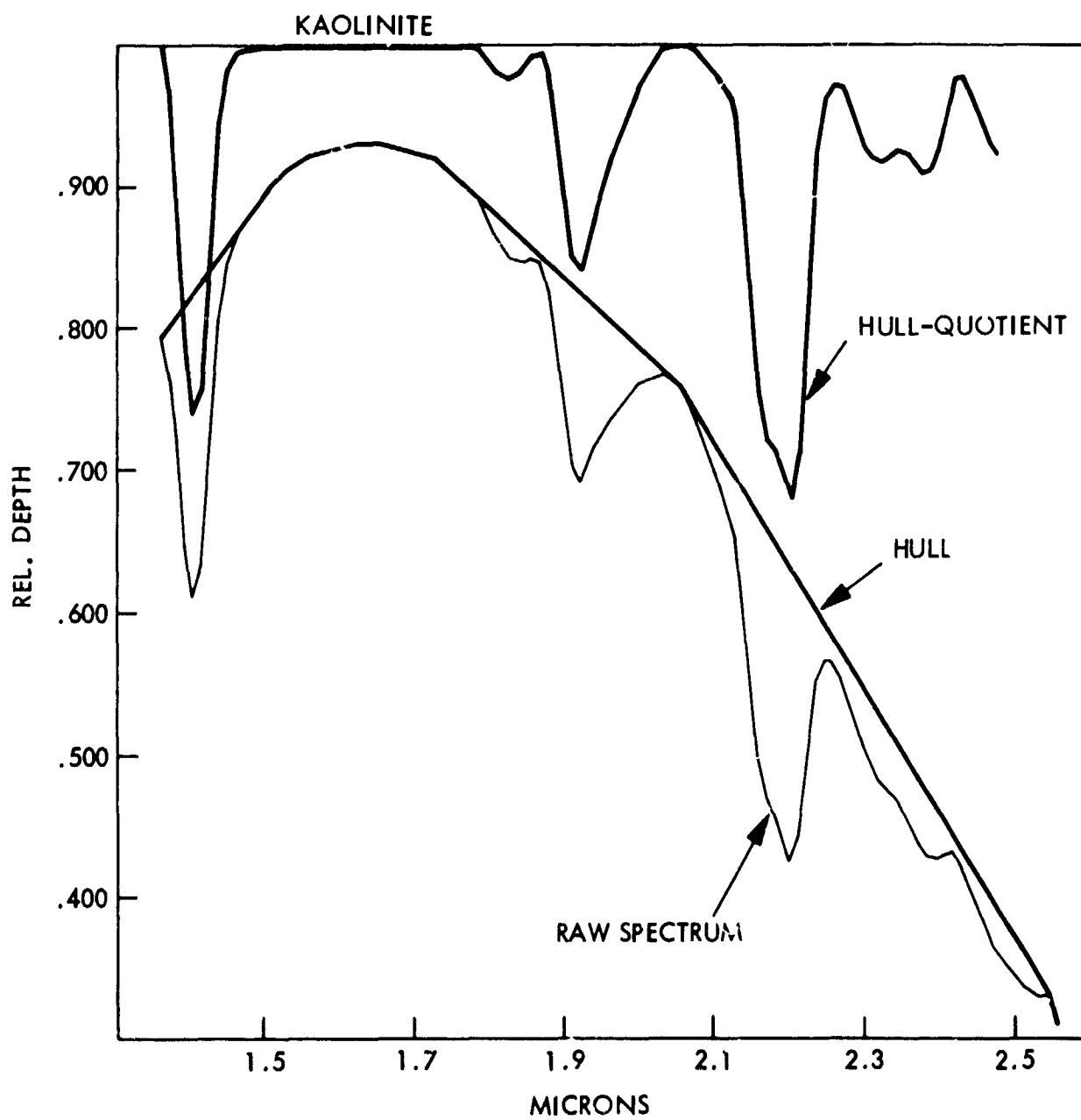


Figure 1. Raw spectrum, hull and hull-quotient for a kaolinite spectrum between 1.4 and 2.5  $\mu\text{m}$ .

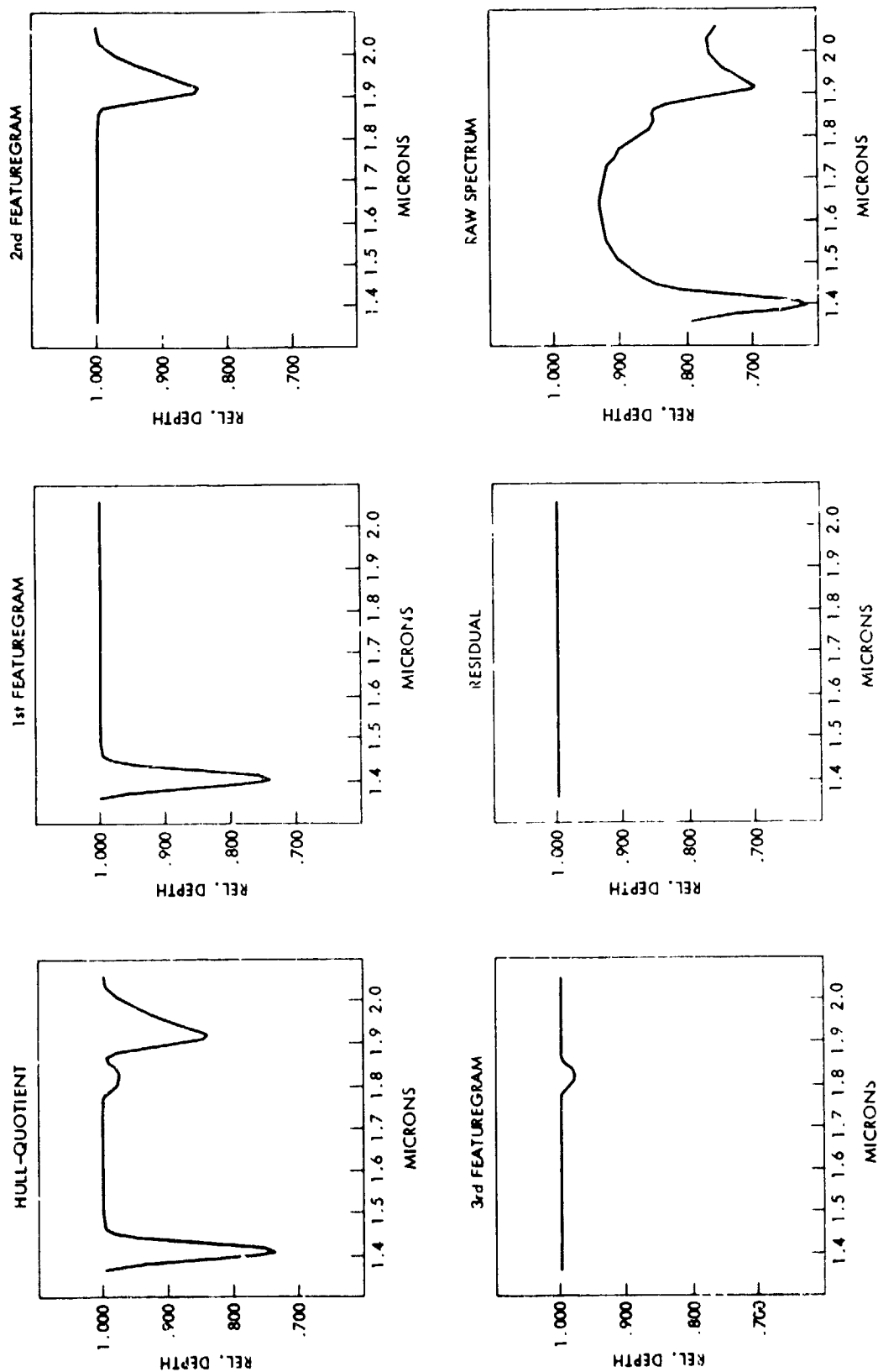


Figure 2. Progressive feature extraction from a hull-quotient spectrum (obtained from the raw reflectance spectrum at lower right). Each featuregram represents a separate absorption feature.

The "topographic" factor  $T_i$  accounts for surface variability with sample number and is constant for all wavelengths, while the "illumination factor"  $I_\lambda$  describes the unknown illumination curve, assumed the same for all points on a single flight line.

Write  $X_{i.}$  to denote the geometric mean of  $X_{i\lambda}$  taken over all channel wavelengths  $\lambda$ . With a similar convention regarding the other new symbols we have from (1)

$$X_{i.} = T_i R_{i.} I. ,$$

hence by division

$$X_{i\lambda}/X_{i.} = (R_{i\lambda}/R_{i.})(I_\lambda/I.), \quad (2)$$

independent of the unknown factor  $T_i$ . The spectra represented by the two sides in (2) may be called the "topographically equalized" (or "albedo equalized") versions of the input spectra (1).

The simplest way of eliminating the unknown illumination factor is by taking the geometric mean over all samples in equation (2). With an obvious notation we find

$$X_{.\lambda}/X_{..} = (R_{.\lambda}/R_{..})(I_\lambda/I.), \quad (3)$$

giving upon division

$$(X_{i\lambda}/X_{i.})/(X_{.\lambda}/X_{..}) = (R_{i\lambda}/R_{i.})/(R_{.\lambda}/R_{..}). \quad (4)$$

We have thus computed from the original radiance spectra  $X_{i\lambda}$  a new set of spectra with the advantage that they are the same as would be obtained by applying the same process to the unknown reflectance spectra  $R_{i\lambda}$ .

The geometric means must, in practice, be computed from arithmetic means of logarithms; hence, it is the logarithm of the quantity in (4) which results from the processing. Such spectra are termed the "logarithmic residuals" of the original spectra  $X_{i\lambda}$ , the quantity in (4) giving then the "exponentiated log residuals" of the  $X_{i\lambda}$ . This residual method has some features in common with that used by Marsh and McKeon (1983) but it is also fundamentally different in the way it removes the  $I_\lambda$  factor.

Log residual spectra lack some of the information originally present. For example, a mineralogical absorption feature present in all samples, even if situated away from the known positions of atmospheric absorptions, will be treated as a component of  $I_\lambda$  and removed by the processing. On the other hand, a mineralogical feature whose presence in a few samples was obscured in the radiance spectra, due to its coincidence with a major atmospheric absorption, will become evident in the log residual data. Thus, despite its limitations, the log residual transformation of radiance spectra from airborne systems has shown itself to be a very useful aid to interpretation.

The log residual technique as described above requires modification to render it compatible with the processing described earlier for reflectance spectra. Suppose, for example, that a particular absorption feature, such as the clay/muscovite feature at 2.2 microns, is strongly represented within a flight line. That

feature will then persist in the geometric mean (3) of the albedo equalized spectra. Samples which do not have an absorption at 2.2 microns will give values at 2.2  $\mu\text{m}$  which are high relative to the mean. The ratio (4) for such samples will thus exhibit what may facetiously be termed an "emission feature" at that wavelength.

Such features will of course defeat the algorithm for (absorption) feature extraction. To overcome the problem we need a replacement for the geometric mean (3) which likewise contains the factor  $X_{\lambda}/I_{\lambda}$ , but is never less than any value (2) which it is to divide. The required quantity is of course the least upper bound spectrum (LUB)

$$\text{LUB}_i (X_{i\lambda}/X_{i.}) = \text{LUB}_i (R_{i\lambda}/R_{i.})(I_{\lambda}/I_{\lambda.})$$

taken over all sample numbers  $i$ . We get in place of (4)

$$(X_{i\lambda}/X_{i.})/\text{LUB}_i (X_{i\lambda}/X_{i.}) = (R_{i\lambda}/R_{i.})/\text{LUB}_i (R_{i\lambda}/R_{i.}), \quad (5)$$

which may be termed the least upper bound (or supremum) residual corresponding to  $X_{i\lambda}$ .

The least upper bound residuals may be computed as well from the earlier log residuals as from the radiance data. We have only to observe that the left member in (5) equals

$$[(X_{i\lambda}/X_{i.})/(X_{\lambda.}/X_{\lambda..})]/\text{LUB}_i [(X_{i\lambda}/X_{i.})/(X_{\lambda.}/X_{\lambda..})].$$

This observation has allowed us to use, as input, an extensive library of early log residual back-up tapes, to generate least upper bound residuals with a minimum of computation.

#### EXAMPLES

Aircraft data were acquired over a number of Australian test sites with the GER spectrometer system (Collins *et al.*, 1981) in September, 1982. The examples used here are taken from a flightline over the Mary Kathleen area in NW Queensland. The data were corrected for instrument response function and processed to log residual spectra and least upper bound spectra as described above.

Figure 3 shows the results of the two procedures when used on data averaged over three uniform areas of distinctly different terrain type.

#### DISCUSSION

The area covered by the flight line used in this example can, to a first degree of approximation, be thought of as being composed of two cover types. These are firstly, a mixture of soil with arid-land grass known as spinifex, and secondly, an anomalous Ca-rich clay which is exposed in the Mary Kathleen open pit. The spectra of both these species are incorporated into the mean reflectance spectrum of the flight line and so will be subtracted from each true spectrum to produce the log residual spectrum for any given sample in the flightline. The result for a region which is typical of the grass/soil mixture is shown in Figure 3(a). The log residual spectrum (upper curve) is what we call a "not - Ca-clay" spectrum.

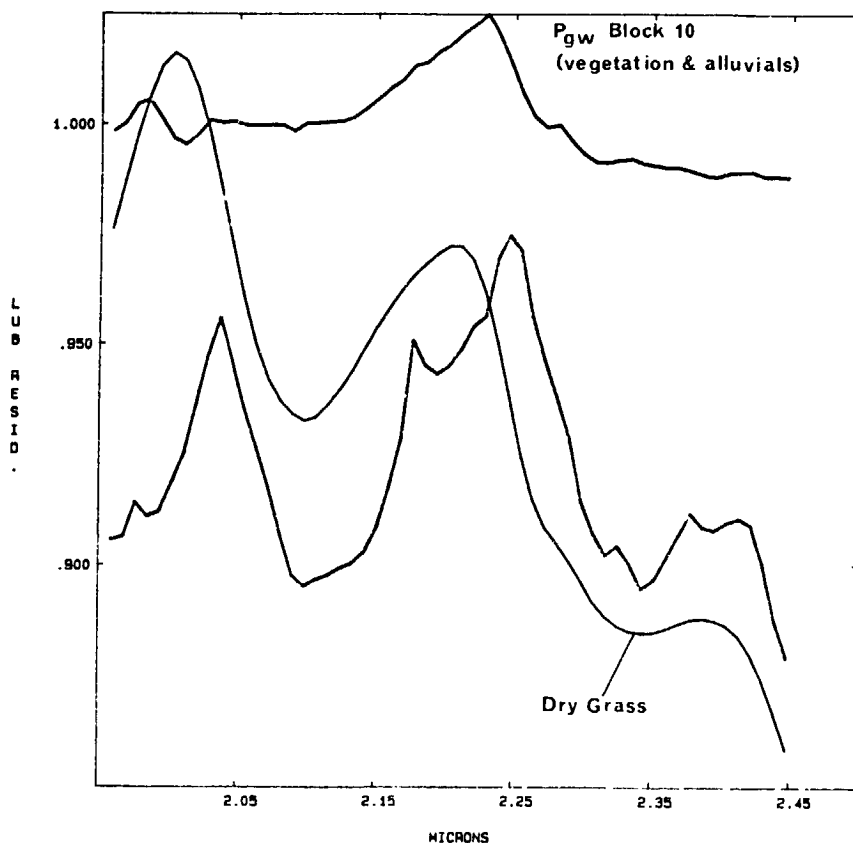
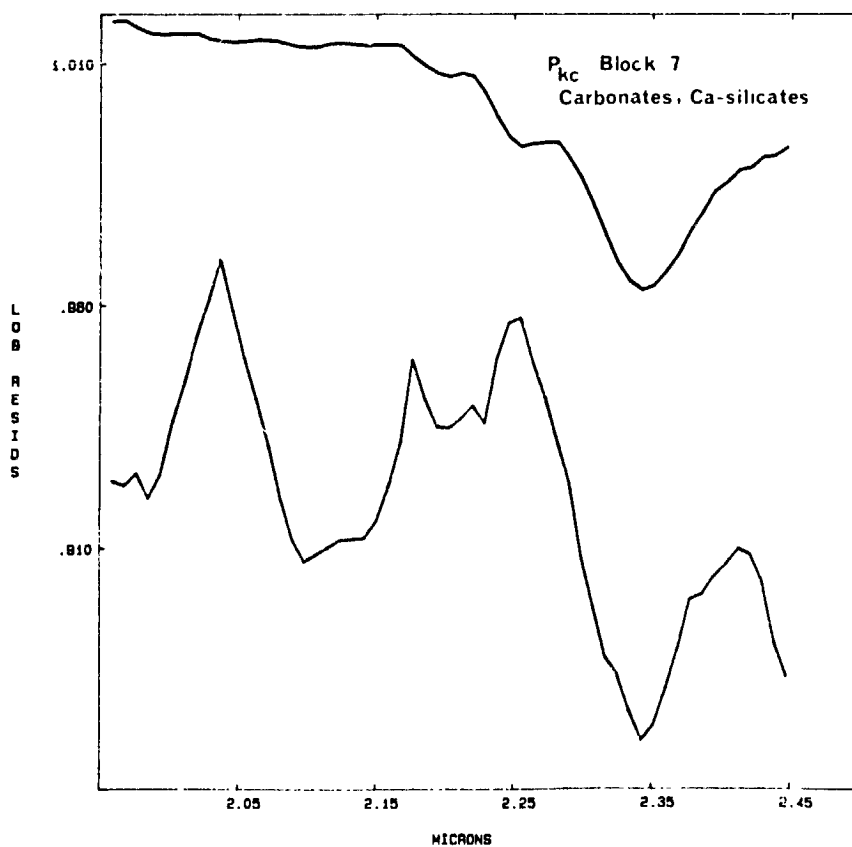
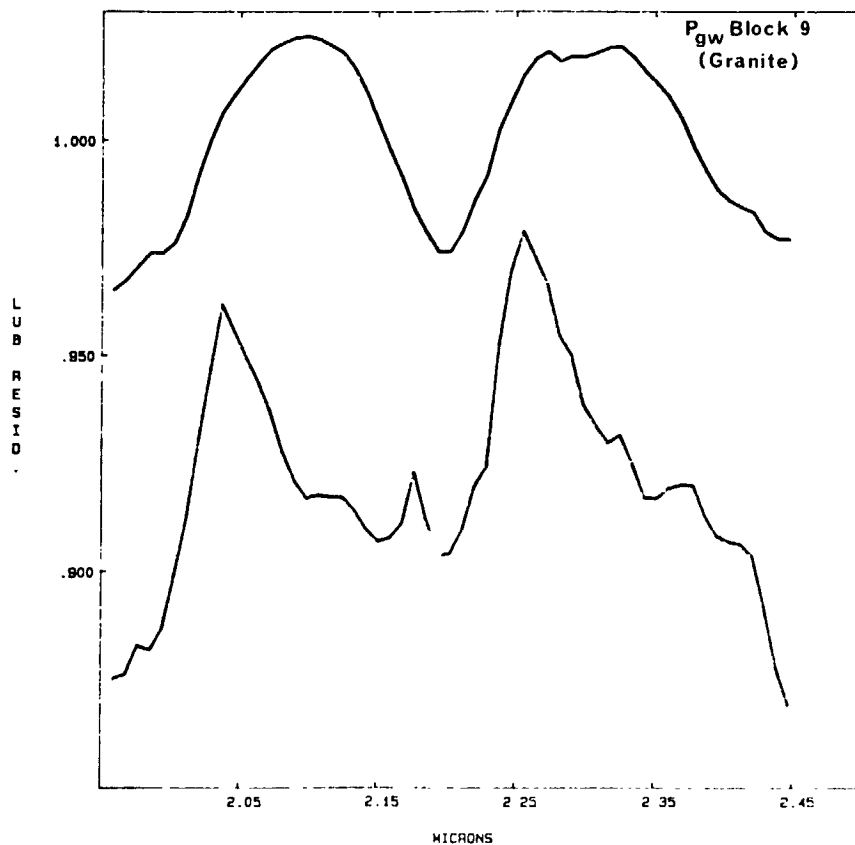


Fig. 3 (a). Log residual spectra (upper curve) and least upper bound residual (lower curve) for an area of dry grass and some soil near Mary Kathleen, Qld. The spectrum of dry grass alone is superimosed for comparison with the LUB curve.



3 (b). Log residual (upper) and LUB (lower) spectra for an area of carbonates and calc-silicates near Mary Kathleen in Qld. The log residual curve shows a typical spectrum for this type of terrain while the LUB residual spectrum shows a dominant vegetation curve perturbed by the carbonate feature at 2.35  $\mu\text{m}$ .



3(c). Log residual (upper) and LUB (lower) spectra for an area of granite. The typical 2.2 absorption feature is much more visible on the log residual than the LUB residuals.

It contains an upward feature with the inverted shape of a Ca-clay absorption feature. In contrast, the least upper bound residual (lower curve) shows a typical spectrum for a mixture of dry grass and a 2.2-absorbing clay. Although the least upper bound procedure does remove obnoxious upward features it superimposes a very strong dry grass spectrum onto the spectra of all samples except those from the open pit. In doing this it is correctly reproducing the reflectance spectra of those samples but it is also masking subtle mineralogical features evident in the log residual spectra, Figures 3(b) and 3(c). From this we can see that, in areas of relatively uniform dry grass cover, the log residual spectra have certain advantages. They remove the unwanted dry grass spectrum, leaving a spectrum which can more easily be allotted to the mineralogy.

#### CONCLUSIONS

Successful analysis of airborne spectrometer data depends on an ability to extract absorption features and measure their wavelength, shape and intensity. Background removal and feature extraction procedures can perform this function on reflectance curves. Radiance spectra can often be converted into "reflectance-like" curves by log residual or least upper bound residual methods which then enable the application of feature extraction procedures.

#### REFERENCES

- Collins, W., Chang, S.H., and Kuo, J.T., 1981. Infrared airborne spectroradiometer survey results in the western Nevada area. Aldridge Lab. Appl. Geophysics, final Report to NASA, Contract JPL 955832.
- Marsh, S.E., and McKeon, J.B., 1983. Integrated analysis of high-resolution field and airborne spectroradiometer data for alteration mapping. Economic Geology 78 p. 618-632.

N86-11637

COMPARISON OF AIS VS. TMS DATA COLLECTED OVER THE VIRGINIA PIEDMONT

R. BELL, NASA/Goddard Space Flight Center, USA; C.S. EVANS, University of Maryland, USA

ABSTRACT

The Airborne Imaging Spectrometer (AIS), NS001 Thematic Mapper Simulator (TMS), and Zeiss camera collected remotely sensed data simultaneously on October 27, 1983, at an altitude of 6860 meters (22,500 feet). AIS data were collected in 32 channels covering 1200-1500 nm. A simple atmospheric correction was applied to the AIS data, after which spectra for four cover types were plotted. Spectra for these ground cover classes showed a telescoping effect for the wavelength endpoints. Principal components were extracted from the shortwave region of the AIS (1200-1280 nm), full spectrum AIS (1200-1500 nm) and TMS (450-12,500 nm) to create three separate three-component color image composites. A comparison of the TMS band 5 (1000-1300 nm) to the six principal components from the shortwave AIS region (1200-1280 nm) showed improved visual discrimination of ground cover types. Contrast of color image composites created from principal components showed the AIS composites to exhibit a clearer demarcation between certain ground cover types but subtle differences within other regions of the imagery were not as readily seen. Verification of these preliminary results is necessary since the AIS data were collected in a fixed grating position with 32 channels compared to a greater spectral coverage of the TMS. Also, no ground checking has been performed. In addition, the AIS data were matched with TMS data from the more distal (from nadir) pixels in the swath coverage where pixels exhibit the most distortion.

DISCUSSION

Remotely sensed data from the Zeiss camera, NS001 Thematic Mapper Simulator (TMS) and Airborne Imaging Spectrometer (AIS) were collected during a flight of the NASA Ames C-130 at an altitude of 6860 meters (22,500 feet) on October 27, 1983, over the Chopawamsic Formation in the Piedmont Province in Central Virginia. This region consists of metamorphosed graywackes, subgraywackes, and impure quartzites interlayered with altered greenstone volcanics. This region is heavily vegetated, and in undisturbed areas is covered with both deciduous and coniferous forest. Due to the relatively flat topography

much of the region is under cultivation, including coniferous plantations.

Nadir pixel resolution for the TMS data was 19 meters and the swath width was approximately five kilometers. In contrast, the AIS data featured a nadir pixel resolution of 14 meters and the AIS data featured a nadir pixel resolution of 14 meters and a relatively narrow swath width of one-half kilometer.

The AIS was operating in the fixed grating mode at (old) position 0 (1200-1500 nm). This grating position includes spectral information associated with vegetation biomass and leaf water (Tucker, 1978). During the 1983 season the AIS utilized a 32x32 element HgCdTe area array detector (JPL, 1984). A video screen was available to the on-board investigator to track collection of the TMS data set but the actual AIS swath was not delineated. It was found post-flight that the AIS was offset from the test area approximately three kilometers to the west. Thus, the following analysis is restricted to a comparison of TMS vs. AIS data since we were unable to evaluate AIS data in a known region of stressed vegetation related to our present geobotanical anomaly project.

Our approach in evaluating the AIS data was three-fold. First we examined AIS spectral information in the 1200 to 1500 nanometer range to determine whether the narrow spectral band data were yielding new information or if redundancy would be evidenced. Second, we compared the TMS band 5 (1000-1300 nm) to the shortwave region of the AIS (1200-1280 nm) for a possible increase in the ability to visually discriminate ground cover classes in the two data sets. Finally, to further assess ability to discriminate ground cover classes, we enhanced three separate color image composites utilizing principal components for the TMS data, shortwave region of the AIS, and full spectrum of AIS, excluding the water absorption channels.

Prior to image processing, a simple atmospheric correction, based upon signal return over a waterbody, was applied to the AIS data. From infrared photography, four classes of ground cover were chosen containing information in a coniferous tree stand, agricultural field, waterbody, and over two separate deciduous tree stands.

To begin appraisal of spectral information in the 1200 to 1500 nm range, the spectra for the above mentioned classes were plotted. From these spectral plots it was usually noted that there appeared to be a telescoping of the actual positioning in the channels from both ends of the grating position. A nominal shift of 10 nm to the longer wavelengths at the 1200 nm position was observed

together with a 10 nm shift to the shorter wavelengths at the 1500 nm position. Otherwise, the relative reflectance values for classes were found to be as expected based upon the color infrared photography for the fall season.

Next, to compare TMS and AIS in an image interpretation context, TMS band 5 (1000-1300 nm) and six AIS principal components (1200-1280 nm) were enhanced. Even though the AIS principal components exhibited vertical striping in several samples due to dead pixel elements (JPL, 1984) and horizontal noise in a periodic manner, certain ground cover classes were more readily defined. Fields not distinguishable from one another with TMS data were separable with the AIS data. Also texture was more apparent in forested areas in the AIS data, allowing demarcation of what are perhaps species assemblage changes within such areas based upon subtle changes in texture. Such forested areas could only be outlined with the TMS data. This result appears to be related to the fact that six orthogonal AIS components overlap spectral information contained in only one TMS channel.

Finally, three color composites were created from principal components using (1) TMS data (450-12500 nm), (2) shortwave region of AIS data (1200-1280 nm), and (3) the full AIS spectrum (1200-1500 nm) excluding the water absorption bands. While the AIS composite enabled a clearer demarcation between certain ground cover types as previously noted, subtle differences within other regions on the image were not as readily seen in the AIS composite.

Verification of these very preliminary results is necessary since no ground checking has been done. The AIS data were matched only by the more distal (from nadir) pixels of the TMS data. In addition, a fixed grating position (1200-1500 nm) was employed for the AIS data collection whereas the TMS recorded data in eight bands covering the 450-12,500 nm range.

#### REFERENCES

- Jet Propulsion Laboratory, 1984, Airborne Imaging Spectrometer, Science Investigator's Guide to AIS Data, p. 15.
- Tucker, C. J., 1978, A Comparison of Satellite Sensor Bands for Vegetation Monitoring, Photogrammetric Engineering and Remote Sensing 44 (11): 1369-1380.

A PRELIMINARY INVESTIGATION OF SYSTEMATIC NOISE  
IN DATA ACQUIRED WITH THE AIRBORNE IMAGING SPECTROMETER

Edward Masuoka, Goddard Space Flight Center/NASA, Greenbelt, MD USA

ABSTRACT

Systematic noise is present in airborne imaging spectrometer (AIS) data collected on October 28, 1983 and May 5, 1984 in grating position 0 (1.2-1.5  $\mu\text{m}$ ). In the October data set the noise occurs as 135 scan-lines of low DN's every 270 scan-lines. The noise is particularly bad in bands nine through thirty, restricting effective analysis to at best ten of the 32 bands. In the May data the regions of severe noise have been eliminated, but systematic noise is present with three frequencies (3, 106 and 200 scan-lines) in all thirty-two bands. The periodic nature of the noise in both data sets suggests that it could be removed as part of routine processing at JPL. This is necessary before classification routines or statistical analyses are used with these data.

BACKGROUND

Data were acquired on October 28, 1983 and May 5, 1984 with the airborne imaging spectrometer (AIS) over the George Washington National Forest in West Virginia in order to examine the utility of sensors with high spectral resolution for geobotanical mapping. The October AIS data covered thirty-two bands in the 1.2-1.5  $\mu\text{m}$  region and while the May data covered 128 spectral bands in the 1.2-2.4  $\mu\text{m}$  region, only the first thirty-two bands were analyzed in this study. The October overflight of the test sites produced data with considerable noise in bands nine through thirty (Figure 1). Histograms of these bands were bimodal with noise forming a significant peak at thirty or less digital counts (Figure 2). The effect of the noise on unsupervised classification was dramatic. Forest communities in areas in which noise was present were placed in separate classes from similar communities in the noise-free regions. Figure 3 illustrates the difference in classified images produced using only noise-free bands and all 32 bands. In the latter case, noise-related classes appear at regular intervals across the image. The May overflight produced data with reduced noise (Figure 4). The large regions of low digital numbers (DN's) present in the October data were gone. However, periodic noise was still present at a level unacceptable for statistical analyses which involve comparisons of reflectance between small test sites.

## ANALYSIS

The noise in the October 1983 AIS data was first recognized in a principal components transformation of the 32 bands. When the first four principal components were displayed, the noise was present in components two and four as regions of lower DN's (Figure 5). An examination of all thirty-two bands revealed that there was substantial noise in bands 9-30, which fell within a region of strong water absorption. The remaining ten bands which fall outside this region were relatively noise free. In plots of columns from band fifteen, noise appeared as 130-140 lines of lower DN's which occur about every 270-300 scan-lines. Similar plots for one of the noise-free bands, band one, did not show a regular pattern of either high or low values.

The large regions of noise which characterize the October data are absent from the May 1984 AIS image (Figure 4). However, noise in the aircraft electrical system, which affects roughly every third scan-line, is worse in the May data. Also new in the May data are spikes and dips in the signal which appear every 106 scanlines. In band 1 these appear as scan-lines with DN's 2000 to 3000 counts lower than surrounding lines. In band 15 the same scanlines are approximately 1500 counts higher than surrounding lines. The occurrence of this noise at a precise interval suggests that its source is within the AIS system. A third type of noise encountered in the May data is saturated scanlines (lines in which all the pixels have the value 4095). The interval between these spikes varies from 4 to 200 scanlines and the spikes occur at the same location in all bands. The irregular interval between spikes suggests that the source of this noise is outside the AIS system. Principal component transformations of this AIS data offer no improvement over the raw data for interpretation (Figure 6) because noise is present in all components and is enhanced in components four and five. However, the results of an unsupervised classification procedure using the data are relatively unaffected by the noise.

The cyclic nature of the electrical noise requires that special care be taken in performing statistical comparisons between test sites along a flight line. The presence of cyclic noise superimposed on the reflectance data creates a situation in which pixels are more similar along rows than down columns and pixels from rows spaced one cycle apart may be more closely related than pixels from adjacent rows. In placing test sites one should try to locate them on scanlines which are at the same place in the noise cycle and the test sites should be large enough to adequately sample

ORIGINAL PAGE IS  
OF POOR QUALITY

the variations in DN due to noise as well as variations due to canopy reflectance. Finally, the means from the sites should be used as observations in the analysis and not the individual pixels. This is particularly important due to the high degree of autocorrelation which stems from the electrical noise.

#### CONCLUSIONS

Noise is present in both the October 1983 and May 1984 AIS data sets acquired over the George Washington National Forest. The noise is for the most part periodic, occurring every three and 106 scanlines. Suitably chosen filters should be used to remove the noise prior to making statistical comparisons between test sites using these data sets.

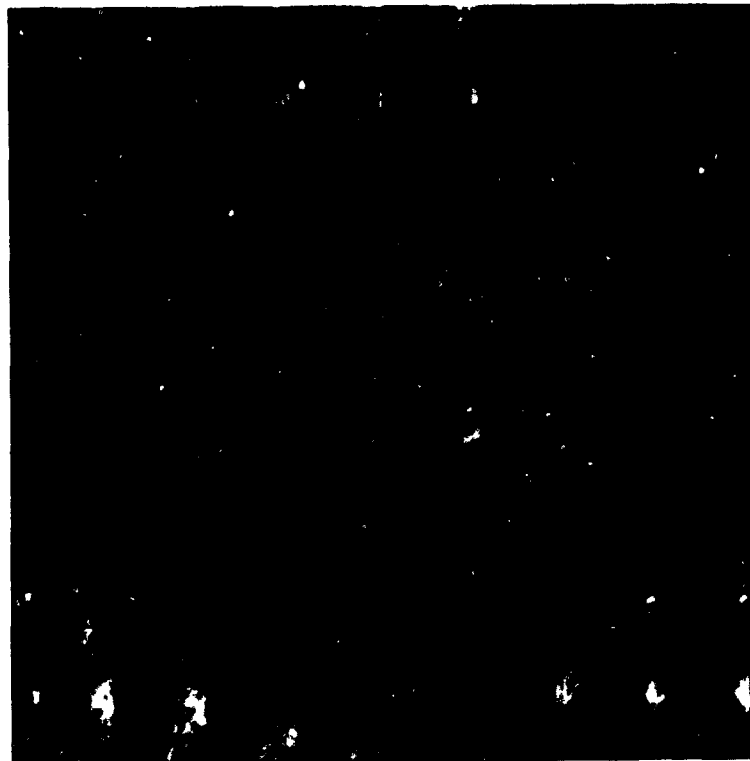
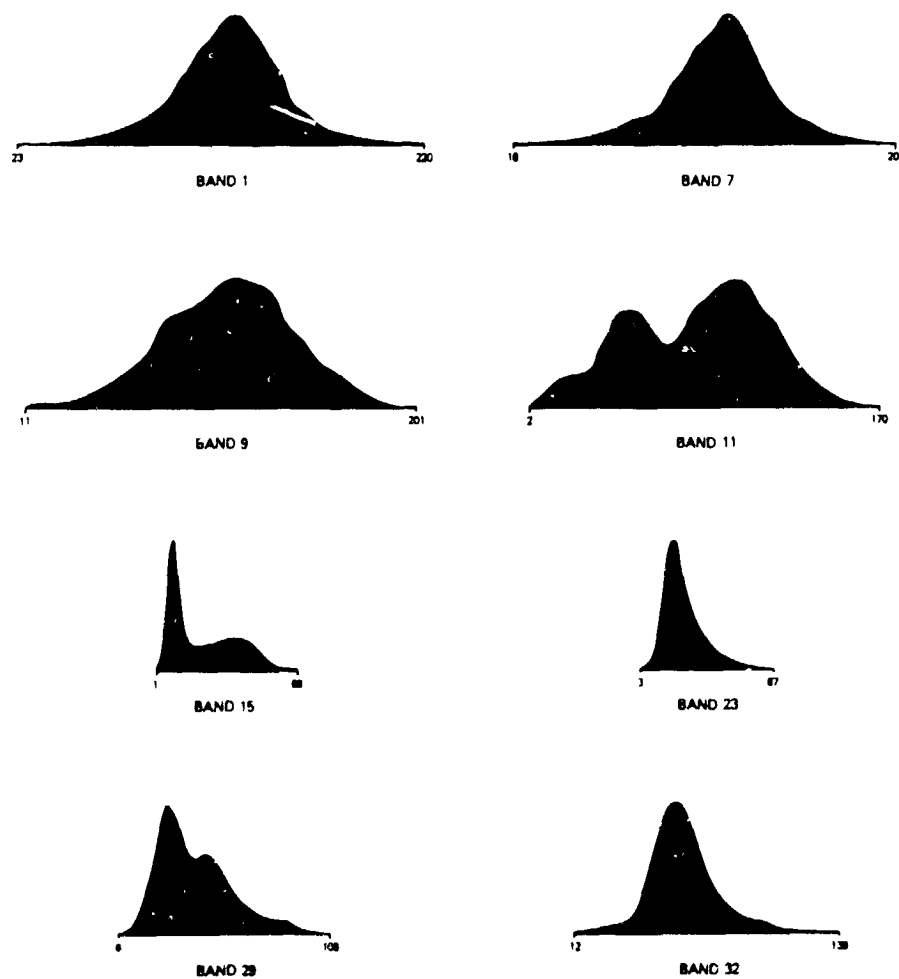


Fig. 1. Eight bands from the October 28, 1983 AIS flight (band numbers appear to the left of the each image)



**Fig. 2. Histograms of DN values for the eight bands in figure 1. Noise appears as a peak in the one-to-thirty DN range.**

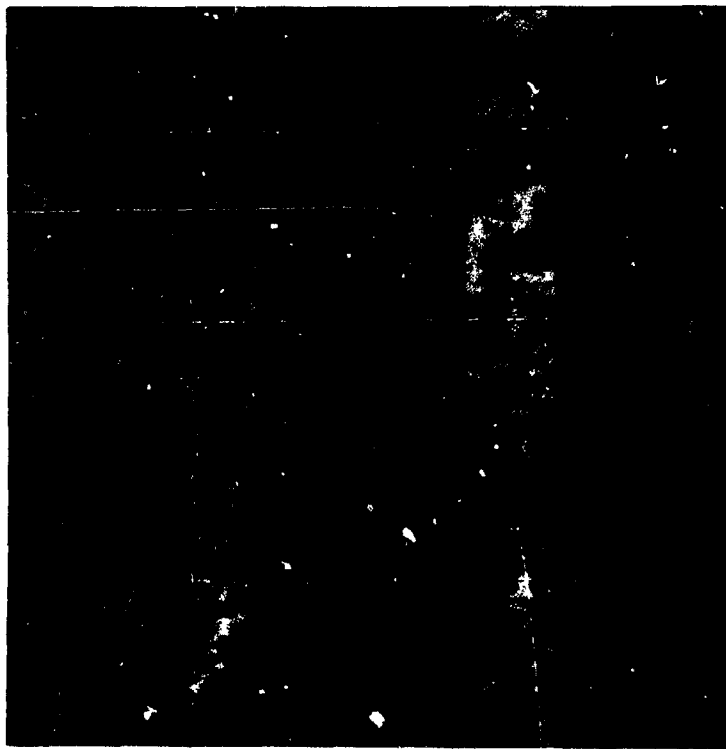


Fig. 3. Two classifications produced by an unsupervised clustering routine, ISOCLS. The left image was produced from only the first eight bands of the October data. The right image was produced using all thirty-two bands. Homogeneous regions in the right image occur where noise is the greatest.

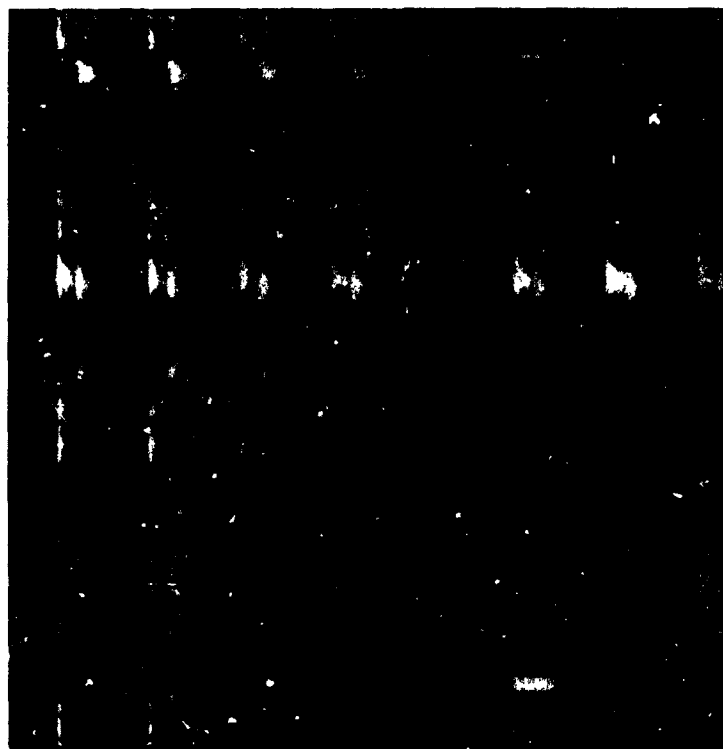


Fig. 4. Eight bands from the May 5, 1984 data.

ORIGINAL PAGE IS  
OF POOR QUALITY

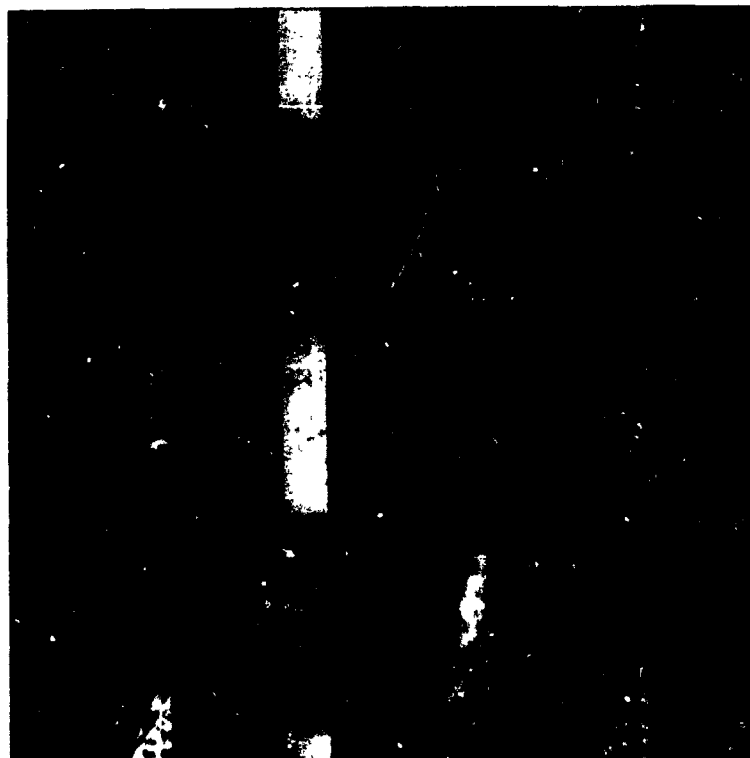


Fig. 5. Principal components analysis all thirty-two bands from the October data. The first principal component is on the left.

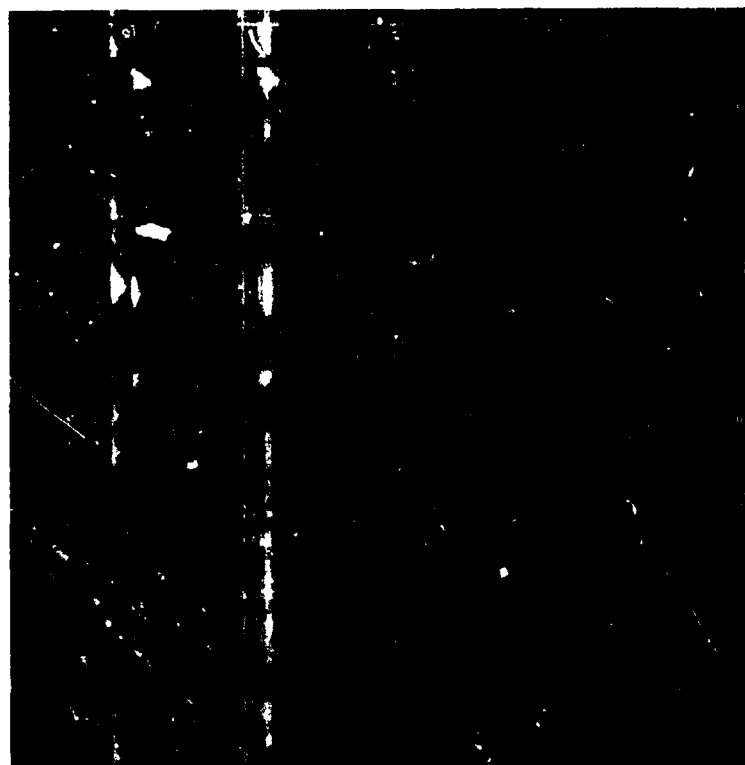


Fig. 6. Five principal components produced from the first thirty-two bands of the May 5, 1984 data.

## DISCRIMINATION OF COASTAL VEGETATION AND BIOMASS USING AIS DATA

MICHAEL F. GROSS AND V. KLEMAS, College of Marine Studies, University of Delaware, Newark, Delaware, 19716, USA.

## ABSTRACT

The AIS was flown over a coastal wetlands region near Lewes, Delaware, adjacent to the Delaware Bay on 16 August 1984. Using the AIS data, it was possible to discriminate between four different types of wetland vegetation canopies: (1) trees; (2) broadleaf herbaceous plants (e.g. Acnida cannabina, Hisbiscus moscheutos); (3) the low marsh grass Spartina alterniflora; and (4) the high marsh grasses Distichlis spicata and Spartina patens. The single most useful region of the spectrum was that between 1.40 and 1.90 $\mu$ , where slopes of portions of the radiance curve and ratios of radiance at particular wavelengths were significantly different for the four canopy types. The ratio between the highest digital number in the 1.40-1.90 $\mu$  and .84-.94 $\mu$  regions and a similar ratio between the peaks in radiance in the 1.12-1.40 $\mu$  and .84-.94 $\mu$  spectral regions were also very effective at discriminating between vegetation types. Differences in radiance values at various wavelengths between samples of the same vegetation type could potentially be used to estimate biomass. Thus, high spectral resolution spectrometry appears to have great potential value for remote sensing studies of wetland vegetation.

## INTRODUCTION

Radiance measurements made using hand-held radiometers have been found to be correlated with, and have been used to predict, biomass of wetland vegetation (Drake 1976, Jensen 1980, Budd and Milton 1982, Hardisky et al. 1984). Landsat imagery has been successfully used to map surface cover types in wetlands (Bartlett and Klemas 1981, Butera 1983). This investigation reports on the potential of AIS data to discriminate between wetland vegetation types and to estimate biomass.

## MATERIALS AND METHODS

The AIS was flown over the Old Mill Creek Marsh near Lewes, Delaware, located at 38°45'N and 75°10'W, on 16 August 1984, at approximately 13:30 EST during low tide. The flight line extended from the head of Old Mill Creek to the Delaware Bay. The swath width was about 320m and the flight line was over 5km long. Spatial heterogeneity and vegetation patchiness within the study site are very pronounced and few monospecific areas exist. For the purposes of this study, the vegetation within the flight line has been grouped into four broad categories based upon dominant

species: (1) SN, low marsh grass S. alterniflora; (2) PD, high marsh grasses S. patens/Distichlis spicata; (3) AH, A. cannabina, H. moscheutos, and other broadleaf low-salinity marsh species; and (4) TR, trees.

The AIS data were processed and corrected for effects of the solar irradiance curve by JPL. It was unfortunately not possible to correct for the striping due to unequal detector response or for water/atmospheric absorption effects in our AIS imagery. In selecting areas for analysis of spectral features, samples 5x5 pixels (50mx50m) in size were chosen in order to lessen the effects that variability in detector response would have on the spectral radiance curves generated.

## RESULTS

Figure 1 displays curves of the reflected radiance of representative AH, TR, SN and PD canopies in the Tree Scan Mode (.84-2.04 $\mu$ ). Four water absorption regions centered at about .94, 1.13, 1.40 and 1.87 $\mu$  are evident. The spectral curves of the four canopy types exhibit the same basic features. In the first reflected radiance region (.84-.94 $\mu$ ), hereafter referred to as region 1, a peak occurs at .87 $\mu$ . The radiance peak is at 1.05 $\mu$  within the second radiance region (.94-1.12 $\mu$ ). The third major radiance region (1.12-1.40 $\mu$ ) is characterized by a peak radiance at about 1.22 $\mu$ , while a radiance peak at 1.70 $\mu$  occurs in the fourth radiance region (1.40-1.90 $\mu$ ). Radiance values between 1.90 and 2.34 $\mu$  (from the Rock Scan Mode) were very low and therefore substantially affected by the variability in detector response, so this spectral region was not extensively analyzed.

The reflected radiance values of SN canopies are lower than those of the other three vegetation types. TR radiance tends to be greater than SN radiance, while the PD and AH canopies exhibit the highest radiance values. The AH curve in region 4 is distinctly different from those of the other three canopy types. A comparison with the PD curve reveals the differences most clearly. The slope of the AH curve between  $\approx$ 1.56 and 1.70 $\mu$  is much greater than that of the PD curve. Also, the AH curve peaks slightly beyond 1.70 $\mu$ , and has a relatively high digital number (DN) value at  $\approx$ 1.82 $\mu$ . The unique features of the AH curves are more obvious in Figure 2, where reflected radiance curves between 1.43-1.89 $\mu$  from representative samples of AH, PD and SN are plotted.

Table 1 lists the mean of several slopes and ratios which were used to successfully discriminate between the four major vegetation types. The first parameter, the ratio between the highest digital number in regions 4 and 1, was significantly different between five out of the six possible vegetation pairs (AH-TR, AH-SN, AH-PD, TR-SN and TR-PD). Only the SN and PD canopies were not distinguishable using this ratio. A similar ratio between the peak DNs in regions 3 and 1 separated all possible pairs but the TR-PD and SN-PD pairs. The other three measures of discrimination between vegetation types shown in Table 1 rely solely upon properties of radiance in the fourth region (1.40-1.90 $\mu$ ). The slope of the straight line drawn between the DN at 1.56 $\mu$  and at 1.47 $\mu$  separated all six possible vegetation pairs, the 1.70 $\mu$  DN/1.82 $\mu$  DN ratio, all but the TR-PD pair, and the slope of the straight line drawn between the 1.70 $\mu$  and the 1.56 $\mu$  DN, all but the TR-PD and AH-PD pairs.

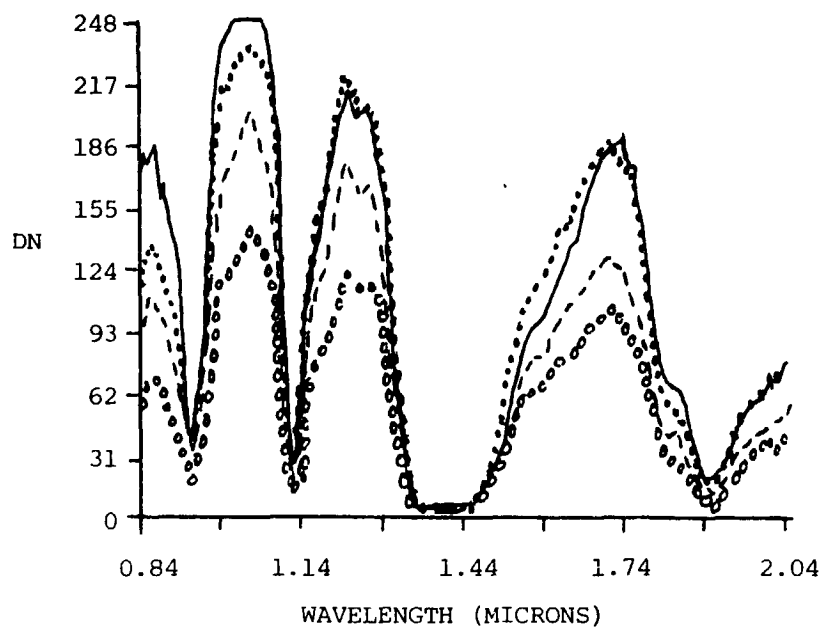


Figure 1. Reflected radiance curves between .84 and 2.04 $\mu$  for four wetland vegetation types (— = AH, ..... = PD, - - - = TR, ooooo = SN).

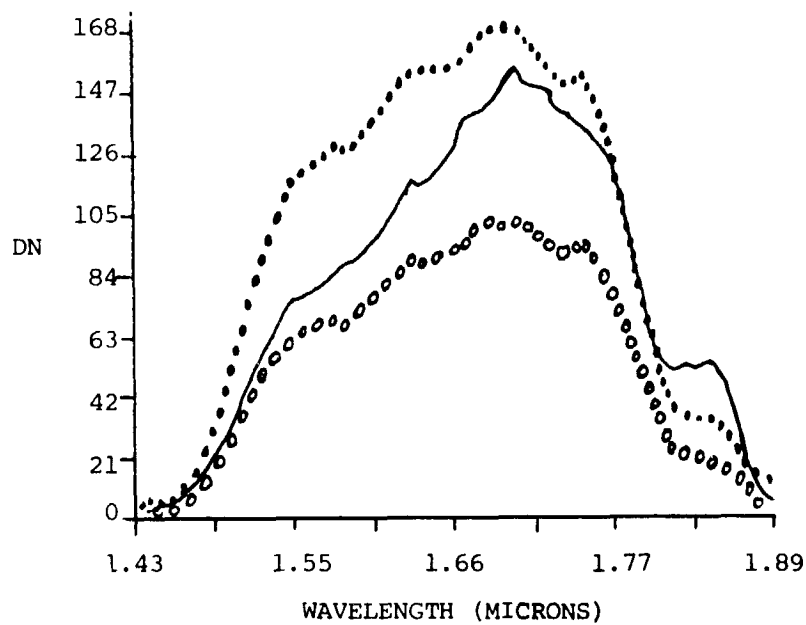


Figure 2. Reflected radiance curves between 1.43 and 1.89 $\mu$  for three wetland vegetation types (— = AH, ..... = PD, ooooo = SN).

Table 1. Parameters successfully used to discriminate between four types of wetland vegetation

Canopy <sup>2</sup>		Parameter <sup>1</sup>									
type	n	I	n	II	n	III	n	IV	n	V	
AH	4	1.04(.04)a	7	1.22(.03)a	5	7.67(.23)a	5	3.06(.04)a	5	5.30(.43)a	
TR	6	1.30(.04)b	7	1.57(.04)b	5	9.02(.14)b	5	3.95(.12)b	5	3.75(.14)b	
SN	4	1.44(.04)c	5	1.73(.04)c	5	6.45(.23)c	5	4.83(.11)c	5	2.71(.05)c	
PD	4	1.47(.03)c	8	1.66(.04)bc	5	11.09(.22)d	5	4.17(.09)b	5	4.55(.36)ab	

Values are means with one standard error of the mean in parentheses. n = number of replicates. Means followed by a similar letter are not significantly different at the .05 probability level.

<sup>1</sup>Parameters: I = ratio of peak radiance value in region 4 ÷ peak radiance value in region 1; II = ratio of peak radiance value in region 3 ÷ peak radiance value in region 1 (regions: 1 = .84-.94μ; 3 = 1.12-1.40μ; 4 = 1.40-1.90μ); III = slope of straight line between 1.56 and 1.47μ radiance values; IV = highest radiance value at 1.70 or 1.71μ ÷ lowest radiance value in the 1.81 to 1.84μ region; V = slope of straight line between 1.70 and 1.56μ radiance values.

<sup>2</sup>Canopy types: AH = broadleaf brackish marsh; TR = tree; SN = Spartina alterniflora; PD = S. patens/Distichlis spicata.

Values are means with one standard error of the mean in parentheses. n = number of replicates. Means followed by a similar letter are not significantly different at the .05 probability level.

<sup>1</sup>Parameters: I = ratio of peak radiance value in region 4 ÷ peak radiance value in region 1; II = ratio of peak radiance value in region 3 ÷ peak radiance value in region 1 (regions: 1 = .84-.94μ; 3 = 1.12-1.40μ; 4 = 1.40-1.90μ); III = slope of straight line between 1.56 and 1.47μ radiance values; IV = highest radiance value at 1.70 or 1.71μ ÷ lowest radiance value in the 1.81 to 1.84μ region; V = slope of straight line between 1.70 and 1.56μ radiance values.

<sup>2</sup>Canopy types: AH = broadleaf brackish marsh; TR = tree; SN = Spartina alterniflora; PD = S. patens/Distichlis spicata.

## DISCUSSION

Although the magnitude of the reflected radiance curves between the four vegetation types (AH, PD, SN, TR) differed substantially, the shape of the curves was generally similar in the five radiance regions bounded by water absorption bands between .84-2.34 $\mu$ , with the exception of the AH curve in the 1.40-1.90 $\mu$  region. The reasons for the peculiarities of the AH curve are not obvious and indicate a need for additional field and laboratory studies. Region 4 (1.40-1.90 $\mu$ ) is the single most useful region for discriminating between wetland vegetation types.

Although the data were not shown, the magnitude of reflected radiance varied among samples of the same vegetation type. Hardisky et al. (1984) demonstrated that an Infrared Index  $[(.76-.90\mu \text{ radiance} - 1.55-1.75\mu \text{ radiance}) / (.76-.90\mu \text{ radiance} + 1.55-1.75\mu \text{ radiance})]$  could be used to successfully predict biomass in Delaware wetlands. This suggests that if field data were collected, the AIS radiance data in the near infrared and in the middle infrared could be correlated with biomass and prove very useful in estimating biomass or productivity of wetland vegetation.

Table 1 indicates that, by using a combination of very basic, easy to compute ratios, it should be possible to map wetlands according to vegetation type. This demonstrates the utility of high spectral resolution data for remote sensing studies of vegetation. None of the ratios in Table 1 could be calculated from Landsat MSS or TM or from SPOT data since these instruments only collect data in very broad spectral bands.

## REFERENCES

- Bartlett, D. S. and V. Klemas. 1981. In situ reflectance studies of tidal wetland grasses. Photogrammetric Engineering and Remote Sensing. 47:1695-1703.
- Budd, J. T. C. and E. J. Milton. 1982. Remote sensing of salt marsh vegetation in the first four proposed Thematic Mapper bands. International Journal of Remote Sensing. 3:147-161.
- Butera, M. K. 1983. Remote sensing of wetlands. IEEE Transactions on Geoscience and Remote Sensing. GE21(3):383-392.
- Drake, B. G. 1976. Seasonal changes in reflectance and standing crop biomass in three salt marsh communities. Plant Physiology. 58: 696-699.
- Hardisky, M. A., F. C. Daiber, C. T. Roman and V. Klemas. 1984. Remote sensing of biomass and annual net aerial primary productivity of a salt marsh. Remote Sensing of Environment. 16:91-106.
- Jensen, A. 1980. Seasonal changes in near infrared reflectance ratio and standing crop biomass in a salt marsh dominated by Halimione portulacoides (L.) Aellen. New Phytologist. 86:57-67.

BYRON L. WOOD, Technicolor Government Services, Inc., NASA/Ames Research Center, Moffett Field, CA, USA; ROBERT C. WRIGLEY, NASA/Ames Research Center, Moffett Field, CA, USA.

#### ABSTRACT

Airborne Imaging Spectrometer (AIS) data were acquired over an agricultural area in eastern San Joaquin County, California in July, 1984. Cover-type information was subsequently collected for all fields along this flight line. The lack of detailed ground data on individual fields, however, limited AIS data analysis to a qualitative comparison of the spectral reflectance curves for a total of nine cover types. Based on this analysis, it appears that cover types with a positive slope in the 1550-1700 nm region have a higher spectral response in the 1200-1300 nm region compared to those cover types with a negative slope in the 1550-1700 nm region. Within cover type, spectral variability was also found to be greater than that between cover types. Given the lack of additional field data, the reason for these differences is a matter of speculation.

#### INTRODUCTION

For several years, the NASA/Ames Research Center (NASA/ARC) has been involved in the application of remote sensing data to agricultural research in California. During the 1983 growing season, researchers at NASA/ARC and the University of California, Berkeley cooperated in the collection of ground data including: crop type, growth stage, percent ground cover, canopy height, surface moisture, weediness, row direction/width and irrigation method on over 200 fields in eastern San Joaquin County, California. The collection of these data was coordinated with the acquisition of Daedalus Thematic Mapper Simulator (TMS) data on seven dates throughout the growing season. These data were used both to evaluate Landsat Thematic Mapper (TM) resolution data for crop identification and mapping and to understand the relationship between changes in surface/crop conditions and spectral reflectivity.

One of the findings of this research was that at the level of TM data resolution, considerable spectral crop confusion results from the relationship between crop canopy structure, percent ground cover and soil moisture content. In an effort to address this issue, Airborne Imaging Spectrometer data were requested for a portion of the San Joaquin County study area. The intent was to coordinate the collection of ground data with the acquisition of the AIS

data. Ground data collection was to include those variables monitored in 1983, as well as plant tissue for laboratory spectral and chemical analysis. In actuality, it proved impossible to coordinate these activities and only cover type information was obtained several weeks after the AIS flight.

#### DATA ACQUISITION AND ANALYSIS

The AIS, mounted on the NASA C-130 aircraft, acquired data along Jack Tone Road in eastern San Joaquin County, California on July 31, 1984. These data cover the wavelengths between 1155 and 2336 nanometers (nm) at a sampling interval of approximately 9.3 nm. Ground resolution of the data is approximately ten meters with a 32 pixel swath width.

The 35-mm black and white photographs, acquired at the same time as the AIS data, were used to locate the flight line, and served as the base on which field cover-type data were recorded. The field reconnaissance took place in late August, 1984. Due to this delay, some of the fields identified as bare soil may have supported a crop at the time of the AIS overflight. Whenever possible, these fields were labeled as to previous cover type. If there was any question about cover type at the time of the AIS overflight, the field was not included in the subsequent analysis.

Analysis of the AIS data was performed on a VAX 11/780 using IDIMS image processing software and additional programs developed specifically for AIS analysis. All AIS channels were registered for analysis purposes. No other preprocessing (i.e., atmospheric correction) was, however, attempted.

For each of the nine cover types identified along Jack Tone Road, one or more two-by-two pixel areas were extracted and labeled. The spectral values for all 128 channels were then plotted. A preliminary analysis of the different cover types was undertaken to determine the maximum reflectance value against which other cover types could be scaled. Of the nine cover types identified, stubble had the highest reflectance values and, therefore, became the reference cover. Other cover types included: corn, alfalfa, beans, sugar beets, tomatoes, peppers, vineyards, and bare soil. An adobe clay soil was found throughout the study area.

#### DISCUSSION

Since the only ground data available to this study was cover type, discussion of results is both preliminary and speculative. Other researchers may opt to interpret these data differently based on a greater knowledge of vegetation

response in the 1155-2336 nm region.

Figures 1 and 2, which show reflectance curves for beans and sugar beets, respectively, are typical of the general patterns observed for most other cover types. The positive slope in the 1550-1700 nm region for beans (.3) and sugar beets (.2) corresponds with higher reflectance values in the 1200-1300 nm region. The negative slope in the 1550-1700 nm region observed in beans (.1) and sugar beets (.1) corresponds with lower reflectance values in the 1200-1300 nm region.

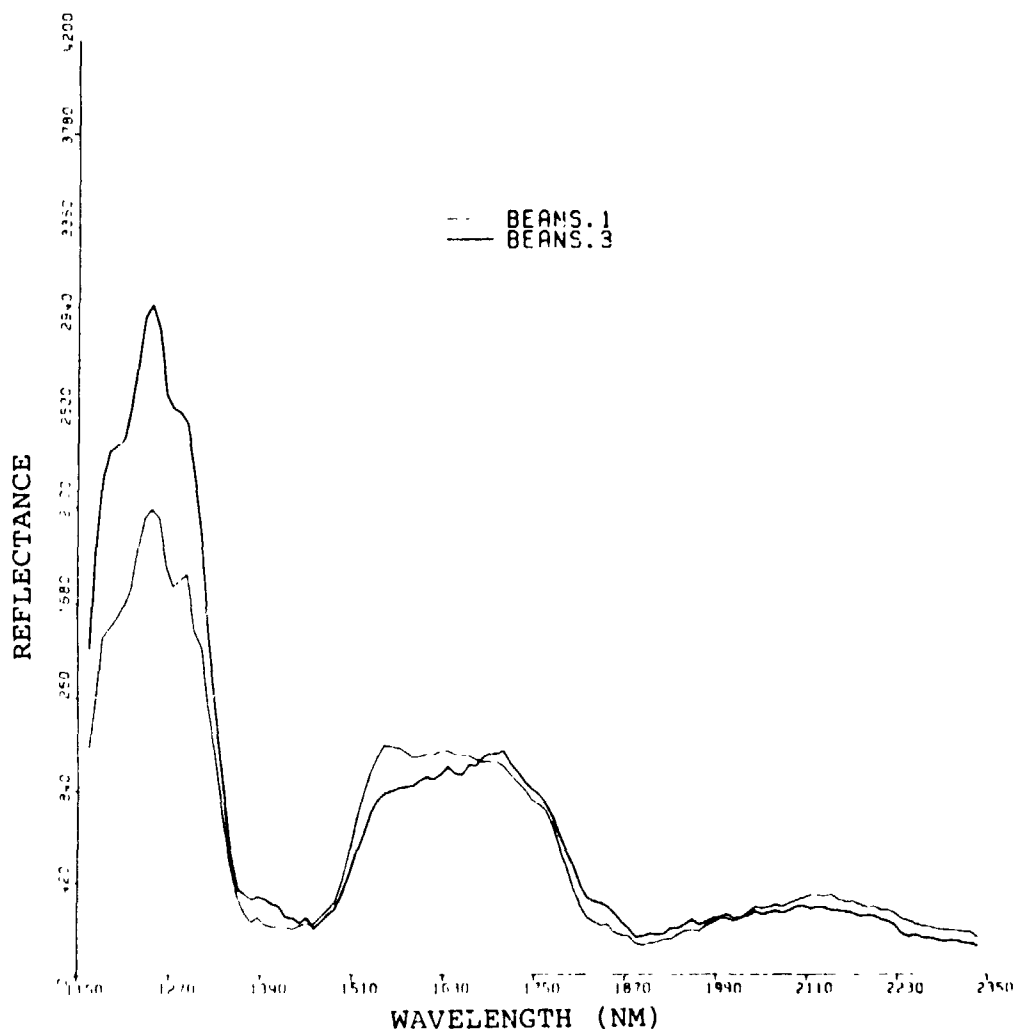


Figure 1. AIS spectra for two bean samples. The positive slope in the 1550-1700 nm region is associated with a higher response in the 1200-1300 nm region. The negative slope in the 1550-1700 nm region is associated with a lower response in the 1200-1300 nm region. Unlike sugar beets, beans are cultivated during a definite season and, as such, all fields should be about the same age. The difference in slope is, therefore, not easily explained on the basis of growth stage or age alone.

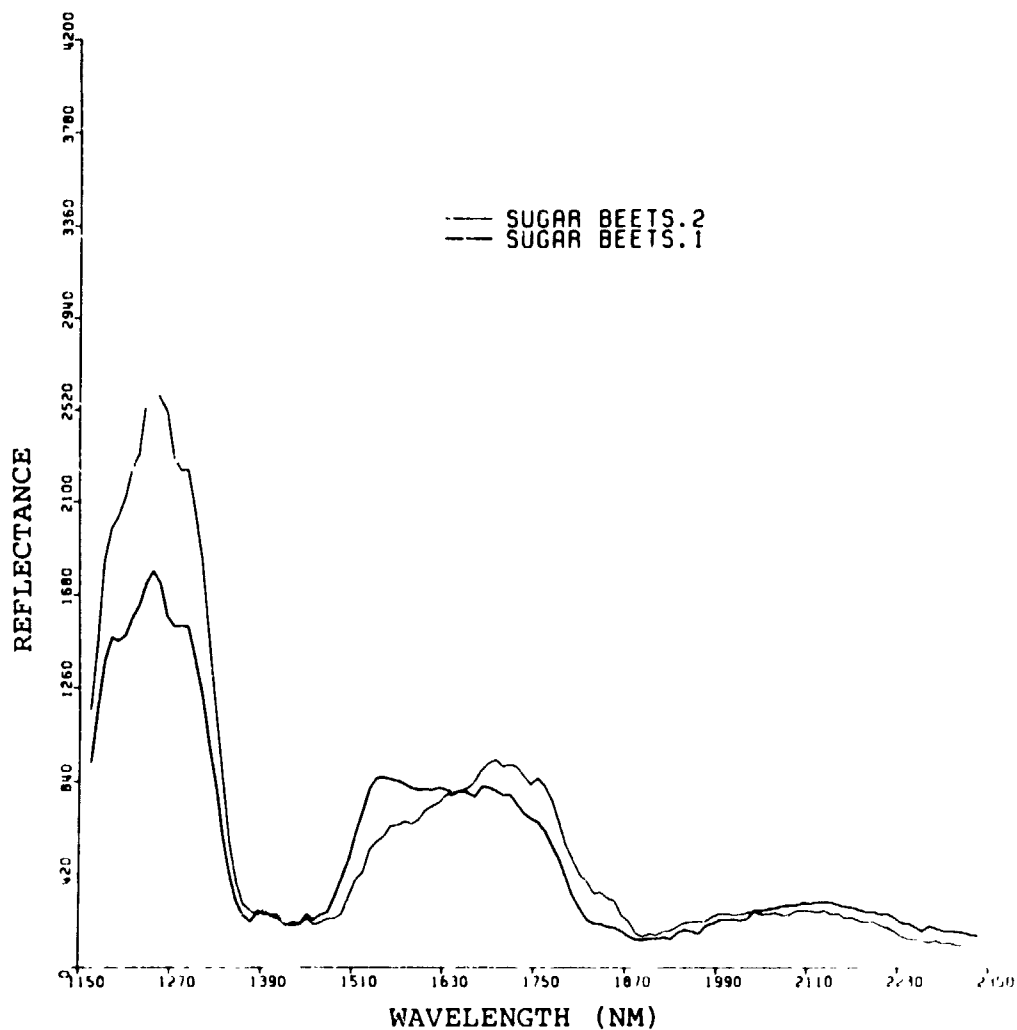


Figure 2. AIS spectra for two sugar beet samples. The positive and negative slopes of the reflectance curves in the 1550-1700 nm region are clearly evident as was the case for beans (Figure 1). Since sugar beets are cultivated year-round, it is nearly impossible to determine the growth stage for the individual fields.

The negative slopes for beans (.1) and sugar beets (.1) are similar to the curves shown in Figure 3. All bare soil plots exhibited this same general shape. The similarity between these curves suggests that either the soil background is influencing the reflectance (lower percent ground cover), field conditions are drier, or the plants are undergoing senescence.

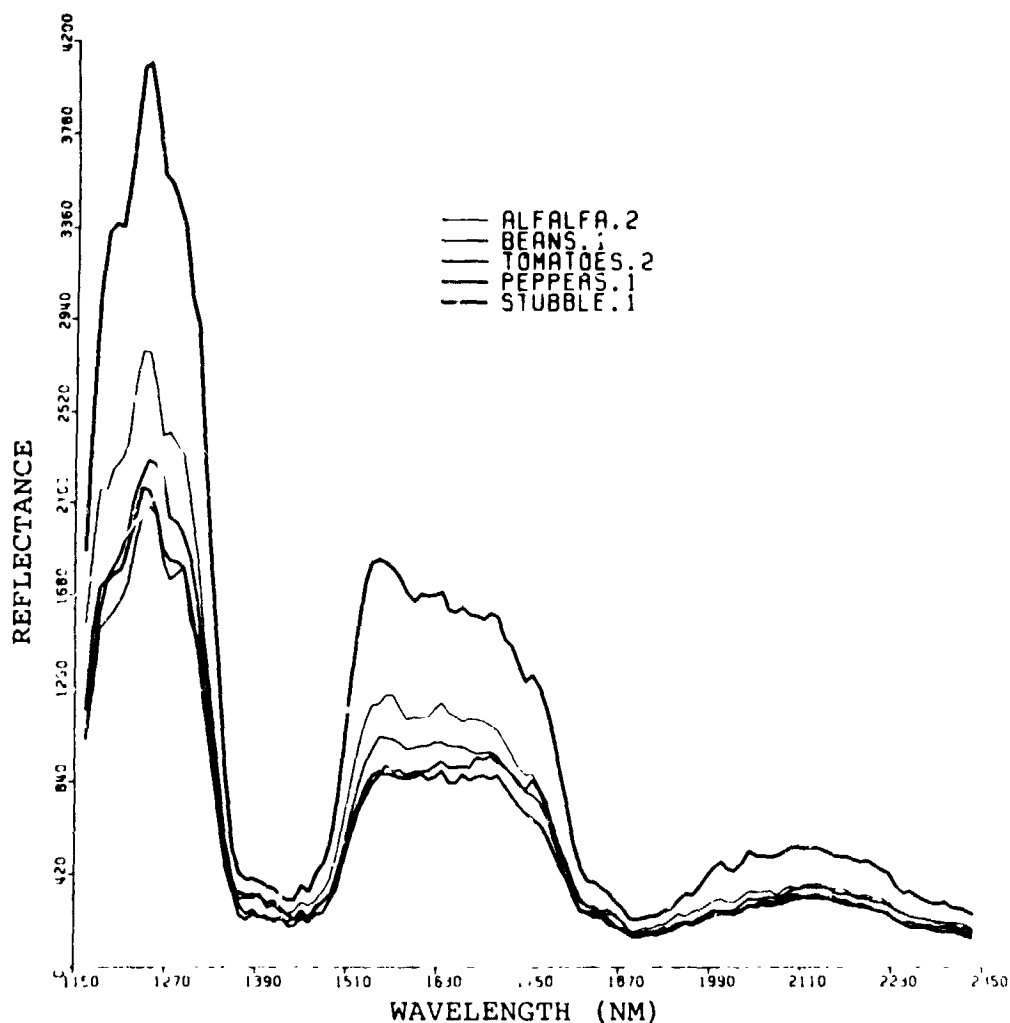


Figure 3. AIS spectra for alfalfa, beans, peppers, tomatoes, and stubble. All these crops have a negative slope in the 1550-1700 nm region. Although the shape of the reflectance curves are similar, the values are different. If not for the similarity of the curves in Figure 4, it would seem likely that the difference was simply a matter of crop-type differences.

Since no ground data were available for well-watered fields, with complete canopy cover, it is difficult to substantiate the idea that the positive slope in the 1550-1700 nm region corresponds to such conditions. This view is supported, however, in part, by the higher reflectance in the 1200-1300 nm region which is characteristic of healthy active-growing crops. Figure 4 shows four fields which follow this general pattern. All have positive slopes in the 1550-1700 nm region and relatively high and consistent values in the 1200-1300 nm region. Not only are the shapes of these curves similar,

but the reflectance values along them are fairly similar. This is surprising, given the considerable differences between the four crops in terms of size, canopy shape, and growth characteristics.

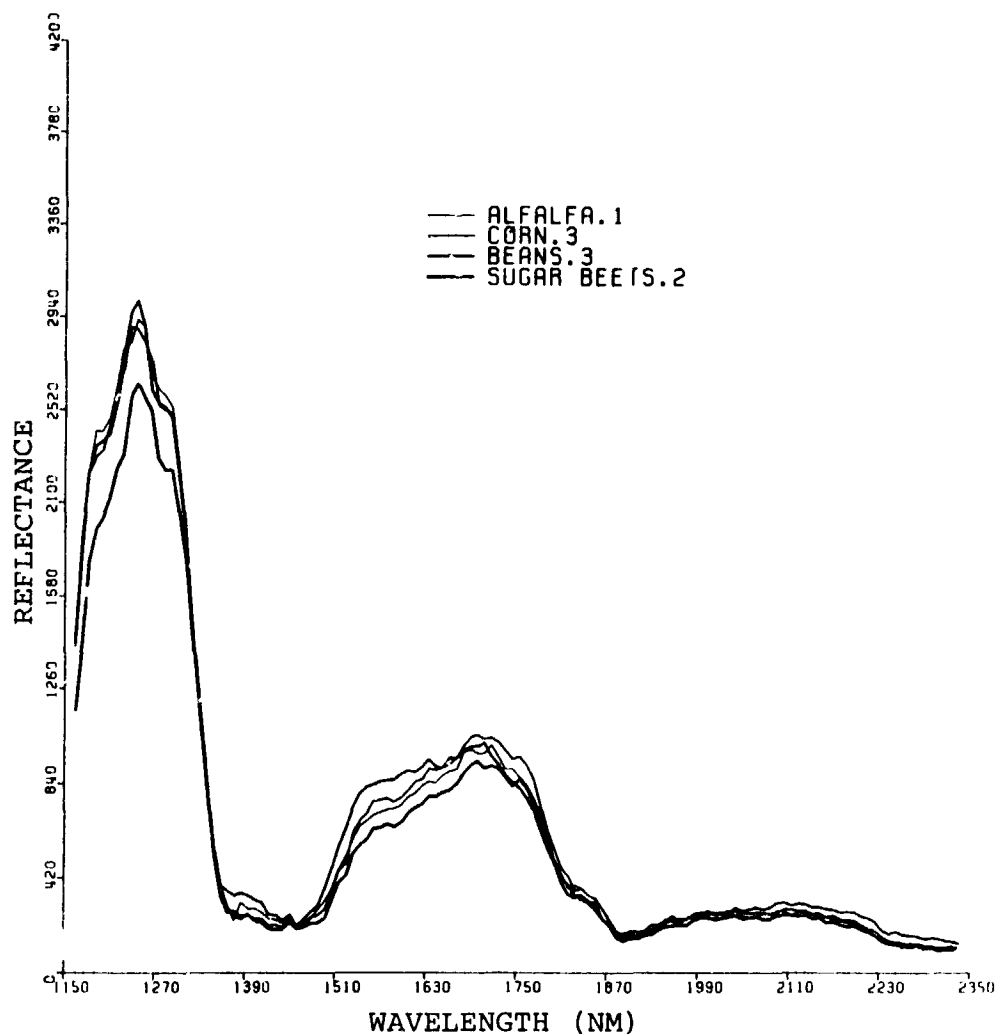


Figure 4. AIS spectra of alfalfa, corn, beans, and sugar beets. All these crops are examples of the positive slope in the 1550-1700 nm region. Although the reflectance curves are similar, the crops are different in terms of structure, canopy, and growth characteristics.

The negative phase in the 1550-1700 nm region is shown for five cover types in Figure 3. Although the curves are similar in terms of overall shape, they exhibit considerable variability in reflectance values. Given the similarity of the curves in Figure 4, this difference in reflectivity can not be explained solely on the basis of different cover type. It may, however, be a function of changes in the plant as it becomes subject to moisture stress or reaches maturity. In either event, reflectivity should change

throughout the spectrum. As moisture content decreases, other leaf components will have a greater influence on reflectivity.

## CONCLUSIONS

Based on a preliminary, qualitative analysis of AIS data acquired over an agricultural area in eastern San Joaquin County, some basic differences between crop spectral profiles have been identified in the 1155-2336 nm region. A positive slope in the 1550-1700 nm region corresponds with higher reflectance values in the 1200-1300 nm region. This does not appear to be related to crop type. A negative slope in the 1550-1700 nm region corresponds with lower reflectance values in the 1200-1300 nm region. This also does not appear to be related to crop type.

The positive and negative slopes in the 1550-1700 nm region seem to be related to plant moisture content, or differences in leaf chemistry growth stage. All crops with the positive slope had similar reflectance curves, regardless of considerable differences in crop structure and growth characteristics. This suggests that whatever factor is the dominant influence on reflectance in the 1155-1336 nm region is common to all of the crops studied.

Crops with a negative slope in the 1550-1700 nm region, although exhibiting similar overall reflectance curves, show considerable differences in terms of absolute reflectance values. These differences may be a result of changes in plant structure, moisture content, mineral uptake and, hence, leaf chemistry as the plant matures and approaches senescence.

In order to answer the questions raised by these spectral curves, one needs to collect considerable and detailed field and laboratory data regarding profiles of the plants of interest over time. Agricultural environments are excellent areas in which to undertake these studies since conditions are uniform over a broad region where they can be easily measured, and since the entire sequence of plant development stages occur in a relatively short period of time.

**Application Of AIS Technology To Forest Mapping**

Stephen R. Yool and Jeffrey L. Star  
Remote Sensing Research Unit  
Geography Department, University Of California  
Santa Barbara, California 93106

**ABSTRACT**

Concerns about environmental effects of large-scale deforestation have prompted efforts to map forests over large areas using various remote sensing data and image processing techniques. Basic research on the spectral characteristics of forest vegetation are required to form a basis for development of new techniques, and for image interpretation. Examination of Landsat data and image processing algorithms over a portion of boreal forest have demonstrated the complexity of relations between the various expressions of forest canopies, environmental variability, and the relative capacities of different image processing algorithms to achieve high classification accuracies under these conditions. AIS data may in part provide the means to interpret the responses of standard data and techniques to the vegetation based on its relatively high spectral resolution.

**INTRODUCTION and OVERVIEW**

Available forest maps are of insufficient accuracy, currency and scale to evaluate the effect massive forest cutting is having on global carbon balance (Houghton and Woodwell, 1981). Scientists are concerned that an imbalance in the global carbon cycle will promote a "greenhouse effect" by the middle of the next century (Sagan et al., 1979). To help evaluate this concern, they have advocated the use of space-based remote sensing to produce accurate maps of the world's forests (Botkin et al., 1984; Woodwell et al., 1983). The accuracies of such maps, particularly in areas of high spatial complexity, may depend upon both the environmental characteristics of the area, and the data processing algorithms used to generate these maps.

This paper summarizes our work on the relative performance of image processing algorithms, and discusses our preliminary findings on the potential of data from the Airborne Imaging Spectrometer (AIS) to supplement existing remote sensing technology for distinguishing forest type classes. We describe our study area in the forests of northern Minnesota, and summarize results of performance tests of standard processing algorithms developed to reduce undesirable variations in spectral reflectance data. This is followed by description of the AIS data from the study site, and a discussion of the potential of these data to complement the vegetation classification process.

Surface spectral variations are needed to classify forest types. Undesirable spectral variations related to the angles of the sun and sensor, the state of the atmosphere, and the type of background soil, however, typically have an adverse effect on

classification accuracy. Algorithms have been developed to reduce these undesirable spectral variations and enhance features in agricultural and rangeland vegetation (Kriegler et al., 1969; Carnegie et al., 1974; Richardson and Wiegand, 1977; Tucker, 1979; Holben and Justice, 1980). We have tested whether such algorithms offer advantages over unprocessed data when large and complex forested areas are classified.

### SUMMARY OF CURRENT WORK

Landsat MSS data from a complex forested area in northern Minnesota were used to analyze the relative performances of waveband ratios, statistical filters, and principal components for classification of natural vegetation in the forests of Northern Minnesota. We analyzed performances of spectral variables produced using standard image processing algorithms (Table 1), grouping categories of ground cover into 9 classes (Table 2).

**Table 1.**  
Spectral Variables of Landsat Data, Minnesota Study Area.

Score (%)	Type	Description	A	B	C	D	E	F	G	H	I
48	14 O	MSS7, MSS5	*	*	*	**	**	**	**		***
47	17 RT	(7/5), MTex	*	**	***	**	*		**		***
46	15 O	MSS6, MSS5	*	*	*	**	**	**	**		***
45	7 R	VI6	*	*	**	**	**		**		***
45	10 R	TVI7	*	*	**	**	*		**		***
44	5 R	MSS7/MSS5	*	*	**	**	*		*		***
44	8 R	VI7	*	**	**	**	*		**		***
44	9 R	TVI6	*	**	*	*	*	*	**		***
43	6 R	MSS6/MSS5	*	*	**	**	*		**		***
42	3 O	MSS6	*	**			**	**	**		***
42	4 O	MSS7		**			**	**	**		***
42	18 C	(7/5)/PC2	*		***	**	*	*			***
38	11 T	MSS5, MTex			*	**	*	**		*	***
37	1 O	MSS4		*	*	*	*	**	*		***
36	2 O	MSS5			**	**	*	**		*	***
28	16 RT	(7/5)SDTex	*			**	*				**
28	19 C	((7/5), SDTex)/PC2	*			***	*		**		
26	21 RT	(7/5)/(7/5), SDTex	**								***
22	20 RT	7, SDTex/5, SDTex			***	*				**	
22	13 T	MSS7, SDTex					*	*		*	***
20	12 T	MSS5, SDTex			*						**
10	22 C	PC1			**						
9	23 C	PC2			**						

**Table 2.**  
**Groundcover Classes**

---

Class A = Evergreen needle-leaved woodland with round crowns, ENLWRC (Pinus banksiana/Jack pine; Pinus resinosa/Red pine; Pinus strobus/White pine)

Class B = Evergreen needle-leaved forest with round crowns, ENLFRC (Pinus banksiana/Jack pine; Pinus resinosa/Red pine; Pinus strobus/White pine)

Class C = Grass

Class D = Dwarf Shrub/Bog (Picea mariana/Black spruce <5m and >10% cover; Sphagnum, Typhus)

Class E = Evergreen needle-leaved woodland with conical crowns, ENLWCC (Picea mariana/Black spruce; Picea glauca/White spruce; Abies balsamea/Balsam fir)

Class F = Evergreen needle-leaved forest with conical crowns, ENLFCC (Picea mariana/Black spruce; Picea glauca/White spruce; Abies balsamea/Balsam fir)

Class G = Deciduous broad-leaved forest, DBLF (Populus spp./Aspen; Betula papyrifera/Paper birch; Acer rubrum/Red maple)

Class H = Mixed evergreen needle-leaved and deciduous broad-leaved forest, MF (Classes B, F, and G)

Class I = Water

---

Differences in performances of the spectral variables apparently result in part from the relative capacities of data processing algorithms to reduce undesirable variations in background reflectance and surface illumination, and to enhance the spectral reflectance of different classes.

Performance differences between two-dimensional ORIGINAL variables and the RATIO variables were insignificant overall. RATIO or "vegetation index" variables appear to be functionally equivalent, and do not perform significantly better than the individual ORIGINAL Landsat variables. Overall classification accuracy for any given RATIO variable is <50%. ORIGINAL MSS6 is the best unprocessed one-dimensional spectral variable overall, while a local-mean filter of MSS7/MSS5 performed best of both processed and unprocessed one-dimensional spectral variables. RATEX and COMPLEX variables performed poorest overall, but RATEX variables 20 and 21 performed best on Classes A and H, respectively.

These results of these tests suggest the complexity of relations between the physical expression of natural vegetation, environmental variability, and data processing techniques that is likely to exist when large geographic areas are surveyed by satellite-borne sensors. Based on these results, the processing of the original Landsat MSS bands does not result in significant increases in performance for the majority of classes. We believe in the excellent performances of certain variables on certain classes. However, further examination into the spectral characteristics of vegetation is required to enable future development of image processing algorithms.

## THE POTENTIAL OF AIS TECHNOLOGY

The AIS was flown over the Northern Minnesota Study Area on August 6, 1983. The time of the overflight was roughly local noon. The instrument was flown at 24,000 feet above the ground, which suggests a 14.8 m pixel size (based on the stated FOV =  $3.7^\circ$ ) at nadir. The data appear blurred, so a precise identification of the ground characteristics is not possible.

Based on our knowledge of ground conditions below the AIS flight path, however, several trends are noticeable.

- \* There are clear gradations in brightness, which show changes in the amount of vegetation along the scan track. The contrast ratios appear to be significantly higher in the 1.4 $\mu$ m than the 1.2 $\mu$ m region.
- \* The dark areas are water bodies. The imagery picks up detail in the water, which probably includes surface and partially-submerged vegetation.
- \* Differences in gray tone patterning and intensity probably relate to the different mixtures of broadleaf and coniferous vegetation typical of this area.
- \* A lake and island are imaged at the bottom of Figure 2. The relative intensity is higher on the island due to the greater amount of bulk vegetation compared with non-island vegetation, which is often patchy due to logging or fire disturbances.

## SUMMARY AND CONCLUSIONS

Previous research completed in the forests of Northern Minnesota demonstrated the complexity of relations between natural vegetation, remotely-sensed data from Landsat, and the algorithms used to process these data. Though the current spectral resolution of AIS is not comparable to Landsat MSS, the Airborne Imaging Spectrometer appears to be a powerful tool for studying the spectral behavior of natural vegetation. AIS data may clarify the results from processing and classification of natural vegetation.

We examined AIS data collected along a corridor within our Minnesota study area. Our data cannot be interpreted precisely, but we are convinced that very subtle changes in the land complex in this area can be detected with the aid of the AIS. The spectral responses to changes in vegetation are particularly apparent in several bandpasses. This information could be useful in the interpretation of data from the Thematic Mapper and SPOT.

## REFERENCES

Botkin, D.B., J.E. Estes, R.M. MacDonald, and Mark V. Wilson

- (1984); Studying The Earth's Vegetation From Space; Biosci; vol. 34, no. 8; pp. 508-514.
- Carneggie, D.M., S.D. deGloria, and R.N. Colwell (1974); Usefulness of ERTS-1 and Supporting Aircraft Data for Monitoring Plant Development and Range Conditions in California's Annual Grassland; BLM Final Report 53500-CT3-266.
- Holben, B. and C. Justice (1980); An Examination Of Spectral Band Ratioing To Reduce The Topographic Effect On Remotely Sensed Data; Tech. Memorandum 80604; NASA Goddard Space Flight Center.
- Houghton, R.A. and G.M. Woodwell (1981); Biotic Contributions To The Global Carbon Cycle: The Role Of Remote Sensing; Proc., Seventh Int'l Symp. Mach. Proc. Rem. Sens. Data; Purdue Univ.; West Lafayette, IN; pp. 593-600.
- Kriegler, F.J., W.A. Mallia, R.F. Nalepka and W. Richardson (1969); Preprocessing Transforms and Their Effects on Multispectral Recognition; Proc., Sixth Int'l Symp. Rem. Sens. Environ.; Environmental Research Institute of Michigan (ERIM); Ann Arbor, MI.
- Richardson, A.J. and C.L. Wiegand (1977); Distinguishing Vegetation From Soil Background; Photog. Eng. & Rem. Sens. vol. 43, pp. 1541-52.
- Sagan, C., O.B. Toon, and J.B. Pollack (1979); Anthropogenic Changes and the Earth's Climate; Science, vol. 206, pp. 1363-68.
- Tucker, C.J. (1979); Red and Photographic Infrared Linear Combinations for Monitoring Vegetation; Rem. Sens. Environ. vol. 8, pp. 127-150.
- Woodwell, G.M., J.E. Hobbie, R.A. Houghton, J.M. Melillo, B.J. Peterson, G.R. Shaver, T.A. Stone, B. Moore, and A.B. Park (1983); Deforestation Measured by Landsat: Steps Toward a Method; U.S.D.O.E.; DOE/EV/10468-1; 62p.

A COMPARISON OF AIS DATA WITH OTHER AIRCRAFT AND GROUND DATA FOR  
THE GEOBOTANICAL DISCRIMINATION OF ROCK TYPES IN SOUTHWEST OREGON

DAVID A. MOUAT, Applied Earth Sciences, Stanford University

ABSTRACT

The use of remote sensing techniques for the geobotanical discrimination of rock types is predicated upon a number of factors. These include an understanding of vegetation response to environmental (especially geochemical) conditions, the establishment of correlations between those vegetation factors and environmental factors, and the use of appropriate remote sensing techniques to discriminate the vegetation.

INTRODUCTION

It has been previously reported (Mouat, 1982) that vegetation can be grouped into three basic categories: 1) Structural, which includes density, plant morphology and structure, phenology, and chlorosis; 2) Taxonomic, which includes indicator species as well as vegetation composition and its distribution; and 3) Spectral, which includes the manner in which vegetation interacts with electromagnetic energy and is usually a function of the other two factors.

This research has been directed toward an understanding of the utility of various sensing systems for discriminating rock types in the Josephine Ophiolite of southwest Oregon (Figure 1). Previous research has involved extensive use of Landsat MSS data for separating

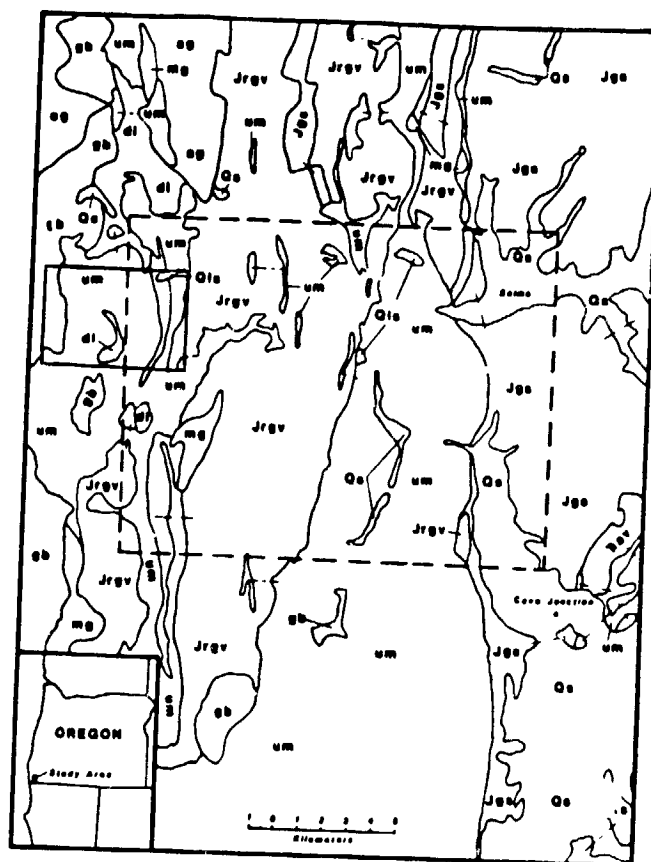


Figure 1. Location and general geology of the Study Area. Area of the AIS flightlines is in solid line. Area studied by Mouat et al. (1982) and Morrissey et al. (1984) in dashed line.

#### LEGEND

Qs	Quaternary sediments	ag	Gneissic amphibolite
Qls	Landslide deposits	di	Quartz diorite
Ks	Marine sedimentary rock	gb	Gabbro
Jgs	Metasedimentary rock	mg	Metagabbro
Jrgv	Metavolcanic rock	og	Olivine gabbro
Jav	Metasedimentary rock	um	Ultramafics

(Morrissey et al., 1984)

unserpentinized peridotite ("harzburgite"), serpentinized peridotite, and sheeted dikes (Harding and Bird, 1984). Vegetation was an important component of that study. Mouat et al. (1982) and Morrissey et al. (1984) reported on the use of simulated thematic mapper imagery for separating general rock types on the basis of associated vegetation. More recently, this author, Nancy Milton, and Mel Podwyssocki (both of the U.S.G.S.) have been undertaking ground-based spectroradiometric work and comparing that data with Airborne Imaging Spectrometer (AIS) data.

#### METHODS AND RESULTS

Five AIS flight lines were flown on July 27, 1984 in a portion of the Josephine Ophiolite (figure 2.). The grating position was in the rock mode between approximately 1150nm and 2350nm. The pixel size was somewhat less than 10 meters; thus, the flight line widths were approximately 300m. Although strong winds and rugged terrain with few discernable landmarks resulted in some crabbing and line displacement, it was felt that most important lithologic and vegetation targets were adequately imaged. These included a variety of rock types within the ophiolitic assemblage and their associated vegetation types. Exceptions included an area of relatively level, unvegetated dunite (a nearly pure olivine as contrasted to harzburgite), and a densely (100% crown closure) vegetated gabbroic intrusive. Ground-based spectroradiometric measurements (with the U.S.G.S. GERS II instrument) were acquired on July 27 and 28. Forty-three of these measurements were obtained.

The AIS imagery was analyzed with the IBM PC-XT image processing system developed at the Stanford Remote Sensing Laboratory. Algorithms useful for AIS image processing as of April 1, 1985 included destriping,

ORIGINAL PAGE IS  
OF POOR QUALITY

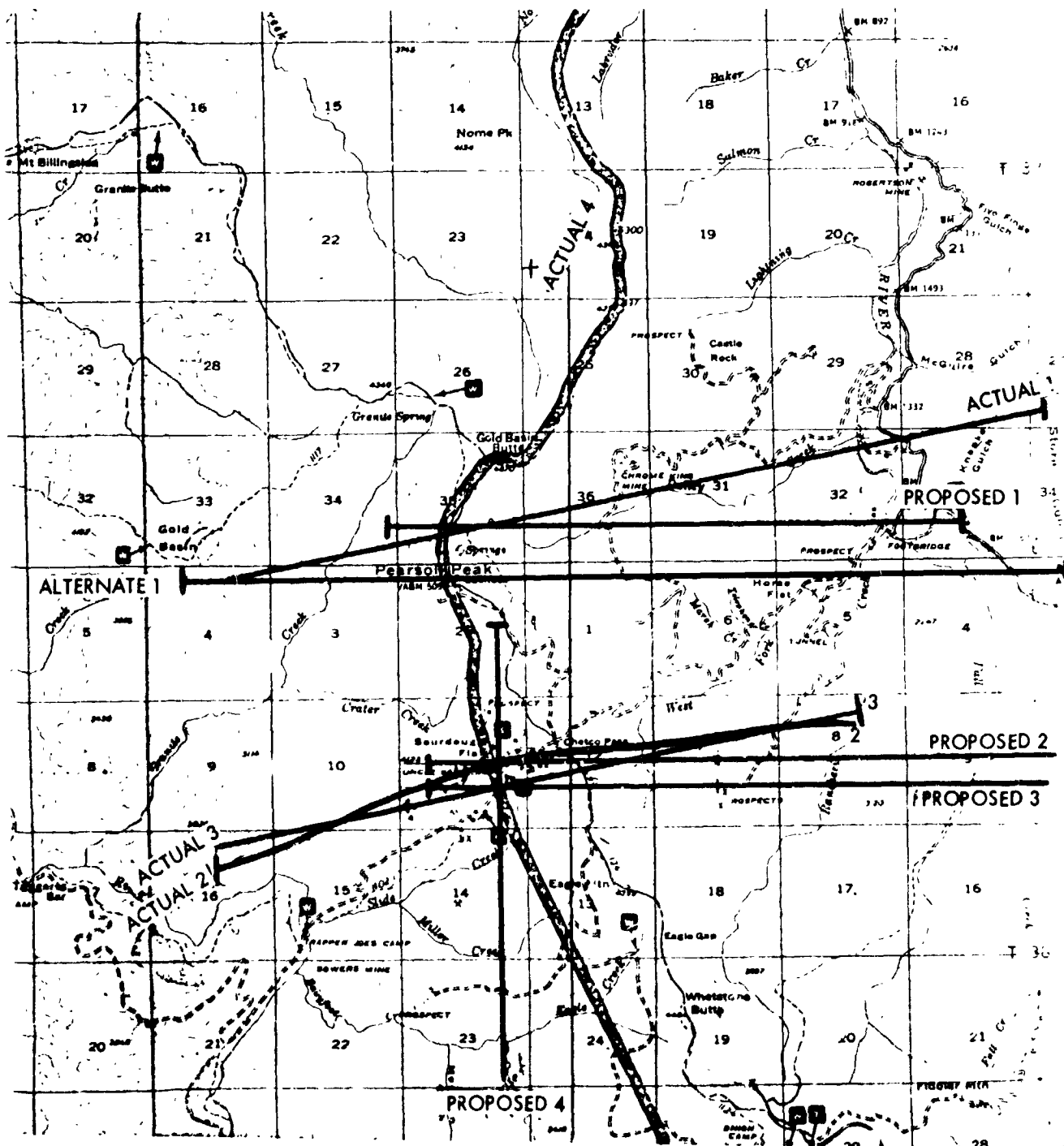


Figure 2. Proposed and alternate AIS flight lines within the southwest Oregon Study Area.

a log residual correction, a multi-channel display, and two spectral representations: graphic and color bar. While the log residual corrections appear to have had some problems (and are being reworked), the others worked satisfactorily. Our spectral representations have successfully spectrally discriminated bare serpentinized harzburgite and nickel laterite, as well as the vegetation growing on those parent materials and also on metavolcanics.

#### ON-GOING PLANS

Continuing work by the investigators involves characterizing vegetation composition and density within the study area, differentiating lithologies on the basis of direct discrimination and through geobotanic inference and applying additional algorithms developed at Stanford and elsewhere to maximize the use of the AIS. It is also hoped that the ground-based spectroradiometric measurements will help us relate the AIS data to reflectance. The NS001 data acquired at the time of overflight and a 1 August 1984 TM scene will be correlated with the AIS data.

#### ACKNOWLEDGEMENTS

The author wishes to acknowledge the essential input of Nancy Milton and Mel Podwysoki to this investigation. In addition, Ron Lyon and Kai Lanz provided invaluable support and assistance with the image processing. Finally, Bob Frenkel and Chris Killgaard of Oregon State University provided earlier detailed ground characterization of the vegetation within the study area.

## REFERENCES

- Harding, D.J. and J. M. Bird. 1984. Mapping Ultramafic Rock Using Landsat Data: The Josephine Peridotite, Oregon and California. Proc. Int'l Symp. of Remote Sensing on Env., Third Them.Conf., Remote Sensing for Exploration Geology, April 16-19, Colo. Springs, pp. 695-709.
- Morrissey, L. A., Weinstock, K. J., Mouat, D. A., and D. H. Card. 1984. Statistical Analysis of Thematic Mapper Simulator Data for the Geobotanical Discrimination of Rock Types in Southwest Oregon. IEEE Trans. on Geoscience and Remote Sensing, Vol. GE-22, No. 6, pp.525-530.
- Mouat, D. A. 1982. The Response of Vegetation to Geochemical Conditions. Proc. Int'l Symp. on Remote Sensing of Environment, Second Them. Conf., Remote Sensing for Expl. Geology, Dec. 6-10, Ft. Worth, Texas, pp.75-84.
- Mouat, D. A., Morrissey, L. A., and E. M. Horn. 1982. Geobotanical Discrimination of Ultramafic Parent Materials: An Evaluation of Remote Sensing Techniques. Proc. of the 16th Symp. on Remote Sensing of Env., Ann Arbor, Mich.

## FOREST SPECIES IDENTIFICATION WITH HIGH SPECTRAL RESOLUTION DATA

CHARLES E. OLSON, JR., School of Natural Resources, The University of Michigan, Ann Arbor, MI 48109-1115, USA; and  
ZHILIANG ZHU, Nanjing Institute of Forestry, Nanjing, China

## ABSTRACT

Data collected over the Sleeping Bear Sand Dunes Test Site and the Saginaw Forest Test Site (Michigan) with the JPL Airborne Imaging Spectrometer and the Collins' Airborne Spectroradiometer are being used for forest species identification. The linear discriminant function has provided higher identification accuracies than have principal components analyses. Highest identification accuracies are obtained in the 450 to 520 nm spectral region. Spectral bands near 1,300, 1,685 and 2,220 nm appear to be important, also.

## INTRODUCTION

Reflectance from plant foliage is largely controlled by plant pigments in the spectral region between 400 and 700 nanometers (nm), by internal leaf structure between 750 and 1,000 nm, and by foliar moisture content between 1,200 and 2,400 nm (Knipling, 1967; Olson, 1967; Rohde and Olson, 1971; Tucker 1980). Any biologic or environmental factor that results in a difference in the amount or nature of pigments present in the leaves, in the amount of cell-wall/air interface inside the leaves, or in the moisture content of the leaves can produce a change in reflectance of those leaves. Many investigators have identified differences between species in response to various biological and environmental factors. Thus, it should not be surprising that differences in reflectance between species have been used to distinguish between species (Krinov, 1947; Olson and Good, 1962; Rohde and Olson, 1962; Roller and Thompson, 1972).

Two recent developments in sensor technology have made it possible to further exploit what is known about reflectance from plants: the Collins' Airborne Spectroradiometer (Chiu and Collins, 1978), and the Jet Propulsion Laboratory Airborne Imaging Spectrometer (Vane, et al., 1983). Both instruments provide data with greater spectral resolution (narrower spectral bands) than has been available before. This report is based on investigations with both of these sensors.

## METHODS

Data were collected over the Sleeping Bear Sand Dunes and Saginaw Forest Test Sites (Fig. 1) in August 1983. The Airborne Imaging Spectrometer (AIS) flight occurred on 7 August and the Collins' Airborne Spectrometer (CAS) flight on 9 August. No precipitation or other significant weather change occurred between the two flights.

Fig. 1. Locations of the two test sites in Michigan's lower peninsula: Sleeping Bear Sand Dunes northwest of Traverse City, and Saginaw Forest west of Detroit.



The Sleeping Bear Sand Dunes Test Site includes a wide variety of natural and modified cover types on rolling glaciated terrain. The Saginaw Forest Test Site is an 80-acre area five miles west of the University of Michigan campus in Ann Arbor, and largely covered by small plantations of different forest tree species. Because of the relative purity of its individual stands, the Saginaw Forest Test Site was selected for initial analysis of the utility of high spectral resolution data for identifying forest tree species.

Broken cumulus clouds over Saginaw Forest on 7 August prevented acquisition of high quality data with the AIS. High quality data were obtained with the CAS on 9 August. Data analyses were based on six flight lines running essentially north-south, parallel to the long axis of the property. Adequate coverage was obtained for nine cover types: red oak (*Quercus rubra* L.), elm and red maple (*Ulmus* spp. and *Acer rubrum* L.), black walnut (*Juglans nigra* L.), cottonwood (*Populus deltoides* Marsh.), hickory (*Carya* spp.), ponderosa pine (*Pinus ponderosa* Dougl. ex Laws.), Scots pine (*Pinus sylvestris* L.), Norway spruce (*Picea abies* L. (Karst.)), and a small lake. Essentially pure spectra from the interior of each cover type were extracted from the CAS data. Principal component (PC) and linear discriminant function (LDF) analyses were made with these spectra (Zhu, 1984).

Because of the high correlation between reflectances in adjacent spectral bands, and because the size of the data set for the total number of spectral bands (570) exceeded available computer storage, Zhu grouped spectral bands into clusters which he called Band Groups. Band Groups were chosen to correspond to the spectral band widths of six of the Landsat Thematic Mapper (TM) spectral channels. Variations in the width of the TM spectral channels resulted in differences in the number of spectral bands in each Band Group (Table 1), but these differences did not cause problems in the subsequent analyses.

Table 1. Spectral ranges of the Band Groups used in the data analyses and their equivalent Thematic Mapper channels.

Band Group	No. of Bands	Spectral Range (nm)	Equivalent TM Channel
1	48	450-520	1
2	54	520-600	2
3	42	630-690	3
4	136	760-960	4
5	14	1550-1750	5
6	18	2080-2350	7

A PC analysis was performed for the spectra in each Band Group. Those bands within each Band Group having the highest correlations with the first PC axis were selected for subsequent cluster analyses with a PC transformation. An LDF analysis was also used to select optimum bands within each Band Group, and to compare results of Band Groups.

Results of these analyses are being used to guide band selections in analyses of the AIS data for the Sleeping Bear Dunes Test Site.

## RESULTS

The PC analyses showed the first principal component accounted for more of the variance in Band Groups 1 through 4 than in Band Groups 5 and 6 (Table 2). When all Band Groups were considered together, the first component accounted for a much lower proportion of the total variance. In every case, however, the first two components accounted for over 95 percent of the variation in the data set.

Table 2. The cumulative variance (in percent) associated with the first and second principal components for Band Groups and for the combination of all Band Groups.

Data Subset	Component 1	Components 1 + 2
Band Group 1	97.72	99.74
Band Group 2	91.72	98.49
Band Group 3	97.61	98.95
Band Group 4	99.86	99.98
Band Group 5	77.43	99.87
Band Group 6	74.52	99.44
Combined	58.85	96.00

Cluster analyses (unsupervised classifications) were performed for each Band Group for PC selected bands from each Band Group, and for the combined PC selected bands from all Band Groups. One set of analyses considered only three cover classes: water, broadleaved forest, and conifer forest. A second set of analyses considered five cover

classes: water; oak, hickory, and walnut; elm and maple; pines; and spruce. Classification accuracy reached 85 percent with the selected bands from Band Group 4 when only three classes were considered, but dropped to 63 percent when the number of classes was increased to five. Because classification accuracies below 80 percent are considered inadequate for most forest resource analyses, PC analyses were not pursued further.

Somewhat better results were obtained with the LDF, and it was decided to attempt a supervised classification with the LDF. The spectra for each cover type were divided into two groups. One group became the training set for that class, and the second group was kept available for testing the classification results. Analyses were made for a two-class case (broadleaved and conifer forests) and for all nine cover classes. As shown in Table 3, results for the combined bands from all Band Groups reached a classification accuracy of 80 percent when all nine classes were considered.

Table 3. Classification accuracies achieved with the linear discriminant function (in percent).

Band Group	Broadleaved/Conifer			All Nine Cover Types		
	Subset 1	Subset 2	All	Subset 1	Subset 2	All
1	83.7	88.1	85.8	91.1	61.2	77.0
2	83.1	90.5	86.8	87.6	51.0	70.4
3	75.5	92.9	83.6	85.7	48.8	68.7
4	79.6	90.5	84.6	87.5	55.0	72.3
5	81.6	90.5	85.7	51.8	40.8	46.6
6	83.7	81.0	82.4	51.8	47.0	49.5
Combined	89.8	*	90.1	94.7	63.2	80.0
* Data not available						

These results indicate that data from Band Group 1 (450-520 nm) provide at least as high a capability for discriminating between the forest species included in this test as data from any other Band Group. In fact, when the nine best individual CAS bands were identified, six were in Band Group 1 and one in Band Group 2. The remaining two were in Band Group 5 (1,684 nm) and Band Group 6 (2,222 nm). Both of these latter bands are within the spectral range of the AIS, and suggest that these two bands should be seriously considered in any attempt to identify tree species from AIS data. These results also point to the desirability of expanding the overall spectral band width of the AIS to include spectral bands at wavelengths shorter than 600 nm.

Work at the Sleeping Bear Sand Dunes Test Site was initially focused on early detection of moisture stress with AIS data. In early July, flexible plastic sheds were built beneath the canopies of trenched forested plots, 20x27 meters in size, to prevent rain from reaching

the soil. When the AIS data were obtained on 7 August, Scholander pressure cell measurements showed xylem water tensions to be 7.7 bars higher in the stressed maple plot, and 9.0 bars higher in the pine plot, than for the control plots. Comparable data for 9 August, when the CAS data were obtained, showed a xylem water tension more than 9 bars above background for both plots. Foliar moisture content, as a percentage of oven-dry-weight, was 15 percent lower in the stressed maple, and 45 percent lower in pine, than in the controls. Laboratory data for leaves from the maple plot showed a small decrease in reflectance between 900 and 1,300 nm, and a progressively higher reflectance from 1,320 to 2500 nm, as compared to comparable data from the maple control. With pine, the laboratory reflectance data showed a slight decrease in reflectance at wavelengths longer than 1,150 nm.

AIS data were obtained for the stressed plots only in grating position 0. Both plots yielded AIS spectra which differed from spectra for their controls in much the same manner as the laboratory reflectance data. In maple, the reflectance cross-over which was observed at about 1,310 nm in the laboratory data was observed in Channels 15 and 16 of the AIS spectra.

Preliminary results with species identification at the Sleeping Bear Test Site indicate there is probably species information in the spectral region between 1,200 and 1,350 nm. While the moisture stress information is relatively broad-band, it appears that the species information is concentrated in bands about 30 nm wide. The optimum spectral band for separating broadleaved species appears to be approximately 20 nm shorter than the optimum band for separating conifers. A single 50-to-60-nm wide band would probably include reflectance cross-overs which could negate the subtle spectral differences we appear to see in the narrow-band data.

#### CONCLUSIONS

Based on work completed to date, it seems safe to conclude that high spectral resolution data can provide improved identification of forest tree species from airborne and spaceborne platforms. It also seems safe to conclude:

1. The linear discriminant function is superior to the principal components technique for identification of forest species.
2. There is significant information about tree species in the spectral band between 450 and 520 nm, in the spectral band between 520 and 600 nm, and in spectral bands near 1,300, 1,685 and 2,220 nm.

#### LITERATURE CITED

- Chiu, H.Y. and W. Collins, 1978. A spectroradiometer for airborne remote sensing. Photogrammetric Engineering and Remote Sensing, 44:507-517.

- Knipling, E.B., 1967. Physical and physiological bases for differences in reflectance of healthy and diseased plants. In Proc. Workshop on Infrared Color Photography in the Plant Sciences, Gainesville, FL, March 2-3. 24 pp.
- Krinov, E.L., 1947. Spectral reflectance properties of natural formations. Academy of Sciences USSR. Translated by G. Belkov, Natural Resources Council of Canada, 1953.
- Olson, C.E., Jr., 1967. Optical remote sensing of the moisture content in fine forest fuels. IST Report No. 4864-8-T, Univ. of Michigan, Ann Arbor. 21 pp.
- Olson, C.E., Jr. and R.E. Good, 1962. Seasonal changes in light reflectance from forest vegetation. Photogrammetric Engineering, 28:107-114.
- Rohde, W.G. and C.E. Olson, Jr., 1971. Estimating foliar moisture content from infrared reflectance data. In Proc. Third Biennial Workshop on Color Aerial Photography in the Plant Sciences. American Society of Photogrammetry. pp. 144-164.
- Rohde, W.G. and C.E. Olson, Jr., 1972. Multispectral sensing of forest tree species. Photogrammetric Engineering, 38:1209-1215.
- Roller, N.E.G. and F.J. Thompson, 1972. Fomes annosus detection by ratio-edited processing of near-infrared and thermal MSS data. IST Report No. 03165-144-L, Univ. of Michigan, Ann Arbor. 17 pp.
- Vane, G., A.F.H. Goetz, and J.B. Wellman, 1983. Airborne imaging Spectrometer: A new tool for remote sensing. In Proc. IEEE 1983 International Geoscience and Remote Sensing Symposium, IEEE Cat. No. 83CH1837-4.
- Tucker, C.J., 1980. Remote sensing of leaf water content in the near infrared. Remote Sensing of Environment, 10:23-32.
- Zhu, Z., 1984. The use of airborne spectroradiometer data: A case of forest composition classification. Unpublished MS thesis, Univ. of Michigan School of Natural Resources, Ann Arbor. 87 pp.

## URBAN, FOREST, AND AGRICULTURAL AIS DATA: FINE SPECTRAL STRUCTURE

V.C. VANDERBILT, Laboratory for Applications of Remote Sensing, Purdue University, West Lafayette, IN 47906-1399, U.S.A.

## ABSTRACT

Spectra acquired by the Airborne Imaging Spectrometer (AIS) near Lafayette, IN, Ely, MN, and over the Stanford University campus, CA were analyzed for fine spectral structure using two techniques: the ratio of radiance of a ground target to the radiance of a standard and also the correlation coefficient of radiances at adjacent wavelengths. The results show ramp-like features in the ratios. These features are due to the biochemical composition of the leaf and to the optical-scattering properties of its cuticle. The size and shape of the ramps vary with ground cover.

## INTRODUCTION

The Airborne Imaging Spectrometer (AIS), developed at the Jet Propulsion Laboratory (JPL), offers the unique capability to obtain high spatial resolution, high spectral resolution, and high radiometric resolution data from an aircraft-borne (NASA C-130) sensor. The instrument provides a synoptic image of any specific ground scene at each of 120 infrared wavelengths between 0.9 (or 1.2) and  $2.4 \mu\text{m}$ . During an extensive data acquisition campaign organized by personnel at JPL during the summers of 1983 and 1984, data were obtained by the AIS instrument over three flightlines: one an agricultural and forested region near Lafayette, IN; an area near Ely, MN, representing the boreal forest; and a rural-urban-residential area including the Stanford University campus in California. Results of an analysis of these data are presented here.

While the AIS instrument does not acquire data in the spectral regions between 0.4 to  $0.9 \mu\text{m}$ , future imaging sensors having high spectral resolution will acquire data in these regions. To anticipate promising areas of future research involving these planned sensors, results of an analysis of high spectral resolution data acquired with an Exotech Model 20C field spectroradiometer are also presented. The data include two spectra from each of more than 250 benchmark soils from locations across the United States as well as more than 800 spectra of four wheat canopies measured in various development stages and sun/view directions and at various times during the day. These spectra and supporting documentation are available in a data library at LARS/Purdue University.

## BACKGROUND AND JUSTIFICATION

Is there fine structure in infrared spectra of foliage? There is reason to believe that in the infrared wavelength region, plants may absorb in narrow spectral bands defined by the structural properties of the organic molecules near the surface of the foliage -- by the resonant frequencies of the translational and rotational vibration modes of the simple bonds (e.g., C-H, C=C, C-CH<sub>3</sub>, N-H, C-NH<sub>2</sub>, etc.) in the larger molecules. For these atoms connected by a covalent bond, the fundamental resonant frequency generally is located at wavelengths longer than 2.5  $\mu\text{m}$ , beyond the wavelength range of the AIS and other passive airborne or spaceborne remote-sensing instruments.

In the 0.7 to 2.4  $\mu\text{m}$  wavelength region (which includes the 1.2 to 2.4  $\mu\text{m}$  range of the AIS), the absorption bands are overtones and harmonics of the fundamental resonant frequencies of these simple structures. The magnitude of the absorption in such a wavelength band usually is not large. And it tends to vary with wavelength, being generally smaller, if the band is located at shorter wavelengths (higher frequency), farther from the fundamental resonant frequency. By the visible wavelengths, this type of light absorption -- involving vibration of organic, covalently bonded atoms -- is nonexistent and light absorption is due to electronic transitions in such organic pigment molecules as chlorophyll.

The observability of the narrow absorption bands may be enhanced if the foliage surfaces are good specular reflectors in the infrared. This is because the magnitude of the specular reflection is determined in part by these absorption properties. And for some plant canopies, the specularly reflected light is a significant part of the total reflected light. For a leaf, the specularly reflected light originates at the interface between air and the cuticle, the multi-layered, wax-covered skin of the leaf. The properties of the cuticle, its topology and chemical composition, are species and possibly variety specific and change with leaf age, plant development stage, plant water status and temperature regime. Because the specularly reflected light never enters the leaf to interact with cell walls or water, its magnitude depends solely on the properties of the cuticle. The magnitude varies with the complex index of refraction of the cuticle and with the optical roughness properties of its surface. Thus, the magnitude would vary in and near a particular narrow absorption band, if these bands exist.

In summary, justifying the search for fine detail in the spectra of vegetation is the potential to discover a new source of information for discriminating species and assessing their condition. The radiometric magnitude and the location in wavelength of absorption in narrow spectral bands, if present in the spectra, may provide such information.

Despite these arguments, narrow absorption bands might not appear in spectra of foliage measured by the AIS instrument. The reasons are identically those explaining, for example, why the sharp absorption

peak at 0.68  $\mu\text{m}$  of chlorophyll measured in vitro does not appear in high resolution spectra of plant canopies. For absorption in the infrared, the many candidate bonds provide a rich plethora of absorbing regions at often adjacent wavelengths. While many molecules throughout the plant will contain any specific bond, for example, C-CH<sub>3</sub>, the absorbing wavelength region of each will not be the same, but rather modified depending on the structural characteristics of the parent molecule and adjacent environment. The absorbing region of wavelengths will be broader for the aggregate of molecules than that for any one molecule. And in canopy spectra, the prominence of the absorption region may be reduced if other bonds absorb at adjacent wavelengths.

Additionally, whether or not absorption is evident in narrow wavelength bands in the AIS spectra will depend on the magnitudes of the instrument noise relative to the absorption "signal" in the spectra as well as the natural variability of the spectra of the scene as a function of wavelength. Almost certainly the change in the spectra due to an absorption band will be small (probably less than 5% of value). Substantial evidence has not been reported for the existence of narrow absorption bands in spectra of individual leaves measured with the Beckman DK-2A spectrophotometer with integrating sphere attachment. Compared to the DK-2A, the AIS has better spectral resolution and has the additional advantage of imaging a synoptic view of the scene. Thus, the AIS is an important tool for readdressing the question -- does foliage preferentially absorb in narrow wavelength bands -- at increased spectral and radiometric resolution.

## RESULTS

To analyze the AIS data for fine spectral structure, the spectral and image analysis system located at the Jet Propulsion Laboratory, Pasadena, CA, was employed to determine, for test fields containing between 50 and 32,000 pixels, two variables (Figs. 1-3) as a function of wavelength: (a) a ratio -- the uncalibrated radiance (as indicated by the digital number, DN) averaged for a test field divided by the DN of a standard -- a large uniform vegetated area in the flightline, and (b) the correlation coefficient of the DN values of adjacent bands. Analysis of the spectroradiometer data of the 500 soil spectra and more than 1200 vegetation spectra involved calculation of the correlation coefficient of data at adjacent wavelengths. A description of procedures used to acquire these data is available.

Figures 1-2 show that the ratio varies as a function of both cover type and wavelength, showing large variations over small wavelength intervals in the two large water absorption bands at approximately 1.4 and 1.9  $\mu\text{m}$ . On each side of these bands the ratio (Fig. 1) varies with wavelength often as an increasing or decreasing ramp, depending upon the cover type in the test field. Plots of ratios (not shown) representing other areas in both the Lafayette and Ely flightlines display similar ramps. The average DN of a large area of deciduous forest served as the standard, or denominator, of the ratio in

Figure 1. The results (Fig. 2) show that the ratios of several cover types of the urban area do not vary with wavelength. This means that the DN values of the cover types vary in conjunction with the DN values of the standard, a large grass area on the Stanford campus. Unlike the results, Fig. 2, the results, Fig. 3, do show variation with wavelengths; the ratios representing clay tile rooftops on the campus (Fig. 3) have minima between 2.05 and 2.15  $\mu\text{m}$ . In the Stanford data, the DN values of some pixels, generally near the extreme left and right edges of the flightline, are saturated with a DN of 2.55. Care was taken to exclude such pixels from the analysis. The minima (Fig. 3) represent the only evidence of fine structure discovered in the analysis of the Stanford flightline.

The results of the analysis of the vegetation and soils acquired by the Exotech spectra radiometer show that the correlation coefficient of data at adjacent wavelengths varies as a function of wavelength. Large variations in the values of the correlation coefficient occur in the vicinity of the water absorption bands at 0.95, 1.15, and 1.4  $\mu\text{m}$ . For the vegetation, additional anomalies are located at 0.56 - 0.60  $\mu\text{m}$  near the peak of the green region and at 0.70 - 0.75  $\mu\text{m}$  at the red edge. The only anomaly found in the soils data was due to the ferric oxide absorption band near 0.9  $\mu\text{m}$ .

#### DISCUSSION

The results (Fig. 1) contain ramp features in the data showing that the spectra of other foliage areas in the flightline vary with wavelength differently than does the spectrum of the forest, the standard whose DN value served as the denominator of the ratio. The variation is not random with wavelength but instead appears to represent fundamental characteristics of the foliage areas. Furthermore, the ramps appear due mainly to chemical and physical properties of the light-scattering foliage -- not to geometric factors related to the canopy architecture -- or to sun-view angle effects (these three factors determine the amount of light scattered by a plant canopy).

The ramps show that the biochemical constituents and/or the optical-scattering properties of the foliage surfaces vary with ground cover. The variation is small and represents a secondary factor in understanding the mean reflectance of all the vegetation in the flightline. Yet when the ratio technique is employed to effectively remove the mean from the data, this secondary factor becomes a primary source of variation between ground covers in the flightline.

The argument that canopy geometry is not the primary cause of the ramp feature is simple; if it were, curves of the ratio would never cross and probably they would have a shape different from that of the ramps (Fig. 1). To prove the point, let us initially assume that the canopy geometry is the primary cause of the ramps in the plots of the ratios. Then we will demonstrate a contradiction. So assume that the light-scattering properties of each infinitesimal piece of foliage in the flightline are identical. Assume that the only difference between

ground covers is due to geometric factors related to canopy architecture (e.g., size of leaf, leaves per unit volume, leaf area per unit volume, etc.). Then the bidirectional reflectance factor (BRF) of the plant canopies would depend only on these geometric factors and on the sun-view direction. For the specific sun-view direction of our flightline, only the geometric factors would determine the BRF of the plant canopies. These geometric characteristics would determine the amount of light, singly and multiply scattered, arriving at the sensor. Under these circumstances, the plots of BRF would be nested; no two curves would cross. Furthermore, two ratios would never cross. As the ratios (Fig. 1) do cross, our initial assumption is not valid; the optical-scattering characteristics of the foliage do vary with species as a function of wavelength. As a second reason why the initial assumption is wrong, consider the region, 1.4 - 1.9  $\mu\text{m}$ , between the large water absorption bands. Again, if the light-scattering properties of all foliage were identical and only geometric differences distinguished canopies, then the amplitude variation of a specific ratio as a function of distance from an absorption band should be similar to the variation with distance in wavelength from other bands. Yet Fig. 1 shows this is not the situation. The ratio (Fig. 1) shows an abrupt rise (or fall) to about 1.5  $\mu\text{m}$  followed by our "ramp" -- a slow fall (or rise) to approximately 1.8  $\mu\text{m}$ . There is no abrupt rise (or fall) near 1.8  $\mu\text{m}$ . Since the geometry of a canopy is not a function of wavelength from 1.5 to 1.8  $\mu\text{m}$  and since light absorption by foliage in each band is comparable, we should see this abrupt rise (or fall) with decreasing wavelength near the 1.9 band. We do not. Thus, for both reasons -- the shape of the ratio curves and the fact that they cross-- we conclude that the geometry of the canopies is not the primary factor for understanding why the ramps exist in the results (Fig. 1); instead the secondary biochemical properties and light-scattering surface properties of the foliage are the important factors.

Three biochemical and physical factors appear potentially important to understanding the appearance of the ramp features in the data: (a) specular reflection; (b) absorption/scattering by the constituent carbohydrates, fats, and proteins in the foliage; and (c) absorption/scattering by the distributed air and water (protoplasm) in and between the cells in the foliage.

Specular reflection requires an optically smooth boundary between two dielectrics--thick compared to the wavelength of incident light. Typically the surface of a leaf is never optically smooth but instead supports structures capable of scattering light according to the size criteria established by Rayleigh and Mie. While the amount of light scattered by the structures on the surface is dependent on wavelength, it is probably of limited importance for remote sensing purposes in the wavelength region 1.2 - 2.4  $\mu\text{m}$ . More important is the optical thickness, the skin depth of the multiple layers containing the epicuticular wax, the cuticle and the cell wall and membrane. All have comparable indices of refraction in the visible wavelength region but not necessarily throughout the infrared. The thickness, more or less three micrometers, is comparable to the wavelength of the incident

light -- more so at 2.4 than 0.9  $\mu\text{m}$ . Because of these structural characteristics, a leaf might be expected to be a better specular reflector in the visible wavelengths than at 2.4  $\mu\text{m}$ . And at some wavelengths, the surface will no longer be a specular reflector. In the transition zone between these extremes (which could include the region 0.9 - 2.4  $\mu\text{m}$ ), the amount of specularly reflected light will decrease to insignificance. Thus, one factor to consider in the explanation of the ramp features in the data (Fig. 1) is the spectral location and importance of the specular reflectance transition zone in each species. It may be possible that all or part of the ramp might be explainable as the waning influence of specular reflection as a function of increasing wavelength, a process dependent on leaf optical properties and thus peculiar to each plant cover -- depending on its species/variety and condition.

The second factor to consider in understanding the presence of the ramp features (Fig. 1) is the amount of light absorbed by the constituent carbohydrates, fats, and proteins of the leaf. As discussed in the Background section above, these molecules absorb preferentially with wavelength. While one of the simple bonds composing one of the larger molecules might absorb at one wavelength, the general trend of the absorption spectrum of the aggregate of all carbohydrate molecules is a decrease, albeit erratic, with decreasing wavelength from 2.4  $\mu\text{m}$ . The absorption curves for fats and proteins show similar trends. Thus, a second factor to consider in the explanation of the ramp features in the data is the relative importance of the absorption spectra of these three constituents of the foliage. The importance will presumably change with wavelength. A composite absorption spectrum might aid in explaining all or some portion of the ramp features in the data (Fig. 1). The composite spectrum would include contributions from all three absorption spectra of carbohydrates, fats, and proteins in a linear combination dependent on species, varieties, and plant condition.

The last factor to consider in the explanation of the ramp features (Fig. 1) is the relative importance of air and water (protoplasm) dispersed in the leaf. If the leaf were optically thick and completely water, then the plant canopy would be quite black. But leaves do contain air in irregular sinuous pathways. The physical properties and thus the optical properties of the emulsion of air and water vary with species. As the transition regions near the large water-absorption bands at 1.4 and 1.9  $\mu\text{m}$  are likely regions to observe such species-dependent optical phenomena, the ramp features may be a manifestation of species-dependent water absorption.

Analysis of the spectroradiometer data, determining the correlation coefficient of reflectances at adjacent wavelengths, provides evidence for fine spectral structure in the orange and red edge spectral regions in the wheat spectra and the ferric oxide,  $\text{Fe}_2\text{O}_3$ , absorption band near 0.9  $\mu\text{m}$  in the soils data. As the wheat data contained spectra from four development stages including data acquired before and after heading and when the wheat was ripe (senescent), the correlation analysis process will tend to identify those regions where

the spectral curves show the maximum change with wavelength and date. Such a region, the red edge, contains an abrupt increase in radiance value between the red and the near infrared before senescence. The increase almost disappears upon senescence as the chlorophyll pigments deteriorate and the red reflectance of the wheat canopy significantly increases. The Collins far-red shift, which has been observed to occur with heading, will add additional diversity to the spectra at the red edge. Thus, the explanation of fine spectral structure at the red edge appears clear. The spectra of the senescent wheat appear to be the contributing factor for finding fine structure at  $0.56 - 0.6 \mu\text{m}$  in the data acquired by the spectroradiometer. Prior to senescence, the wheat spectra have a peak reflectance at  $0.56 \mu\text{m}$ ; the peak disappears after senescence and the reflectance increases monotonically with increasing wavelength in the green and red spectral regions. The correlation process is identifying this abrupt change that occurs at senescence.

#### ACKNOWLEDGEMENT

This research would not have been possible without the generous and friendly assistance of Greg Vane, Barry Rock, and Jim Vogelmann, all of JPL.

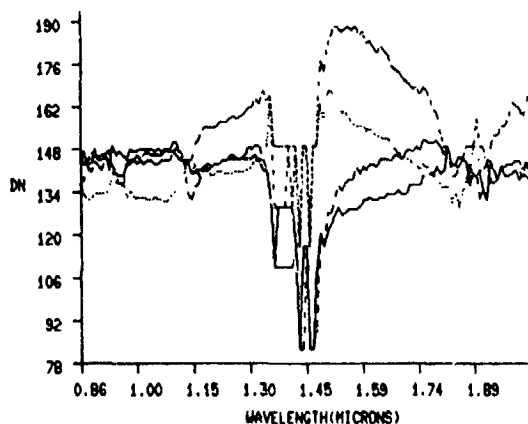


Fig. 1. Using the AIS data from the Lafayette flightline, the ratios, the digital numbers (DN) of four ground covers divided by the DN value of a deciduous forest used for comparison purposes as a standard, were calculated using the formula:  $\text{ratio} = 50 + 100 * \text{target/standard}$ . As best as can be determined, the four ground covers are alfalfa (top curve at  $1.5 \mu\text{m}$ ), deciduous forest (bottom curve), and probably corn and/or soybeans (middle curves).

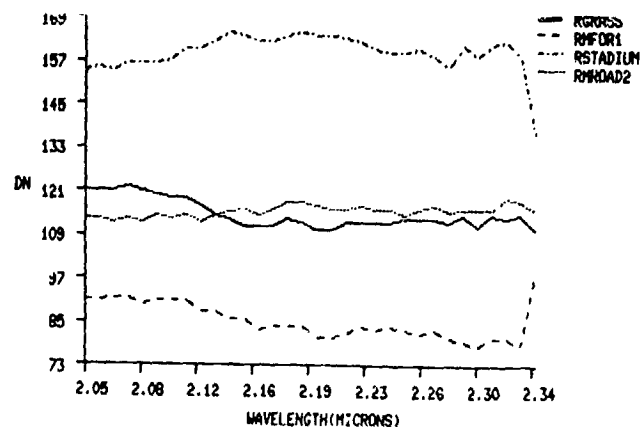


Fig. 2. The ratios of four ground targets in the Stanford flightline were determined from the formula:  $\text{ratio} = 50 + 75 \times \text{target/standard}$ . The ground targets are bleachers in the football stadium (top curve), forest (bottom curve), playing field in stadium (solid curve), and a road surface. A large grass area served as the standard.

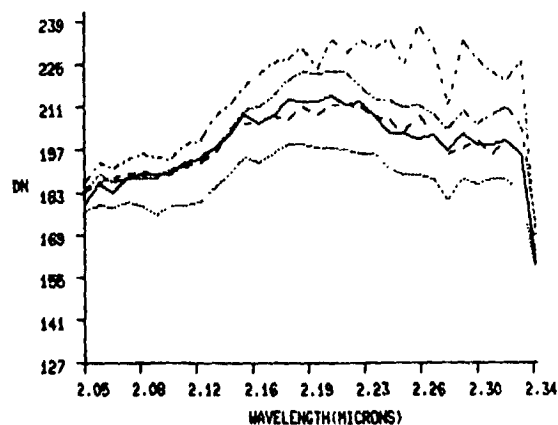


Fig. 3. The ratios of the Stanford data representing four rooftops from the section of the Stanford campus containing red tile roofs were determined from the formula:  $\text{ratio} = 50 + 75 \times \text{target/standard}$ . The grass area of Fig. 2 served as the standard.

APPENDIX 1  
ATTENDEES OF THE AIS DATA ANALYSIS WORKSHOP  
APRIL 8-10, 1985

<u>Name</u>	<u>Representing</u>
Abrams, Mike	JPL
Adams, John	University of Washington
Adams, Steven	JPL
Albee, Arden	California Institute of Technology
Allen, Jim	NSI
Bailey, Jeff	Australian Mineral Industry Research Association, Australia
Balick, Lee	EG & G Energy Measurement Inc.
Banninger, Cliff	Institute for Image Processing and Computer Graphics, Graz, Austria
Barge, Lisa	JPL
Barney, Terry	University of Missouri, Columbia
Berry, Wade	University of California, Los Angeles
Blad, Blaine	University of Nebraska
Blake, Pamela	University of Hawaii
Brown, Hal	General Electric Space Division
Conel, Jim	JPL
Curtis, Brian	California Institute of Technology
Dickinson, Stan	NASA/Ames Research Center
Donis, Paul	Self
Dykstra, Jon	Earth Satellite Corporation
Elvidge, Chris	JPL
Evens, Carla	NASA/Goddard Space Flight Center
Evans, Diane	JPL/NASA Headquarters

<u>Name</u>	<u>Representing</u>
Feldman, Sandra	Mackay School of Mines, University of Nevada
Ford, John	JPL
Fownes, Jim	University of Wisconsin, Madison
Gardner, Bronson	Standard Oil of Ohio
Gillespie, Alan	JPL
Goetz, Alex	JPL
Gross, Michael	University of Delaware
Henderson, Fred	Geosat Committee
Herring, Mark	JPL
Higgins, Robert	NSI
Hoover, Gordon	JPL
Huntington, Jon	CSIRO, North Ryde, New South Wales Australia
Jordan, Bob	Lockheed Missiles & Space Company
Kahle, Ann	JPL
Krohn, Dennis	U.S.G.S., Reston
Kruse, Fred	U.S.G.S., Denver
Laity, Julie	California State University, Northridge
Lang, Harold	JPL
Lawton, Wayne	JPL
Lyon, Ron	Stanford University
MacDonald, John	MacDonald Detweiler & Associates, Vancouver, British Columbia, Canada
Mahoney, Colin	JPL
Martucci, Louis	Battelle Northwest Laboratories
Mason, Robert	NASA/Ames Research Center

<u>Name</u>	<u>Representing</u>
McFarland, William	University of Missouri, Columbia
Meesong, Lee	JPL
Michael, Richard	Earth Satellite Corporation
Milton, Nancy	U.S.G.S, Reston
Monson, Richard	NASA Headquarters
Morris, Bob	NASA/Ames Research Center
Mouat, David	Stanford University
Murphy, Robert	NASA Headquarters
Mustard, John	Brown University
Nemani, Ramakrishna	University of Montana, Missoula
Ocampo, Adriana	JPL
Olson, Charles, Jr.	University of Michigan, Ann Arbor
Palluconi, Frank	JPL
Paylor, Earnie	JPL
Peterson, Dave	NASA/Ames Research Center
Pieters, Carle	Brown University
Podwysocki, Mel	U.S.G.S, Reston
Reimer, John	JPL
Ridd, Merrill	University of Utah
Rinker, Jack	U.S. Army Topographic Laboratory
Ripple, William	ERSAL, Oregon State University
Roberts, Dar	Stanford University
Rock, Barry	JPL
Rode, Jon	Rockwell International
Rowan, Larry	U.S.G.S, Reston
Rundquist, Don	University of Nebraska

<u>Name</u>	<u>Representing</u>
Ruzek, Martin	JPL
Samson, Scott	University of Nebraska
Schenck, Leslie	JPL
Settle, Mark	ARCO Oil & Gas Company
Singer, Bob	University of Hawaii
Smith, Milt	University of Washington
Smythe, William	JPL
Solomon, Jerry	JPL
Spanner, Mike	NASA/Ames Research Center
Steinkraus, Ron	JPL
Strahler, Alan	Hunter College of C.Y.N.Y.
Taranik, Jim	Mackay School of Mines, University of Nevada
Tucker, Deanne	JPL
Ustin, Susan	University of California, Davis
Vanderbilt, Vern	Purdue University
Vane, Gregg	JPL
Vogelmann, Jim	JPL
Westman, Walt	Technicolor Government Services
Wickland, Diane	JPL/NASA Headquarters
Wilson, Peter	CSIRO, Perth, Australia
Wood, Byron	NASA/Ames Research Center
Wukelic, George	Battelle Northwest Laboratories
Yamaguchi, Yasushi	Geology Survey of Japan/Stanford University
Yool, Steve	University of California, Santa Barbara
Zak, Alex	JPL

## APPENDIX 2

### AGENDA OF THE AIS DATA ANALYSIS WORKSHOP HELD APRIL 8-10, 1985

Meeting all Three Days in the Building 167 Conference Room  
at the Jet Propulsion Laboratory

#### Monday, April 8

- 8:00 Shuttle Bus leaves Holiday Inn for JPL
- 8:30 WELCOME AND WORKSHOP OVERVIEW  
Gregg Vane
- 9:00 IMAGING SPECTROMETER PROJECT REVIEW AND STATUS  
Alex Goetz
- 9:45 Break
- 10:00 AIS 1984 OPERATIONS SUMMARY AND 1985 PLANS  
Gregg Vane
- 10:45 AIS DATA HANDLING AND ANALYSIS  
Jerry Solomon
- 12:00 Lunch
- 1:00 MINERALOGICAL MAPPING IN THE CUPRITE, NEVADA, MINING DISTRICT  
Alex Goetz, JPL
- 1:30 REMOTE STRATIGRAPHIC ANALYSIS: COMBINED TM AND AIS RESULTS IN  
THE WIND RIVER/BIGHORN BASIN AREA, WYOMING  
Harold Lang, Ernie Paylor, and Steve Adams, JPL
- 2:00 FIELD UTILIZATION AND ANALYSIS OF AIS 128-CHANNEL IMAGERY USING  
MICROCOMPUTERS: APPLICATION TO YERINGTON, NV FIELD AREA  
Ron Lyon and Kai Lanz, Stanford University
- 3:00 Break
- 3:30 PRELIMINARY ANALYSIS OF AIS SPECTRAL DATA ACQUIRED FROM  
SEMI-ARID SHFUB COMMUNITIES IN THE OWENS VALLEY, CALIFORNIA  
Susan Ustin, U.C. Davis, and Barry Rock, JPL
- 4:00 AIS SPECTRA FOR STRESSED AND UNSTRESSED PLANT COMMUNITIES IN  
THE CAROLINA SLATE BELT  
Diane Wickland, JPL
- 4:30 SPECTRAL CHARACTERIZATION OF SUSPECTED ACID DEPOSITION DAMAGE  
IN RED SPRUCE (PICEA RUBENS) STANDS FROM VERMONT  
Jim Vogelmann and Barry Rock, JPL

- 5:00 Wrap Up
- 5:30 Shuttle Bus departs JPL for Holiday Inn

Tuesday, April 9

- 8:00 Shuttle Bus departs Holiday Inn for JPL
- 8:30 A FIRST LOOK AT AIRBORNE IMAGING SPECTROMETER (AIS) DATA IN AN AREA OF ALTERED VOLCANIC ROCKS AND CARBONATE FORMATIONS, HOT CREEK RANGE, SOUTH CENTRAL NEVADA  
Sandra Feldman and Jim Taranik, University of Nevada/Reno, and Dave Mouat, Stanford University
- 9:00 INTERPRETATION OF AIS IMAGES OF CUPRITE, NEVADA USING CONSTRAINTS OF SPECTRAL MIXTURES  
Milton Smith and John Adams, University of Washington
- 9:30 SPECTRAL ANALYSIS OF AIS DATA FOR THE WIND RIVER BASIN, WYOMING  
Bob Singer and Pam Drake, University of Hawaii
- 10:00 Break
- 10:30 EVALUATION OF AIS DATA FOR AGRONOMIC AND RANGELAND VEGETATION: PRELIMINARY RESULTS FOR AUGUST 1984 FLIGHT OVER NEBRASKA SANDHILLS AGRICULTURAL LABORATORY  
Blaine Blad, Patrick Starks, and Cynthia Hays, University of Nebraska, and Bronson Gardner, Standard Oil Company
- 10:50 SITE DESCRIPTION FOR THE UNIVERSITY OF NEBRASKA'S SANDHILLS AGRICULTURAL LABORATORY  
Bronson Gardner, Standard Oil Company, and Blaine Blad, University of Nebraska
- 11:20 PRELIMINARY EVALUATION OF AIS SPECTRA ALONG A TOPOGRAPHIC/MOISTURE GRADIENT IN THE NEBRASKA SANDHILLS  
Don Rundquist, University of Nebraska
- 11:40 THE USE OF AIS DATA FOR IDENTIFYING AND MAPPING CALCAREOUS SOILS IN WESTERN NEBRASKA  
Scott Samson, University of Nebraska
- 12:00 Lunch
- 1:00 CALIBRATION OF AIS DATA USING GROUND-BASED SPECTRAL REFLECTANCE MEASUREMENTS  
Jim Conel, JPL
- 1:30 ANALYSIS OF AIS DATA OF THE RECLUSE OIL FIELD, RECLUSE, WYOMING  
Jon Dykstra and Don Segal, EarthSat Corp.

- 2:00 AIS DATA FORM A BASIS FOR RELATIVE DATING OF GRANITIC ALLUVIAL FANS  
Alan Gillespie, JPL
- 2:30 AIS DATA FROM ALLUVIAL FANS AND EVAPORITE DEPOSITS IN DEATH VALLEY  
Anne Kahle, JPL
- 3:00 Break
- 3:30 FOREST BIOGEOCHEMICAL CYCLING AND REMOTE SENSING  
Dave Peterson and William Acevedo, Ames Research Center
- 4:00 HIGH RESOLUTION SPECTROMETRY OF LEAF AND CANOPY CHEMISTRY FOR BIOCHEMICAL CYCLING  
Mike Spanner, Dave Peterson, William Acevedo, and Pam Matson, Ames Research Center
- 4:30 FOREST CANOPY CHEMISTRY FROM BLACKHAWK ISLAND, WISCONSIN  
Jim Fownes and John Aber, University of Wisconsin
- 5:00 Wrap Up
- 5:30 Shuttle Bus departs JPL for Holiday Inn

Wednesday, April 10

- 8:00 Shuttle Bus departs Holiday Inn for JPL
- 8:30 ANALYTICAL TECHNIQUES FOR EXTRACTING MINERALOGICAL INFORMATION FROM MULTICHANNEL IMAGING SPECTROMETER DATA  
Fred Kruse, Gary Raines, and Kenneth Watson, U.S.G.S.
- 9:00 SPECTROSCOPY OF MOSES ROCK KIMBERLITE DIATREME  
Carle Pieters and John Mustard, Brown University
- 9:30 ANALYSIS OF AIRCRAFT SPECTROMETER DATA WITH LOGARITHMIC RESIDUALS  
Andy Green and M. Craig, CSIRO, Australia (to be presented by Jon Huntington)
- 10:00 Break
- 10:30 COMPARISON OF AIS VS. TMS DATA COLLECTED OVER THE VIRGINIA PIEDMONT  
Robin Bell, Goddard Space Flight Center, and Carla Evans, University of Maryland
- 11:00 DISCRIMINATION OF COASTAL VEGETATION AND BIOMASS USING AIS DATA  
Mike Gross and Vic Klemas, University of Delaware

- 11:30 AIS INVESTIGATION OF AGRICULTURAL MONOCULTURES  
Byron Wood and Bob Wrigley, Ames Research Center
- 12:00 Lunch
- 1:00 APPLICATION OF AIS TECHNOLOGY TO FOREST MAPPING  
Steve Yool and Jeff Star, U. C. Santa Barbara
- 1:30 A COMPARISON OF AIS DATA WITH OTHER AIRCRAFT AND GROUND DATA  
FOR THE GEOBOTANICAL DISCRIMINATION OF ROCK TYPES IN SOUTHWEST  
OREGON  
Dave Mouat, Stanford University
- 2:00 FOREST SPECIES IDENTIFICATION WITH HIGH SPECTRAL RESOLUTION DATA  
Charles E. Olson, University of Michigan, and Zhiliang Zhu,  
Nanjing Institute of Forestry
- 2:30 URBAN, FOREST, AND AGRICULTURAL AIS DATA: FINE SPECTRAL  
STRUCTURE  
Vern Vanderbilt, Paul Anuta, and Craig Daughtry, Purdue  
University
- 3:00 Break and Wrap Up
- 5:00 Shuttle Bus departs JPL for Holiday Inn